The role of the claustrum during eyeblink conditioning

María del Mar
Reus García

Pablo de Olavide University Department of Physiology, Anatomy and Cellular Biology Seville, 2021

Pablo de Olavide University

Department of Physiology, Anatomy and Cellular Biology

MARÍA DEL MAR REUS GARCÍA

THE ROLE OF THE CLAUSTRUM DURING EYEBLINK CONDITIONING

Doctoral Thesis directed by:

José María Delgado García

Seville, 2021.

División de Neurociencias

Universidad Pablo de Olavide

Carretera de Utrera, Km. 1

41013 Sevilla (España)

El Dr**. José María Delgado García**, Profesor Emérito de Fisiología, adscrito al Departamento de Fisiología, Anatomía y Biología Celular de la Universidad Pablo de Olavide,

CERTIFICA:

Que el Trabajo de Investigación titulado **"The role of the claustrum during eyeblink conditioning"**, correspondiente al Programa de Doctorado en Neurociencias, ha sido realizado bajo mi dirección y supervisión por Dña. María del Mar Reus García, Licenciada en Biología por la Universidad de les Illes Balears y Máster en Neurociencia y Biología del Comportamiento por la Universidad Pablo de Olavide. A su vez, considero que el presente trabajo reúne las condiciones y el rigor científico necesarios para ser presentado y defendido como Tesis Doctoral.

Sevilla, 11 de febrero de 2021

José M. Delgado García

To my beloved friends in and outside the lab,
and to my mum, who inadvertently
encouraged me to become a neuroscientist.

RESUMEN

El claustro es una estructura de materia gris y forma laminar escondida en el límite interior del neocórtex, localizada entre el putamen y la ínsula. Está presente en todos los mamíferos, y se han encontrado estructuras homólogas también en aves y reptiles. Cuando fue descrito por primera vez, hace ya un siglo, se pensó que se trataba de una mera estación de relevo debido a sus densas y recíprocas conexiones con el resto del cerebro. Hoy en día, gracias al trabajo de cada vez más científicos, sabemos que el claustro está implicado en procesos atencionales, detección de saliencia, integración multisensorial, sincronía de las oscilaciones cerebrales, e incluso en la consolidación del aprendizaje y la memoria durante el sueño. También ha sido probado que las células del claustro pueden responder a estímulos sensoriales simples, particularmente si éstos implican novedad o alerta, aunque para concretar la función del claustro es necesario más trabajo.

Dadas estas sorprendentes características, la presente Tesis Doctoral se centra en evaluar la participación de las neuronas del claustro en el aprendizaje asociativo, específicamente en el condicionamiento clásico de la respuesta palpebral, en conejos. Para ello, se utilizó un paradigma de retraso simple: un tono de 350 ms se usaba como estímulo condicionado, y 250 ms después de su inicio, se presentaba un soplo de aire en el ojo de 100 ms a modo de estímulo incondicionado; ambos estímulos terminaban simultáneamente. El registro de la actividad electromiográfica del músculo *orbicularis oculis* sirvió para monitorizar el proceso de aprendizaje. La contracción de dicho músculo durante el periodo de tiempo comprendido desde el inicio del tono hasta el del soplo se consideró una respuesta condicionada y dependiente del aprendizaje; la actividad durante los 100 ms que dura el soplo, o más, se consideró una respuesta refleja o incondicionada, y es independiente del aprendizaje.

Para alcanzar nuestro objetivo, primero se obtuvieron registros electrofisiológicos extracelulares y unicelulares de la actividad de las neuronas del claustro durante el condicionamiento palpebral. Las neuronas se localizaron mediante su estimulación sináptica y/o antidrómica desde las cortezas motora, prefrontal y cingulada. Después, registramos los potenciales de campo en el claustro, la corteza motora y corteza prefrontal, también durante el condicionamiento. Por último, hicimos uso del método vINSIST para bloquear sinápticamente las eferencias del claustro antes o después de la adquisición del reflejo de parpadeo.

Se analizaron los registros unicelulares de dos sesiones de habituación (en las que se presentaba solo el estímulo condicionado), ocho de condicionamiento (se presentaban el estímulo condicionado e incondicionado emparejados) y seis de pseudocondicionamiento (se presentaba ambos estímulos desparejados). Durante las sesiones de habituación y pseudocondicionamiento la actividad de la mayoría de las neuronas no se vio afectada por las presentaciones de ninguno de los estímulos desparejados. Sorprendentemente, algunas neuronas del claustro (llamadas tipo A) respondieron con un brote de actividad después de la presentación de los estímulos emparejados, especialmente durante la fase de adquisición del condicionamiento. Sin embargo, la actividad de estas neuronas no estaba linealmente relacionada con el área de las respuestas condicionadas. En contraposición, las neuronas del tipo B se inhibieron tras presentar los estímulos pareados. Así mismo, los estudios de patrones de disparo y duración de las espigas revelaron que las células tipo A eran neuronas de proyección, mientras que las de tipo B eran interneuronas. Los potenciales de campos registrados en el claustro, la corteza motora y la corteza prefrontal, cambiaron sus poderes espectrales a través de las sesiones de condicionamiento en todas las bandas de frecuencia seleccionadas. Además, se detectó una significante comodulation en las bandas espectrales delta y gamma en claustro y prefrontal durante ciertas fases del condicionamiento. Finalmente, la inactivación de la conectividad sináptica del claustro afectó al número y a la amplitud de las respuestas condicionadas a través del condicionamiento, pero no a las respuestas reflejas.

Estos resultados, respaldados por la literatura previa, indican que la actividad de las neuronas del claustro está directamente relacionada con el aspecto cognitivo —no con el motor— del proceso de adquisición del reflejo palpebral, incluso en un sencillo paradigma de retraso (anteriormente atribuido únicamente a otras estructuras). Por lo tanto, el claustro podría ser una nueva diana para tratar los déficits cognitivos relacionados con la atención y el aprendizaje, como los que se producen en diversos trastornos del neurodesarrollo y la salud mental.

ABSTRACT

The claustrum (CL) is a sheet-shaped grey matter structure hidden beneath the inner surface of the neocortex and located between the putamen and the insular cortex. It is present in all mammals, and also birds and reptiles have a homologous structure. When first described, a century ago, it was thought to be a mere relay station given its dense, reciprocal connections to the rest of the brain. Nowadays, thanks to the great effort of a growing number of scientists, we know it is related to attentional processes, salience detention, multisensory integration, brain oscillation synchrony, and even learning and memory consolidation during sleep. It has also been proved that CL cells can respond to single sensorial stimuli, particularly when they involve novelty or alertness, although more research will be needed to elucidate the CL function.

Given these outstanding characteristics, the present Doctoral Thesis focuses on assessing the involvement of claustral neurons during associative learning, specifically in classical eyeblink conditioning, in rabbits. A simple delay paradigm was used: a 350 ms tone was presented as the conditioned stimulus (CS); 250 ms after the CS onset, a 100 ms air puff aimed at the eye was used as the unconditioned stimulus (US); thus CS and US co-terminated. Electromyographic recordings of the activity of the *orbicularis oculi* muscle were used to monitor the learning progress. The contraction of this muscle during the 250 ms after the CS onset was considered a conditioned response (CR) and was learning-dependent; if the movement happened in the 100 ms after the US onset or later, it was considered a reflex or unconditioned response (UR) and was unrelated to learning.

To achieve our purpose, we firstly attained electrophysiological extracellular single-unit recordings from the activity of CL neurons during eyeblink conditioning. CL neurons were located by synaptic and/or antidromic activation from motor (MC), medial prefrontal (mPFC), and cingulate cortices (CC). Secondly, the local field potentials (LFPs) were recorded for CL, MC, and mPFC, also during eyeblink conditioning. As a last step, we used the vINSIST method to synaptically block the CL output before or after the acquisition of the conditioned eyeblinks.

Single-unit recordings were analyzed from two habituation (only the CS was presented), eight conditioning (paired CS/US), and six pseudoconditioning sessions (unpaired CS and US). During habituation and pseudoconditioning sessions, the activity of most recorded cells was rarely distorted by the unpaired CS or US. Remarkably, some CL neurons (type A) responded with a burst of activity after the paired CS/US

presentation, especially during the acquisition phase of the conditioning. However, the activity of type A cells was not linearly related to the area of the CRs. In contraposition, type B neurons were inhibited after the CS/US. Firing pattern and spike duration analyses revealed that type A cells were projection neurons, while type B cells were interneurons. LFPs recorded in CL, MC, and mPFC changed their spectral powers across conditioning sessions for all the selected frequency bands. Moreover, significant delta-gamma comodulations were detected at CL-mPFC network nodes during certain conditioning phases. Finally, inactivation of CL synaptic connectivity affected the number and the amplitude of CRs across the conditioning, but not the URs.

These results, which are consistent with previous reports, indicate that claustral neurons' activity is directly involved in cognitive aspects —rather than in the kinematics of the CRs— of the process of acquiring eyeblink CRs, even using a simple delay paradigm (previously ascribed to other structures). Therefore, the CL could be an important new target in treating cognitive deficits related to attention or learning, such as those reported in several neurodevelopmental disorders.

LIST OF ABBREVIATIONS

ACC	Anterior cingulate cortex
ANOVA	Analysis of variance
AP	Antero-posterior
CC	Cingulate cortex
cCC	Caudal cingulate cortex
CS	Conditioned stimulus
CR	Conditioned response
CL	Claustrum
D	Depth
Dox	Doxycycline
EGFP	Enhanced green fluorescent protein
EMG	Electromyography
IN	Interneurons
INSIST	Inducible silencing of synaptic transmission
L	Lateral
LFP	Local field potential
mPFC	Medial prefrontal cortex
M1	Primary motor cortex
MC	Motor cortex
NPY	Neuropeptide Y
O.O.	*Orbicularis oculi*
PN	Projecting neurons
Ptetbi	Bidirectional tetanus promoter
PV	Parvalbumin
rCC	Rostral cingulate cortex
rAAV	Recombinant adeno-associated viruses
rtTA	Reverse tetracycline-controlled transactivator
SST	Somatostatin
SW	Slow wave
tdTOM	Tandem dimer tomato
TeTxLC	Tetanus toxin light chain
tTA	Tetracycline-controlled transactivator
US	Unconditioned stimulus
UR	Unconditioned response
VIP	Vasoactive intestinal peptide

INDEX

1. INTRODUCTION 1
1.1. The claustrum through the XX century 2
1.1.1 Neuroanatomy 3
1.1.2. Connectivity 5
1.1.3. Basal firing activity of the claustrum 8
1.1.4. Putative functions of the claustrum 9
1.1.5. The claustrum in mental illness 12
1.2. Specific characteristics of the rabbit claustrum 14
1.3. Learning and memory, or how brain adapts behavior to changes 16
1.3.1. Associative learning 18
1.3.2. Classical (or Pavlovian) conditioning 19
1.3.3. Classical conditioning of the eyelid response 22
1.3.4. Why could the claustrum play a role in eyeblink conditioning? 26
1.4. Claustrum and eyeblink conditioning: cortical structures under study 27
1.4.1. Medial prefrontal cortex, Brodmann area 32 28
1.4.2. Motor cortex, M1 29
1.4.3. Rostral and caudal cingulate cortex, Brodmann area 24 31
2. HYPOTHESIS AND OBJECTIVES 35
3. MATERIALS AND METHODS 37
3.1. Experimental animals 38
3.2. Anesthesia and surgeries 38
3.2.1. Ex. 1 - For extracellular recording and stimulation 40
3.2.2. Ex. 2 - For recording of Local Field Potentials 41
3.2.3. Ex. 3 - For injections of the vINSIST viruses 42
3.3. Classical conditioning of eyelid responses 43
3.3.1. Training and adaptation sessions 43
3.3.2. Eyeblink conditioning paradigm 44
3.4. Recording and stimulation procedures 46
3.4.1. Ex. 1 - Extracellular unitary recording and stimulation 47
3.4.2. Ex. 2 - Local Field Potentials recording procedure 48
3.5. Ex. 3 - The vINSIST method 48
3.6. Perfusion 51
3.7. Histology 51

3.7.1. Rabbit brain slices infected with vINSIST viruses 52
3.8. Data collection and analysis 52
3.8.1. Ex. 1 - Extracellular unitary activity analysis 52
3.8.2. Ex. 1 - Parameters to classify CL neurons 53
3.8.3. Ex. 2 - Analysis of the recorded Local Field Potentials 55
3.8.4. Ex. 3 - Analysis of the CRs of vINSIST-infected rabbits 55
3.8.5. Statistical analysis 56
4. RESULTS 58
4.1. Ex. 1 - Location and identification of claustral neurons 59
4.2. Ex. 1 - Firing activity of claustral neurons during eyeblink conditioning 62
4.2.1. Type A: Activated neurons 64
4.2.2. Type B: Inhibited neurons 66
4.2.3. Type C: Non-related neurons 67
4.2.4. Number of type A, B, and C neurons during eyeblink conditioning and pseudoconditioning 68
4.2.5. Firing rate profiles and spike duration study 70
4.3. Ex. 1 - Changes in the firing rate of type A claustral neurons in relation to the development of conditioned responses (CRs) across conditioning 72
4.3.1. EMG area vs. integrated firing rate 73
4.3.2. Conditioned responses vs. latency of neuronal activation 74
4.4. Ex. 2 - Analysis of Local Field Potentials recorded in CL, mPFC, and MC during classical eyeblink conditioning 75
4.4.1. LFPs in the claustrum during eyeblink conditioning 77
4.4.2. Comparison of LFPs in CL, mPFC, and MC during eyeblink conditioning. 81
4.5. Ex. 3 - Effect of blocking claustrum output on the acquisition curve and on the EMG activity of the *orbicularis oculi* muscle during eyeblink conditioning 83
4.5.1. Effect of claustrum partial inhibition on the learning curve 84
4.5.2. Quantitative analysis of cumulative areas of the EMG 85
5. DISCUSSION 87
5.1. Ex. 1 - Location and identification of claustral neurons 88
5.1.1. Differences between claustrum and surrounding structures 88
5.2. Ex. 1 - Firing activity of claustral neurons 89
5.2.1. Basal firing activity of claustral neurons 89
5.2.2. Firing activity of claustral neurons during classical eyeblink conditioning.. 90
5.2.3. Why claustrum activity is not related to the kinematics of the CRs 91

5.3. Ex. 2 - Analysis of the Local Field Potentials recorded in CL, MC, and mPFC during classical eyeblink conditioning 92

5.3.1. Changes in LFPs recorded in claustrum across PHASE I, II, and III 92

5.3.2. Comparison of changes in LFPs recorded in CL, mPFC, and MC across PHASE I, II, and III 93

5.4. Ex. 3 - Blocking claustrum output delayed learning during classical eyeblink conditioning 94

5.5. The claustrum is involved in the cognitive aspect of the classical eyeblink conditioning 95

5.6. Limitations and future prospects 96

6. MAIN FINDINGS AND CONCLUSIONS 99

6.1. Ex. 1 – Claustrum cells are involved in the acquisition of the eyeblink conditioning 100

6.2. Ex. 2 – Local Field Potential oscillatory patterns are correlated in delta and low gamma bands in CL and mPFC, but not in MC, during eyeblink conditioning 100

6.3. Ex. 3 - Partial inhibition of claustrum output delays the acquisition of the conditioned responses (CRs) 101

7. REFERENCES 102

8. ANNEXES 125

8.1. The claustrum is involved in cognitive processes related to the classical conditioning of eyelid responses in behaving rabbits. 126

1. INTRODUCTION

1.1. The claustrum through the XX century

A century ago, the claustrum (CL) was described as a thin sheet of grey matter located between the insular cortex and the putamen (Landau, 1919). Since the original proposal of the CL as a structure involved in the integration of many different cortical and subcortical neural centers in order to generate conscious sensations (Crick, 1994), we have seen a notable increase in the number of structural and hodological studies dealing with its peculiar central place in the brain and regarding its putative integrative role in higher brain functions.

The CL has been identified in all mammals and recently —using a variety of techniques, including single-cell transcriptomics and viral tracing connectivity— a homologue of the CL has also been described in reptiles (Norimoto et al., 2020) and birds (Puelles et al., 2016). Consequently, the CL should be an ancient structure that was probably already present in the brain of the common vertebrate ancestor of reptiles, birds, and mammals.

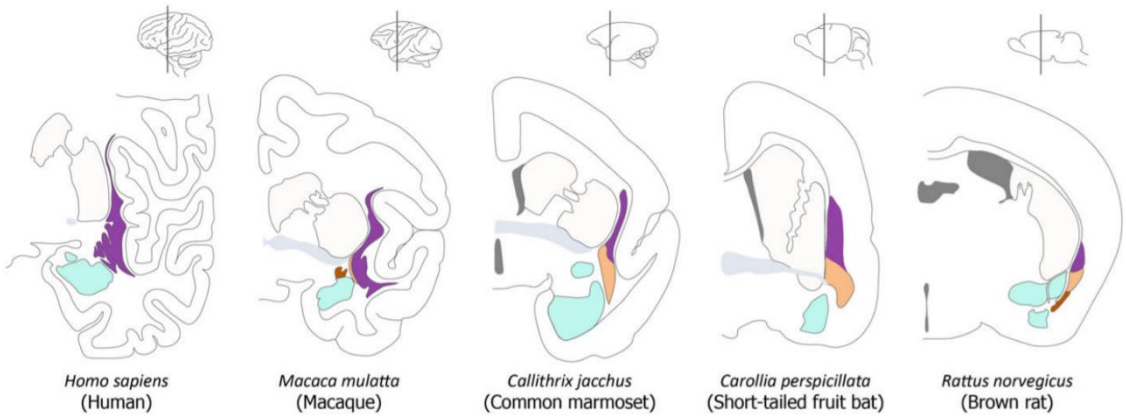

Figure 1.1. Coronal sections from brain atlases for human, macaque, marmoset, bat, and rat showing the delineation of the CL (purple), dorsal endopiriform nucleus (beige), ventral endopiriform nuclei (brown), amygdala (cyan), caudate-putamen (white), cortex (white), and anterior commissure (grey). Note the lack of endopiriform designation in human and the obscure location of the endopiriform nucleus in macaque compared with other species. Taken from Smith et al., 2018.

Throughout this section, the featuring characteristics regarding the physiology, anatomy, and connectivity of the CL, reported by many neuroscientists over the last 100 years, are going to be summarized and presented in order to give this dissertation an accurate scientific context.

1.1.1 Neuroanatomy

The CL is a telencephalic pallial subcortical structure hidden beneath the inner surface of the neocortex, between the insular cortex and the striatum (**Fig. 1.1**; Binks et al., 2019). In species in which it is well developed (e.g., cat, rabbit, and monkey), the CL is limited by the external capsule medially and the extreme capsule laterally. However, in some insectivores and other basal mammals (namely monotremes, *afrotheria*, and bats), the extreme capsule is poorly developed or absent, so that the CL cell population is scarcely distinguishable from the deep insular cortical layers (Kowiański et al., 1998; Puelles, 2014).

"Claustrum" often collectively refers to both "dorsal claustrum" (or *insular claustrum*) and a structure that is ventrally contiguous called "ventral claustrum" —otherwise known as the *endopiriform nucleus*— (Druga, 1966; Druga et al., 1990, 1993; Smith et al., 2018). Embryologically, the CL originates from the ventrolateral dorsal pallium, forming through the dorsal migratory stream from where it settles into the cortical subplate and then also expands into the lateral pallium (Smith et al., 2018; Bruguier et al., 2020). Here, we will use the term "claustrum" to refer to the "dorsal claustrum".

In contrast to those of the cerebral cortex, the CL has few neuronal types and an non-laminar, simple internal architecture. Two common cell types can be distinguished (**Fig. 1.2**).

The first have medium to large cell bodies, are spiny stellate or fusiform, and are the most common cell type (≈ 90%) (LeVay and Sherk, 1981; Braak and Braak, 1982; Druga, 2014). These spiny cells possess long, coarse axons, and they send and receive projections to and from the cerebral cortex —usually leaving the CL either laterally or medially— and rarely form synaptic connections with one another (Kim et al., 2016). They have varied soma shapes, including pyramidal, fusiform, and spherical, and their dendrites do not have a preferred orientation. They are glutamatergic (Real et al., 2006), and we will refer to them as *projecting neurons*.

CL neurons of the second type are small, granular, aspiny cells with axons forming dense local arborizations. Their axons do not leave the CL and they are GABAergic. Thus, they are *interneurons* whose activity generates the inner circuitry of the CL. These cells can be subdivided according to their intrinsic properties and histochemically by the

presence of different neuropeptides or calcium-binding proteins such as parvalbumin (PV), vasoactive intestinal peptide (VIP), somatostatin (SST), neuropeptide Y (NPY), and others (Graf et al., 2020; Marriott et al., 2020). Interneuron subtypes are differentially localized to the core and shell of the CL, with the core region most notably identified by intense neuropil staining for PV-positive cells (Real et al., 2016; Marriott et al., 2020).

As a matter of fact, CL cells express receptors for dopamine, acetylcholine, and serotonin (Rahman and Baizer, 2007; Norimoto et al., 2020; Terem et al, 2020), and they receive direct input from areas that are involved in wake–sleep control.

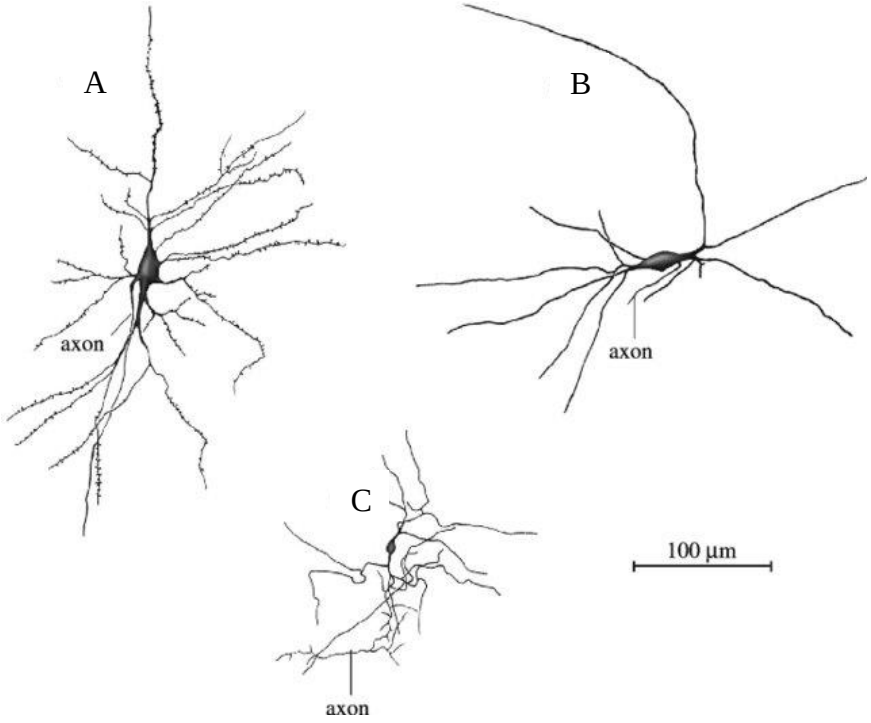

Figure 1.2. Neuronal cell types in the human CL as seen in Golgi preparations. ***A***, The dominant cell type (projecting neurons). This type both receives input from cortex and sends its axons back there. Its dendrites are covered with spines. ***B-C,*** At least two types of interneurons whose dendrites are lacking spines have been identified. Their axons do not leave the claustrum. Modified from Braak & Braak, 1982.

1.1.2. Connectivity

The CL is the most connected region per volume in the mammal brain (Milardi et al., 2013; Torgerson et al., 2015*;* Wang et al., 2017), ranging from rodents to primates.

It is generally accepted that the CL is highly interconnected with all the areas of the cortex (**Fig. 1.3**; Druga, 1968; Minciacchi et al.,1985; Crick and Koch, 2005; Mathur, 2014; Torgerson et al., 2015), including prefrontal, parietal, and visual cortices (Riche and Lanoir, 1978; LeVay and Sherk, 1981; Ungerleider et al., 1984; Druga et al., 1990; Reser et al., 2014; Gattass et al., 2014), as well as prelimbic and cingulate cortices (Smith and Alloway, 2010; Smith et al., 2012; White et al., 2017; Wang et al., 2017; Atlan et al., 2017). CL-cortical connections usually terminate in layer IV, and VI while cortico-CL projections arise predominantly from layer VI (Olson and Graybiel, 1980; LeVay and Sherk, 1981; LeVay, 1986). Nonetheless, the CL is not equally connected to all cortical areas (Alloway et al., 2009; Colechio and Alloway, 2009; Smith and Alloway, 2010) and although it does exist contralateral projection from CL to cortex, ipsilateral CL-cortical projection is generally stronger. Inversely, contralateral cortico-CL projections are denser than their ipsilateral counterparts (Olson and Graybiel, 1980; Colechio and Alloway, 2009; Mathur et al., 2009; Smith and Alloway, 2010). A general feature repeatedly described by these authors is that CL projections are topographically organized: the CL core projects predominantly to frontal-midline cortical regions, whereas the dorsal and ventral shell projects to the cortical motor system and temporal lobe, respectively (Marriott et al., 2020).

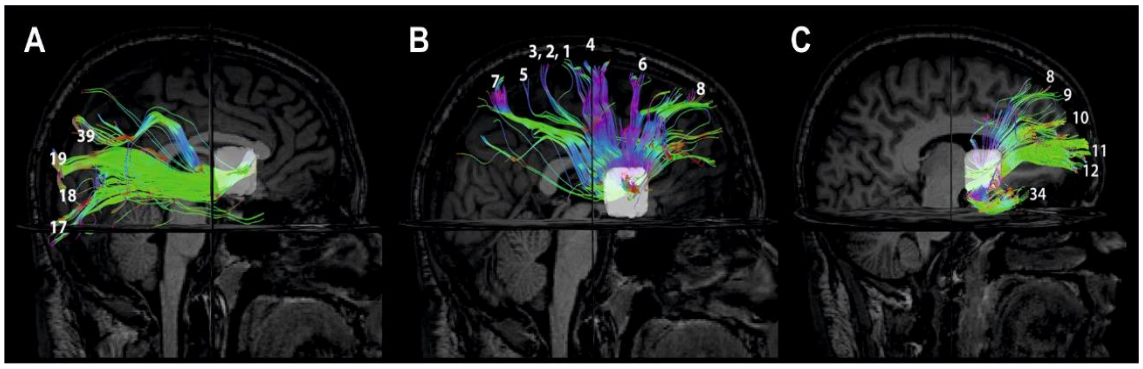

Figure 1.3. Cortico-claustral connections. Right sagittal view of the posterior (***A***), superior (***B***), and anterior (***C***) cortico-claustral pathways. The prevalent colour (green) indicates that the orientation of the fibers was antero-posterior. The right CL is represented by a white volume. Brodmann areas reached by the pathways are also indicated. Modified from Milardi et al., 2013.

In their recent experiments, Chia and colleagues (2020) showed that CL-anterior cingulate cortex (ACC) neurons co-labeled consistently with other frontal and limbic regions, but that the same CL-ACC population rarely co-labeled with sensorimotor regions. Therefore, they proposed that CL projection neurons have at least two distinct targeting systems: one to frontal cortex and one to sensorimotor cortex. Consistent with that, full re-constructions of single-cell neurons by Wang et al. (2019) support their conclusion: the population of claustral neurons projecting to frontal areas represents the CLA-I population described by Wang and colleagues, while the population of claustral neurons projecting to sensorimotor areas represents the CLA-II population of Wang.

Likewise, the CL is also widely connected to many subcortical structures (**Fig. 1.4**), mainly the thalamus, hypothalamus, striatum, amygdala, and caudate nucleus (Amaral and Cowan, 1980; LeVay and Sherk, 1981; Arikuni and Kubota, 1985; Jiménez-Castellanos and Reinoso-Suárez, 1985; Amaral and Insausti, 1992; Edelstein and Denaro, 2004; Fernández-Miranda et al, 2008; Zingg et al., 2018; Chia et al., 2020). Interestingly, in many of these experiments the retrogradely labeled somata in the CL formed a ring-like pattern around the body of the claustrum.

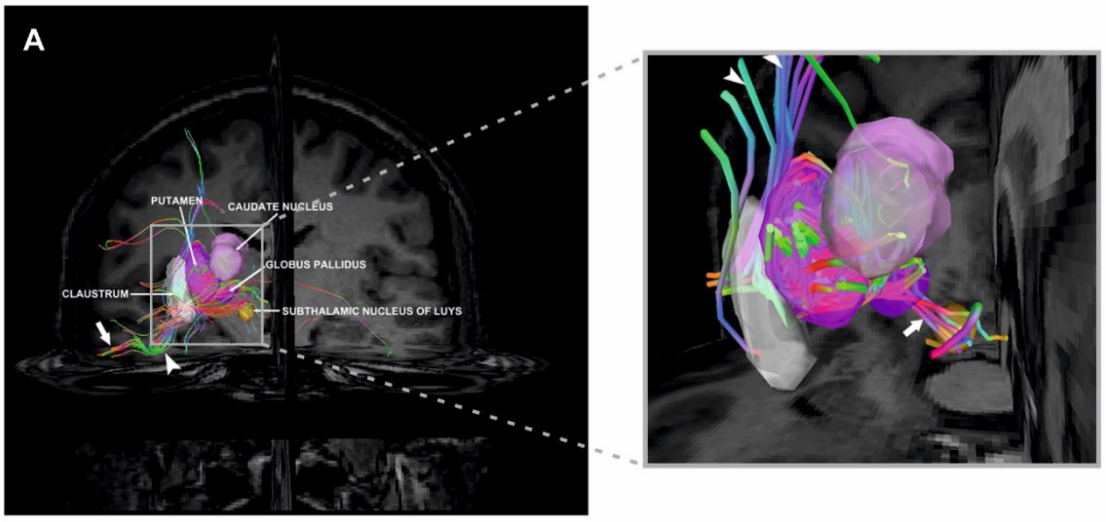

Figure 1.4. Subcortico-claustral connections. ***A***, Coronal view shows the pathway spreading between CL and basal ganglia. The fibers of the lateral pathway reaching the hippocampus (arrowhead) and the temporal cortex (arrow) can be clearly seen on the coronal view. An enlarged view focused on the medial pathway (grey square on the right) shows the close relationship between the fibers and the basal ganglia. Since the fibers spread in a complex 3D way, they appear green-, red-, and blue-colored in different segments accordingly to their main changing direction. In addition, fibers of the superior claustral pathway are visible (arrowheads) passing mainly through the *capsula externa*. Modified from Milardi et al., 2013.

The significance of a potential subcortico-CL connection has not yet been deeply studied, although there is evidence that the CL receives serotonergic innervation from the brainstem dorsal raphe nucleus (Rahman and Baizer, 2007) and from basal forebrain cholinergic centers, such as the *substantia innominate*.

According to the comprehensive classification of claustral neurons reported by Graf et al. (2020), claustral strongly-adapting (SA) neurons project to the cortex (Kim et al., 2016), while mildly-adapting (MA) neurons project to the subcortical structures. Real et al. (2006) suggested that the core of the CL may be connected with cortex, while the shell might be connected to subcortical sites, although Graf and colleagues did not describe such distribution in the SA and MA neurons described by themselves, and Marriott et al. (2020) reported CL shell neurons that do project to cortex, so this issue is not yet clear.

Excitatory CL afferences target mostly cortical interneurons and provide a robust feedforward inhibition (Kim et al., 2016; Atlan et al., 2018; Jackson et al., 2018; Narikiyo et al., 2020). Regarding cells projecting from cortex to CL, Kim et al. (2016) reported that cortico-CL afferences formed monosynaptic connections onto both CL-cortical projecting neurons and PV-positive interneurons.

Additionally, early in the 1960s, Carman et al. (1964) found that the connections to the neocortex are the largest source of claustral afferents. After Carman, Andersen (1968), Fallon and Moore (1978) and LeVay and Sherk (1981) also found that CL–cortical connections are greater than the CL's connections to subcortical regions.

With regard to the inner CL circuitry, several differentiated types of CL interneurons have been described (Kim et al., 2016; Graf et al., 2019, 2020): two of them, PV-positive and SST-positive, are likely to inhibit the projecting neurons (SA and MA), and the third, VIP-positive, might inhibit the other two interneurons. Marriott et al. (2020) indicated that CL inhibitory cells also show unique topographical distribution. CL interneurons (especially PV-positive cells) are highly interconnected to one another —with both electrical and chemical synapses— and also to projecting neurons (Kim et al., 2016).

This is interesting because its dense reciprocal connections to the rest of the brain give the CL a privileged position to act as a switching mechanism for information between areas involved in sensation, learning, and motor output.

1.1.3. Basal firing activity of the claustrum

It is commonly accepted that the CL has a low basal firing rate in awake resting animals (Spector et al., 1974; Olson and Graybiel, 1980; Shrek and LeVay, 1981; Remedios et al., 2010).

Spector, Hassmannova, and Albe-Fessard, in 1974, were among the first to report that the majority of claustral neurons either are silent until stimulated or have quite low basal firing rates in awake immobilized cats (Spector et al., 1974). Firing rates higher than 1 spike/s were observed in only 20% of claustral neurons, and cells with firing rates of over 10 spike/s were seldom observed even when excited. They also noticed that anterior CL neurons fired at higher rate and with shorter latency than posterior CL cells. Spector and colleagues also recorded in the cat CL during the presentation of visual, auditory, and somatic stimuli. According to their report, 31% of the analyzed CL cells did not respond to any of the stimuli, although most cells (69%) responded to all the tested sensory modalities in both subdivisions of the CL. Of the responding neurons, 75% changed their activity after presented with multimodal stimulation while 25% of them responded to single-modality stimuli. They also described the general pattern of CL discharge, recorded repeatedly after presenting a stimulus: a brief burst of activity (1-3 spikes) followed by a silent period.

Thirty years later, Chachich and Powell (2004) obtained similar results recording in rabbit CL. The claustral cells that they recorded also presented a low spontaneous firing rate, with frequencies under 10 Hz. The authors also presented the animals with visual, auditory, and somatic stimuli, and reported some 28% of neurons whose activity remained unchanged after any stimulus presentation and with a basal firing rate of over 3 Hz. Nevertheless, most of the recorded units (72%) did respond to one (36%) or various (36%) stimulus modalities, and neurons responding to all three stimuli (around 11%) exhibited the highest basal firing rate (≈ 8 Hz). In contrast to Spector et al. (1974), Chachich and Powell described single-firing patterns instead of bursts of activity.

A few years ago, Remedios et al. (2010) also supported the fact that the spontaneous firing rate in CL is quite low, and usually becomes activated only after the presentation of a sudden sensory stimulus in awake monkeys.

Jankowski and O'Mara (2015) reported in 2015 the result of their chronic single-cell recordings in anterior CL of freely-moving rats. In their electrophysiological

recordings of activity from almost 900 cells, they distinguished spatial-, object-, and boundary-responsive cells, and their basal firing rate was around 1 Hz. However, they also reported the presence of *fast-firing bursting neurons* (11%) that presented a much higher basal firing rate, between 20 and 30 Hz.

Regarding the activity of CL neurons during a different brain state, in the last few years a particular interest in studying the CL during sleep has arisen. Recently, Narikiyo et al. (2020) have reported that CL glutamatergic neurons' activity is related to the presence of neocortical slow wave (SW) activity. They saw that most CL neurons presented high firing rates during SW periods, reaching even 20 Hz, but in non-SW periods it is only 1 to 8 Hz —which is consistent with the information reported before for awake animals.

1.1.4. Putative functions of the claustrum

Because of the widespread claustro-cortical connections, early theories back in the 1980s regarding CL function, described the CL as a satellite of the cortex, having some regulatory role, or acting as a relay station (Olson and Graybiel, 1980; LeVay and Sherk, 1981). Nevertheless, in the last fifteen years, researchers agree that the CL is much more than a simple relay station. Since Francis Crick and Christof Koch's paper in 2005 (Crick and Koch, 2005) in which they suggested a possible role of the CL in multimodal integration and conscious experiences, the number of projects aimed at figuring out the enigmatic function of the CL has increased notably, and it is today a topic of interest among neuroscientists.

Lately, modern neuroscience tools and genetic and viral technology have become available in many laboratories around the world. Hence, new data about CL connectivity, anatomy, and physiological properties are being considered in order to elucidate its real function.

A number of reviews have proposed a role of the CL in the integration of multisensory information, perceptual binding, and internal functional states to generate cognitive-related processes (Ettlinger and Wilson, 1990; Edelstein and Denaro, 2004; Crick and Koch, 2005; Mathur, 2014; Goll et al., 2015; Citri and Barretta, 2016; Jackson et al., 2018). Other surveys assess that CL neurons are involved in very diverse tasks. Jankowski and O'Mara (2015) reported the presence of CL cells in rat anterior CL that

responded to the position of the animal in space, to boundaries enclosing the environment, and to the presence of objects in the environment. Also, Smythies et al. (2012) and Smith et al. (2012) suggested that the CL is important for coordinating motor behaviors involved in redirecting spatial attention and is involved in organizing and synchronizing cortical activity; in line with that, Smythies et al. (2012 and 2014) suggested that the claustrum can thus synchronize oscillations between distant cortical areas without the requirement for multimodal neurons. This coordination of cortical oscillatory activity was suggested to be involved in cognitive tasks.

Nevertheless, given the normally quiescent nature of CL cells that respond transiently to suddenly presented stimuli, and that the CL is most strongly connected with frontal areas, a role in directing executive, higher-order functions —such as segregation of attention (Mathur, 2014; Goll et al., 2015; Atlan et al., 2018) and salience processing (Smythies et al., 2012; Remedios et al., 2010, 2014; Chia et al., 2017; Smith et al., 2019)— has recently gained supporters.

Regarding the implication of the CL in salience detection, Chia et al. (2017) studied the insula-CL-ACC pathway in mice. The ACC and insular cortex (IC), two structures classically involved in the salience network (controlling attention and processing valence, respectively) are not directly connected (Medford and Critchley, 2010). Chia and colleagues showed that the CL, which has dense connections with both structures, might serve as a link between them. Therefore, the IC-CL-ACC pathway that they described may underlie the salience network. After them, recent studies from Smith et al. (2019) and Jackson et al. (2020) using resting-state fMRI to analyze CL functional connectivity support this hypothesis, both in rodents and in humans.

On the other hand, several behavioral surveys have revealed a clear role of the CL in attention and discrimination of relevant/irrelevant sensory events. According to White et al. (2018), the CL amplifies top-down information coming from the ACC for the purpose of cognitive control over actions; similarly, Atlan et al. (2018) showed that mice were more likely to be distracted by disruptive noise during a nose spoke task with a visual cue if the CL was inhibited; likewise, Fodoulian et al. (2020) demonstrated recently that specific ensembles of CL and of medial prefrontal cortex (mPFC) neurons are activated during a task requiring the ability to shift attention towards newly relevant

stimulus-reward associations while disengaging from irrelevant ones. These findings indicate that the CL filters out distractions and focusses attention on rewarding clues.

Furthermore, Terem et al. (2020) have recently shown that the CL plays a role in reward and reinforcement, and in incentive salience (i.e., an otherwise rather neutral cue acquires desirability). In this study, they found that the activity of the CL is necessary for the development of behavioral sensitization to cocaine, and the activity of $D1R^{+}$ claustral neurons is required for the appearance of cocaine-conditioned place preference; moreover, the optogenetic activation of these CL cells can drive the development of place preference.

In addition, the CL–PFC pathway regulates methamphetamine-induced impulsivity, suggesting a critical role of this neural pathway in regulating impulsivity-related disorders such as drug addiction (Liu et al., 2019). Morys et al. (1996) and Naqvi et al. (2007) also associated it to repetitive behaviors and addiction.

It is true that numerous surveys regarding the function of the CL in awake and/or behaving animals have been published since Cricks and Koch's paper in 2005, but the interest in what the CL is doing during sleep is relatively new.

In 2015, Renouard et al. (2015) were working on determining which cortical neurons remained active during sleep in rats. Combining FOS staining, retrograde labeling, and neurochemical lesions, they provided evidence that FOS overexpression occurring in the cortex during REM sleep is due to projections from the supramammillary nucleus and the CL. In agreement with that, Luppi and colleagues (2017) also reported that the CL is notably active during REM sleep; they stated that the CL was the only subcortical structure containing more FOS-positive neurons projecting to ACC and retrosplenial cortices after REM sleep than in the awake state.

Furthermore, these results suggest that tonic activation of limbic cortical neurons during REM sleep is moderately due to projections from glutamate neurons of the CL. The limbic structures activated during sleep (retrosplenial, medial entorhinal, and anterior cingulate cortices and the dentate gyrus) have all been implicated in spatial memory and learning, and it is therefore likely that such activation is crucial for memory consolidation.

Other recent studies have shown that stimulation of the CL activates inhibitory interneurons in the cortex in a particularly prominent way during periods of sleep or

quiescent wakefulness. Narikiyo et al. (2020) suggest that the CL coordinates SW activity generated by the neocortex during sleep and awake rest. In their study, Narikiyo and colleagues developed CL-specific transgenic tools in mice and showed that a population of CL excitatory neurons regulates SW activity over widespread cortical areas in a state-dependent manner by synchronizedly silencing the cortical neurons. Moreover, genetic ablation of CL neurons attenuated SW activity in the frontal cortex. Thus, they consider the CL output necessary for regulating cortical interneurons and enabling offline cognitive processing and propose it as a major subcortical hub for the synchronization of neocortical SW activity. Meanwhile, Norimoto et al., (2020) reported that a homologue of the CL also exists in reptiles and underlies the generation of sharp waves during SW sleep: the CL does not generate the sleep rhythm itself, but unilateral or bilateral lesions of the CL suppress the production of sharp-wave ripples during SW sleep unilaterally or bilaterally, respectively.

Even though it seems paradoxical that the CL may be involved in such different processes as sleep and attention or the salience network, it could participate in both through its ability to suppress cortical activity *via* strong feedforward inhibition. Also, it could play a role in memory consolidation of attention-related learning.

With all this said, it is easy to come to the conclusion that the CL may also be somehow implicated in associative learning, which certainly requires all the higher brain functions mentioned —including especially attention and salience detention— as well as the consolidation mechanisms that take place during sleep.

1.1.5. The claustrum in mental illness

Even though the CL is not the principal cause of any specific disorder, under- or overactivity of the CL has been reported in quite a few neurological diseases. For instance, almost all the above-mentioned functions are disturbed in autistic patients. It has been reported that autistic subjects present a reduced claustral volume, especially comparing autistic and control children. At older ages, the differences in mean volume diminish, which suggests that autistic infants suffer a late development of the CL. (Wegiel et al., 2014a). This observation is consistent with Davis' (2008) MRI studies of high-functioning (IQ 85) autistic and control males ranging from 7 to 12 years of age. The mean numerical density of neurons in the CL was almost identical in the autistic and control subjects. Nevertheless, a few important structures showed an increase in the total

number of neurons when comparing with control —PFC and IC— while others showed a diminution —fusiform gyrus and cerebellum. CL connectivity is also compromised in autism (Wegiel et al., 2014b). The imbalance between the number of cells in several brain structures, and the delayed development of CL cells and its projections, could be a cause of desynchronization over the brain, and contribute to the clinical manifestations of autism, such as cognitive impairment and altered processing of sensory signals, among others.

In regard to the alleged role of the CL in segregation of attention, it is of interest to ask whether Attention-Deficit/Hyperactivity Disorder (ADHD) subjects present affected CL, since these patients manifest an age-inappropriate level of hyperactivity, impulsivity, and incapability of attention. In fact, in resting state, ADHD patients show more brain activity than control subjects, with the basal ganglia, IC, precuneus, cingulate cortex (CC), thalamus, and cerebellum being especially affected (Wang at al., 2013). Indeed, Dickstein et al. (2006) and later Castellanos et al. (2008) reported that the CL is also abnormally overactive in subjects with ADHD, and Wang and colleagues (2013) found similar results, particularly in hyperactive and impulsive patients.

In bipolar disorder patients with first-episode mania, an increased left CL volume was found (Chen et al., 2012). In contraposition, patients with late-life depression presented reduced claustral volumes (Du et al., 2014; Bernstein et al., 2016).

Remarkably, Bernstein et al., (2016) showed that claustral volumes are bilaterally reduced in schizophrenia as well. Researchers (Cascella et al., 2011; Cascella and Sawa, 2014) using MRI scans in schizophrenic patients found negative correlations between the volume of grey matter in the CL and the severity of auditory hallucinations and delusions. Moreover, Shapleske et al. (2002) observed that patients with schizophrenia presented a white matter excess in the CL, especially among patients with predominance of hallucinations. In point of fact, in 1996 a girl who suffered temporarily bilateral lesion in the CL presented epileptic seizures, loss of vision, and psychotic behavior during that time (Sperner at el., 1996). More recently, Ishii et al. (2011) reported that a 21-year-old man diagnosed with an infection of mumps virus that resulted in bilateral claustrum lesions suffered visual and auditory hallucinations. Therefore, the disruption of the binding or synchronization of sensory, cognitive, and motor information due to a reduction of grey matter in the CL could contribute to positive symptoms of schizophrenia, such as hallucination and delusions (Patru and Reser, 2015).

Likewise, it is no surprise that some CL neurons experiment severe neurodegeneration in Alzheimer's disease patients (Morys et al., 1996; Venneri and Shanks, 2014); thus, the CL could be among the structures whose alteration generates its characteristic cognitive and memory dysfunction.

In the case of epilepsy, in 1996, Wada and Tsuchimochi (1996) tested the role of the primate CL in the convulsive evolution of the visual afferent and amygdaloid seizure and the specificity of the CL lesions effect. They concluded that anterior CL regulates the convulsive evolution of partial seizures originated from the limbic system. Since then, the CL has repeatedly been implicated in the generation and maintenance of seizures in kindling models in primates, cats, rats, and mice (Mohapel et al., 2000; Zhang et al., 2001; Meletti et al., 2015; Bayat et al., 2018; Kurada et al., 2019; Bickel and Parvizi, 2019). Mohapel et al. (2000) reported that small lesions in CL were effective in delaying, but not blocking, amygdaloid kindling. In the same direction, Zhang et al. (2001) suggested that the rapid rate of kindling from the anterior CL after electrical stimulation, and the strong connections with areas involved in generating seizures, are indicators that the CL is functionally close to the mechanisms of seizure generalization.

Very recently, Kurada et al. (2019) have reported alterations of consciousness resulting from electrical stimulation of the CL *via* a deep electrode in a woman with refractory focal epilepsy. Additionally, they indicated that some seizures induced by kainate injections showed an early involvement of the CL with later propagation to the hippocampi. However, a few months later, Bickel and Parvizi (2019) reported that no changes in patients' awareness were elicited after uni- or bilateral electrical perturbations in the CL; instead, their patients reported severe motor jerking, loss of tone, or strong somatosensory sensations. Thus, more research will be needed.

Either way, the CL could be an attractive new target for epilepsy therapy.

1.2. Specific characteristics of the rabbit claustrum

The previous section has shown that different species, ranging from humans to mice, have been used in the study of the CL (**Fig. 1.5**). Rodents are the most used despite the fact that their CL is small and is not well-separated from the cortex (Binks et al., 2019). Consequently, targeting the CL may be complicated, and single-unit recordings are difficult to attain.

CL volume increases with the size of cerebral hemispheres (Kowiański et al., 1999), thus the CL of rabbits and guinea pigs is more favorable for this kind of experiment, because of its larger volume. Compared with that of mice (**Fig. 1.5*B***), the rabbit CL (**Fig. 1.5*E***) is a prominent structure that is seven times larger in volume than the CL of mice. Furthermore, the rabbit CL is distinctly separated from surrounding structures (i.e., the insular cortex and the putamen) by the fibers of well-developed external and extreme capsules (Girgis and Shih-Chang, 1981; Kowiański et al., 1999). These advantages facilitate targeting the CL during *in vivo* recordings, such as those performed here. In addition, although CL volume and shape vary across species, vast connectivity with the cortex seems to be a well-conserved characteristic of the CL in monkeys (Druga et al., 1990), cats (Druga, 1982), mice (Atlan et al., 2017), rats (Majak et al., 2000), and rabbits (Kowiański et al.,1998, 2000).

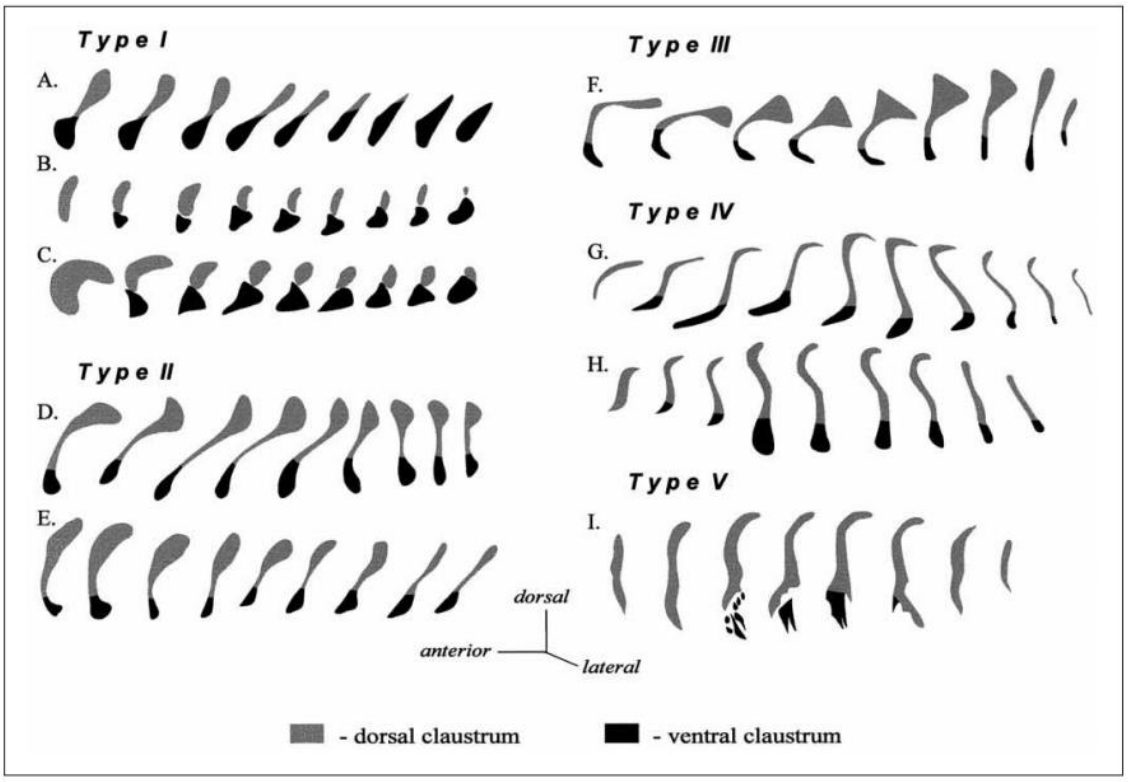

Figure 1.5. The schematic transverse sections of the CL (from rostral to caudal) representing the five morphological types of CL (based on differences in volume, shape, and degree of separation from surrounding structures) appearing in the species examined. **A**, Sorex; **B**, mouse; **C**, rat; **D**, guinea pig; **E**, rabbit; **F**, cat; **G**, macaque; **H**, *cercopithecus*; **I**, human. Taken from Kowiański et al., 1999.

Although it is not an extended practice, rabbits have previously been successfully used to assess a putative implication of the CL in associative learning (Chachich and Powell, 2004).

1.3. Learning and memory, or how brain adapts behavior to changes

In Cognitive Neuroscience, the terms "learning" and "memory" are so close that usually they could be interchanged, and one would not exist without the other. Today, learning and memory processes are one of the most studied subjects, and researchers use extremely diverse techniques and models to determine the neural functions underlying them. Therefore, many different definitions have previously been used to characterize these concepts. Nevertheless, most neuroscientists agree on the statement that learning is the mechanism by which the nervous system adapts to environmental changes by developing appropriate and suitable new behaviors, while memory could be defined as the preprocess that allows the encoding, storage, and retrieval of this information, to be used in the future (Kandel et al., 2000).

During actual learning, neural information needs to be encoded and stored properly in order to be retrieved through memory processes the next time it is needed. Also, it seems clear that memory cannot be defined as a single skill, but as several processes covering different stages of the task. These processes, coordinated and working together, generate the capability called "memory" (Tulving, 1985; Schacter, 1987; Squire, 1987).

In terms of the different systems of memory storage, the Atkinson-Shiffrin theory (**Table 1.1**; Atkinson and Shiffrin, 1968) is widely accepted. Their model established that memory can be classified according to two considerations: the time of storage coursed, and the nature of the information stored.

Table 1.1. Types of memory according to the Atkinson-Shiffrin theory.

Sensory memory (< 1 s)	The ability to retain impressions of sensory information after the original stimuli have ended.
Short-term memory (< 1 min)	Cognitive system used for holding sensory events, concepts, or items for brief period of time. It can be selectively transferred to long-term memory. *Working memory* is a discussed subtype of short-term memory to briefly retain relevant knowledge for a specific goal (Baddeley and Hitch, 1974).

<table>
<tr><td rowspan="6">Long-term memory
(days to years)</td><td rowspan="2">Declarative / Explicit

Conscious form of recovering early experiences and remembering information about places, people, or things.</td><td>Episodic: Events.</td></tr>
<tr><td>Semantic: Ideas, concepts, words.</td></tr>
<tr><td rowspan="4">Non-declarative / Implicit

Unconsciously acquired knowledge or ability manifested in an automatic manner.</td><td>Procedural: skill learning.</td></tr>
<tr><td>Perceptual: priming learning.</td></tr>
<tr><td>Associative: To learn about the association between two stimuli.</td></tr>
<tr><td>Non-Associative: To learn about the properties of a single stimulus.</td></tr>
</table>

As reflected above, the numerous processes that we call “memory” can be divided into different types, although the limits between these subtypes are usually unclear and can generate controversy among scientists. Even so, it is likely that every one of the subtypes could be supported by different brain structures and circuits. For example, the different types of long-term memory are assumed to be stored in different brain structures and undergo different functional processes (Zola-Morgan and Squire, 1993).

Briefly, explicit memories (e.g., the date of your wedding day) are thought to be encoded by the medial temporal lobe (hippocampal and rhinal cortices) but are consolidated and stored in the temporal cortex and elsewhere. On the other hand, implicit memories, such as procedural learning (e.g., riding a bike), that requires motor control, could recruit the activity from cerebellum, putamen, caudate nucleus, and motor cortex (MC), besides hippocampus. It is assumed that cerebellum is involved in timing and coordination of body skills, but they are likely to be stored in the putamen. Instinctive behaviors, such as grooming, are stored in the caudate nucleus. However, there is a lot to discover in order to be able to draw the whole map of brain structures involved in every kind of memory. While a molecular approach can be useful to figure out the principles underlying learning and memory, behaving animals may be the most challenging and helpful option to study those processes under physiological conditions.

The present dissertation focuses specifically on associative learning, one type of implicit, long-term memory.

1.3.1. Associative learning

Associative learning is defined as the development of a relationship between two stimuli, or between a stimulus and a behavior. As summarized in **Table 1.1**, it is a type of implicit or non-declarative memory (because it is a knowledge or skill learned unconsciously) and it requires long-term memory procedures. In contrast to non-associative learning (i.e., single or repeated presentations of one type of stimulus; it comprises sensitization and habituation), associative learning is dependent on the timing of the two stimuli, and is based on the assumption that experiences reinforce one another and can be linked to enhance the learning process.

Two main forms of associative learning have been widely studied in the past, and are still today frequent in many laboratories (Schacter and Wagner, 2013):

(1) *Classical conditioning* entails learning the relationship between two stimuli. This kind of learning involves involuntary behaviors as a response to the conditioned stimulus, such as salivating in front of a picture of candy. The responses driven by this type of learning are not chosen, as they are reflexes.

(2) *Operant conditioning*, or instrumental conditioning, involves associating a specific action or behavior with a reinforcing or penalizing outcome. Even though acquiring this learning (as well as the other types of associative learning) is unconscious, it implies the voluntary choice of repeating a reinforcing behavior (such as opening the biscuit jar) or avoiding a penalizing one (such as touching a hot pan).

Another kind of associative learning derived from the other two is the *Vicarious conditioning* or observational learning (Carlier and Jamon, 2006; Burke et al., 2010; Jurado-Parras et al., 2012). It implies that the subject (or *observer*) learns by watching others (*models*) to acquire conditioned responses. An example could be a child learning to say “please” or “thank you” because it has been rewarding to his older sibling.

Until now, only a few laboratories have considered the involvement of the CL in associative learning. In 1965, Chorazyna, Stepien, and Sychowa (as cited in Spector et al., 1974) realized that during an auditory discrimination task in dogs, the ability to differentiate two tones was not altered by the ablation of the auditory cortex, although this task was irrevocably impaired when both CL and auditory cortex were ablated. Later, in 1972, Kalashnikova (1972) found that CL ablation in cats abolished the conditioned

alimentary response. Additionally, they reported that electrical stimulation of the CL inhibited the conditioned alimentary response, and this inhibition could be complete or have different components depending on the time when the CL was stimulated. A few years ago, Chachich and Powell (2004) related the CL to the Pavlovian heart-rate conditioning in rabbits. They reported that CL cells were more active when presented with a previously reinforced tone than to a non-reinforced tone. Moreover, they found that CL lesions attenuated the bradycardic response evoked by the tone reinforced by a periorbital shock. Lastly, Bayat et al. (2018) reported that deep brain stimulation in rat CL interfered with operant conditioning performance.

Even though they provided future generations with extremely valuable information, and a lead to follow in the study of the CL as an important missed piece in associative learning, they were not able to evaluate the activity of CL cells *during* the learning, so *when*, *which neurons*, and *with what specific purpose* these CL neurons fire are still unsolved questions. Here, we tried to assess the activity of CL neurons during the learning of a classical conditioning task.

1.3.2. Classical (or Pavlovian) conditioning

The classical conditioning is one of the simplest forms of learning, thus it has been truly useful to address the physiological mechanisms that underlie learning and memory processes.

It was first described in 1903 by Ivan Petrovich Pavlov, a Russian physiologist and psychologist who dedicated his scientific career to the study of the fundaments of the digestive system of dogs. Such were his findings in the physiology of digestion that he was awarded the Nobel Prize in Physiology and Medicine in 1904. In his physiological studies, Pavlov developed a procedure to collect and measure the amount of gastric secretions and saliva produced under different experimental situations called fistulae. He and his colleagues realized that gastric secretions were produced spontaneously —as a reflex response— when dogs were presented with food powder. Moreover, they also noticed that dogs drooled with the presence of the person who usually fed them, even when that person did not carry any food, so they hypothesized that dogs had associated those two stimuli that were usually presented together in time.

This observation led Pavlov to design his universally known experiment, comprehensively studied in psychology (**Fig. 1.6**): the presentation of an unconditioned stimulus (US, food) evoked a reflex response (i.e., salivation); this innate response is called unconditioned response (UR). In contrast, animals did not salivate when presented with a neutral stimulus (NS), such as a tuning fork sound. Nevertheless, when the neutral sound was presenting right before the food again and again, the dogs associated the sound with the food; therefore, eventually, the animals began to salivate merely with the tuning fork sound. The sound became a conditioned stimulus (CS), and the salivation a conditioned response (CR) (Pavlov, 1927). Usually, UR and CR are similar but not identical (i.e., in composition, duration, and/or magnitude) (Trigo et al., 1999; Gruart et al., 2000a).

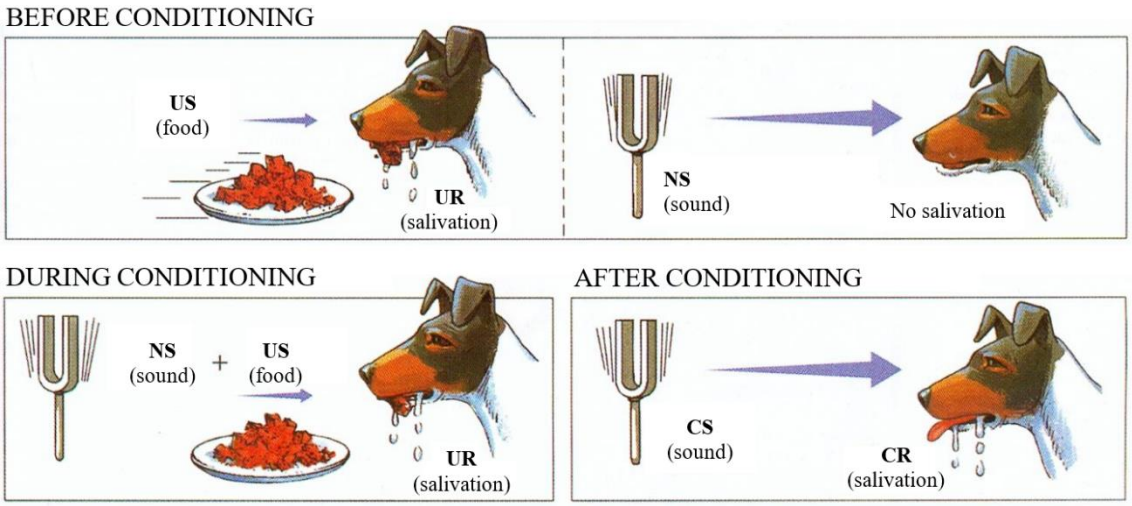

Figure 1.6. Description of Pavlov's classical conditioning paradigm. Dogs were taken into the training room and were prepared for the collection and quantification of saliva. *Before conditioning*, animals salivated as a reflexed, unconditioned response (UR) when presented with food, the unconditioned stimulus (US), whereas they remained quiescent (no salivation) when presented with a neutral stimulus (NS), a tuning fork sound. *During conditioning*, Pavlov repeatedly delivered the US (the food) right after presenting the NS (the tuning fork sound), which also produced the UR (salivation). Finally, *after conditioning*, the sound of the tuning fork itself was able to produce salivation, so it became a conditioned stimulus (CS) and salivation turned into a conditioned response (CR).

Since Pavlov's paradigm, several forms of classical conditioning have been developed and used in cognitive science aiming to cement the basis of associative learning in behaving animals. CS and US can be of a great variety. Some famous experimental procedures of classical conditioning include fear conditioning (which involves learning

that certain environmental stimuli predict aversive events; Watson and Rayner, 1920; Maren, 2001), taste aversion learning (in which animals appear to be innately predisposed to avoid eating food that caused illness in the past; Gaston, 1978; Logue, 1979; Welzl et al., 2001), or the heart-rate conditioning mentioned before (where animals present conditioned bradycardia as a response to the CS when the US is aversive; Kapp et al., 1979; Cohen and Randall, 1984; Chachich and Powell, 2004), among many others.

Even though there is a vast variety of paradigms, most classical conditioning models present different stages during training, as in Pavlov's experiment (1904). Authors may differ regarding the terms for each phase (Black and Prokasy, 1972; Rescola and Wagner, 1972; Lattal and Lattal, 2012; Fernández-Lamo et al., 2018), but it is commonly accepted that conditioning takes place following these stages:

i) Phase I, *pre-learning*. In this stage, the training has not even started, or repetitions of the paired NS and US are not enough to produce a CR (i.e., the NS does not trigger a response because it is not associated to the US yet).
ii) Phase II, *acquisition*. This is the process when the NS gradually pairs with the US —becoming the CS— and the first CRs appear. During the acquisition phase, small CRs start appearing, and their number and magnitude increase with the training, until reaching asymptotic values. Usually, it takes several repetitions to achieve the learning, although this process can be very different across different tasks: in some kinds of learning, especially aversive ones, the association between the NS and US is so fast that a single NS/US presentation is enough to generate a CR.
iii) Phase III, *after learning*. By this time, the learning has been achieved. The NS has become the CS, then most times its presentation produces large CRs. The number of CRs reaches asymptotic values, therefore learning has finished, even if training keeps on.
iv) *Extinction*. Although it is not a learning phase *per se*, extinction is an important process. Once learning is achieved, if the CS is repeatedly presented unpaired with the US, the CS will gradually stop eliciting a CR. Hence, the association between the CS and US will eventually be revoked, and the CS will become neutral again.

In the present study, we have recorded the activity of claustral neurons during the three main phases of the classical conditioning of the eyelid response.

1.3.3. Classical conditioning of the eyelid response

The conditioning of the eyelid reflex, commonly known as eyeblink conditioning, is a well-known experimental procedure for studying the neural basis of associative learning in mammals (Thompson, 2005). Eyeblink paradigms in awake experimental animal became popular during the 1960s (Gormezano et al., 1962), although they were being used in human scientific investigations from the early 1920s. Since the 1960s, the classical eyeblink conditioning has been extensively used by multiple researchers as a satisfactory experimental animal model for the investigation of neuronal mechanisms and pathways underlying the acquisition of new somatomotor capabilities (Gormezano et al., 1962, 1983; Woody et al., 1970; Gruart et al., 2000a; Medina et al., 2002; Márquez-Ruiz et al., 2012, 2016; Pacheco-Calderón et al., 2012; Carretero-Guillén et al., 2015; Ammann et al., 2016).

Delay and trace paradigms (**Fig. 1.7**), and the principal structures involved in them, are quite well established. Delay conditioning refers to a type of classical or Pavlovian conditioning in which the onset of the NS (usually a tone; from now on, to simplify, we will call the NS, *CS*, even in the pre-learning phase) is followed repeatedly with the onset of an eliciting stimulus (usually a weak air puff in the eye, the US); the CS and US co-terminate (**Fig. 1.7*C***). After several CS/US presentations, animals begin to present a conditioned or learned response (CR) following the CS, which typically mimics the response spontaneously produced later by the US, the unconditioned response (UR) —namely, an eyeblink. Even though there is a variety of stimuli eligible to use as CS and US (flashlights, electric shocks), the combination of a tone as CS and an air puff as US seems to be the one with best results, and the optimal interval for the acquisition of delay conditioning is between 200 and 400 ms (Thompson, 1988).

In contrast, during trace conditioning, the onset of the CS and US are separated by a blank time interval, so that the subject must hold the memory for the CS during the "trace" period before the US is presented. This gap is usually within 0.1 to 0.5 s; longer intervals might produce a failure in the acquisition of the CR. Normally, the trace paradigm is more difficult to learn than the delay because CS and US do not overlap in time (Christian and Thompson, 2003; Oswald et al, 2008).

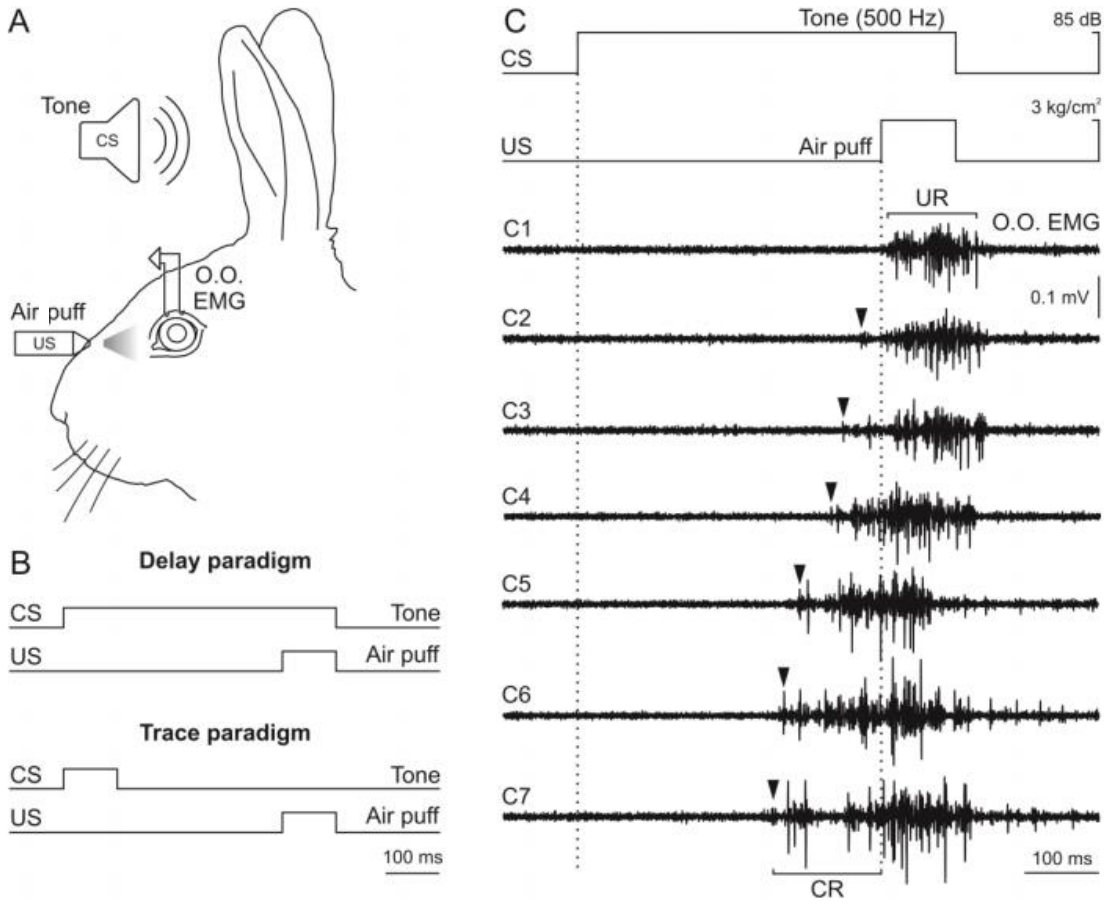

Figure 1.7. Description of eyeblink conditioning paradigms. ***A***, Experimental design of eyeblink conditioning in rabbits: a tone (as CS) is followed by an air puff aimed at the left cornea (as US) while the electromyographic activity of the *orbicularis oculi* (O.O. EMG) provides information about the eyelid position. ***B***, Schematic representation of the CS and US during delay and trace paradigms. Notice that in delay paradigm, CS and US coexist for a brief period, and co-terminate, whereas in trace paradigm a silent period separates CS and US. ***C***, Development of the CRs across conditioning sessions during a delay paradigm: under the representation of the conditioning stimuli (CS and US) can be seen an example of the electromyographic activity from seven consecutive conditioning sessions (C1-C7). Black arrows point to the onset of the CRs, which grow bigger across sessions; URs remain practically unchanged. Modified from Cheron et al., 2013.

Eye movements (CRs and URs) can be measured and quantified using different methods: the search-coil technique (Gruart et al., 1995), with Hall-effect devices (Koekkoek et al., 2002), or by means of the electromyographic (EMG) activity of the *orbicularis oculi* (O.O.) muscle ipsilateral to the US presentation (Márquez-Ruiz et al., 2012; Ammann et al., 2016).

It was commonly accepted that classical eyeblink conditioning requires the participation of the cerebellum during delay paradigms, or the hippocampus during trace

paradigms, as exclusive structures (Thompson, 2005; Gerwig et al., 2007; Green and Arenos, 2007; Thompson and Steinmetz, 2009). Nevertheless, several studies carried out during the last few years concluded that this is a dated notion and a simplistic model, since multiple brain regions have been successfully proved to be involved in the proper performance, acquisition, storage, or retrieval of conditioned eyeblinks.

Regarding delay paradigms, it is undeniable that an essential part of this learning —namely the acquisition and storage— takes place in the cerebellum (Krupa et al., 1993; Christian and Thompson, 2003, 2005; Ten Brinke et al., 2017), or at least that the timed performance of the acquired responses (Welsh and Harvey, 1991; Sánchez-Campusano et al., 2007) and its retention (Christian and Thompson, 2005) do so.

Delgado-García and colleagues (Gruart and Delgado-García, 1994; Gruart et al., 2000b; Delgado-García and Gruart, 2002, 2005) used the search-coil technique to measure the movement and position of the eyelid (instead of the passive movement of the nictitate membrane, as had been done before). They found that the anterior interpositus nucleus of the cerebellum of the cat (previously considered necessary for acquisition, retention, and generation of the CRs; Chapman et al., 1990; Nicholson and Freeman, 2002; Christian and Thompson, 2005; Green and Arenos, 2007; Halverson et al., 2010) starts its firing *with* the onset of the UR and the CR, rather than *before* it —thus interpositus cannot be the site of generation of the CRs. Instead, they suggest that interpositus may be involved in the proper timing and the correct performance of the CRs.

With regard to trace conditioning, it is especially related to cortical structures (Clark et al., 1984; Takehara-Nishiuchi et al., 2005; Gruart et al., 2006; Oswald et al., 2009). It is understood that the hippocampus is involved in the acquisition of conditioned eyeblinks, since apparently this requires hippocampal-dependent declarative memory (Berger et al., 1983; Thompson, 2005). In this regard, Solomon et al. (1986) reported that large bilateral hippocampal lesions performed before training prevented trace conditioning CRs but not delay CRs; also, if hippocampal lesions were made immediately after learning, trace CRs were abolished, while delay CRs prevailed. Surprisingly, later in 1995, Kim et al. (1995) produced hippocampal lesions a month after trace conditioning and the CRs remained intact.

Nonetheless, the activity of hippocampal pyramidal neurons is related to the salience of CS presentations across training and/or to the increasing CS/US associative strength (Rescorla, 1988; Múnera et al., 2001) in both trace and delay paradigms, but not

to the biomechanics of eyelid CRs, a coding property ascribed to the rostral CC (Weible et al., 2003; Hattori et al., 2014).

All these investigations generated a still ongoing debate. Yet authors agreed that the neural correlates of the learning of conditioned eye movements could be dependent on the functional activity of multiple brain structures.

For example, MC pyramidal neurons fire well in advance of CR initiation (Aou et al., 1992; Ammann et al., 2016) in delay training. Moreover, electrical stimulation of the eyelid primary motor area (M1) evoked motor responses with profiles and kinematics similar to those of CRs during classical conditioning (Ammann et al., 2016). Other cortical structures have been implicated in non-motor, cognitive components of the acquisition, storage, and retrieval of eyelid CRs. Likewise, specific areas of the mPFC have been proposed to participate in proper determination of CS/US time intervals (Siegel and Mauk, 2013; Caro-Martín et al., 2015) and in partial reinforcement (Powell et al., 2005). The mPFC also plays a permissive role in the initial release of eyelid CRs because electrical stimulation of mPFC prevents the expression of CRs, but not CR acquisition (Leal-Campanario et al., 2007, 2013).

Many more structures have also been proved to be involved somehow in the generation and/or expression of conditioned eye blinks, both cortical —namely, the cingulate (Weible et al., 2003) and somatosensory cortices (Leal-Campanario et al., 2006; Ward et al., 2012) and neuronal premotor networks (Morcuende et al., 2002)— and subcortical structures —such as the striatum (Blázquez et al., 2002), the amygdalar complex (Boele et al., 2010; Sakamoto and Endo, 2010), some thalamic nuclei (Sears et al., 1996; Bahro et al., 1999; Campolattaro et al., 2007), and the red nucleus (Haley et al., 1988; Sakamoto and Endo, 2010; Pacheco-Calderón et al., 2012).

Several authors (Alexander et al., 1991; Powell et al., 1991; Powell, 1999; Weiss & Disterhoft, 1996) even suggested that there is a standard pathway for the simplest types of the associative learning of the eyeblink reflex (such as delay paradigm), and when a task requires heavier cognitive loads (such as trace paradigm), a complementary circuitry (probably involving hippocampus, mediodorsal thalamic nuclei, PFC, and amygdala among others, depending on the specific task) is used to deliver precise responses to more challenging trainings.

1.3.4. Why could the claustrum play a role in eyeblink conditioning?

Taken together, the previously described experimental studies indicate that to generate a conditioned eyelid response, many sensory and motor structures, as well as functional circuits, need to be activated, even for the simpler forms of learning. Only then would it be possible to obtain the required movement, with the appropriate kinematics as well as the correct timing. Here, we hypothesize that the CL could be one of those structures.

Given the dense reciprocal connections between the CL and many of the cortical structures described above, and its demonstrated involvement in salience detection and attention (Chia et al., 2017; Atlan et al., 2018), CL neurons could also play an important role in motor and/or non-motor functions involved in classical eyeblink conditioning. Furthermore, it has been reported that CL neurons respond to numerous sensory stimuli (Spector et al., 1974; Olson and Graybiel, 1980; Shrek and LeVay, 1981; Chachich and Powell, 2004; Remedios et al., 2010), a crucial requirement for this specific type of associative learning.

Eyeblink conditioning was used as the learning task in order to study the involvement of the CL in associative learning for several reasons:

i) It is a simple and well-studied form of learning.
ii) To learn the relationship between an auditory stimulus and a somatosensorial one requires multisensory integration. Additionally, attention and salience detention, processes tightly associated to the CL, are also challenged to perform properly.
iii) The set-up allows the head-immobilization needed for the extracellular *in vivo* recording.
iv) Using a weak air puff as a US (rather than an electric shock; Chachich and Powell, 2004) makes it possible to record during all the conditioning phases while avoiding electrical noise. Also, it is less aversive, so animals are more relaxed during the sessions (Rescorla and Wagner, 1972).

Besides bigger CLs, other advantages of using the rabbit as a model for eyeblink conditioning experiments are their high tolerance for movement restriction, the absence of eyelid reflex response to the tone used as CS (Grant and Adams, 1944; Gruart et al., 2000a), and easy acquisition of eyelid responses compared with other smaller animals such as rodents. Previous research has established that the integral of the rectified EMG

activity of the O.O. muscle can precisely determine eyelid position (Gruart et al., 1995; Schade Powers et al., 2010). Therefore, implanting a recording electrode in the O.O. muscle, we could ascertain whether animals closed the eye due to CS presentations (i.e., as a CR), or to US presentations (i.e., as a UR), and monitor the learning process (Gruart et al., 2000a; Leal-Campanario et al., 2007). However, there are eyeblink conditioning paradigms designed for use in other animal models, and they have proved to be successful in cats (Norman et al., 1974; Gruart et al., 1994), rats (Schmajuk and Christiansen, 1990; Stanton et al., 1992), and mice (Aiba et al., 1994; Chen et al., 1996; Heiney et al., 2014) among others.

Furthermore, as previously mentioned, a few laboratories have already reported alterations in the proper performance or execution of an associative learning in relation to variations in the claustral functions; therefore, we are positive that the CL could be active during eyeblink conditioning, even in the simplest training. To prove that, and for the reasons described above, here we examine the extracellular unitary activity of CL neurons using glass micropipettes during different learning phases of classical eyeblink conditioning in rabbits using a simple delay paradigm.

1.4. Claustrum and eyeblink conditioning: cortical structures under study

The CL is a small, thin group of cells; recording within it without invading surrounding structures —i.e., IC and striatum— can be a challenging task. Because of this, during the extracellular recording performed here, induced activity from CL-projecting cortices was used to verify that the activity recorded was generated by CL cells.

As comprehensively described in previous sections, a large and growing body of literature has investigated the connections from CL to the rest of the brain and vice-versa. Its connections reach nearly every single corner of the brain cortex, and a good part of the subcortical structures. The following cortical areas have been chosen from among the others for two main reason:

i) there is a vast literature about their strong, reciprocal connections with the CL;
ii) they have all been proved to be involved in modulating the proper acquisition, generation, and/or retrieval of classically conditioned eyeblink responses.

1.4.1. Medial prefrontal cortex, Brodmann area 32

The PFC is known for being involved in the proper timing, representation, selection, and execution of intentional behaviors and in a set of cognitive processes such as anticipation, choice of objectives, planning, behavior selection, self-regulation, self-control, and feedback (Damasio, 1994; Fuster, 1997; 2001; Kolb and Whishaw, 1999).

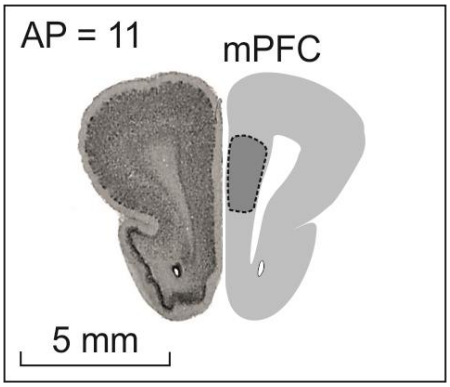

Figure 1.8. Diagram showing the location of mPFC in the rabbit brain. The left hemisphere is a coronal section (AP = 11) taken from "Brain atlas of the domestic rabbit" (http://neurosciencelibrary.org/), while the right hemisphere shows a drawing from the same slice (mPFC is indicated by the grey dotted area).

There are many published studies (Chachich and Powell, 2004; Goll et al., 2015; Wang et al 2017; Jackson et al., 2018) that describe how the CL is bidirectionally connected to PFC.

In 1984, Buchanan et al. found in rabbits that the CL is activated when the mPFC is stimulated using 3H-2 deoxyglucose autoradiography. They also reported that mPFC stimulation produced greater activity in the ipsilateral CL than in the contralateral CL. Later, Minciacchi et al. (1985) and Chachich and Powell (2004) obtained the same results. Besides that, Buchanan and colleagues realized that relative optical density was higher in the anterior CL and gradually decreased into the posterior CL. A similar topographical organization in the projections from PFC to CL was described later by Kowiański et al. (1998) using retrograde fluorescent tracers. Kowiański and colleagues also reported that CL-cortical projections in rabbits were similar to those in other animal models.

Very recently, Fodoulian et al. (2020) found that the CL-mPFC network is activated during a task requiring cognitive control such as attentional set-shifting.

Publications regarding the role of Brodmann area 32 (namely, mPFC or prelimbic area) in eyeblink conditioning are also numerous, in both trace and delay paradigms. Most of the published works in rabbits, rats, and mice agree on that mPFC participates in the retrieval of information from a permanent memory store, rather than its acquisition or encoding, in this somatomotor conditioning. Powell et al. in 2001, induced lesions in

rabbits mPFC before the eyeblink conditioning training and found no effect on the acquisition of the conditioned eyeblinks, whereas damage after acquisition produced a deficit in the performance of the learning respons. Simon et al., in 2005 and Oswald et al., in 2008, reported similar results when inducing lesions in Brodmann area 32: post-training lesions produced a deficit in conditioned eyeblink performance, especially during the first day of retraining, but those lesions did not disrupt the ability to relearn the task.

Leal-Campanario et al. (2007) was able to substantially inhibit both the CRs and URs by stimulating rostro-medial PFC during a delay eyeblink conditioning, probably producing freezing behavior. Surprisingly, even though the performance of the conditioned and unconditioned eyeblinks was lessened, acquisition of the learning was not affected, since once prefrontal stimulation stopped, animals showed a nearly normal learning curve.

With all these reports, it has conclusively been shown that mPFC is involved in the proper development of eyeblink conditioning.

1.4.2. Motor cortex, M1

The CL has connections with the motor cortices in both hemispheres (Minciacchi et al., 1985; Sloniewski et al., 1986, Alloway et al., 2009; Smith and Alloway, 2010), in accordance with its role in coordinating neural processes in separate cortical areas.

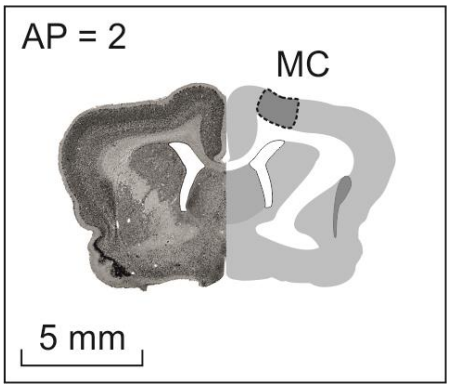

Figure 1.9. Diagram showing the location of MC in the rabbit brain. The left hemisphere is a coronal section (AP = 2) taken from "Brain atlas of the domestic rabbit" (http://neurosciencelibrary.org/), while the right hemisphere shows a drawing from the same slice (MC is indicated by the grey dotted area). CL is represented in dark grey.

In each hemisphere, the M1 whisker regions are directly interconnected by dense sets of axons that project through the corpus callosum (Donoghue and Parham, 1983; Reep et al., 1987; Miyashita et al., 1994). The afferences and efferences with the CL provide another route, probably monosynaptic, that complements the direct connections between M1 in each hemisphere *via* the corpus callosum. It has been proved that rat CL receives bilateral projection from M1, but contralateral projection is more prominent

(Alloway et al., 2009; Smith and Alloway, 2010). In contrast, rat CL efferences project to the ipsilateral motor region and do not project to the contralateral hemisphere (Colechio and Alloway, 2009).

By including an intervening synapse along this CL-MC route, the CL might be able to integrate cortical information from the ipsilateral hemisphere with information received from the MI in the contralateral hemisphere (Smith and Alloway, 2010).

The MC has traditionally been assumed to be one of the main neural sites involved in the acquisition and proper performance of new motor abilities (Evarts et al., 1983; Doyon and Benali, 2005; Gloor et al., 2015; Hayashi-Takagi et al., 2015). As a matter of fact, MC dynamic activities have been described as interacting with cerebellar and striatal contributions to different types of motor sequence learning (Houk et al., 1996; Hikosaka et al., 2002; Penhune and Steele, 2012). Accordingly, it is not surprising that a number of authors have also considered the involvement of MC in the generation of learned eyelid movements.

Woody and his group, in the 1970s, were among the first to suggest a role for the MC in associative learning (Woody et al., 1970; Woody and Yarowsky, 1972). They recorded increased unit activity mediated through neurons whose microstimulation evoked eye blinks. The enhanced firing activity preceded the CRs by a delay suitable for conduction between MC and O.O. muscles. Furthermore, they showed impaired acquisition of CRs with bilateral lesions of cortical motor areas (Woody et al., 1974). Then, in the early 1990s, Aou et al. (1992) reported similarly increased spike activity within the MC after eyeblink conditioning in cats, supporting Woody's hypothesis that the increase of cortical excitability facilitates the responsiveness to the CS, and that the generation of CRs may depend on neural circuitry and mechanisms of the MC.

However, a few years later, those reported electrophysiological measurements were questioned by other authors suggesting that the behavioral response determined by Woody and colleagues was not representative of a typical long-latency CR. Instead, Christian and Thompson (2003) indicated that their results were due to a short-latency response caused by sensitization of the unconditioned reflex blinks to the CS.

By that time, Birt's laboratory was studying in more detail the motor neurons' response to a CS and a US in awake cats and noticed that both stimuli induced an increase

in unitary activity; however, less activity was observed for the CS compared with the US (Birt et al., 2003).

Likewise, more recently (Pacheco-Calderón et al., 2012), the hypothesis about the role of the MC during eyeblink conditioning was strengthened by Pacheco-Calderón's report: reversible inactivation of MC produced a decrease in CR acquisition, and an initial defacilitation of CR-related neuronal activity of red nucleus neurons. Additionally, the observed reduction of CRs provoked by the loss of N-methyl-Daspartate (NMDA) receptor function (hypothesized to play a crucial role in the processes of learning and memory formation) provided evidence that the memory of acquired CRs is localized in MC (Hasan et al., 2013).

A few years ago, Ammann et al. (2016) showed that the firing activities of identified MC neurons are related to the generation and profiles of eyelid CRs. She reported three types of conditioning-related MC neurons recording in the eyelid motor area in rabbits; the firing of all of them started during the CS/US interval well in advance of CR onset (≥90 ms) and changed with it. Type A and B were activated antidromically from the facial nucleus, and Type C from the red nucleus. The reversible inactivation of the facial MC area during conditioning evoked a significant reduction in the percentage and in the integrated amplitude of CRs, with a lesser effect on unconditioned responses. In contrast, train stimulation of the MC simulated the profile and kinematics of CRs.

With those results, Ammann concluded that MC neurons from the eyelid motor area were involved in the acquisition and performance of conditioned eyeblinks during delay conditioning.

1.4.3. Rostral and caudal cingulate cortex, Brodmann area 24

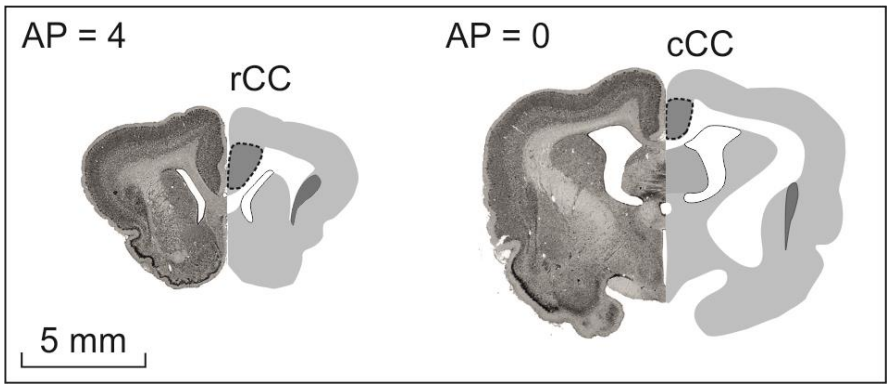

Figure 1.10. Diagram showing the location of CC in the rabbit brain. Two locations are represented: rostral CC (AP = 4) and caudal CC (AP = 0). In both, the left hemisphere is a coronal section taken from "Brain atlas of the domestic rabbit" (http://neurosciencelibrary.org/), while the right hemisphere shows a drawing from the same slice (rCC or cCC is indicated by the grey dotted area). As a clarification, rCC is likely to be equivalent to ACC in rodents. CL is represented in dark grey.

More than 30 years ago, Witter et al. (1988) found that the CL is reciprocally connected to the CC. Todays, it is well-known that the strongest reciprocal connection across species is between the CL and frontal cortical regions such as the ACC (Zingg et al., 2014; Torgerson and Van Horn, 2014; White et al., 2017; Atlan et al., 2017).

While the dense connectivity between ACC and CL had been described and studied in depth, little was known about the function of these pathways. That is why in 2017, Chia et al. initiated a study of the CL–ACC connections by characterizing the intrinsic properties of CL cells that project to the ACC. Retrograde labeling revealed that the input to the ACC comes mostly from the dorso-ventral CL core, rather than the shell region, and that the ipsilateral projection is stronger than the contralateral one, which agreed with previous works (Torgerson and Van Horn, 2014; Zhang et al., 2016; Atlan et al., 2017). Furthermore, White et al. (2018) reported that ACC input monosynaptically targets inhibitory CL neurons.

Recently, Chia et al. (2020) have identified several types of CL-ACC projecting neurons, based on their waveforms and action potential adaptation. These CL-ACC neurons were distributed heterogeneously with one type (moderately adapting; cell type 1) prominent in the central CL, and a second type (strongly adapting; cell types 2, 3 and 4) predominant in the anterior and posterior CL. Surprisingly, they found a sexual dimorphism in the distribution of the ACC-projecting neurons labeled in anterior CL.

The ACC plays an essential role in higher cognitive functions (Bush et al., 2000; Shenhav et al., 2013; Heilbronner and Hayden, 2016) and it is involved in top-down attention (Zhang et al., 2014, 2016). Consequently, given its dense connection with the CL, Mathur (2014) and White et al. (2018) hypothesize that this pathway is related to top-down input for cognitive control. Furthermore, White and Mathur (2018) assured that ACC-CL input participates in modulating attentional behavior in rodents. Meanwhile, the ACC is a key node in the salience network, as well as the IC (Seeley et al., 2007; Sridharan et al., 2008; Medford and Critchley, 2010; Menon and Uddin, 2010; Mechling et al., 2014;

Pagani et al., 2016), but they are not directly connected (Medford and Critchley, 2010). The report of Chia and collaborators (2020) supports the hypothesis that CL neurons could contribute to the salience network by serving as a link between ACC and IC.

Turning now to the involvement of the CC in associative learning, several studies indicate that it may be involved in eyeblink conditioning.

During the 1980s, Buchanan and Powell (1982) assessed the contribution of the anterior and posterior CC in heart-rate conditioning and eyeblink conditioning in rabbits. They reported that anterior cingulate lesions reduced conditioned heart-rate decelerations, relative to posterior cingulate or sham lesions, but enhanced the magnitude of the bradycardic component of the orienting reflex. Posterior cingulate lesions enhanced the bradycardic component of the conditioned response, particularly late in training, compared with anterior or sham lesions. However, somatomotor eyeblink conditioning, shock thresholds, and heart-rate UR were unaffected by cingulate lesions.

Contrarily to that report, several years later numerous authors realized that the temporal separation of the CS and US requires the input of forebrain structures, in order to achieve a successful acquisition of the trace conditioned response. Those structures included the hippocampus (Kim et al. 1995; Solomon et al. 1986; Weiss et al. 1999) and also the caudal region of the ACC, since Kronforst-Collins and Disterhoft (1998) and Weible et al. (2000) showed that lesions of the caudal CC in rabbit disrupted acquisition of trace eyeblink conditioning. Additionally, Preston et al. (2000), using functional magnetic resonance imaging techniques, observed event-related activation in the human ACC during conditioning.

Later, in 2003, Weible and colleagues recorded activity from cingulate neurons during trace eyeblink conditioning to assess how CC could contribute to this task. They reported that the first presentations of both the CS (tone) and the US (air puff) produced an excitatory response from caudal ACC neurons, regardless of whether using trace paradigm or pseudoconditioning. This initial excitatory response to the CS was maintained during all conditioning sessions but was more prominent in the first two training sessions. In contrast, after a few unpaired CS and US presentations, the activation of caudal ACC neurons to the CS rapidly declined as the stimulus became familiar and non-significant. This suggests that these neurons in the ACC are involved in attending to

stimuli with associational significance because they are more active before the learning has even started (first and second training sessions).

Instead, Oswald et al. (2008) trained rabbits in trace eyeblink conditioning and afterwards performed ibotenic acid lesions in CC; then they evaluated the performance during retraining. They reported that lesions in area 24 did not produce any deficit during the retesting. Nevertheless, these data do not contradict the results of Weible et al. (2003): here, Oswald shows that ACC lesions have no effect in either the retention or the retrieval of eyeblink conditioning, but the ACC may be involved in the acquisition, as Weible suggested.

An attentional role of the ACC had been proposed before in rabbits (Freeman and Gabriel, 1999). In fact, Gabriel and colleagues (1991) demonstrated retarded acquisition rates after ACC damage.

As a final comment, the area 24 is quite large, so, in order to obtain specific information, two locations within area 24 are going to be studied. Also, the ACC is not entirely equivalent in mice and rabbits. Therefore, in this Thesis the terms *rostral* (rCC) and *caudal* (cCC) CC are used. In this study, the location that most approximates the mouse ACC corresponds to the rabbit rCC.

2. HYPOTHESIS AND OBJECTIVES

Although surveys about the function of the CL are more numerous every year, and many of them involve the CL in cognitive processes related to segregation attention, salience processing, synchronization of oscillations, or even memory consolidation during sleep state, not much work has been done regarding the putative role of the CL in associative learning. With the development of new technology in neuroscience, previous work addressing this issue is todays dated and/or incomplete, and to our knowledge, activity of claustral neurons has never been recorded during the acquisition of new motor and/or cognitive abilities in behaving animals.

The purpose of this thesis is to assess the involvement of the CL during associative learning —in particular, classical eyeblink conditioning— and evaluate whether such a putative role affects its motor or cognitive component.

Therefore, the **hypothesis** of this dissertation is that the CL is involved in eyeblink conditioning (probably in the initial phase of the learning, when stimuli need to be paired) even in the simplest training: a delay paradigm. The vast connectivity of the CL, its demonstrated participation in attention and salience detention, and previous reports of activity in the CL when presented with different stimuli, all support this hypothesis.

Accordingly, the **general aim** of this study was to observe and record activity from CL cells through all the phases of the learning and try to elucidate the role of the CL in delay eyeblink conditioning. For this purpose, the following **specific objectives** were experimentally addressed:

1. To characterize the firing activity of CL neurons, ortho- and/or antidromically identified from electric stimulation of mPFC, MC, rCC, and/or cCC, during the three main phases of eyeblink conditioning: *before*, *during*, and *after* learning.
2. To explore the contribution of the CL to the local field potentials generated in the brain during eyeblink conditioning.
3. To analyze whether the activity generated by CL neurons contributes to the motor or to the cognitive component of the conditioned eyeblinks learning process.
4. To assess the consequences of partially inhibiting both CL afferences before or after the acquisition of the CRs in the learning curve.

3. MATERIALS AND METHODS

3.1. Experimental animals

Experiments were carried out in male rabbits (New Zealand white albino) obtained from an authorized supplier (Isoquimen, Barcelona, Spain). Animals were 2.5-3 months old and weighing 2-2.4 kg on arrival at the Animal House facilities of Pablo de Olavide University (Seville, Spain). Upon their arrival, animals were housed in individual cages provided with a burrow and different environmental stimuli, where they were maintained for the whole experiment. The room was kept on a 12/12 h light/dark cycle with constant ambient temperature (21 ± 1°C) and humidity (55 ± 7%). Food and water were available *ad libitum*.

Experiments were carried out following European Union Council (2010/276:33–79/EU) guidelines and Spanish (BOE 34:11370-421, 2013) regulations for the use of laboratory animals in chronic experiments. Experiments were also approved by the local Ethics Committee of Pablo de Olavide University.

3.2. Anesthesia and surgeries

All the operated rabbits fasted 12 hours prior to surgery. They were anesthetized with an intramuscular injection of a ketamine–xylazine cocktail (Ketaminol, 50 mg/mL; Rompun, 20 mg/mL; and atropine sulfate, 0.5 mg/mL) at an initial dosage of 1.0 mL/kg. Once the animal was asleep, the upper part of the head was shaved and disinfected with an antiseptic solution (Betadine®, Mundipharma GmbH, Germany). Anesthesia was maintained during the whole surgery by intravenous perfusion (93% saline, 4% Ketaminol, and 3% Rompun) supplied through a cannula (Abbocath®) implanted in the marginal vein of the right ear, at a flow rate of 10 mL/kg/h. A transparent gel (Methocel® 2%, CIBA vision) was applied on both corneas to prevent ocular damage by desiccation.

Afterwards, the heads of the animals were fixed to the stereotaxic apparatus (Model 1240, David Kopf Instruments, CA, USA) by means of zygoma clamps, adjustable tooth bar and a nose clamp. Surgical material and area were sterilized before use. Subsequently, the skull was exposed by mean of an anteroposterior incision in the skin and the removal of the periosteum. The rabbit's head was accurately positioned in the stereotaxic apparatus with a depth variation of 1.5 mm between *Bregma* and *Lambda*. This position was established as stereotaxic zero and served as the reference point whenever using stereotaxic coordinates (following the Rabbit Atlas, Girgis and Shih-Chang, 1981) in the different surgical procedures described below. The holes in the skull

for electrode implantation or virus injections were performed with a dental drill (NSK Volvere max, Nakanishi Inc., Japan). As a ground, a silver electrode in contact with the dura mater was attached to the right bone with a small screw. Another silver wire (1 mm in diameter) was shaped forming a loop to facilitate the grasping by the amplifier equipment during the recordings (**Fig. 3.1*C***).

Also, all the animals were implanted with bipolar hook electrodes in both O.O. muscles to record their EMG activity (**Fig. 3.1*B***) in order to evaluate the CRs during the classical conditioning of the eyelid response. These electrodes were handmade from seven-stranded Teflon-coated stainless-steel wire (A-M Systems, Everett, WA, USA) with a total external diameter of ≈ 0.2 mm and bared ≈ 0.5 mm at the tip. The prepared wire was inserted into the muscle with the aid of a syringe needle (21 G).

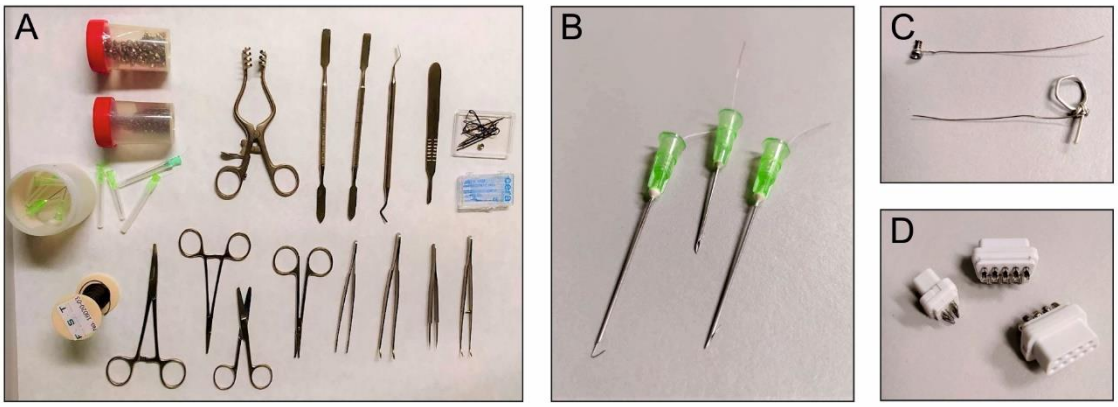

Figure 3.1. General surgical materials. ***A,*** Tools and instruments used in surgery; this material was previously sterilized using a dry-heat cycle of 150ºC for 60 min. ***B,*** Bipolar hook electrodes made from multistranded Teflon-coated steel wire used to record O.O. muscle EMG activity; hypodermic needle (21 G) facilitates implantation. ***C,*** Handmade grounds. ***D***, 9-pin sockets.

For head fixation during recordings and eyeblink conditioning, animals were implanted with a head-holding device (**Fig. 3.5*B***) made from three bolts (20 mm long, ø 2 mm) attached to the skull with dental cement (Duralay, Dental Mfg. Co., IL, USA) perpendicular to the stereotaxic plane. When animals were not being tested, a triangular metal plate was screwed to the three bolts to prevent the rabbits from getting jammed in their home cages. Stimulating and/or recording electrodes, EMG wires, and grounds were connected to 9-pin sockets (**Fig. 3.1*D***) affixed to the holding system, forming a single, solid turret.

Finally, operated animals were injected with 1 mL benzylpenicillin (Penilevel®) in order to prevent infections, and they were taken back to their home cages to rest for 7 days until fully recovered from surgery.

Depending on the experimental goal, three different surgical procedures were carried out in addition to the common ones described so far. These extra steps, specific to experiments 1, 2 and 3 (*Ex. 1*, *2*, and *3* respectively) are detailed below.

3.2.1. Ex. 1 - For extracellular recording and stimulation

The first group of animals (n = 7) were prepared for the chronic recording of unitary activity in the CL during classical eyeblink conditioning (n = 5) and pseudoconditioning (n = 2). For this, besides the procedures described above, a window (2 mm × 5 mm) was drilled through the parietal bone centered overlying the right rostral CL (rostral corners from bregma: AP = 4 mm, L = –4 mm to –6 mm; caudal corners: AP = –1 mm, L = –7.5 mm to –9.5 mm; Girgis and Shih-Chang, 1981; **Fig 3.2*A***, pink rectangle). A recording chamber was built with acrylic cement around the window, and a sterile stainless-steel needle (21G) was fixed to one anterolateral corner of the recording window for reference purposes. The dura mater remained exposed and intact (except for tiny holes made with a sterile needle just before each recording session, to insert the recording electrodes). At the end of the surgery, and between sessions, the cortical surface was protected with an inert silicone cover (Silastic®, BioPlexus Corporation, CA, USA) and a sterile gauze on which a small amount of antibiotic (Gentamycin 0.3%) was applied. Finally, the hole was sealed with a layer of bone wax (Ethicon®, Johnson & Johnson Intl., NJ, USA).

All these animals were implanted bilaterally with stimulating electrodes in the M1 subdivision of the MC (AP = 2 mm, L = +2 mm and –2 mm; D = 1.5 mm, with respect to brain surface; **Fig 3.2*A***, orange dots) corresponding to the eyelid motor area (Girgis and Shih-Chang, 1981; Ammann et al., 2016). In addition, five of them were also implanted with electrodes aimed at the prelimbic area of the mPFC (AP = 11 mm, L = +1 mm and –1 mm; D = 2.5 mm; **Fig 3.2*A***, magenta dots), while the other two were implanted in the CC (AP = 4 and 0 mm, L = –0.8 mm; D = 1.5 mm; **Fig 3.2*A***, light and dark blue dots, respectively) (Girgis and Shih-Chang, 1981; Oswald et al., 2008). These three regions are related with eyeblink conditioning (Weible et al., 2003; Leal-Campanario et al., 2006; Caro-Martín et al., 2015; Ammann et al., 2016) and project to

the CL (Smith and Alloway, 2010; Atlan et al., 2017; White et al., 2017; Jackson et al., 2018). Stimulating electrodes were handmade with varnished silver wire (200 µm in diameter; California Fine Wire Company, CA, USA) bared ≈ 0.5 mm at the tip (**Fig. 3.2*C***).

Stimulating electrodes, EMG wires, and ground were connected to 9-pin sockets affixed to the holding system.

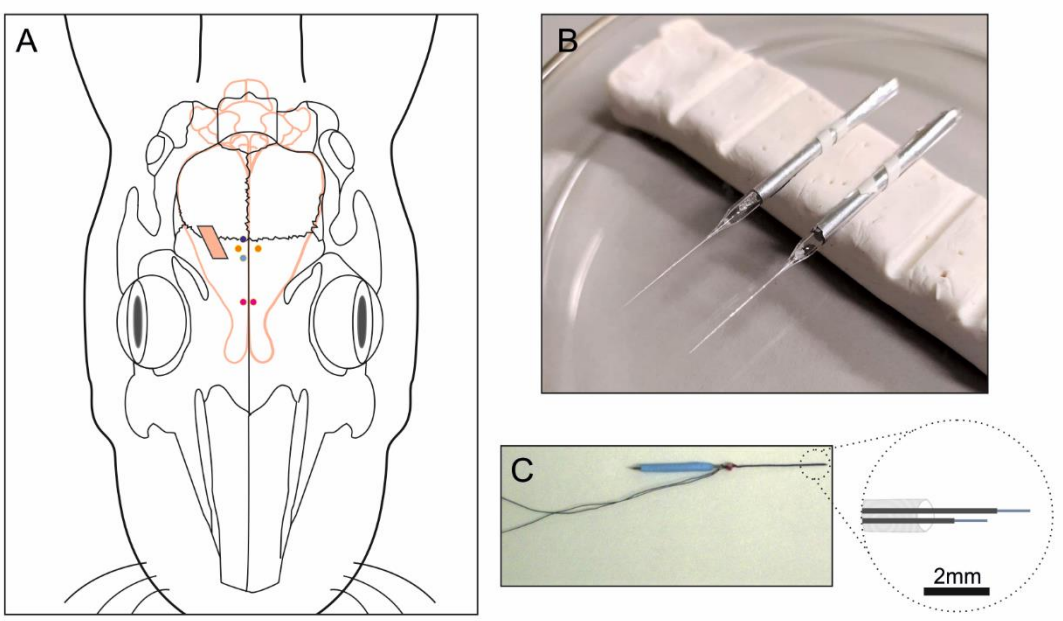

Figure 3.2. Surgical procedures for experiment 1. ***A***, Schematic view of the recording window (pink rectangle) and the stimulating electrodes over the rabbit skull. All rabbits (n = 7) were implanted with bilateral MC stimulating electrodes (orange dots); five of them were also implanted with bilateral mPFC electrodes (magenta dots), while the other two were implanted in rCC (light blue) and cCC (dark blue). ***B,*** Glass micropipettes used for unitary recordings from CL. They were filled with 2M NaCl (3–5 MΩ of resistance) and partially covered with aluminum foil to reduce electromagnetic noise while recording. ***C,*** Stimulating electrodes, handmade with 200 µm varnished silver wire bared ≈ 0.5 mm at the tip; the large, dotted circle is an amplified view of the smaller.

3.2.2. Ex. 2 - For recording of Local Field Potentials

A second group of animals (n = 4) were prepared for the chronic recording of local field potentials (LFP) in CL, MC, and mPFC (**Fig. 3.3*A***; the CC was excluded for technical limitations). For this experiment, animals were implanted bilaterally with recording tetrodes in the rostrodorsal part of the CL (AP = 1 mm, L = +6.5 mm and –6.5 mm; D = 6.5 mm; Girgis and Shih-Chang, 1981) and with bipolar recording electrodes in

the mPFC (AP = 11 mm, L = +1 mm and –1 mm; D = 2.5 mm; Girgis and Shih-Chang, 1981) and in the MC (AP = 2 mm, L = +2 mm and –2 mm; D = 1.5 mm; Girgis and Shih-Chang, 1981).

These electrodes (**Fig. 3.3*B***) were handmade from two (bipolar) or four (tetrodes) threads of 50 µm, Teflon-coated tungsten wire (Advent Research Materials Ltd., Eynsham, England). Three 9-pin sockets affixed to the holding system were needed to connect the LFP recording electrodes, EMG wires, and ground.

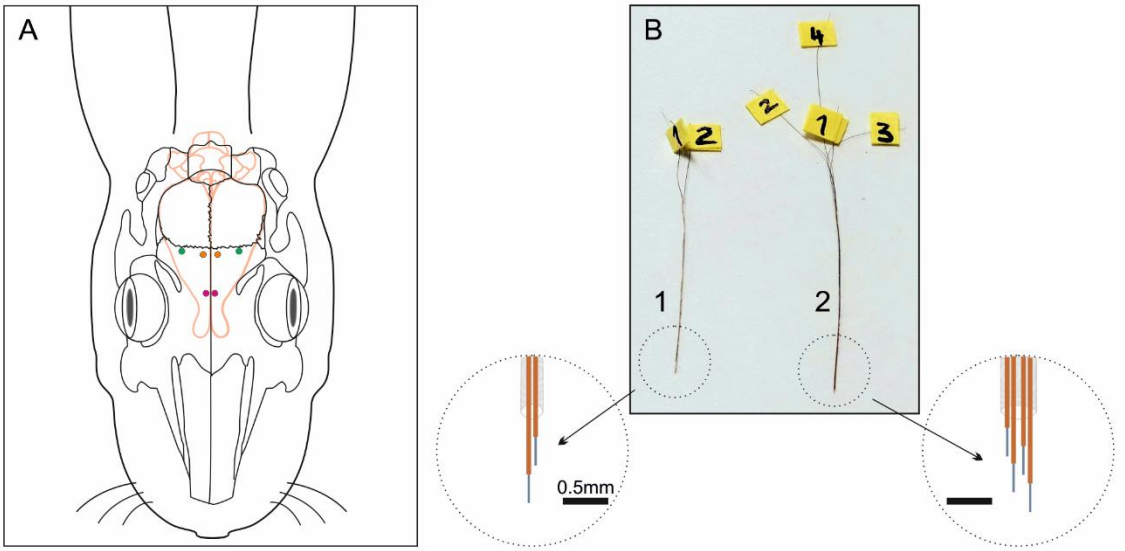

Figure 3.3. Surgical procedures for experiment 2. ***A***, Schematic view of the LFP recording electrodes over the rabbit skull. Rabbits (n = 4) were bilaterally implanted with bipolar recording electrodes (***B*1**) in MC (orange dots) and mPFC (magenta dots) and with tetrodes (***B*2**) in CL (green dots). ***B,*** Recording electrodes were handmade from two (**1**) or four (**2**) threads of 50 µm, Teflon-coated tungsten wire bared ≈ 0.5 mm at the tip; the latge, dotted circle is an amplified view of the smaller.

3.2.3. Ex. 3 - For injections of the vINSIST viruses

A third group of animals (n = 8) were infected with a mix of recombinant adeno-associated viruses (rAAVs) equipped with doxycycline-dependent tetracycline-controlled genetic switches, which release tetanus toxin (TeTxLC) and tandem dimer Tomato (tdTOM) when activated, and enhanced green fluorescent protein (EGFP) to identify the infected cells (vINSIST method, see below; **Fig. 3.4*A***). To accomplish an acceptable level of infection, these animals received a total of six microinjections (each of 2 µL) of the viral suspension: three in each CL (rostral, AP = 4 mm, L = +5 mm and –5 mm; D = 5 mm; medial, AP = 2 mm, L = +7 mm and –7 mm; D = 5.5 mm; and caudal, AP = 0.5 mm, L = +8 mm and –8 mm; D = 6 mm; Girgis and Shih-Chang, 1981).

Injections were carried out in both CLs since there is a powerful functional compensation system (Duffau et al., 2007). A 5 µL microsyringe (Hamilton®, Reno, NV, USA) was used for injecting the rAAVs (**Fig. 3.4*B***). EMG wires and ground were soldered to one 9-pin connector. After the surgery and the viral infection, animals were given a period of 20 days to recover so that the correct level of viral expression could be achieved.

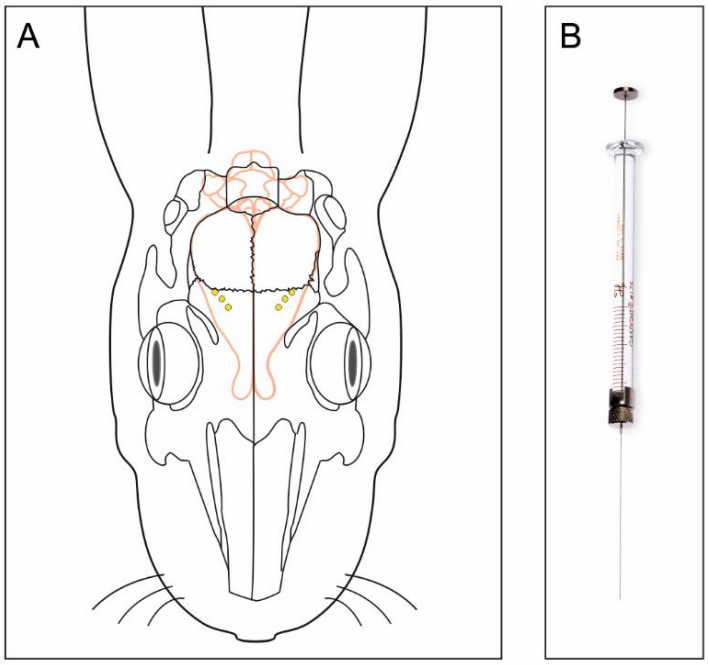

Figure 3.4. Surgical procedures for experiment 3. ***A***, Schematic view of the bilateral vINSIST viruses injections (yellow dots) in three locations within the CL. The animals (n = 8) received a total of six microinjections (each of 2 µL) of the viral suspension, using a 5 µL Hamilton® microsyringe (***B***).

3.3. Classical conditioning of eyelid responses

3.3.1. Training and adaptation sessions

The training period started one week after surgery —once no discomfort was shown by the animals— and lasted for 5 days in which rabbits got used to the Perspex® box (**Fig. 3.5*A***) designed to limit their movements (Gruart et al., 2000; Leal-Campanario et al., 2007). The box was placed on a table in front of the set-up for 5, 10, 15, 20, and 30 min each day respectively. The experiment room was kept softly illuminated and the conditioning table was surrounded by a black cloth. After those 5 training sessions, animals went through two 45-min sessions aimed at adapting them to the experimental conditions (including head immobilization and connected cables). A few random stimuli were presented during these sessions, only to test the well-functioning of the conditioning set-up and the EMG recordings.

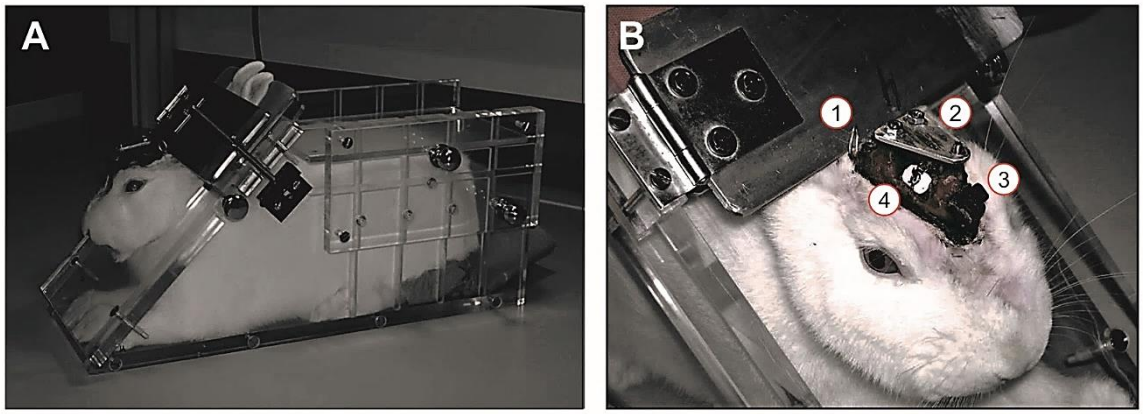

Figure 3.5. ***A,*** Plexiglass restraining box for rabbits. This box allowed adjusting the internal space according to the size of the animal, and the position of the head could be fixed with a padded clamp. Before each experiment, the animals underwent a training period described below. ***B,*** Image of the head-holding system (**2**) made from three bolts attached to the skull with dental cement with a metal plate on top. Also attached with dental cement there are (**1**) the loop-shaped silver ground, (**3**) the 9-pin connector, and (**4**) the window over the CL (only in experiment 1 subjects), all forming a solid turret.

3.3.2. Eyeblink conditioning paradigm

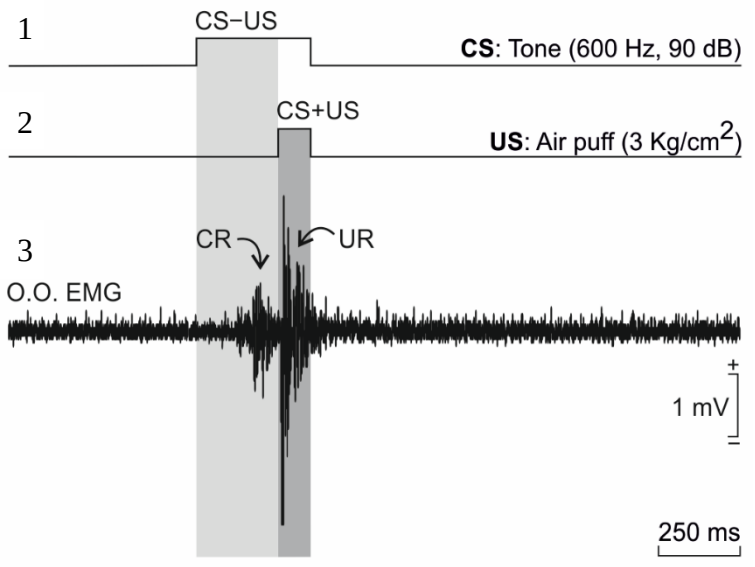

Figure 3.6. Illustration of the delay paradigm. From top to bottom are shown: (**1**) the CS; (**2**) the US; (**3**) one example of the EMG activity of the left O.O. muscle. Note the presence of the CR in the CS-US gap (light gray area) as a learning-dependent response and the UR in the CS+US period (in dark gray area) as a reflex reaction.

Eyeblink conditioning was achieved using a delay conditioning paradigm (see **Fig. 3.6** and Leal-Campanario et al., 2007). A 350 ms tone (600 Hz, 90 dB) was presented as CS and a 100 ms air puff (3 kg/cm^2) aimed at the left cornea was used as US. The US was prepared to coterminate with the CS. The concept "CS/US" refers solely to the presentation of the pair of stimuli. We term "CS-US" the first 250 ms of the CS, right

before the start of the US. It is during this time frame that CRs are expected to be found throughout conditioning. We considered a "CR" the presence, during the CS-US period, of the EMG activity of the left O.O. muscle lasting > 10 ms and initiated > 50 ms after CS onset (Gruart et al., 2000). We use "CS+US" to refer to this 100 ms coexisting period; the UR will appear during this period. Recordings from the right O.O. muscle were used as a control for spontaneous and/or voluntary eyelid movements.

Following five training and two adapting sessions, conditioned animals received two habituation sessions (during which the CS was presented alone; **Fig. 3.7*A***) and eight conditioning sessions (paired CS/US; **Fig. 3.7*B***).

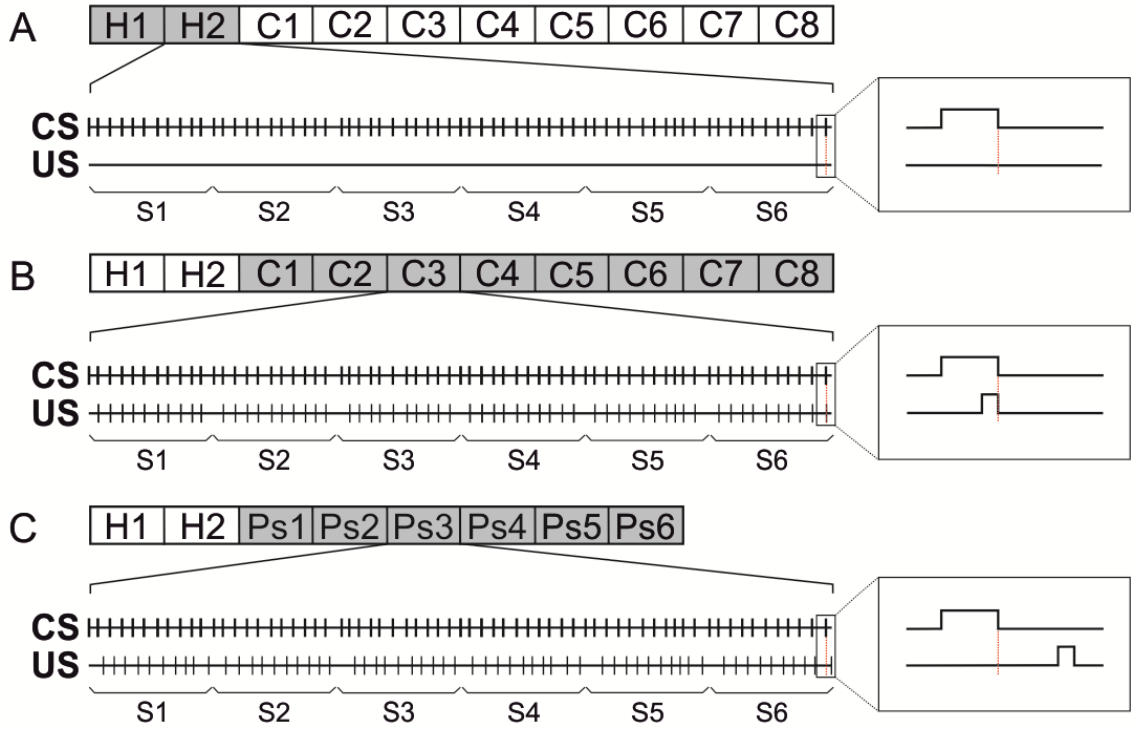

Figure 3.7. Representations of the conditioning and pseudoconditioning paradigms. All sessions (habituation, conditioning, and pseudoconditioning) consisted of 66 trials (6 series of 11 trials each) separated at random by intervals of 45-60 s. ***A-C,*** Scheme of a habituation (single CS presentations; ***A***), conditioning (paired CS/US; ***B***), and pseudoconditioning session (unpaired CS and US; ***C***). Note the six test trials (CS only) in conditioning and pseudoconditioning sessions. The large rectangular insets are a magnification of the smaller ones. All sessions lasted ≈ 70 min.

All sessions consisted of 66 trials (6 series of 11 trials each). Successive trials were separated at random by intervals of 45–60 s (3.2-Microstim, Cibertec). During conditioning sessions, the 1st trial of each one of the six series consisted of a test trial in which the CS was presented alone (a total of 6 test trials per session). As selected criterion

for learning, the animals had to generate ≥ 80% of CRs in two successive conditioning sessions.

Pseudoconditioned animals received two habituation sessions as described above and six pseudoconditioning sessions (all conditioned animals learned the task and reached the criterion before the 6th conditioning session) with unpaired, randomized CS and US presentations (**Fig. 3.7*C***). Successive CS were also separated at random by intervals of 45–60 s (3.2-Microstim, Cibertec). US were delivered at a random interval of 10–30 s after the CS. The first trial of each serie was a test trial as in conditioning sessions.

The EMG activity of the O.O. muscle was recorded during all the forementioned sessions using Grass P511 differential amplifiers with a bandwidth of 0.1 Hz to 10 kHz (Grass-Telefactor, West Warwick, RI, USA). A function generator (AFG 3022B, Tektronix, Miami, FL, USA), triggered by a digital programmer (3.2-Microstim, Cibertec), was used to generate the train with tone characteristics (600 Hz, sine wave, 1 V). An amplifier (PA Amplifier FS-2035, Fonestar Systems, Madrid, Spain) converted the pulse to a tone (90 dB) *via* a loudspeaker located 60 cm in front of the animal. Air puffs were delivered from an air compressor (Biomedical Engineering, Thornwood, NY, USA) and applied through the opening of a plastic pipette (3 mm in diameter) attached to the animal's holding system and located 1 cm from the left cornea.

3.4. Recording and stimulation procedures

The five training sessions were carried out as described above. During the adapting sessions, recording set-up was added to the conditioning table and served to test the level of noise of the recordings (unitary or LFPs), besides reduce the stress level of the animals and familiarize them with the recording conditions (head fixation, connected cables, and conditioning equipment). A few random stimuli were presented to assess the well-functioning of the conditioning set-up and the EMG recordings. As indicated before, the recording room was kept softly illuminated and the conditioning table was surrounded by a black cloth throughout the experiment. Recordings were carried out during habituation and conditioning or pseudoconditioning sessions. All sessions lasted ≈ 70 min.

3.4.1. Ex. 1 - Extracellular unitary recording and stimulation

Once the animal inside the Perspex® box was positioned on the recording table, its heads was fixed to the holding device attached to an arm of the table. First of all, the bone wax and gauze which sealed the recording window were removed. Using a surgical microscope (M 400-E, Leica, Leica Microsystems, Switzerland) the silicone cover was also removed, and the brain surface was exposed. The dura mater was carefully cleaned with super-fine tweezers. The recording electrode (glass micropipette) was fixed to a specific holder attached to a micromanipulator (Model Camberra, Narishige, Japan). Using the needle affixed in the rostral-medial corner of the window as a stereotaxic reference, the micropipette was placed in the coordinate of interest. A tiny hole was made in the dura mater with a sterile needle (to avoid breaking the electrode). Afterwards, the micropipette was gradually lowered with the micromanipulator until reaching the desired depth.

The glass micropipettes used for unitary recordings from CL neurons were manufactured a few days before the experiment (**Fig 3.2*B***). The pipettes were produced with a glass microelectrode puller (Model PE-2, Narishige, Japan) from glass rods with an external and internal diameter of 3 and 2.5 mm, respectively (Corning, MA, USA). Parameters of the puller were adjusted to produce pipette tips with an adequate length (~20 mm). The pipettes were initially sealed until their tips were gently broken under an optical microscope, obtaining tips with a diameter between 4 and 5 µm. Lastly, they were filled with 2M NaCl (3–5 MΩ of resistance) and partially covered with aluminum foil to reduce electromagnetic noise while recording. During the experiment, a silver wire inside the conducting solution connected it to a NEX-1 preamplifier (x100) (Biomedical Engineering, NY, USA). The recorded activity was filtered analogically in a bandwidth of 1 Hz to 10 kHz (AC/DC differential amplifier; model 3000, A-M Systems, Everett, WA, USA). On occasion, we used tungsten microelectrodes of 5 MΩ of resistance (A-M Systems) for unitary recordings and local microlesions.

The recording area was approached with the help of the reference needle and stereotaxic coordinates (Girgis and Shih-Chang, 1981), and antidromic or orthodromic field and unitary potentials were evoked by electrical stimulation of MC, CC, and/or mPFC. To determine whether the recorded and the activated neuron were the same, we used the collision test (i.e., the antidromic invasion of a soma is prevented if the antidromic action potential collides with a spontaneous orthodromic action potential; see

Múnera et al., 2001; Ammann et al., 2016). At the end of each recording session, the recording chamber was sterilized and closed with the silicone cover and sterile gauze, and it was sealed with bone wax.

Electrical stimulation of electrode-implanted sites (mPFC, MC, and/or CC) consisted of single (square, 50 µs, 0.1-0.5 mA, positive-negative pulses with 20 µs of interval) or paired (1-2 ms of interval) pulses programmed with a CS-20 stimulator across an ISU-200-BIP isolation unit (Cibertec, Madrid, Spain).

To facilitate the location of recording sites in the CL a small electrolytic lesion (0.2-0-4 mA of anodic current for 30 s; CS-220 stimulator across an ISU-200-BIP isolation unit; Cibertec) was carried out during the final recording sessions.

3.4.2. Ex. 2 - Local Field Potentials recording procedure

Since LFP recording electrodes were implanted chronically and no stimulation was used, the experiment set-up was simpler. Animals inside the Perspex® box were placed on the recording table and their heads were fixed to the holding device attached to an arm of the table. Conditioning devices were placed, and cables were connected to the three 9-pin connectors each animal had in the cement structure on its head.

LFPs in CL, mPFC, and MC were recorded using Grass P511 differential amplifiers with a bandwidth of 0.1 Hz to 10 kHz (Grass-Telefactor, West Warwick, RI, USA).

3.5. Ex. 3 - The vINSIST method

For the inhibition of CL transmission, we used an advanced method for doxycycline-controlled virus-delivered inducible silencing of synaptic transmission (vINSIST) between connected circuits (**Fig. 3.8**; Reus-Garcia et al., 2021). The injected mix contained three rAAVs: 1. rAAV-PhSYN-rtTA, 2. rAAV-Ptetbi-TeTxLC/tdTOM, and 3. rAAV-PhSYN-EGFP. The tetanus toxin light-chain coding sequence (TeTxLC) for selective cleavage of synaptobrevin-2 (Syb-2) blocked synaptic transmission (Sweeney el al., 1995) into a bidirectional tetracycline promoter (P_{tet}bi) (Hasan et al., 2013, Dogbevia et al., 2015, 2016) with TeTxLC on one side and tandem dimer Tomato gene (tdTOM, expressing red fluorescent protein) on the other (rAAV-Ptetbi-TeTxLC/tdTOM). A reverse tetracycline transactivator (rtTA) and enhanced green fluorescent protein (EGFP) are independently expressed under the human synapsin

promoter (rAAV-PhSYN-rtTA and rAAV-PhSYN-EGFP), so that rtTA-infected cells will be traceable in green.

With the addition of doxycycline (Dox), a hydrophobic derivative of tet that rapidly crosses the blood-brain barrier, rtTA binds P_{tet}bi and activates the expression of TeTxLC (to silence synaptic transmission) and tdTOM (thus the inhibited location will glow in red).

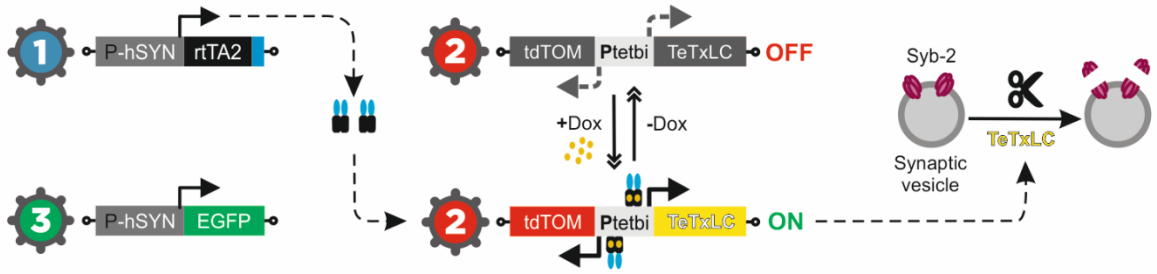

Figure 3.8. The vINSIST method. Viral preparation for classical eyeblink conditioning following virus-delivered inducible silencing of synaptic transmission (vINSIST) of CL neurons. The three injected viruses were as follows: (**1**, blue) rAAV-**P**$_{hSYN}$-rtTA; (**2**, red) rAAV-**P**$_{tet}$bi-TeTxLC/tdTOM; and (**3**, green) rAAV-**P**$_{hSYN}$-EGFP. With the vINSIST method, the reverse tetracycline trans activator (rtTA; 1) is expressed under a human synapsin specific promoter (**P**$_{hSYN}$; 1, 3) and the tetanus toxin light chain (TeTxLC; 2) and tdTomato (tdTOM; 2) are under a bidirectional tet responder promoter (**P**$_{tet}$bi; 2). Only under doxycycline (Dox) treatment, rtTA binds the **P**$_{tet}$bi to express simultaneously TeTxLC, which blocks synaptic transmission, and tdTOM, a tracer used to identify the inhibited zone. Virus 3 acts as a *post hoc* histological tracer for validating the degree of precision and the expression of rtTA.

After the period of 20 days for recovery from surgery and viral infection, all rabbits were trained for classical conditioning as described before. For comparative purposes, the participating animals (n = 8) were divided in two experimental groups (**Fig. 3.9*B***): in the first (n = 4), Dox injection and resultant inhibition of CL transmission was produced after the 2nd habituation session, and in the second group (n = 4) Dox was administrated after the 6th conditioning session (i.e., before and after the learning, respectively).

Dox injections were carried out immediately after the indicated session (the 2nd of habituation for group 1 and the 6th of conditioning for group 2) once the rabbits were taken out of the retraining box. Experimental animals received a single dose of 100 mg of powdered Dox dissolved in 10 mL of saline solution. This was delivered intraperitoneally in two 5 mL shots, one on each side of the animal's body, to avoid

injecting an excess of solution in a single point. Afterwards, the rabbits were put back in their home cages and rested for at least 22 h before the next session. Animals were sacrificed the day after the 8th conditioning sessions.

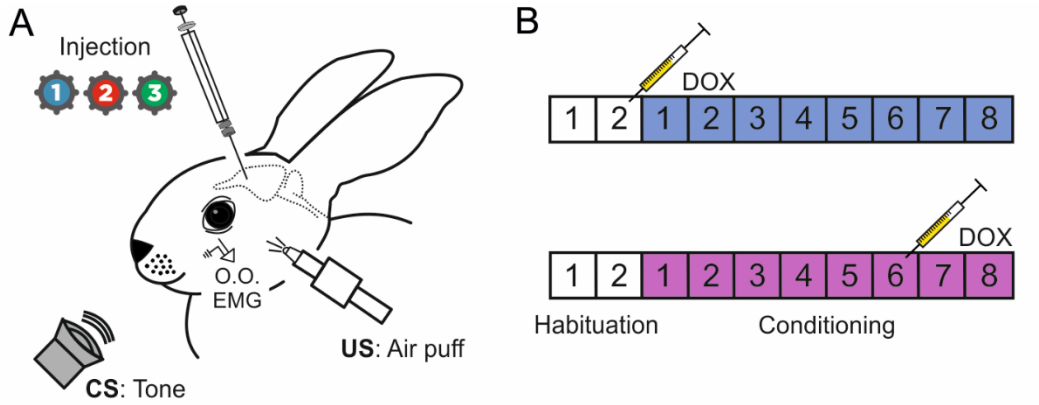

Figure 3.9. Inhibition protocol. ***A,*** Diagram illustrating the animal's injections with the rAAVs during surgery and its preparation for the classical conditioning of eyelid responses. ***B***, Rabbits were classically conditioned using a delay paradigm following two protocols: half of them (blue group) were injected with Dox after the 2nd habituation session and the other half (magenta group) after the 6th conditioning session.

As a synopsis of the contents, **table 3.1** provides a summary of the surgeries, procedures, and experiments described so far.

	Training (5) + Adaptation (2) + Habituation (2) + CONDITIONING (8)	**Training (5) + Adaptation (2) + Habituation (2) +** PSEUDOCOND. (6)
Ex. 1 Unitary recording and stimulation **Surgery 3.2**	**n = 5 rabbits**	**n = 2 rabbits**
Ex. 2 Recording of LFPs **Surgery 3.3**	**n = 4 rabbits**	**-**
Ex. 3 CL inhibition by viral infection **Surgery 3.4**	**Group 1, n = 4 rabbits** **Group 2, n = 4 rabbits**	**-**

3.6. Perfusion

Once the electrophysiological experiments were finished, animals were deeply anesthetized with an intravenous injection of a mixture of the muscular relaxant Xylazine (Rompun®, 3 mg/kg of animal weight) and the hypnotic Ketaminol (Imalgene®, 25 mg/kg of animal weight) and perfused transcardially with saline and 4% paraformaldehyde. Once the animals were deeply asleep, the heart was exposed by making a U-shaped incision in the thoracic cage and separating the pericardial tissue. An injection of 0.5 mL of sodium heparin (1000 UI/mL, Chiesi-Spain S.A.) in the ventricular cavity was used as anticoagulant. To amplify and accelerate the effect of the fixation solution, the descendent portion of the aorta was clamped. After that, a cannula was inserted in the right atrium, and with the assistance of a peristaltic pump (Master Flex® L/S®, Thermo Fisher Scientific Cat. Nº 7524-45, USA) 1 L of saline solution cleaned the circulatory system of blood and facilitated the posterior fixation, which was achieved with 2 L of 4% paraformaldehyde in phosphate buffer (0.2 M, pH 7.4).

3.7. Histology

After perfusion, the brains were extracted and preserved at 4 ºC overnight, in paraformaldehyde (4%) to ensure a proper fixation. Then, the brains were moved first to a 15% saccharose cryoprotectant solution (15% saccharose in a 0.2M phosphate buffer solution) and when they sank (1-2 days), they were transferred to a more concentrated cryoprotectant solution (30% saccharose in a 0.2M phosphate buffer solution). When, 2-3 days after that, the brains had completely sunk, they were ready to be sliced (in coronal sections 50 µm thick) using a microtome (Leica SM200R, Leica Microsystems, Nusslock GmbH, Germany). These slices were sorted into a multi-well dish containing a phosphate-buffered solution (0.2M) until they were placed on gelatinized glass slides and stained if they contained information about the stimulation and recording locations. Relevant sections were processed for Nissl staining with 0.1% toluidine blue. After the staining and the dehydration process, the slices were immersed in two consecutive cuvettes containing xylene (100%) for 5 min each time. Finally, mounting media (Distrene Plasticizer Xylene) was applied to the tissues, they were covered with a glass coverslip and let dry.

Preparations were observed and photographed using an optical microscope (Leica DMRE type 020-525-025, Leica Microsystems, Wetzlar GmbH, Germany). Recording sites were adjusted according to the collected stereotaxic coordinates and with the location of the electrolytic marks.

3.7.1. Rabbit brain slices infected with vINSIST viruses

Brains from the vINSIST-injected rabbits (experiment 3) were fixed in paraformaldehyde (4%) at 4 ˚C overnight. Brains were then cut by a vibratome (Leica VT 1000 S) in sections 140 µm thick. The sections were mounted in glycerol (80% in phosphate-buffered saline + 2.5% DAPCO). Slices were imaged on a confocal laser scanning microscope (Leica TCS SP5) using a 10x air objective and a 20x oil immersion objective and a 488 nm argon laser. Images were taken in z-stacks of 2 µm and 3 µm on the 10x and the 20x objectives, respectively.

3.8. Data collection and analysis

The EMG activity of the left O.O. muscle, the unitary activity of CL neurons, LFPs recorded in CL, mPFC, and MC, and 1-volt rectangular pulses corresponding to CS and US presentations were acquired online through an 8-channel analog-to-digital converter (CED 1401-plus, CED, Cambridge, UK) and transferred to a computer for quantitative offline analysis. Data were sampled at 4 kHz for LFP recordings, 5 kHz for EMG activities, and 25 kHz for unitary recordings, with an amplitude resolution of 12 bits.

Computer programs (Spike2, version 7 and SIGAVG from CED, UK) were used online to display unrectified and rectified EMG, unitary activities and LFPs.

3.8.1. Ex. 1 - Extracellular unitary activity analysis

The recorded neuron was generally easy to identify. In the case of multiple unitary recordings in which identifying a single cell was difficult, a spike-sorting procedure (from Spike2, version 7, CED, UK; and VISSOR software, see Caro-Martín et al., 2018) was conducted. In all cases, an event channel was created for each identified neuron in which every event corresponded to a single spike. Representation programs enabled displaying event rasters of unitary activity and post-stimulus time histograms (PSTHs). Following Rieke et al. (1997), PSTHs were converted to firing rates as a function of time (i.e., in spikes/s) for the characterization of the firing properties of the CL neurons. For the

classification of the CL neurons in different groups, we used not only their firing rate profiles but also spike duration parameters, both explained in detail below.

3.8.2. Ex. 1 - Parameters to classify CL neurons

Firing rate profiles: transformation of PSTHs to firing rate as a function of time.

PSTHs were converted to firing rate $r(t)_i$ as a function of time (i.e., in spikes/s), according to the equation (1):

$$r(t)_i = Nspikes_i/(Ntrials * \Delta bin) \quad (1)$$

In equation (1), $Nspikes_i$ is the average number of spikes in each bin, $Ntrials$ is the number of repetitions (or number of trials in the raster), and Δbin is the bin size (in ms). The optimal bin size (Δbin) was dependent on the mean and the variance of the number of spikes in the *i*th-interval.

In this way, we used the firing rate profiles for a functional characterization of CL neurons and for their classification in different putative groups. As a result, three types (A, B, and C) of firing rate recorded from CL neurons were identified during classical eyeblink conditioning (see **Figs. 4.8, 4.9, 4.10** in Results section).

Spike shape features: extraction of the spike duration from the neural recordings.

The proposed methodology for the extraction of spike duration was based on the analysis of regular differentiations (first-order and second-order derivatives) of the raw CL neuron recording. The first-order $D^1_\propto f(t)$, and second-order $D^2_\propto f(t)$ derivatives were calculated through a convolution between the derivatives of the kernel function $G^j_\propto(t)$ and the raw recording $f(t)$.

$$D^j_\alpha f(t) = \left(f * G^j_\alpha\right)(t) = \sum_\alpha f(\alpha)G(t-\alpha) \quad (2)$$

In equation (2), α was a dummy variable of the convolution that reflected the displacement of $G^j_\alpha(t)$ across of $f(t)$ and j was the order of the derivative (1, first-order; and 2, second-order). The study of these regular differentiations (based on the convolution) provided a proper preprocessing of the data, obtaining the smoothed j-order derivative of the raw recording, as well as an optimal way for computation of the spike duration (for further details see Aksenova et al., 2003). **Table 4.5** (in Results) summarizes the main quantitative results about the spike durations for discriminating between putative principal and non-principal neurons.

Next, there is a diagram (**Fig. 3.10**) illustrating the feature extraction methodology, with emphasis on the parameters of spike duration.

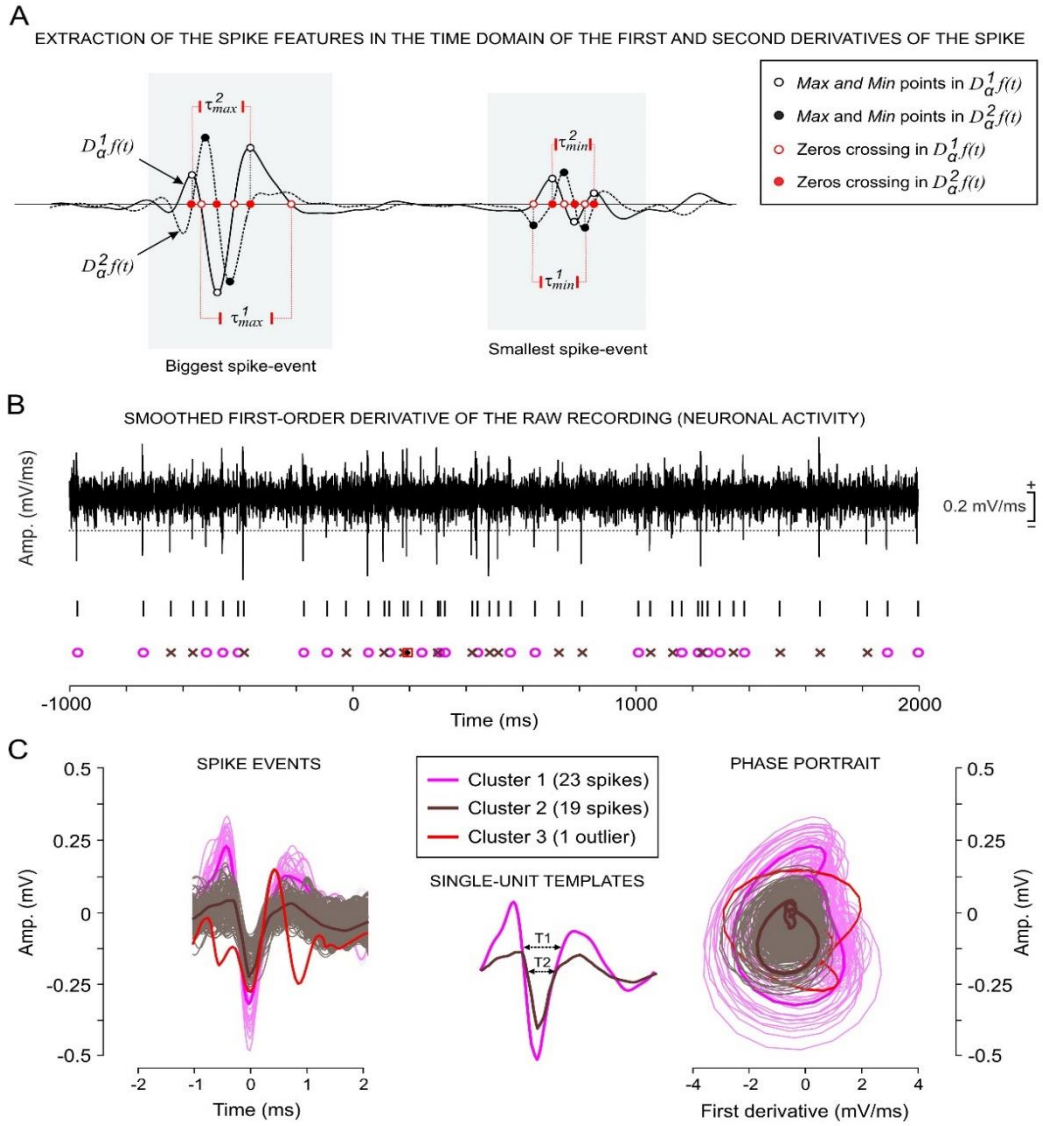

Figure 3.10. Neuron classification considering firing rate profile and spike duration parameters. ***A***, Diagram illustrating the extraction of the spike duration from two simulated spike-events with maximum peak amplitude (biggest spike-event; on the right) and with minimum peak amplitude (smallest spike-event; on the left). The solid line indicates the first-order derivative $[D_\alpha^1 f(t)]$ while the dotted line indicates the second-order derivative $[D_\alpha^2 f(t)]$. Parameters τ1min and τ1max (from the first-order derivative) and τ2min and τ2max (for the second-order derivative) are the durations of the two simulated spike-events. ***B***, Smoothed first-order derivative of the raw recording (sampling frequency of 25 kHz, epoch of 3 s). The horizontal dotted line indicates the amplitude threshold, and the small vertical markers indicate the detected spike-events before classification. ***C***, Three clusters were obtained (cluster 1, 23 spikes; cluster 2, 19 spikes; cluster 3, 1 outlier) and all the spikes were represented in both time domain and phase portrait. The single-unit templates from the two significant clusters were determined and the spike durations were calculated. In this way, the principal and non-principal units were classified.

3.8.3. Ex. 2 - Analysis of the recorded Local Field Potentials

From spectral analyses, we selected LFP epochs lasting 3.5 s (1.5 s preceding and 2 s following CS presentation). Analyses in the frequency domain were carried out in accordance with the following frequency bands: delta (1-5 Hz), theta (5-12 Hz), beta (12-35 Hz), low gamma (35-50 Hz), and high gamma (50-100 Hz). The processing of LFP recordings both in the frequency domain by means of fast Fourier transforms (FFT) and in the time-frequency domain by means of multitaper Fourier transforms (mTFT) were carried out using homemade programs (Jurado-Parras et al., 2013; Fernández-Lamo et al., 2016) written in the MATLAB platform (version 9.4, R2018a. The MathWorks, Natick, MA, USA) and customized scripts of Chronux software (versions 2.11/R2014 and 2.12/R2018. Website: http://chronux.org/; Mitra and Bokil, 2008; Bokil et al., 2010; **Figs. 4.19** and **4.20**).

Probability maps (**Fig. 4.21**) for the comparison of pairs of spectrograms were generated following previous descriptions by our group (Fernández-Lamo et al., 2016). These maps enabled us to locate the significant differences between LFP recordings in the time-frequency plane. In addition, to assess the putative spectral couplings between different oscillatory activities from LFP recordings, the cross-frequency correlation (Masimore et al., 2004) as a measure of comodulation and the power-power spectral ratios were calculated (see Reus-Garcia et al, 2021).

3.8.4. Ex. 3 - Analysis of the CRs of vINSIST-infected rabbits

For the qualitative analysis of the EMG activity, a CR was understood as the presence, during the CS-US period, of EMG activity of the left O.O. muscle lasting > 10 ms and initiated > 50 ms after CS onset (Gruart et al., 2000). The number of CRs was counted for each rabbit (n = 8), animal group (n = 2), and session (n = 10, two of habituation and eight of conditioning) to obtain the corresponding learning curves (see **Fig. 4.25**). In addition, a quantitative analysis of cumulative areas under the rectified O.O EMG (in mV × s) was performed during the CS-US interval (corresponding to the CR) and during the 250 ms following it (corresponding to the UR) (see Results section). The evolution of the rectified O.O. EMG activity across different sessions for the two groups of animals is represented in **Fig. 4.26**.

3.8.5. Statistical analysis

Statistical analyses for all the measured physiological parameters were carried out using the Sigma Plot 11.0 package (Sigma Plot, San Jose, CA, USA), the Statistics MATLAB Toolbox for Windows (version 9.4, R2018a. The MathWorks, Natick, MA, USA), and customized mini-packages of Chronux (Mitra and Bokil, 2008; Bokil et al., 2010) for the jackknifed estimates of the variance and of Z-statistics.

For multivariate statistics assessments, both parametric (Fisher ANOVA F-tests, without or with repeated measures) and non-parametric [ANOVA tests on ranks, without repeated measures (Kruskal-Wallis ANOVA)] methods were used to assess the statistical significance of differences between groups, followed by the appropriate test (Holm-Sidak, Tukey-Kramer, or Student-Newman-Keuls tests, in this order of priority when the group sizes are equal; and Dunn's test when the sizes are different) for all the pairwise multiple-comparison analyses (Jurado-Parras et al., 2013; Fernández-Lamo et al., 2016), for a predetermined statistical significance level of $P < 0.05$.

When the normality (Shapiro-Wilk test) and equal variance of the errors (Levene Median test) assumptions were satisfied, the significance (P-value) and the statistic $F(m-1, l-m)$, with its corresponding orders m (number of groups) and l (number of multivariate observations), were reported. When the normality assumption was not verified, the significance (P -value) of the Chi-square ($\chi 2$) was calculated using the ranks of the data rather than their numeric values. Unless otherwise indicated, data are represented by the mean ± SEM (standard error of the mean). For all the statistical tests, the significance level (P-value) is indicated. It is common to declare a result significant if the estimated P-value is < 0.05 (*), < 0.01 (**), or < 0.001 (***).

Spike2 (version 7, CED, UK) and MATLAB (version 9.4, The MathWorks, Natick, MA, USA) also enabled quantifying the following physiological parameters: [1] the percentage of recorded neurons (in %) from the different groups (n = 3; types A, B, and C) classified according to their firing rates (in spikes/s), [2] the corresponding integrated firing rate [in (spikes/s) × s], and [3] the rectified O.O. EMG areas (in mV × s) (Caro-Martín et al., 2015; Ammann et al., 2016).

Linear and nonlinear regression analyses for the trend of the parameter 1 through training sessions [i.e., recorded neurons (in %) vs. sessions (in days); see **Fig. 4.11** and **Table 4.4**, in Results section], and also between the parameters 2 and 3 [i.e., EMG area vs. Integrated firing rate] (see **Figs. 4.13** and **4.14**, and **Table 4.6**, in Results section),

allowed us to report the correlation coefficient (r), the corresponding P-value, and the fit equation coefficients, all of them as measures of the relationships (linear or not) between the CL kinetic neural commands and the eyelid kinematics during classical eyeblink conditioning. In a similar way, the regression analysis between the percentage of CRs and the latency of the neuronal response to CS presentation was reported (see **Fig. 4.15** and **Table 4.6**).

4. RESULTS

4.1. Ex. 1 - Location and identification of claustral neurons

Because of its substantial connectivity with the MC, CC, and mPFC (Kowiański et al., 1998; Majak et al., 2000; Smith and Alloway, 2010; Mathur, 2014; White et al., 2018; Smith et al., 2019) and its significantly larger size, the rostral and central portion of the dorsal CL was targeted for electrophysiological recordings. In accordance with Kowiański et al. (1998), in rabbits this region corresponds to somatosensory and motor protection zones, and perhaps includes the auditory and PFC projection zones of the CL. The recording area was initially approached using available stereotaxic coordinates (Girgis and Shih-Chang, 1981).

Small electrolytic lesions made with tungsten electrodes at the end of the recording sessions indicated that most neurons examined were located in the dorsal part of the rostral CL. These lesions, as well as stereotaxic coordinates, indicated the location of the CL neurons (n = 315) included in this study (**Fig. 4.1**). These neurons formed a cell column (AP = 0-3 mm; L: 5.5-6.25 mm) between the striatum and the insular cortex. (Note that the rabbit CL can be up to 1 mm thick; Girgis and Shih-Chang, 1981; Kowiański et al., 1999).

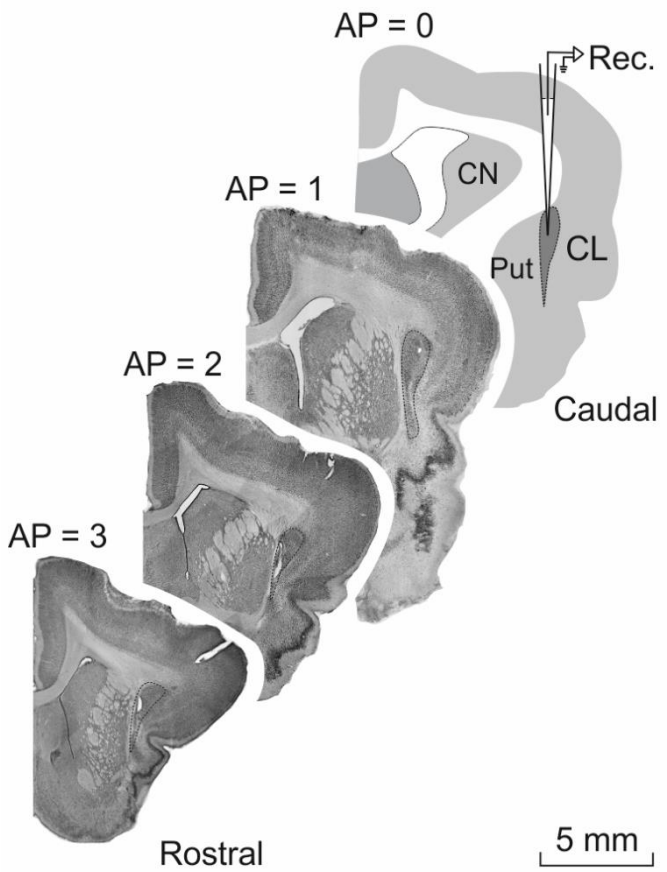

Figure 4.1. Diagram of recording sites and images from targeted CL in four anteroposterior sections. The activity of CL neurons was recorded with glass micropipettes from rostral and central parts of the right dorsal CL (dotted area). Drawing in AP = 0 follows the atlas of Girgis and Shih-Chang (1981); CN, caudate nucleus; Put, putamen.

CL neurons were identified by their orthodromic (i.e., synaptic) activation following stimulation of the MC or the mPFC. Occasionally CL neurons were also activated when the rCC or cCC were stimulated. Synaptic and/or antidromic activation was recorded when stimulating MC, mPFC, or CC in 81.9% (258/315) of the cases (**Table 4.1**). In the absence of conditioning stimuli, the spontaneous activity of CL neurons (n = 315 neurons from 7 rabbits) exhibited irregular firing at low rates (5-15 Hz).

Table 4.1 Electrical stimulation from cortex (MC, mPFC, and CC) to CL.

		SYNAPTIC activation		ANTIDROMIC activation	
MC (AP = 2)	Ipsilateral	186/278	66.90%	29/186	15.59%
	Contralateral	99/251	39.44%	6/99	6.06%
mPFC (AP = 11)	Ipsilateral	18/179	10.06%	0/18	0%
	Contralateral	13/142	9.15%	0/13	0%
CC (AP = 4 or 0)	Ipsi. Rostral	11/25	44.00%	1/11	9.10%
	Ipsi. Caudal	8/25	32.00%	1/8	12.50%

Electrical stimulation of the two MCs evoked both early (≈10 ms) and late (≈150 ms) activation of most CL neurons (contralateral: 39.4%; ipsilateral: 66.9%), including an intermediate period of low activity (**Fig. 4.3**). Repeated MC stimulation (at 0.1 Hz) increased the mean firing rate of CL neurons (to 50 spikes/s) for ≈ 300 ms following the low-activity period. CL neurons were also antidromically activated from the ipsilateral MC (15.6%) with the help of the collision test (see Materials and Methods and **Fig. 4.2**). Mean activation latencies were 3.12 ± 0.13 ms (mean ± SEM; n = 20; range: 2.02-4.53 ms). Additional support for the antidromic nature of spike activation was that it followed stimulation frequencies of up to 300 Hz.

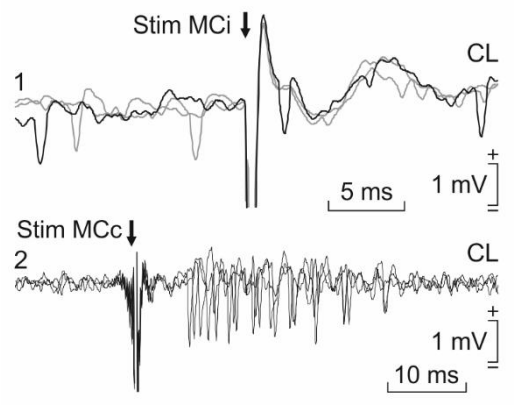

Figure 4.2. Collision test. Three superimposed recordings illustrating a CL neuron antidromically activated from the ipsilateral MC during the spike-triggered collision test (1). (2) illustrates the synaptic activation of a representative CL neuron from the contralateral MC.

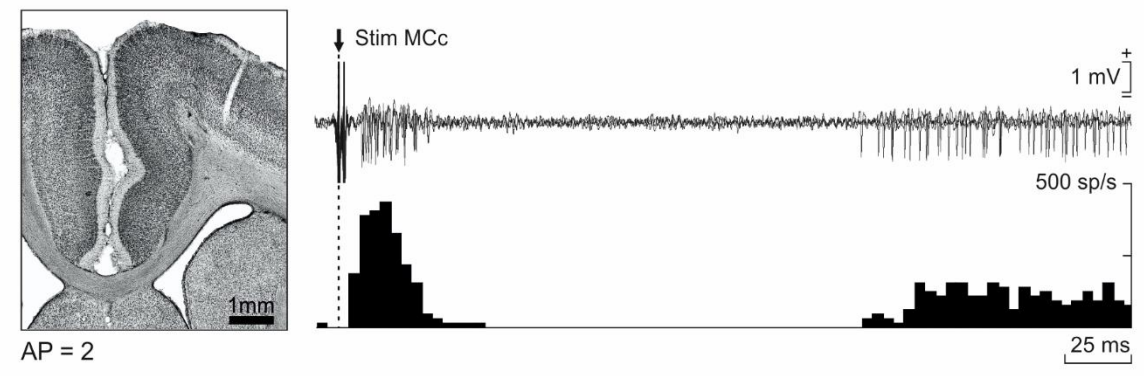

Figure 4.3. Photomicrograph of coronal section illustrating the location of stimulating electrodes in MC (AP = 2). Next to it, three overlapped recordings illustrating short- and long-term synaptic activation of a CL neuron activated from the ipsilateral MC. Below the recordings, the peristimulus time histogram of 15 recordings is illustrated.

Electrical stimulation of the mPFC preferentially activated neurons located deeper in the CL (contralateral: 9.15%; ipsilateral: 10.06%). The responses of these neurons were similar to the responses to MC stimulation —brief and late excitation separated by a silent period; **Fig. 4.3**)— but response latency was longer and the increase in firing rate was smaller (to 25 spikes/s) (**Fig. 4.4**).

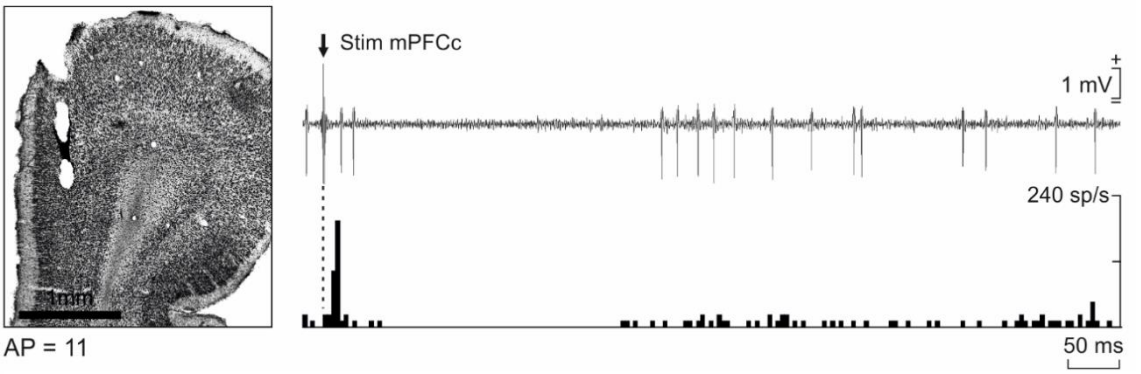

Figure 4.4. Photomicrograph of coronal section illustrating the location of stimulating electrodes in mPFC (AP = 11). Next to it, three overlapped recordings illustrating short- and long-term synaptic activation of a CL neuron activated from the ipsilateral mPFC. Below the recordings, the peristimulus time histogram of 15 recordings is illustrated.

Almost half (44%) of the CL neurons responded to stimulation of the ipsilateral rCC (AP = 4 mm) (**Fig. 4.5**), while 32% responded to stimulation of the ipsilateral cCC (AP = 0 mm). These CL neurons were also activated antidromically after stimulation in rCC (9.1%) and cCC (12.5%), showing the bidirectional projections between the CL and the CC (Chia et al., 2020).

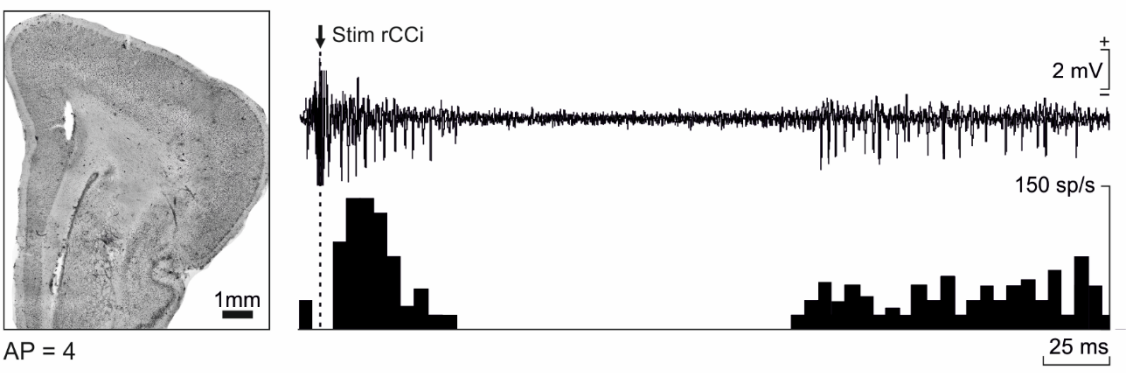

Figure 4.5. Photomicrograph of coronal section illustrating the location of stimulating electrodes in rCC (AP = 4). Next to it, three overlapped recordings illustrating short- and long-term synaptic activation of a CL neuron activated from the ipsilateral rostral CC. Below the recordings, the peristimulus time histogram of 15 recordings is illustrated.

Finally, as previously reported (Ammann et al., 2016), the MC area that we stimulated was clearly related to eyelid movements: stimulation there (twin pulses separated by a 2 ms interval) evoked short-latency activation (16.6 ± 0.4 ms; range 15.1-18.7 ms) of the contralateral O.O. muscle (**Fig. 4.6**). In contrast, applying similar stimuli to the CL, mPFC, rCC or cCC, did not activate this muscle.

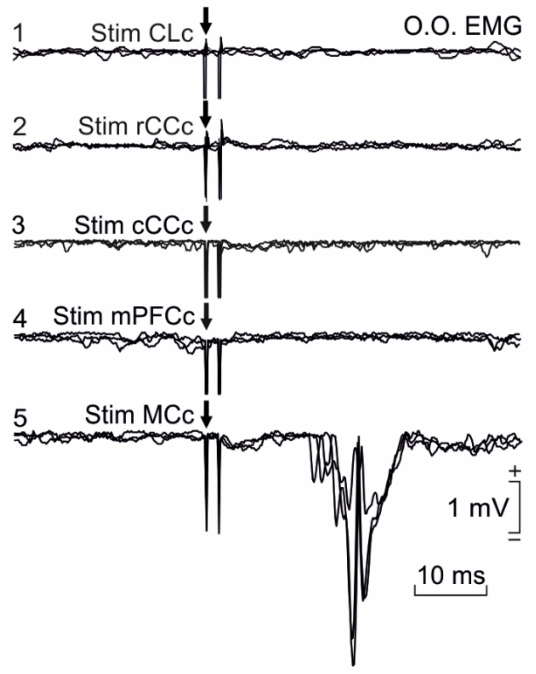

Figure 4.6. Effect of cortical stimulation in O.O. EMG. From top to bottom are illustrated the EMG activity evoked in the left O.O. muscle by double pulses (2 ms interval) applied to contralateral CL (1), rCC (2), cCC (3), mPFC (4), and MC (5).

4.2. Ex. 1 - Firing activity of claustral neurons during eyeblink conditioning

We next examined the activity of CL neurons during classical eyeblink conditioning. To produce eyeblink conditioning, animals were presented with a CS (tone) that was followed 250 ms later by the US, a 100 ms air puff onto the left cornea. The activity of CL neurons was recorded for two habituation sessions (where only the CS was presented) and eight conditioning sessions where the CS and US were paired (n = 5 rabbits), or six pseudoconditioning sessions where the CS and US were randomized (n = 2 rabbits). The mean learning curves of conditioned and pseudoconditioned animals are illustrated below (**Fig. 4.7**).

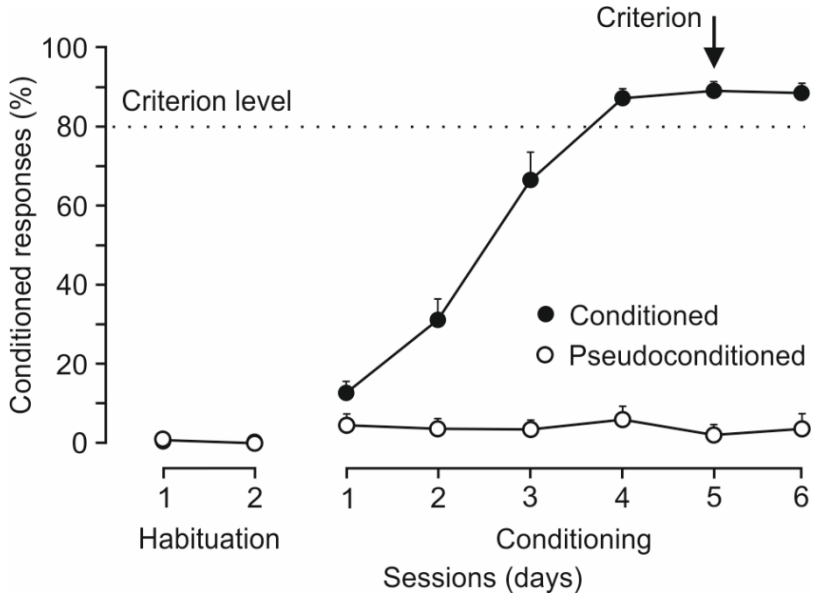

Figure 4.7. Mean learning curves of conditioned and pseudoconditioned animals. Evolution of the percentage of CRs across six conditioning sessions for five conditioned and two pseudoconditioned rabbits. Note that conditioned animals reached the selected criterion (≥ 80% of CRs for two consecutive days) by the 5th conditioning session.

Although the CR of conditioned animals reached the criterion level by the 5th session, training was maintained up to the 8th session. This allowed us to measure neuronal activity both during the acquisition process and after learning was established. Our acquisition values were similar to those previously observed in rabbits when using the same delay conditioning paradigm and recording characteristics (Gruart et al., 2000a; Leal-Campanario et al., 2007; Caro-Martín et al., 2015; Ammann et al., 2016).

Three different types of CL neuron (A-C, summarized in **Table 4.2**) could be distinguished by their different responses during presentation of paired CS/US stimuli.

The following analysis includes only neurons whose activity was recorded for ≥ 8 trials during conditioning (n = 130 neurons from 5 rabbits) or pseudoconditioning sessions (n = 47 neurons from 2 rabbits). All the selected neurons were also activated by at least one of the stimulating electrodes placed in MC, mPFC, and/or CC, which allowed us to use the procedures described above to determine that they were within the CL.

Table 4.2. Characteristics of the activity recorded from the different types of neuron as a response to the CS/US presentations.

Neuron type	Nº	Baseline firing rate (spikes/s)	Change in firing rate (%)	Change onset (ms after CS)	Change ending (ms after CS)	Change duration (ms from onset)	Peak activity (ms after CS)
Type A	59	15-20	+ 293.02 ± 29.56	175.5 ± 11.5	650.0 ± 35.2	476.8 ± 33.5	380 ± 39.5
Type B	16	20-30	- 59.59 ± 5.82	60.0 ± 18.7	266.3 ± 25.2	206.3 ± 21.8	-
Type C	55	20-30	No change	-	-	-	-

4.2.1. Type A: Activated neurons

Type A neurons recorded during conditioning sessions (n = 59) were characterized by a > 30% increase in their firing rate in response to CS/US presentations (**Fig. 4.8**). In the absence of the paired stimuli, type A neurons fired at an irregular, low rate (15-20 spikes/s). Type A neurons were rarely activated during single-stimulus presentation of any sensory modality (including the CS and US, but also different tones and light flashes). The mean firing rate of type A neurons increased by 293 ± 29.6% over baseline values measured immediately before CS presentation [H = 50.900 with one degree of freedom; P < 0.001; Kruskal-Wallis one-way ANOVA on ranks]. Activation of these neurons occurred 175.6 ± 11.5 ms (n = 57; range 50–430 ms) after the CS, well after the start of CRs (mean 156.7 ± 13.8 ms; range 76–231 ms). CL neuron activity lasted for 477 ± 33.5 ms, which is much longer than the CS+US interval. In addition, the activity of type A neurons occurred slightly after presentation of the CS/US, with a mean time to peak of 380 ± 39.5 ms after the CS onset.

Figure 4.8 illustrates the activity of two type A neurons recorded from a well-trained animal during the 5th conditioning session. The first one (**A**) was activated 164 ms after CR initiation, which occurred 129 ms after CS onset. The firing of this neuron increased steadily, increasing by a mean value of 330% compared with its baseline [$F_{(1,8)}$ = 58.533; $P < 0.001$; one-way ANOVA *F*-test], and persisted > 600 ms beyond the end of the US. The activity of this cell peaked just before US presentation, at 229 ms after the CS, and reached a maximum rate of ≈ 50 spikes/s. In contrast, the other type A neuron (**B**) increased its firing rate almost at the same time as CR onset (≈ 160 ms after the CS) but also reached its peak firing rate before the US (208 ms). The increase in firing rate (594% more than its baseline) extended beyond the end of the US by > 600 ms [$F_{(1,8)}$ = 80.365; $P < 0.001$; one-way ANOVA *F*-test].

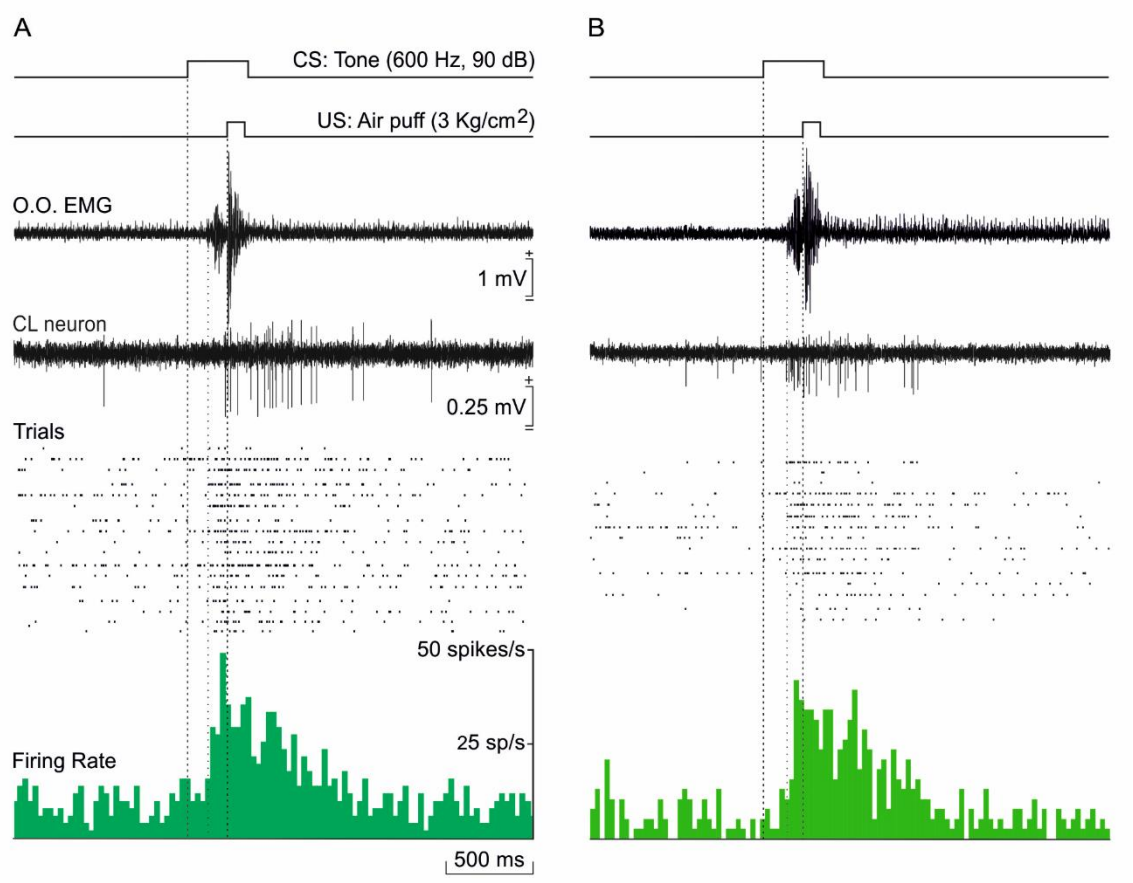

Figure 4.8. Examples of two type A neurons, activated in advance of US onset, and recorded during the 5th conditioning session. ***A,*** Representation of the delay paradigm and the firing activity of a selected CL neuron. From top to bottom are shown: (1) the CS (a tone; 600 Hz, 90 dB, 350 ms); (2) the US (a corneal air puff; 3 kg/cm^2, 100 ms); (3) one example of the EMG activity of the O.O. muscle; (4) the firing activity of a CL neuron during a CS/US presentation; (5) a raster plot of 15-20 successive CS/US trials; and (6) the peristimulus time histogram of all of them (in spikes/s). ***B,*** Another example of a selected type A neuron. Traces illustrated from top to bottom and calibrations in ***A*** are also for ***B***.

4.2.2. Type B: Inhibited neurons

Type B neurons (n = 16) exhibited a ≥ 30% decrease in their firing rate in response to CS/US presentation during conditioning. In the absence of paired stimuli, type B neurons had irregular spontaneous firing, with a mean rate of 20-30 spikes/s), which was 133-150% higher than that of type A neurons. As already described for type A neurons, type B cells rarely responded during presentation of a CS or a US alone. The mean firing rate of type B neurons decreased by 59.6 ± 5.8% compared with baseline values [H = 38.434 with one degree of freedom; P < 0.001; Kruskal-Wallis one-way ANOVA on ranks]. This inhibition of type B neuron activity occurred from 60.0 ± 18.7 ms to 266.7 ± 25.2 ms after CS presentation, typically during the CS-US interval; hence, their response occurred before the mean time of CR initiation (156.7 ± 13.8; range 76–231 ms). **Figure 4.9** illustrates the response of a type B neuron recorded from a well-trained animal during the 8th conditioning session. This neuron was inhibited 65 ms following CS presentation, well before CR onset (111 ms after the CS), and recovered back to baseline levels of activity by ≈ 250 ms after the CS; i.e., at the time of US presentation. The activity of this neuron decreased by 79.2% during the 185 ms that the inhibitory response occurred [$F_{(1,7)}$ = 62.395; P < 0.001; one-way ANOVA F-test].

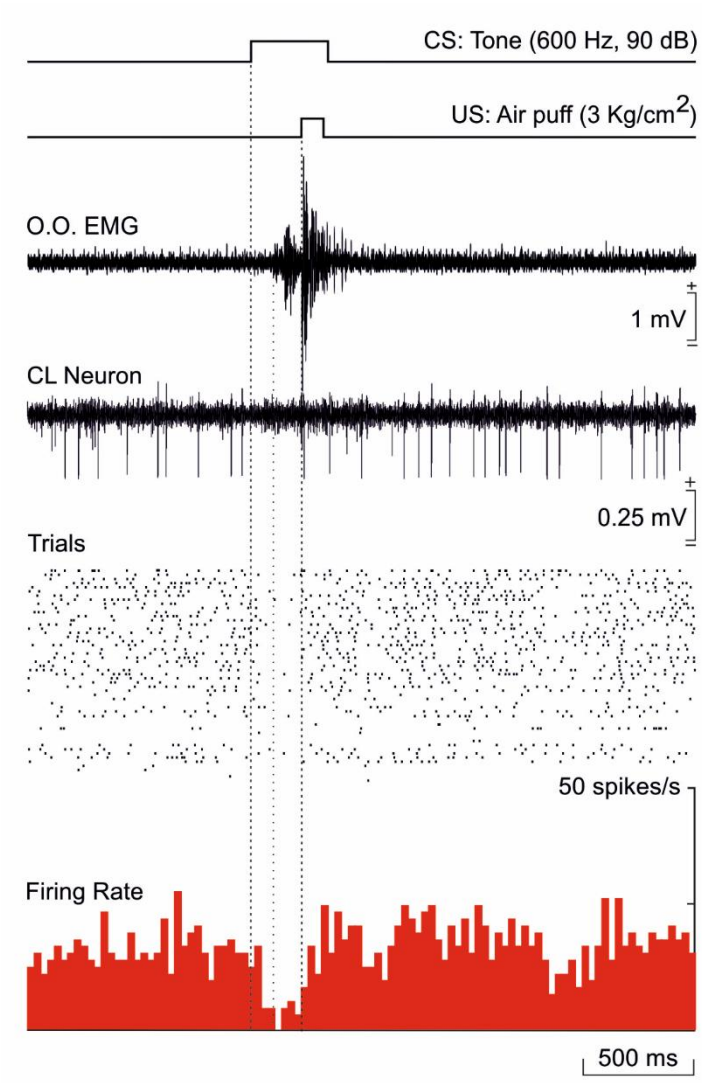

Figure 4.9. Example of a type B neuron inhibited well in advance of the beginning of the CR and recorded during the 8th conditioning session. Representation of the delay paradigm and the firing activity of a selected type B CL neuron. Traces illustrated from top to bottom as in **Fig. 4.8.**

4.2.3. Type C: Non-related neurons

The activity of type C neurons (n = 55) recorded during conditioning was irregular, with a firing rate of 20-30 spikes/s. The activity of these cells was not affected by any stimulus present in the recording room, including the paired CS/US presentation or the presentation of CS or US alone [H = 0.678 with one degree of freedom; P = 0.41; Kruskal-Wallis one-way ANOVA on ranks]. An example of the activity of a type C cell is shown in **Figure 4.10**. This neuron did not change its firing rate in response to CS/US presentation; its baseline activity, measured 500 ms before CS onset, was very similar to that 500 ms after the CS (25.74 and 26.50 spikes/s respectively) [$F_{(1,8)}$ = 0.127; P = 0.731; one-way ANOVA F-test].

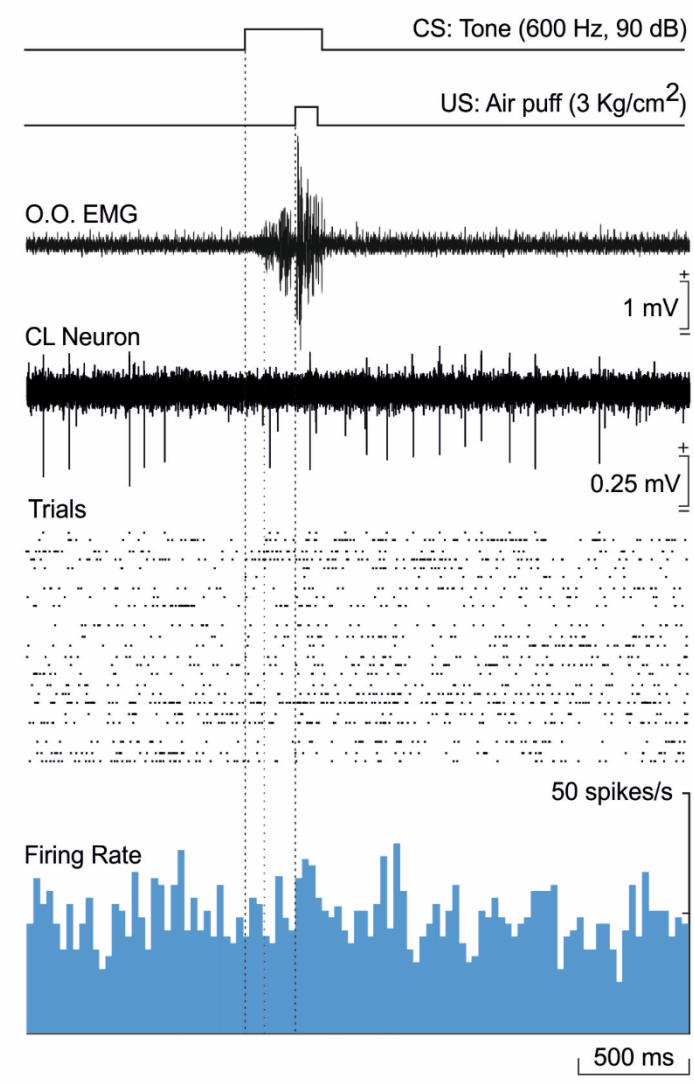

Figure 4.10. Example of a type C neuron, unrelated to the classical conditioning task, and recorded during the 3rd conditioning session. Representation of the delay paradigm and the firing activity of a selected type C CL neuron. Traces illustrated from top to bottom as in **Fig. 4.8.**

4.2.4. Number of type A, B and C neurons during eyeblink conditioning and pseudoconditioning

Remarkably, the relative abundance of these three types of neuron changed across habituation and conditioning sessions, but not during pseudoconditioning.

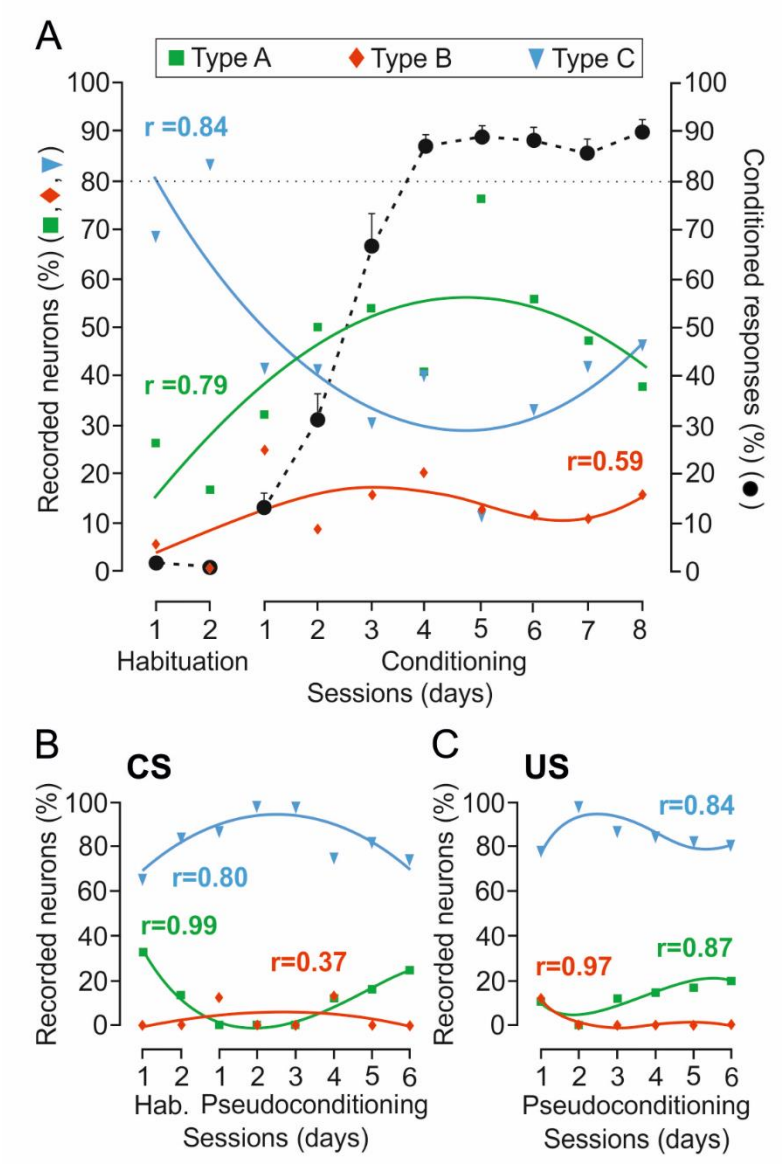

Figure 4.11. ***A,*** Percentages of claustral neurons (n = 130 from n = 5 rabbits) activated by (green squares and lines), inhibited by (red diamonds and lines), or unrelated to (blue triangles and lines) the CS and/or the US in habituation and eight conditioning sessions. The black dotted line indicates the learning curve. ***B-C***, Percentages of CL neurons activated by, inhibited by, or unrelated to CS (n = 47 from n = 2 rabbits; ***B***) or US (n = 40 from n = 2 rabbits; ***C***) presentations during habituation and six pseudoconditioning sessions. Collected neuronal data in ***A-C*** were best represented with quadratic or higher-order polynomial fits. The regression coefficients (r) for the illustrated polynomial fits are indicated. The statistical performance was calculated according to the confidence interval (95%, $P < 0.05$)

During the 1st and 2nd habituation sessions, type C neurons represented 68.4% and 83.3% of recorded cells respectively, while type A neurons were only 26.3% and 16.7%, and type B less than 5% (**Fig. 4.11*A***). During the first five conditioning sessions (pre-learning and learning phase, up until rabbits reached the selected criterion), these percentages changed notably for type A and C neurons. The number of type A neurons increased, reaching its highest value during the 5th conditioning session to become 76.5% of all cells. At the same time, the number of type C neurons decreased to 11.8%. After the percentage of CRs reached asymptotic values, this trend reversed, until type C neurons again became the most numerous (46.2%) compared with 38.5% for type A. The fraction of type B cells was relatively low and maintained constant values (mean 12.3 ± 2.26%, range 0-25%) across sessions, and no trend was detected.

In contrast, no changes were observed in the relative percentages of type A, B, and C neurons during pseudoconditioning (**Fig. 4.11*B*-*C***). In response to presentation of single CS, the percentage of the recorded type C neurons remained at high levels, while the percentages of type A and B neurons maintained low levels across training [**Fig. 4.11*B***, types A (10.6%), B (4.3%), and C (85.1%)]. Similar results were collected during presentation of single US [**Fig. 4.11*C***, types A (12.5%), B (2.5%), and C (85%); **Table 4.3**].

Table 4.3 Number of neurons whose activity was recorded during conditioning (CS/US) and pseudoconditioning (single CS and single US).

Conditioning	**H1**	**H2**	**C1**	**C2**	**C3**	**C4**	**C5**	**C6**	**C7**	**C8**	**Total**
Type A	5/19	1/6	4/12	6/12	7/13	4/10	13/17	5/9	9/19	5/13	59/130
Type B	1/19	0/6	3/15	1/12	2/13	2/10	2/17	1/9	2/19	2/13	16/130
Type C	13/19	5/6	5/12	5/12	4/13	4/10	2/17	3/9	8/19	6/13	55/130
Pseudo. - CS	**H1**	**H2**	**P1**	**P2**	**P3**	**P4**	**P5**	**P6**	**-**	**-**	**Total**
Type A	1/3	1/7	0/8	0/4	0/7	1/8	1/6	1/4			5/47
Type B	0/3	0/7	1/8	0/4	0/7	1/8	0/6	0/4			2/47
Type C	2/3	6/7	7/8	4/4	7/7	6/8	5/6	3/4			40/47
Pseudo. - US	**-**	**-**	**P1**	**P2**	**P3**	**P4**	**P5**	**P6**	**-**	**-**	**Total**
Type A			1/9	0/5	1/8	1/7	1/6	1/5			5/40
Type B			1/9	0/5	0/8	0/7	0/6	0/5			1/40
Type C			7/9	5/5	7/8	6/7	5/6	4/5			34/40

The evolution in the relative percentage of types A (green), B (red), and C (blue) neurons across training was best represented with quadratic or higher-order polynomial fits shown in the table below (**Table 4.4**).

Table 4.4. Polynomial fits for the types of neuron recorded during conditioning (CS/US) and pseudoconditioning (single CS and single US).

Stimulus	**Neuron type**	**Nº**	**Polynomial fits**	**r**	***P***
Paired **CS/US**	Type A	59/130	$y = - 1.2x^2 + 17x - 0.14$	0.79	< 0.05
	Type B	16/130	$y = 0.033x^4 - 0.6x^3 + 3x^2 - 0.86x + 2$	0.59	< 0.05
	Type C	55/130	$y = 1.6x^2 - 21x + 99$	0.84	< 0.05
Single **CS**	Type A	5/47	$y = - 0.4x^3 + 7.8x^2 - 42x + 69$	0.99	< 0.05
	Type B	2/47	$y = - 2.7e\text{-}16x^3 - 0.45x^2 - 4x - 3.6$	0.37	< 0.05
	Type C	40/47	$y = - 1.9x^2 + 18x + 54$	0.80	< 0.05
Single **US**	Type A	5/40	$y = - 0.74x^3 + 8.3x^2 - 25x + 27$	0.87	< 0.05
	Type B	1/40	$y = - 0.51x^3 + 6.4x^2 - 25x + 30$	0.97	< 0.05
	Type C	34/40	$y = 1.2x^3 - 15x^2 - 49x + 44$	0.84	< 0.05

Taken together, recorded CL cells did not respond to single stimuli (even when presented at high intensities), as during pseudoconditioning. Type A neurons did respond with an increase of firing activity to the same stimuli when they were presented together (paired CS/US); in this situation, their percentage increased in conjunction with the development of CRs, until animals reached the learning criterion —i.e., when the acquisition phase was finished. The burst of activity presented by type A neurons followed the initiation of CRs. In contrast, type B neurons decreased their activity during the CS-US interval, but the number of recorded units remained low across sessions and no particular evolution was observed. Their inhibition preceded CR onset. Interestingly, the number of recorded neurons not related to CS and US presentations (type C) decreased during the first conditioning sessions until animals reached criterion. This suggests a recruitment of type A CL neurons, at the expense of type C cells, during CR acquisition.

4.2.5. Firing rate profiles and spike duration study

It is well known that in many brain regions, projecting neurons and interneurons differ in their intrinsic electrical properties (McCormick et al., 1985). Because firing rate profiles and spike durations vary between pyramidal cells and interneurons (Buzsáki and Kandel, 1998; Csicsvari et al., 1999; Constantinidis and Goldman-Rakic, 2002; Barthó et

al., 2004; Viskontas et al., 2007), these two criteria were used to determine whether the three types of CL neuron are principal cells (projecting neurons) or non-principal cells (putative interneurons). Following the analytical procedures detailed in the Materials and Methods section (**Fig. 3.10**), no significant differences ($P > 0.05$) were observed between the durations of spikes recorded from type A and type C neurons.

In contrast, the spikes of type B neurons were shorter in duration (0.88 ± 0.01, range 0.80–0.92 ms) than those of type A neurons (1.04 ± 0.01, range 0.94–1.09 ms). These mean spike duration values are significantly different [$H = 16.26$ with one degree of freedom; $P < 0.001$; Kruskal-Wallis one-way ANOVA on ranks] for these two cell types.

Table 4.5. Summary of the statistical analyses for spike durations (in ms) computed from type A (n = 13) and type B (n = 10) CL neurons. Data were collected from epochs of 3 s in CL recordings. Abbreviations: STD (standard deviation); SEM (standard error of the mean).

Type A	**Size**	**Mean**	**STD**	**SEM**	**Min.**	**Max.**	**Median**	**25%**	**75%**
ACT1	62	1.0540	0.1620	0.0206	0.6000	1.4800	1.0400	0.9600	1.0400
ACT2	56	1.0720	0.1730	0.0232	0.6000	1.4800	1.0400	0.9600	1.1600
ACT3	33	1.0760	0.1620	0.0282	0.7200	1.4800	1.0400	0.9600	1.2000
ACT4	23	1.0730	0.1900	0.0397	0.7200	1.4400	1.0400	0.9300	1.2400
ACT5	41	1.0210	0.1250	0.0196	0.8000	1.4000	1.0000	0.9200	1.0800
ACT6	72	1.0730	0.1740	0.0205	0.8400	1.4800	1.0400	0.9400	1.2000
ACT7	37	1.0520	0.1570	0.0258	0.8800	1.4800	1.0400	0.9500	1.0400
ACT8	83	0.9900	0.1120	0.0123	0.8000	1.3600	1.0000	0.8900	1.0400
ACT9	60	1.0190	0.1730	0.0223	0.2400	1.4800	1.0400	0.9600	1.0400
ACT10	79	1.0920	0.1640	0.0184	0.7600	1.4800	1.0800	0.9600	1.2400
ACT11	91	1.0800	0.2040	0.0213	0.5600	1.4800	1.0400	0.9200	1.2700
ACT12	61	0.9530	0.1500	0.0192	0.7200	1.4400	0.8800	0.8400	1.0400
ACT13	85	0.9360	0.1960	0.0213	0.1200	1.4800	0.8800	0.8300	1.0400
Type B	**Size**	**Mean**	**STD**	**SEM**	**Min.**	**Max.**	**Median**	**25%**	**75%**
INH1	36	0.8060	0.1280	0.0213	0.4800	1.0400	0.8400	0.7000	0.9200
INH2	19	0.9180	0.1510	0.0347	0.4400	1.0800	0.9200	0.8400	1.0400
INH3	19	0.8820	0.1470	0.0337	0.6000	1.1200	0.9200	0.7600	1.0000
INH4	33	0.9050	0.1400	0.0244	0.5200	1.0800	0.9200	0.8800	1.0000
INH5	39	0.8960	0.1150	0.0184	0.5600	1.0400	0.9200	0.8400	0.9600
INH6	69	0.8690	0.1670	0.0201	0.4800	1.4800	0.8400	0.7900	0.9600
INH7	70	0.8640	0.1700	0.0204	0.4400	1.3200	0.8800	0.7600	1.0000
INH8	78	0.8890	0.1390	0.0157	0.5600	1.2400	0.9200	0.8000	0.9600
INH9	49	0.9080	0.1930	0.0275	0.4800	1.4800	0.9200	0.8000	1.0400
INH10	19	0.9030	0.1390	0.0318	0.6000	1.4800	1.0400	0.8400	1.0400

These differences in spike duration, together with differences in their firing patterns suggest that type B neurons are CL interneurons (IN), while type A and type C cells are likely to be CL projection neurons (PN).

4.3. Ex. 1 - Changes in the firing rate of type A claustral neurons in relation to the development of conditioned responses (CRs) across conditioning

Frequently, CRs and the burst of activity of type A neurons happened simultaneously. In order to assess whether the activity of type A claustral neurons was related to the development of the conditioned responses, we examined the relationship between the firing of type A neurons during the acquisition process and the EMG activity of the left O.O. muscle collected during the same sessions and trials.

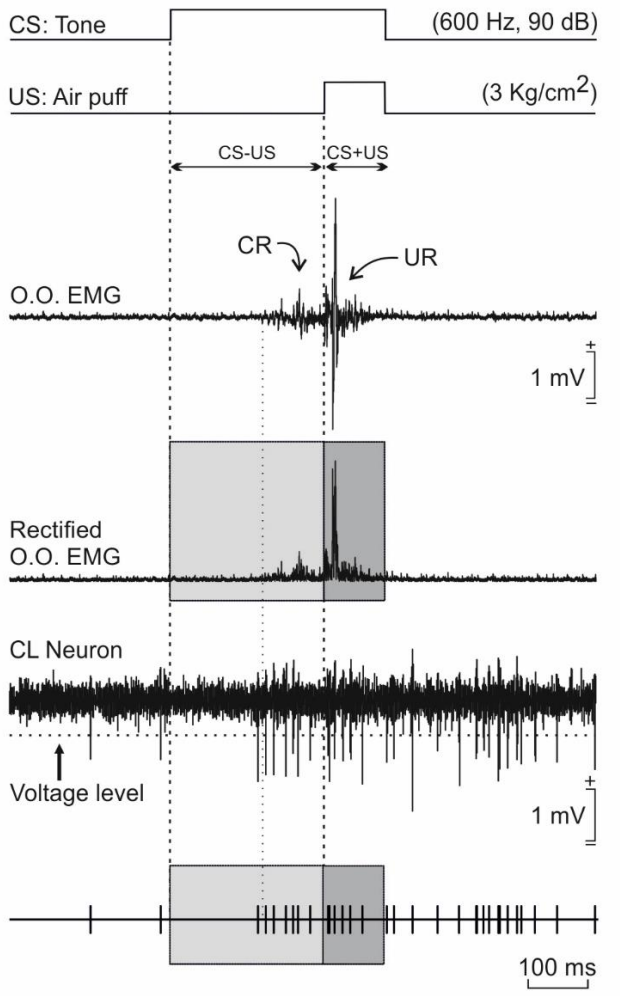

Figure 4.12. Relationship between changes in the firing rate of type A neurons and the EMG activity of the O.O. muscle and the percentage of CRs across conditioning. From top to bottom are shown: a representation of the conditioning stimuli, one example of the EMG activity of the O.O. muscle with its rectified version below, the firing activity of a type A CL neuron during a CS/US presentation, and a representation of action potentials reaching the selected voltage level. For these analyses, we quantified the EMG area (mV × s) vs. the integrated firing frequency [in (spikes/s) × s] during the CS-US period (light gray area) and also during CS+US interval (dark gray area) (n = 5 rabbits).

4.3.1. EMG area vs. integrated firing rate

Initially, we measured the integrated firing rate [in (spikes/s) × s] of type A neurons during the CS-US and CS+US periods and plotted it against the area (in mV × s) of the rectified EMG activity of the left O.O. muscle (n = 5 animals). We determined the relationships between these two variables in early (from 1st to 3rd) and late (from 4th to 8th) conditioning sessions.

As a first step, we analyzed the CS-US interval (**Fig. 4.13**), when CRs are expected to appear and learning is measurable, in early conditioning (1st to 3rd; weak and small CRs) and late conditioning (4th to 8th; strong and well-developed CRs).

Then, we studied the CS+US period (also in early and late conditioning; **Fig. 4.14**), when learning-nondependent responses appear (i.e., URs) —hence they are not expected to change across learning.

None of these four relationships exhibited a significant correlation ($r \geq 0.6$), indicating that the firing rate of type A neurons appears not to determine the magnitude of the O.O. muscle response.

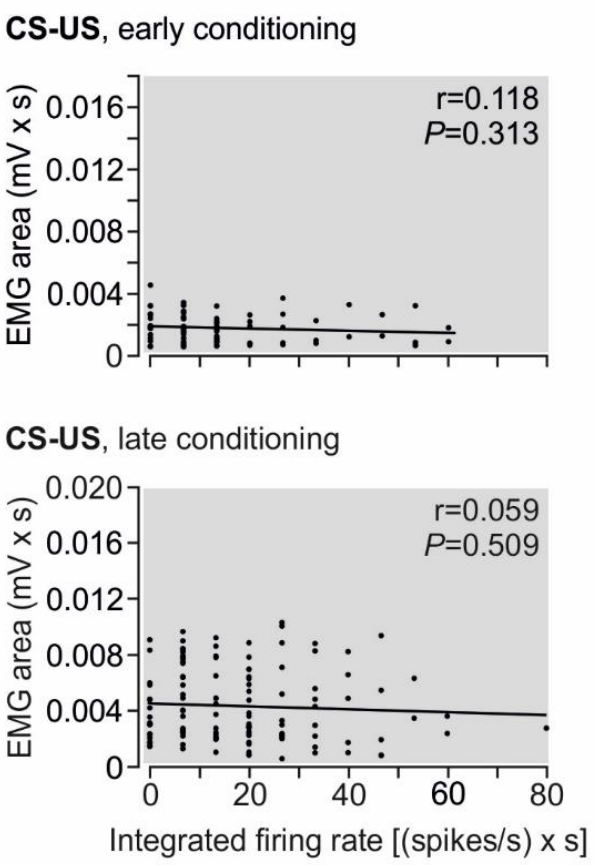

Figure 4.13. Linear relationships between the O.O. EMG area and the integrated firing frequency of type A neurons for the CS-US interval, first during early conditioning sessions (n = 75 trials from n = 17 neurons), and below, during late conditioning sessions (n = 127 trials from n = 25 neurons).

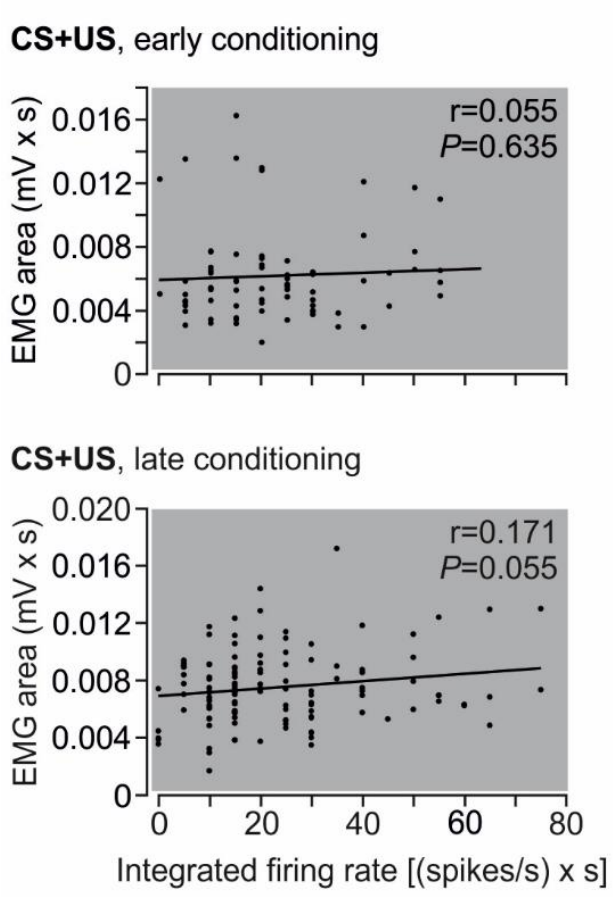

Figure 4.14. Linear relationships between the O.O. EMG area and the integrated firing frequency of type A neurons for the CS+US period, first during early conditioning sessions (n = 75 trials from n = 17 neurons), and below, during late conditioning sessions (n = 127 trials from n = 25 neurons).

4.3.2. Conditioned responses vs. latency of neuronal activation

Finally, it is well known that training reduces the latency of CRs relative to the time of CS presentation (see Gruart et al., 1995). If CL neuron activity is related to the development and/or expression of CRs, then the response of type A neurons in well-trained animals should occur earlier relative to CS onset. Accordingly, we checked whether the activation latency of type A neurons to CS presentation was inversely correlated to the percentage of CRs (**Fig. 4.15**). We found that there was no clear relationship (r = 0.097) between these two variables.

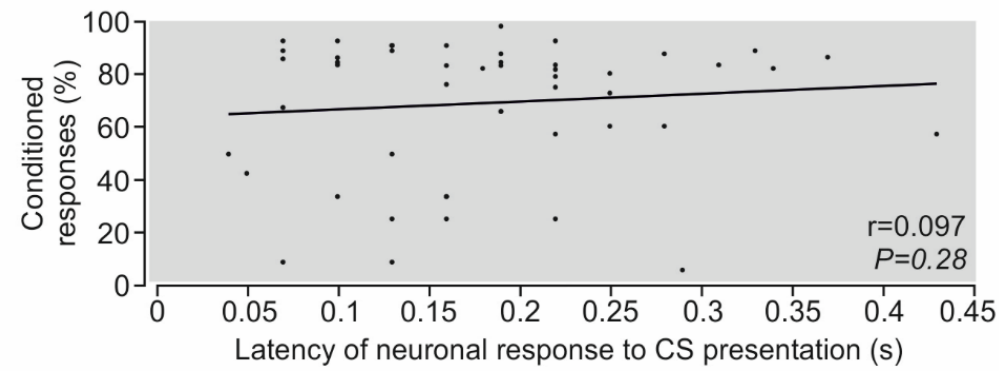

Figure 4.15. Relationship between the activation latency of type A neurons after CS presentations and the percentage of CRs (n = 51 neurons).

Taken together, these results (compiled in **Table 4.6**; note the low values of regression coefficients (r) for all the illustrated relationships) indicate that type A neurons are not responsible for changes in the CRs that occur during the acquisition process.

Table 4.6. Linear relationship between EMG area and type A neurons' firing rate.

Interval	Conditioning	Trials	Neurons	Equation	r	*P*
CS-US	Early	75	17	$y = -7*10^{-6} x + 0.0019$	$r_{(75,0.05)} = 0.118$	0.313
	Late	127	25	$y = -9*10^{-6} x + 0.0045$	$r_{(126,0.05)} = 0.059$	0.509
CS+US	Early	75	17	$y = 1*10^{-5} x + 0.0059$	$r_{(74,0.05)} = 0.055$	0.635
	Late	127	25	$y = 3*10^{-5} x + 0.0069$	$r_{(126,0.05)} = 0.171$	0.055
CRs vs. Activation latency			51	$y = 0.0318 x + 0.16$	$r_{(50,0.05)} = 0.097$	0.28

4.4. Ex. 2 - Analysis of Local Field Potentials recorded in CL, mPFC, and MC during classical eyeblink conditioning

During unitary recording sessions, we noticed the presence of specific changes in LFPs recorded in the CL across conditioning, particularly in the gamma band (**Fig. 4.16*B***; Cebolla and Cheron, 2019). In order to have consistent recordings of selected CL sites during all training sessions, we prepared four additional rabbits with chronically implanted tetrodes in the right CL. For comparative purposes, those animals were also chronically implanted with recording bipolar electrodes in mPFC and MC (**Fig. 4.17**; CC was excluded due to technical limitations). To avoid any distortion of LFP recordings, no electrical stimulation of the implanted sites was carried out in this group of animals.

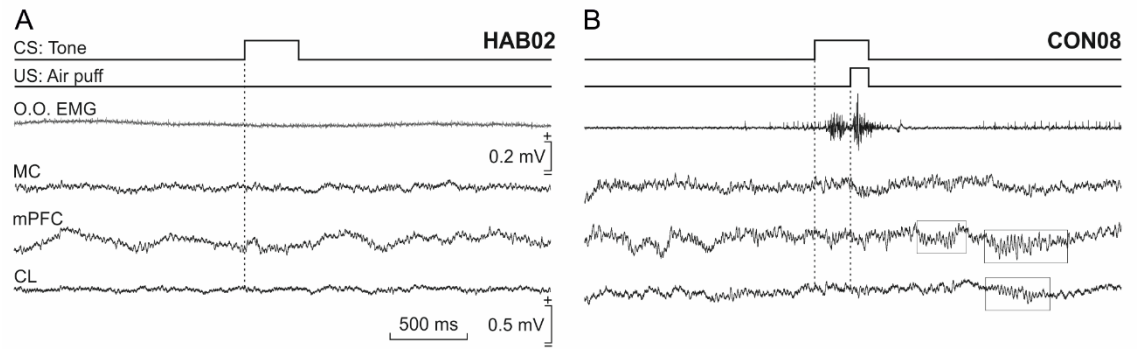

Figure 4.16. Recording of LFPs in CL, mPFC, and MC during classical eyeblink conditioning. ***A***, ***B***, From top to bottom are shown: the conditioning stimuli —a tone (600 Hz, 90 dB, 350 ms) as CS and an air puff (3 kg/cm^2, 100 ms) in the cornea as US, an example of the EMG activity of the O.O., and a representative example of LFPs recorded from the indicated sites (MC, mPFC, and CL) during the 2nd habituation (***A***) and 8th conditioning sessions (***B***); calibrations in ***A*** are also for ***B***. Note the high-frequency oscillation presented in mPFC and CL following the paired CS/US presentation during CON08.

Representative LFPs collected from CL, MC, and mPFC are shown above (**Fig. 4.16**). These examples exhibit frames of 3.5 s (from 1.5 s before to 2 s after CS presentations) taken from the 2nd habituation and the 8th conditioning sessions. It can be seen that conditioning increases LFP amplitudes in the three recording sites and evokes the presence of a high-frequency oscillation following the paired CS/US presentation in CL- and mPFC-recorded traces.

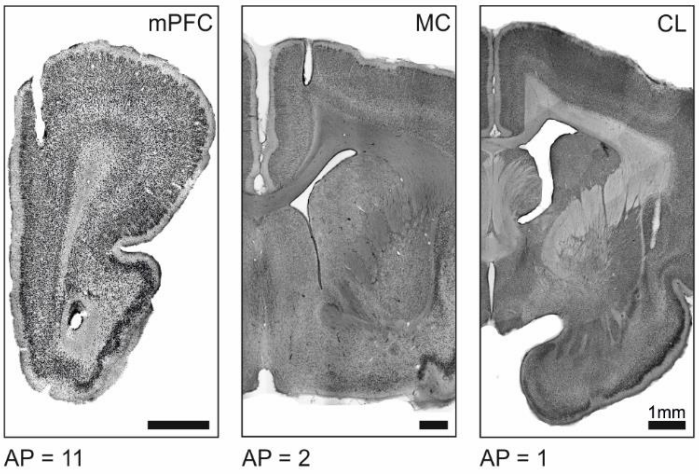

Figure 4.17. Photomicrographs of coronal sections illustrating the location of the LFP recording electrodes in mPFC, MC, and CL.

In the next section, we illustrate the spectral analysis of LFPs (in frames of 3.5 s, such as those shown in **Fig. 4.16**) recorded during baseline and the 2nd habituation session, and also during three conditioning sessions that represent different learning stages: PHASE I (before learning, < 12% of CRs, 5.95 ± 2.16%; mean ± SEM); PHASE II (during acquisition, ≈ 50% of CRs, 47.45 ± 2.93%); PHASE III (after learning, > 85%

of CRs, 94.27 ± 2.22%; **Fig. 4.18**). Time frames from PHASES I-III included the paired CS/US presentations, while habituation sessions included only the CS, and baseline sessions did not include any stimulus.

Those phases were defined following a previous study from our laboratory (Fernández-Lamo et al., 2018).

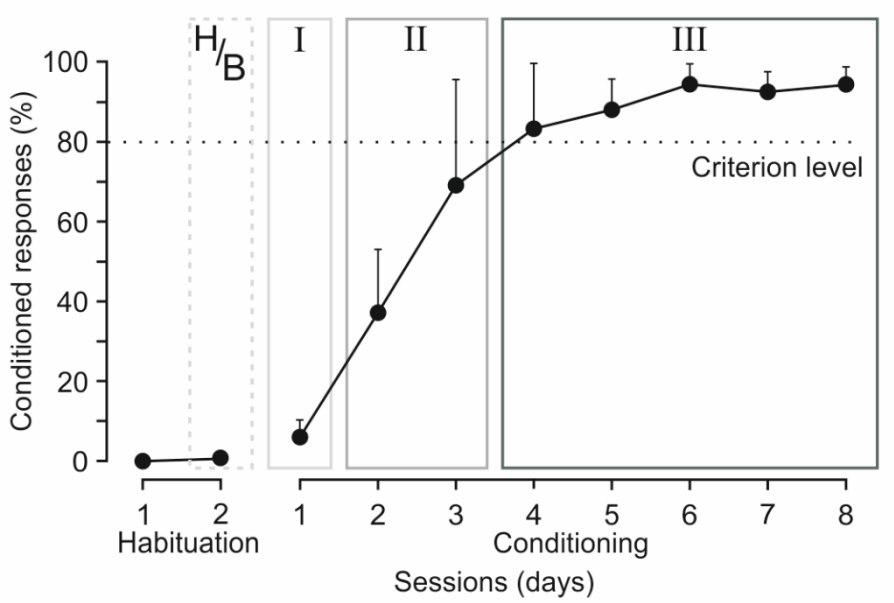

Figure 4.18. Evolution of the percentage of CRs across eight sessions (n = 4 rabbits). Different learning phases are indicated: PHASE I (< 12% of CRs; mostly, the 1st day of conditioning); PHASE II (20-70% of CRs, comprises the 2nd and/or the 3rd day of conditioning); PHASE III (> 85% of CRs; animals have reached the learning criterion, generally from the 4th conditioning session on). All the analyzed frames last 3.5 s. Habituation (H) and Baseline (B) frames were all taken from the 2nd habituation recording: Habituation frames started 1.5 s before the CS onset (hence, it is included) while Baseline frames started 10 s before the CS onset (thus they did not include any stimulus). PHASE I, II, and III frames were taken from the 1st, 2nd or 3rd (depending on each rabbit's performance) and the 8th conditioning sessions, respectively. All of them include the paired CS/US.

4.4.1. LFPs in the claustrum during eyeblink conditioning

Fig. 4.19 shows the results for the analysis of the LFP recordings carried out in the CL. As plotted in **Fig. 4.19*A, B***, baseline and habituation did not show any difference in the mean spectral power of the five selected bands [delta (1-5 Hz), theta (5-12 Hz), beta (12-35 Hz), low gamma (35-50 Hz), and high gamma (50-100 Hz)], whereas during the conditioning phases it increased significantly in all the frequency bands (Tukey-Kramer multiple comparison test: HAB02 and Baseline vs. PHASES I, II, and III; $P <$

0.001; ***). Although the fundamental contribution to the CL power spectrum was determined by delta and theta frequency bands, prominent (well-differentiated) power peaks appeared in delta and low gamma bands during PHASES I and III. Therefore, the resulting delta-gamma comodulation is also indicated in the figure.

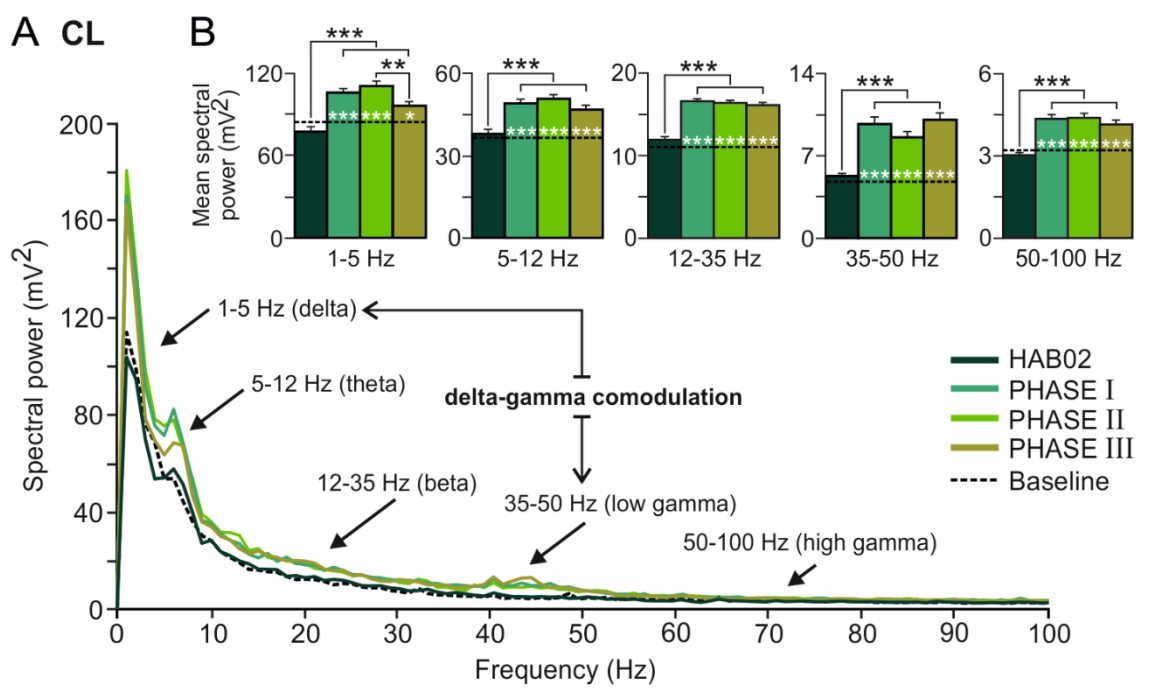

Figure 4.19. Spectral analyses of LFPs recorded in the CL during classical eyeblink conditioning. LFPs were recorded during habituation and conditioning phases (n = 4 rabbits). ***A***, Mean power spectra of LFPs recorded in the CL for 120 3.5 s frames (between 1.5 s before and 2 s after CS presentation) for four of the conditions (HAB02, PHASE I, PHASE II, and PHASE III) and for 3.5 s baseline frames (taken from HAB02 sessions but including no stimulus). The black arrows indicate the spectral ranges. ***B***, Histograms of mean spectral powers for all the defined frequency bands. Note that baseline values (dotted black line) were very similar to those collected during the presentation of the unpaired CS (HAB02) while the start of conditioning phases considerably increased the spectral powers in the five frequency bands.

Following Fernández-Lamo et al. (2016), for a more-precise dynamic analysis of spectral powers computed from LFPs, we selected moving time-windows of 500 ms (shifted in increments of 10 ms) and we calculated mTFT. Thus, time-frequency representations were computed for the 3.5 s LFP frames recorded in the CL for habituation and PHASE I, II, and III (**Fig. 4.20**). The illustrated spectrograms correspond to 600 tapered Fourier transforms, each corresponding to the average of 120 frames × 5 tapers. Collected results indicate that the maximum power values appeared during the CS+US interval and the 0.75 s following it, throughout the subsequent conditioning

phases. This is particularly visible in lower frequency bands (delta, theta; white arrows) but it is also present in the higher frequency bands (beta, low gamma, and high gamma). Likewise, notice the increase of the spectral power in the low gamma band 1 s after the CS/US presentation shown in PHASE I and III spectrograms (black arrows), but not in PHASE II.

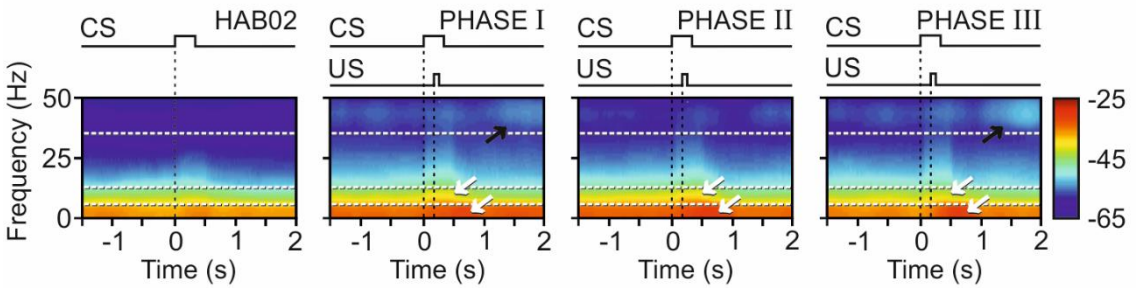

Figure 4.20. Time-frequency representations (spectrograms; $N_T \times K = 600$ tapered Fourier transforms) corresponding to data from HAB02 and conditioning phases I, II, and III illustrated in **Fig. 4.19**. Note that maximum spectral powers (see the color calibration bar at the right) for delta and theta occurred during and shortly after CS/US presentations, in the three conditioning phases (white arrows), but maxima for low gamma appeared 1 s after the CS/US, during PHASE I and III (black arrows).

Figure 4.21 represents a probabilistic map for the multiple comparisons between pairs of spectrograms, where red (inference type +1) and blue (inference type -1) indicate significant statistical differences ($P < 0.05$; jackknifed estimates of the variance), and white (inference type 0) indicates no significant differences ($P > 0.05$). It can be seen clearly that spectral powers of LFPs recorded during conditioning sessions were higher than those recorded during habituation (red, inference type +1), mainly during and after CS/US presentations. Specific differences were observed when comparing the three selected conditioning phases: between PHASES I and III versus PHASE II, mainly the in low gamma band (see the black arrows 1 s after the CS/US presentation), and between PHASES I and II versus PHASE III for low frequencies (red arrows).

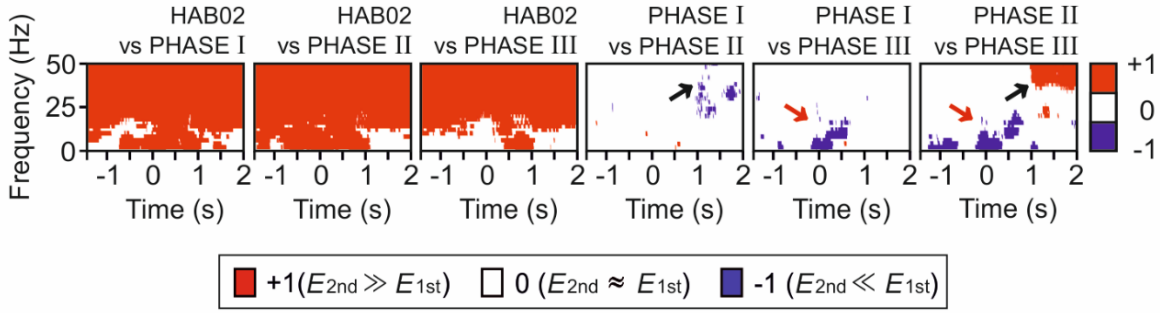

Figure 4.21. Multiple comparisons between the different spectrograms and their corresponding probabilistic maps. Red (inference type + 1; power in first spectrogram ≫ power in second spectrogram) and blue (inference type − 1; power in first spectrogram ≪ power in second spectrogram) indicate significant statistical differences ($P < 0.05$; jackknifed estimates of the variance), and white (inference type 0; power in first spectrogram ≈ power in second spectrogram) indicates no significant differences ($P > 0.05$). Black arrows indicate that the spectral powers in the low gamma frequency band were higher in PHASE I and (especially) III when comparing with PHASE II; that increment occurred at the end (range between 1 s and 2 s after the CS/US presentation) of the analyzed epoch. Red arrows show how, in contrast, spectral powers in low frequencies were higher in PHASE I and (especially) II when comparing with PHASE III during and slightly after the CS/US presentation.

The probability density histograms (**Fig. 4.22**) below allowed us to verify these results.

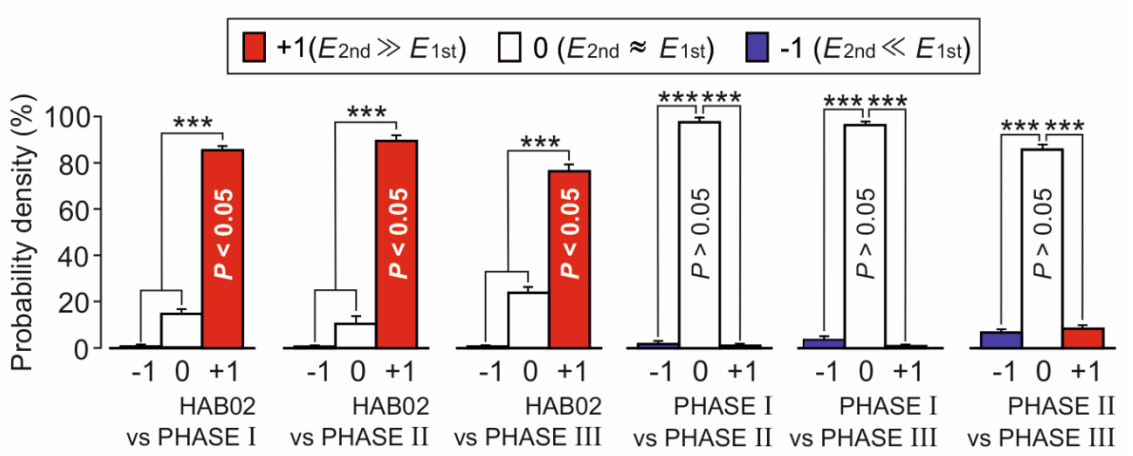

Figure 4.22. Histograms of mean probability densities. Here it is very evident (***, $P < 0.001$, Tukey-Kramer test) that there are statistically significant differences ($P < 0.05$, red bars) between the habituation (HAB02) and the conditioning (I, II, and III) phases in practically the whole time-frequency range. Although they present some specific significant differences in delta, theta, and low gamma bands, the three conditioning sessions are not statistically different overall ($P > 0.05$, white bars).

It is noticeable in all the representations that spectral power of PHASE II is the highest in low frequencies before and during the CS/US presentations (in which it is similar to PHASE I). In contrast, the peak in the low gamma frequency 1 s after the CS/US present in PHASES I and III is missing in PHASE II. The increment of the low gamma spectral power during PHASES I and III with respect to PHASE II in this specific temporal range (between 1 s and 2 s after CS presentation) could be a CL cognitive-control inference.

4.4.2. Comparison of LFPs in CL, mPFC, and MC during eyeblink conditioning

Figure 4.23 shows a comparative spectral analysis of the LFP recordings carried out in CL (green), mPFC (magenta), and MC (orange) simultaneously. **Figure 4.23*A*-*C*** shows mean spectra (***A***), histograms of mean spectral power (***B***), and time-frequency spectrograms (***C***) of these three recording sites during habituation. **Figures 4.23*D*-*F***, **4.23*G*-*I***, and **4.23*J*-*L*** provide the same information about conditioning phases I, II, and III respectively. In addition, in the multiple comparison histograms (**Fig. 4.23*B, E, H, K***) the difference from the baseline values is shown (dotted black line). The histograms also further illustrate that the forementioned changes in spectral power for LFPs collected in the CL when comparing habituation versus any of the conditioning phases were present in mPFC and MC as well, and they were even stronger (Tukey-Kramer multiple comparison test: HAB02 and Baseline vs. PHASES I, II, and III; $P < 0.001$, white asterisk).

CL results were described and analyzed in detail above; hence data from mPFC and MC LFP recordings will be evaluated next. The changes we observed in CL LPF spectra seem to be present and even greater in mPFC ones. Apparently, the two structures follow a similar spectral pattern. Both structures increased their LFP spectral power in delta (1-5 Hz) during PHASE I and II (although both increased, power values from mPFC became statistically different to those from CL, $P < 0.001$), and reduced it notably in PHASE III. In addition, they both remarkably raised their spectral power for low gamma band (35-50 Hz) in PHASE I and PHASE III (**Fig. 4.23*E, K***, 35-50 Hz plots; **Fig. 4.23*F, L***, see black arrows). Curiously, mPFC is the one recording site whose theta band (5-12 Hz) spectral powers grew the most compared with the habituation session, but its values remained unchanged throughout the three conditioning phases. On the other hand, LFP recordings from MC did not follow the same spectral patterns as those from CL and mPFC. Its spectral powers did increase in PHASE I and II, especially for low frequencies (delta and theta), but in contrapositions to CL and mPFC, LFP from MC did not experience any noticeable change for the low gamma values across PHASES I, II, and III. (*, $P < 0.05$; **, $P < 0.01$; ***, $P < 0.001$; Tukey-Kramer test).

None of the three structures presented any marked change in beta (12-35 Hz) and high gamma (50-100 Hz) bands, except the general increase of spectral power in all the five bands produced presumably due to the conditioning itself.

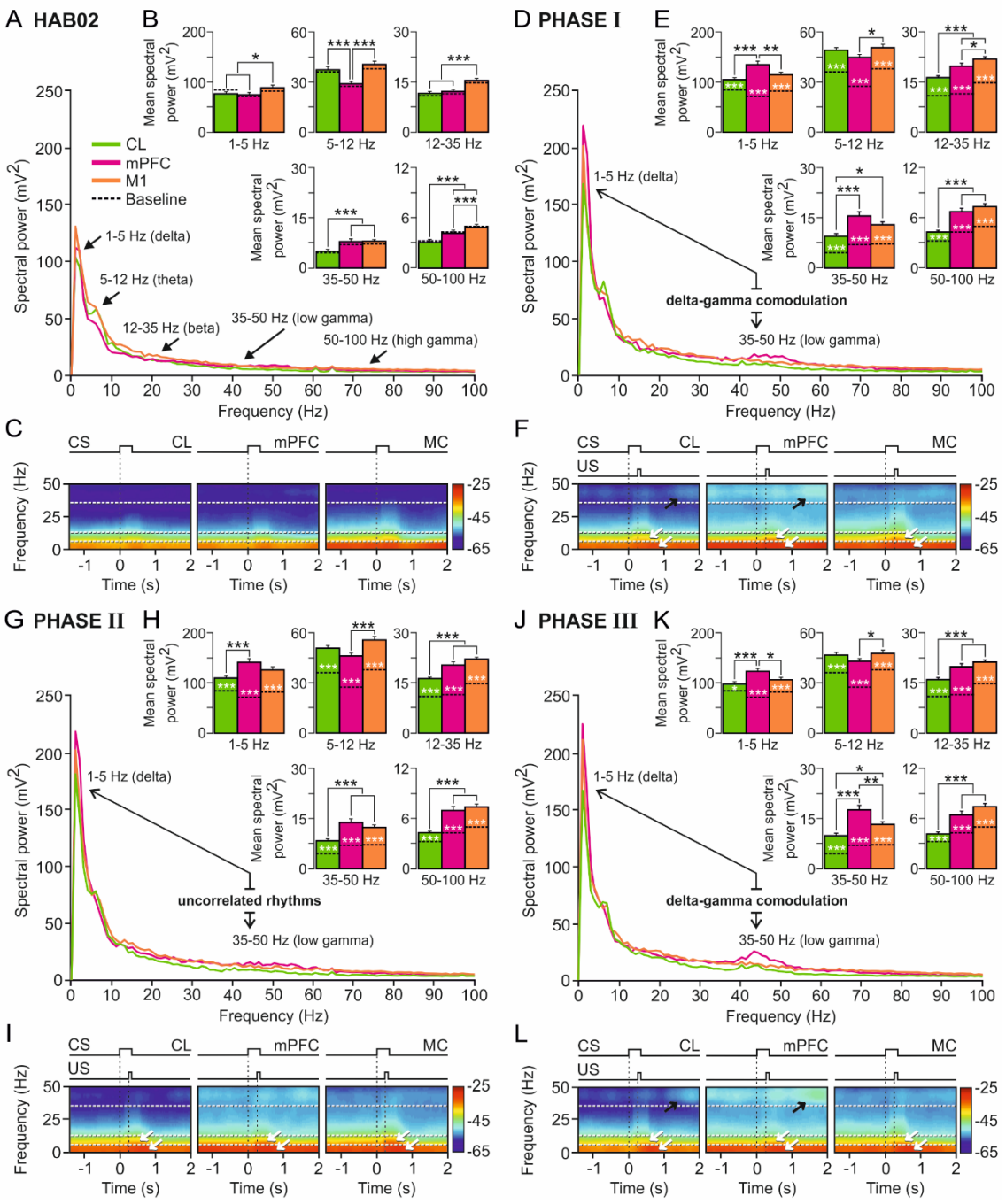

Figure 4.23. Spectral analyses of LFPs recorded in CL (green), mPFC (magenta), and MC (orange) during classical eyeblink conditioning. ***A***, Mean power spectra of LFPs recorded in the three recording sites between 1.5 s before and 2 s after the CS initiation during the 2nd habituation session (HAB02). Black arrows indicate spectral ranges. ***B***, Histograms of mean spectral powers for all frequency bands. Baseline values (collected from HAB02 sessions, including no stimulus) are also represented (dotted black line inside the bars); note that they are very similar to those collected during the presentation of the unpaired CS (HAB02). ***C***, Spectrograms corresponding to data illustrated in ***A***, ***B***. Note that the maximum values of spectral power (see the color calibration bar at the right) appeared during and after CS presentations, and the fundamental contribution to the spectral power was determined by delta and theta bands. ***D-L***, Same representations and analyses for LFPs recorded in CL, mPFC, and MC during PHASE I (***D-F***), PHASE II (***G-I***), and PHASE III (***J-L***).

Finally, comodulation analysis by means of the cross-frequency couplings and the computation of the power-power spectral ratios between different frequency bands indicated that the strength of these cross-frequency interactions changes, dynamically and differentially, between the LFP oscillatory activities from CL, mPFC, or MC. In summary, the LFP oscillatory patterns at CL-mPFC network nodes were correlated with coordinated dynamic changes in delta and low-gamma powers. In contrast, at the CL-MC network nodes the power dynamics in delta and gamma frequency bands were uncorrelated. In relation to the above, see further comments and detailed statistical results in Reus-Garcia et al., 2021 (Supplementary Appendix S3).

4.5. Ex. 3 - Effect of blocking claustrum output on the acquisition curve and on the EMG activity of the *orbicularis oculi* muscle during eyeblink conditioning

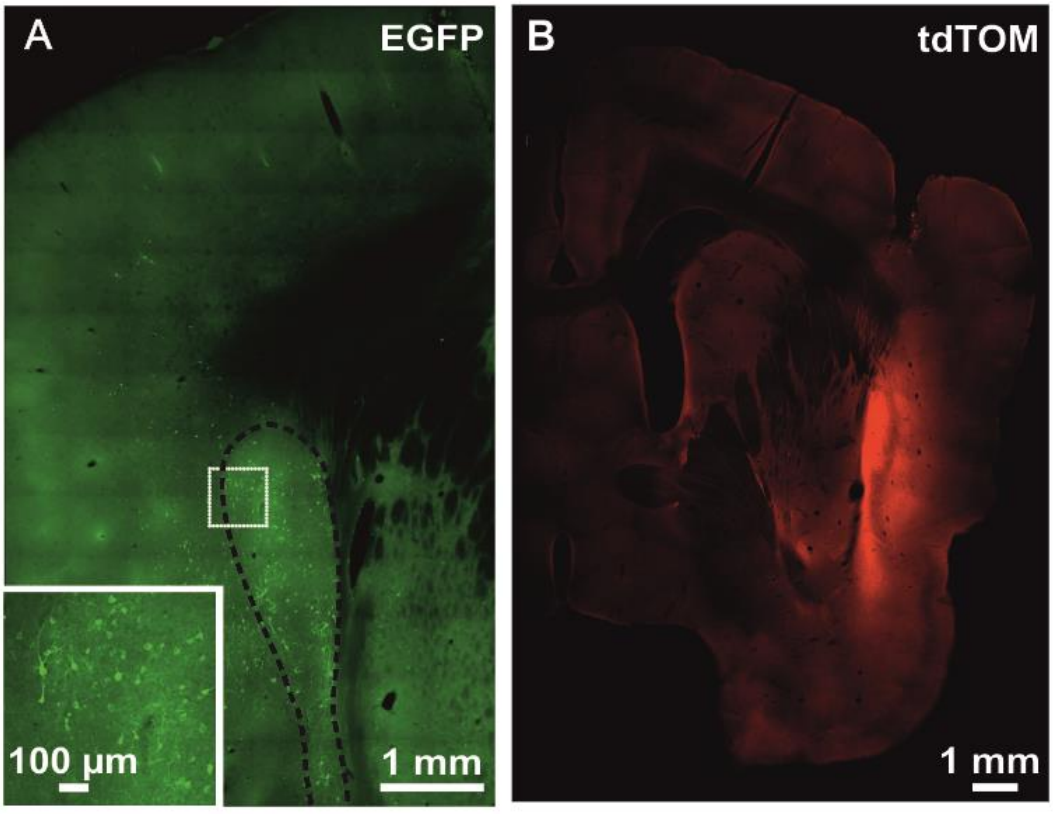

Figure 4.24. Photomicrographs from CL taken from postmortem tissues. **A**, Infected CL neurons glowing green due to the generation of EGFP fluorescent protein encode in virus 3, under $\mathbf{P}_{hSYN}$ promoter. The large white square is an amplification of the smaller one. ***B,*** Inhibited CL glowing red due to tdTOM fluorescent protein generated by the activation of the $\mathbf{P}_{tet}$bi by Dox administration.

To ask whether CL activity is directly involved in classical eyeblink conditioning, we examined the effects of blocking CL neuron output on learning and/or performance of conditioned eyeblink responses. For this, we used a novel method for virus-delivered inducible silencing of synaptic transmission (vINSIST). A homogeneous cocktail of three rAAVs was injected at three different sites (2 µL each) bilaterally in CL. With the vINSIST technology, we were able not only to silence synaptic transmission in CL after doxycycline treatment, but also to mark targeted (EGFP, green; **Fig. 4.24*A***) and silenced (tdTOM, red; **Fig. 4.24*B***) CL neurons (see Materials and Methods and Reus-Garcia et al., 2021).

4.5.1. Effect of claustrum partial inhibition on the learning curve

A total of eight rabbits were injected with rAAV and then classically conditioned using a delay paradigm; four were injected with doxycycline following the 2nd habituation session, before learning began (blue group), while the other four were injected following the 6th conditioning session, after learning had occurred (magenta group).

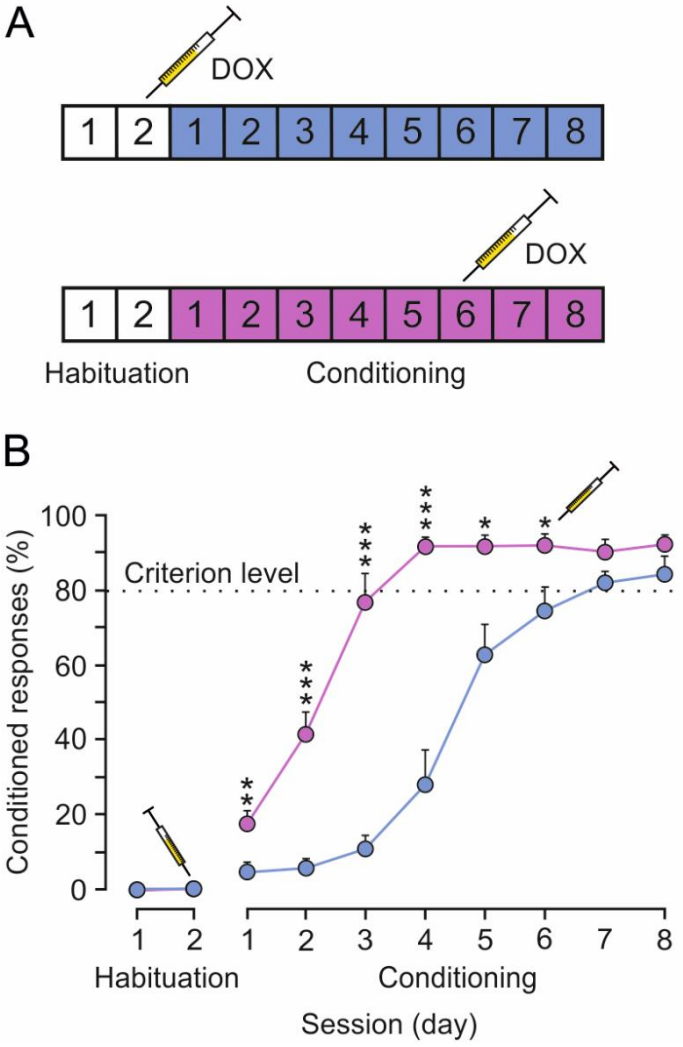

Figure 4.25. Classical conditioning of eyelid responses during the inhibition of both CLs. CL neurons were inhibited by the local injection of a cocktail of rAAVs equipped with doxycycline (Dox)-dependent tetracycline-controlled genetic switches, which release tetanus toxin (TeTxLC) when activated. ***A***, Animals (n = 8) were classically conditioned using a delay paradigm following two protocols: half of them (blue group) were injected with Dox after the 2nd habituation session and the other half (magenta group) after the 6th conditioning session. ***B***, Learning curves corresponding to the two groups of animals. Data are presented as mean ± SEM (see the multiple comparison reports: *, $P < 0.05$; **, $P < 0.01$; ***, $P < 0.001$; Holm-Sidak or Tukey-Kramer tests).

As illustrated in **Fig. 4.25*B***, animals included in the blue group, where CL output was silenced prior to learning, learned much more slowly [$F_{(7,42)}$ = 14.179; P < 0.001; two-way ANOVA F-test, with one factor repetition] compared with rabbits in the magenta group, where the CL was not silenced until learning was achieved.

In contrast, silencing of CL neurons after the 6th conditioning session (magenta group) produced no noticeable effects on the learning curve.

4.5.2. Quantitative analysis of cumulative areas of the EMG

In regard to the EMG activity of the O.O. muscle during the CS-US interval, the early inactivation of both CLs in the blue group significantly decreased the mean area of the rectified EMG during the intermediate conditioning sessions, but control values were reached by the 8th conditioning session [$F_{(3,18)}$ = 7.287; P = 0.002; two-way ANOVA F-test, with one factor repetition; see inset in **Fig. 4.26*C***]. In contrast, there were no significant differences for the evoked URs shown during the CS+US period [$F_{(3,18)}$ = 3.036; P = 0.056; two-way ANOVA F-test, with one factor repetition].

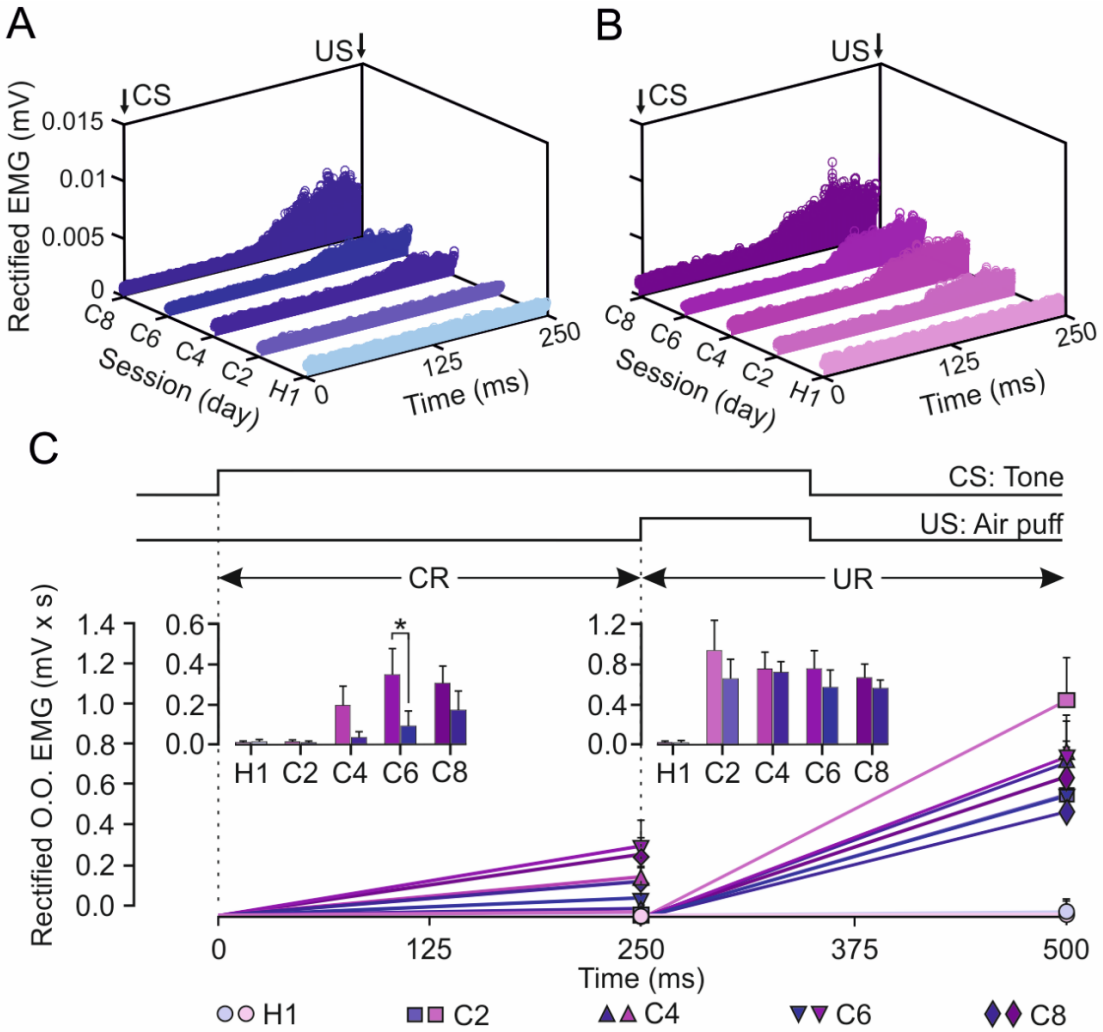

Figure 4.26. ***A***, Rectified EMG activity of the left O.O. muscle from the blue group during the CS-US interval (CRs time gap) and collected for the indicated habituation and conditioning sessions (n = 50 trials per session from n = 4 animals). ***B***, Same representation for magenta group. Note the earlier and larger CRs attained by this group during CS-US interval. ***C***, Quantitative analysis of cumulative areas (in mV x ms) of the rectified EMG activity of the left O.O. muscle recorded during the CS-US interval (CRs time gap) and during the 250 ms following it (CS+US interval plus 150 ms, URs time gap) for the five indicated sessions. The insets illustrate the differences in net EMG areas between the two groups (*, $P < 0.05$) during the CS-US (CRs) and the CS+US intervals (URs). No differences were found between groups for URs.

In summary, early inactivation of CL output delayed the acquisition of a classical conditioning task without affecting its performance, while inactivation in well-trained animals had no effect. Therefore, we conclude that CL neurons are involved in the cognitive component of the eyeblink conditioning, rather than the motor.

5. DISCUSSION

In this Doctoral Thesis it was found that CL neurons exhibit changes in their activity during classical eyeblink conditioning in behaving rabbits. Apparently, their firing properties were related to cognitive aspects of the acquisition process rather than the kinematics of the CR. Below, these findings are discussed in detail and the potential role of the CL in cognitive-like functions involved in associative learning is considered.

5.1. Ex. 1 - Location and identification of claustral neurons

Because it is a small and thin structure, we carefully arranged our experimental procedures to ensure that recordings were carried out within the CL. Although the rabbit CL is far easier to access, due to its significantly larger size compared with the mouse CL, we employed specific criteria to determine that we were recording the activity of CL neurons. The differential, dense, and bidirectional connectivity of the CL with the MC, mPFC, and CC (Carman et al., 1964; Crick and Koch, 2005; Mathur, 2014; Chia et al., 2017; Atlan et al., 2018; White et al., 2018) and the spontaneous firing rate of CL neurons (Spector et al., 1974; Chachich and Powell, 2004) were key to identifying the recordings of CL neuron activity. Furthermor, *post-hoc* electrolytic lesioning confirmed that our electrodes were placed in the CL.

Neurons were identified by their anti- and/or orthodromic activation from MC, mPFC, and CC; they were observed to be synaptically activated in response to stimulation of these cortices, although their antidromic activation was seldom observed. This could be the result of the extensive branching of claustral axons into different cortical areas (Marchi et al., 1983; Minciacchi et al., 1985; Majak et al., 2000), which could hinder antidromic invasion of action potentials into their somata (Steriade et al., 1971; Lipski, 1981). As supported by the present results and in the multiunit recordings carried out in rabbit CL during Pavlovian heart-rate conditioning by Chachich and Powell (2004), CL neurons had a low, irregular spontaneous firing that was not affected by the presentation of CS or US alone. This characteristic firing helped to differentiate CL cells from neurons in nearby nuclei: insular cortex (lateral) and striatum (medial).

5.1.1. Differences between claustrum and surrounding structures

On the one hand, insular neurons in rabbits exhibit inconstant, low-magnitude responses during classical conditioning (Gibbs et al., 1992). Moreover, insular neurons in

monkeys seem to be involved in integrative complex processing of sounds and vocal communications (Remedios et al., 2009), while —as we have observed— CL neurons are not very active when presented with single stimuli of any sensory modality. Finally, the inactivation of the insular cortex by tetrodotoxin (Bermudez-Rattoni, 1991) produces different effects from those reported here after blocking the CL output with TeTxLC.

On the other hand, striatal cells have a characteristic stable, low-frequency tonic firing that is modulated during classical eyeblink conditioning (Blázquez et al., 2002) but with response profiles that differ from what we found for type A and B CL neurons.

Finally, action potentials recorded in fiber tracks and long dendrites have a shape that differs from action potentials recorded near neuronal somata (Delgado-García et al., 1990; Deligkaris et al., 2016). That allows us to conclude that we were not recording responses from the extreme or external capsule nor from dendrites located outside the CL.

With those facts taken together, we are positive that the neuronal activity analyzed in this work was recorded within the CL.

5.2. Ex. 1 - Firing activity of claustral neurons

5.2.1. Basal firing activity of claustral neurons

As indicated in the Introduction section, most researchers agree that the CL basal firing activity is rather low (≈ 1 to 10 Hz) in awake resting animals. Nevertheless, different brain states —such as attention, learning, or sleep— can increase it notably (Spector et al., 1974; Chachich and Powell, 2004; Remedios et al., 2010; Jankowski and O'Mara, 2015; Narikiyo et al., 2020); for example, here we report higher basal firing rate (≈ 10 to 25 Hz) for claustral neurons recorded during eyeblink conditioning sessions.

However, it was especially difficult, using a glass micropipette, to maintain the extracellular recording of neurons that barely fire spontaneously. That is why, in order to be sure that almost-silent neurons were still being recorded (instead of simply having lost track of them), we needed to activate them using electrical stimulations from MC, mPFC, or CC. That frequent activation of the recorded CL cells could contribute to the rise of their firing rate. Also, it is much easier finding and keeping the recording of cells with higher spontaneous firing activity —thus our results regarding the basal firing rate may be skewed by that fact.

Even so, our results are consistent with other authors' research: CL basal firing rate is typically low in resting state, but it increases during learning and attention.

5.2.2. Firing activity of claustral neurons during classical eyeblink conditioning

According to their firing profiles during the CS/US presentations, and their spike duration, neurons whose activity was recorded throughout the eyeblink conditioning sessions were classified in three differentiated groups.

Type A neurons reported here had activation profiles similar to what has been reported for rabbit cortical neurons during delay eyeblink conditioning. For instance, Leal-Campanario et al. (2013) identified mPFC pyramidal neurons that exhibited delayed firing with respect to CS presentation. Caro-Martín et al., 2015 ('late mPFC neurons') and Ammann et al., 2016 ('type C pyramidal MC neurons') also found comparable cells.

In a similar way, Weible et al. (2003) recorded excitatory activity in CC neurons —tightly related to CL— during the first trials in both conditioning and pseudoconditioning, a probable consequence of the novelty of the stimuli. As we also reported for CL neurons during pseudoconditioning, CC activity declined as the stimuli became familiar and non-significant. Nevertheless, claustral type A cells became even more active while the animals were learning the task.

Also, CL neurons recorded by Chachich and Powell (2004) one day after the conditioning had a late and longer-lasting increase in their discharge rate as a response to only the CS. Their firing patterns were similar to the responses of type A neurons reported here, although their recordings were taken not *during* but *after* the learning.

In contrast, Chachich and Powell (2004) did not report CL cells that were inhibited as a consequence of the conditioning (*type B* neurons). With the single-unit extracellular recordings used here, it was challenging to find type B neurons: inhibition was perceptible only when neurons had high baseline firing rates and the recording was held for a long time.

Type C neurons did not respond to any stimuli, including paired CS/US presentations. They represented more than 75% of the cells examined during habituation and pseudoconditioning sessions (when single or unpaired stimuli were presented), but they became less frequent during the learning phase. In fact, they seemed to be replaced by type A neurons, whose number increased considerably (**Fig. 4.11**). The spike durations

of type A and type C neurons were similar, and they presented an inverse relation across conditioning. Nevertheless, to ensure that they are members of the same CL population, more research would be needed since they had different baseline firing rates.

5.2.3. Why claustrum activity is not related to the kinematics of the CRs

The demonstration that type A and B neurons respond to CS/US pairing indicates that these neurons must play some role in associative learning. Claustral type A neurons increased their activity with the association of the paired CS/US during the acquisition of the CRs. However, their function during the learning phase is not related to motor performance of the eyelid CRs, because:

(1) CRs appeared mostly before type A neurons discharged (156.7 ± 13.8 ms and 175.5 ± 11.5 ms after the CS respectively), so their activity could not produce or modulate eyelid movement.

(2) CRs appeared very early during training and became larger and more numerous until the learning curve reached asymptotic values, around the 5th session. If type A neurons were necessary for the proper execution of the CRs, their activation should be maintained specifically during the last conditioning sessions, when more and bigger CRs are delivered. On the contrary, we found that the number of recorded type A neurons decreased after the 5th session.

(3) Furthermore, regression analyses rule out any linear relationship between the discharge rates of type A neurons and the EMG activity of the O.O. muscle ($r \geq 0.6$), both for the CS-US period, where CRs are expected, and for the CS+US interval, when URs appeared.

(4) Finally, on a trial-by-trial basis we often found CS/US trials with type A neuron firing activity and no CR, and *vice versa*.

Thus, we conclude that type A neurons are not responsible for the accurate performance of eyelid CRs. A more plausible possibility is that CL neuron activity is related to attentional, cognitive processes. Type A cell activity is mainly required during the acquisition phase: once the CRs are fully developed and learning has been achieved, no further activation of these cells was observed. Moreover, claustro-cortical connections are expected to produce inhibition of their target cortices, particularly in the PFC (Jackson

et al., 2018). Therefore, we postulate that Type A cell activity serves to suppress cortical areas during the learning phase.

In contrast, given their firing profiles during conditioning and the short duration of their spikes, type B neurons are expected to be interneurons and thus do not project out of the CL. They did respond to the CS/US prior to CR initiation (60 ± 18 ms and 156.7 ± 13.8 ms after the CS respectively), but it is improbable that their inhibition is involved in CR performance. Instead, they are likely to participate in local inhibitory circuitry, and they might be responsible for the noticeable silent period after synaptic stimulation of the CL (**Figs. 4.3**, **4.4**, **4.5**). More data will be needed to clarify the role of type B neurons.

5.3. Ex. 2 - Analysis of the Local Field Potentials recorded in CL, MC, and mPFC during classical eyeblink conditioning

5.3.1. Changes in LFPs recorded in claustrum across PHASE I, II, and III

According to data obtained from LFPs recorded in the CL (**Fig. 4.19**), habituation and baseline results barely differed, and single CS presentations did not produce any change in LFP spectral powers, as has already been observed in single-unit recordings. In contrast, the CS/US association increased the spectral power of all the frequency bands. Comparing spectral power changes (**Fig. 4.20**) with single-unit activation (**Fig. 4.11*A***) throughout PHASE I, II, and III, we noticed several remarkable details:

i) In the pre-learning stage (PHASE I) there was a perceptible increase of low frequency (delta and theta) spectral powers, and simultaneously (during and slightly after the CS/US presentation) a few type A neurons started firing. One second after the CS, there was a slight increase of low gamma spectral power.

ii) During the acquisition stage (PHASE II), delta and theta spectral powers were the highest (during and slightly after the CS/US presentation) simultaneously with the increased firing of type A neurons. One second after the CS, the low gamma peak had disappeared.

iii) When learning had been achieved (PHASE III), delta and theta bands presented the lowest spectral powers during and slightly after the CS/US, while type A neurons were rarely recorded. Yet, one second after the CS, the low gamma band presented its highest value, with a prominent peak.

To sum up, the spectral patterns (power-power ratio and amplitude-amplitude comodulation) suggest that the couplings in which delta-gamma comodulation appears in the LFPs recorded in CL depend on the learning phase. Not only are they absent during habituation sessions, but also, the strength of these cross-frequency interactions changed differentially during phases I, II, and III. Moreover, those patterns seem to be tightly related to the single-unit activities. Available information concerning LFP recordings carried out in the CL of behaving rats indicates a similar modulation between two frequency bands (1-4 Hz and 8-12 Hz) during spontaneous behaviors (Jankowski et al., 2017), although frequency bands in rats and rabbits are not equivalent.

5.3.2. Comparison of changes in LFPs recorded in CL, mPFC, and MC across PHASE I, II, and III

Data collected from LFP recordings carried out in CL, mPFC, and MC are quite intriguing. Despite the fact that MC recordings seem to follow a pattern completely different from that of CL ones, mPFC recordings also presented a distinctive increment of spectral power in low gamma frequencies during some conditioning phases, as described above for CL recordings.

LFPs recorded from CL-mPFC network nodes show an amplitude-amplitude coupling between delta and low gamma frequency bands during PHASES I and III. In contrast, during the acquisition stage (PHASE II) the low gamma peak disappeared in CL and mPFC, and delta-gamma comodulation was not found. For single-unit recording experiments, it was also during the acquisition sessions that the percentage of type A neurons was greater, reaching its highest value at the end of this stage (**Fig. 4.11*A***). These cells fired from 175.5 ± 11.5 ms to 476.8 ± 33.5 ms after the CS presentations, and ≈ 500 ms after that, the expected low gamma peak was missing. Thus, firing activity of CL neurons could prevent the presence of low gamma oscillations.

Additionally, as Jackson et al. (2018) have reported using optogenetic activation of CL neurons, it is likely that CL type A cells target PFC interneurons which inhibit pyramidal neurons. Those inhibited mPFC neurons could generate the low gamma oscillations described in PHASES I and III (especially considering that spectral power values for low gamma were higher in mPFC than in CL). After the acquisition period (i.e., in PHASE III), CL neurons become silent and mPFC might again generate low gamma oscillations. This would also explain why in PHASE I the low gamma peak is

small: there are already a few CL neurons firing, but not sufficient to inhibit PFC activity, as they do in PHASE II.

Indeed, results presented here further support evidence of a cognitive control system (White et al., 2018), where the CL is subservient to network function (mainly top-down) rather than an integrator of sensory cortical information. Likewise, last year Fodoulian et al. (2020) also reported that the CL-mPFC network is activated during a task requiring cognitive control. Even further, cortical PV interneuron networks (likely, the main target for type A CL neurons) play a role in synchronizing the activity of cortical projection neurons and in generating brain rhythms, including gamma oscillations in the cortex (Galarreta and Hestrin, 2001; Bartos et al., 2007; Cardin et al., 2009; Sohal et al., 2009).

In contrast, MC does increase its spectral power values for low frequencies (delta and theta) across conditioning, but not for low gamma. This fact helps to verify that this peak in the low gamma band is specific and is not occurring all-brain-wide due to signal contamination. In accordance, it can be suggested that the power dynamics at CL nodes could be related to cognitive-like functions (CL and mPFC LFPs are correlated) rather than to motor neural control (CL and MC LFPs are uncorrelated) during classical eyeblink conditioning (contrary to the predominant motor control role played by MC circuits for the generation of eyelid conditioned responses as described by Ammann et al., 2016).

Note that for LFP experiments we use special electrodes to avoid multiunitary recording that could affect low- and/or high gamma amplitudes. Thus, the delta-gamma couplings in the CL-mPFC network nodes were due to genuine interactions between spectral patterns of two LFP oscillations, and not to spike contamination from the local firing of CL and/or mPFC neurons. These LFP spectral patterns should endorse the proposal of the delta-associated gamma oscillations described here as a new type of CL-mPFC coupling, directly involved in cognitive processes related to this type of associative learning.

5.4. Ex. 3 - Blocking claustrum output delayed learning during classical eyeblink conditioning

When inhibiting CL neuron output with vINSIST, injections of rAAVs were minimal and local to avoid spillover into adjacent structures. As a result, it is unlikely that the entire

CL was silenced. Nevertheless, such partial inactivation evoked a noticeable delay in the acquisition of CRs, without affecting URs. This delay in CR acquisition was evident not only qualitatively —fewer CRs in early conditioning sessions (**Fig. 4.25*B***)— but also quantitatively: when CRs started appearing, they were considerably smaller in amplitude (**Fig. 4.26**). In contrast, we could not find any significant difference between the URs of blue and magenta groups; thus, CL shutdown affected the cognitive component of the task, but not the motor one. Chachich and Powell (2004) observed similar effects —namely a delay in achievement of an associative learning task (heart-rate conditioning)— following permanent bilateral electrolytic lesions in the CL of rabbits.

These results, together with the regression analyses showing that CL neural activity is not related to the kinematics of eyelid CRs, further support our conclusion that the CL is involved in cognitive components of this type of associative learning.

5.5. The claustrum is involved in the cognitive aspect of the classical eyeblink conditioning

In contraposition to the role in the motor aspects of conditioned eyeblinks played by the cerebellum (Welsh and Harvey, 1991; Krupa et al., 1993; Christian and Thompson, 2003; Sánchez-Campusano et al., 2007; Ten Brinke et al., 2017) and the MC (Aou et al., 1992; Ammann et al., 2016), the CL may be one of several brain structures that participate in the cognitive component of conditioning. These include the hippocampus (Rescorla, 1988; Múnera et al., 2001), the CC (Weible et al., 2003; Hattori et al., 2014), and the mPFC (Powell et al., 2005; Leal-Campanario et al., 2007; Siegel and Mauk, 2013; Caro-Martín et al., 2015) among others.

The cognitive role of CL neurons could be related to the attentional process triggered by CS/US association, as reported by Goll et al. (2015). Furthermore, this potential role of the CL in the attentional and cognitive components of classical eyeblink conditioning has also been proposed for CL in other learning tasks, as a sort of resilience to distraction (Atlan et al., 2018). In addition, we found that reduction of claustral output produces a cognitive deficiency that generates learning difficulties. It has also been reported that CL activity is heightened in patients with Attention Deficit Hyperactivity Disorder (Dickstein et al., 2006; Castellanos et al., 2008; Wang at al., 2013). Therefore,

it is possible that a specific activation-inhibition balance of the CL cell population is needed to cope with complex cognitive challenges that require recruiting attention.

According to our present results, CL neurons are not activated by single and/or irrelevant stimuli of any sensory modality. In fact, they are activated by paired CS/US associations until the time when CRs are maximal during conditioning. Thus, we conclude that the CL plays an important role in the proper acquisition of classical conditioning tasks, mostly in attentional processes related to CS/US association.

5.6. Limitations and future prospects

Despite the extraordinarily high degree of interconnectivity between the CL and the rest of the brain, the CL has been grossly understudied. While recent work has started to implicate the CL in sensorimotor integration and higher cognitive functions, interpreting the effects of experimental manipulations of the CL have yielded inconsistent results. This is largely due to a lack of knowledge of the types of CL neurons being manipulated.

A few investigators —using several methods in a variety of animal models— have examined the effects of activating (Dickstein et al., 2006; Castellanos et al., 2008; Wang at al., 2013) and inactivating (Atlan et al., 2018; Reus-Garcia et al., 2021; Terem et al., 2020) the CL during different cognitive-related tasks. Paradoxically, all alterations in CL activity have been found to worsen performance; hence, more-precise control of neuronal activity is needed to understand the circuits underlying these cognitive processes. Part of the difficulty in interpreting such experimental manipulations is that it was unclear which specific types of CL neurons were being manipulated.

It is known that the claustrum includes at least two different types of projecting neurons (PN) (Shibuya et al., 1998; Kim et al., 2016; Chia et al., 2017; White et al., 2018) and at least one type of interneuron (IN) that expresses the calcium-binding protein parvalbumin (Kim et al., 2016; White et al., 2018).

Recently, Graf et al. (2020) have done a comprehensive survey that identified all types of CL neurons. That work provides a detailed characterization of these neurons and provides objective criteria for distinguishing them, including strategies for genetic targeting of each neuron type. This contribution to the field opens many new opportunities for dissecting CL function. Graf reported that the CL consists of two subgroups of PN:

strongly-adapting neurons (SA) that project mainly to cortex, and mildly-adapting neurons (MA) that project largely to subcortical structures. They therefore hypothesized that these PN will be involved in different cognitive processes: SA neurons are expected to be involved in sensory or executive roles, while MA neurons should be involved in appetitive or affective components. The three types of IN in the CL should be involved in regulation of CL local circuitry. Two of these, PV-IN and SST-IN, preferentially inhibit both types of PN, while a third, VIP-IN, preferentially inhibits the other two IN types (Graf and Augustine, 2019). Thus, the activity of PV-IN and SST-IN should be inversely correlated with the activity of PN in behavioral tasks, while the activity of VIP-IN should be correlated with PN activity.

Accordingly, type A neurons described in the present dissertation are expected to be Graf's SA cells, mostly. Presumably that is because classical eyeblink conditioning is related to cognitive processes happening mainly in cerebral cortex since it requires sensorimotor integration, rather than appetitive or affective components developed in subcortical structures. Type B cells, according to their firing rate profile and their spike durations, are likely to be interneurons, but we cannot be positive as to whether they correspond to PV or SST in Graf's work; nevertheless, we can rule out VIP interneurons since their activity is assumed to be correlated to PN activity. Unfortunately, the vINSIST method used here is not specific either for the whole CL, or for its distinct cell types. Consequently, we assume that in our inhibition experiment all cells infected with the viruses will be synaptically blocked, regardless of the cell type. Hence, although the experiment gives information about its role in associative learning, it does not help find out how the CL local circuitry works.

Benefiting from the recent insights into the cellular composition of the CL, it will now be possible to selectively perturb and measure the activity of precisely known CL neuron types. This should yield much more interpretable data regarding the role of the CL in various cognition-related behaviors.

Different types of CL neuron are likely to be differentially active during different cognitive-related tasks. Behavioral tests have been very useful in probing the function of the CL (Smythies et al., 2012; Atlan et al., 2018; Terem et al., 2020). While these works have yielded extremely valuable information on the role of the CL in various cognitive-related tasks, all of them lacked information about the types of CL neuron involved. Thus,

it would be useful first to revisit the role of the CL in those different cognitive tasks (i.e., salience detection, sensorimotor associative learning, resilience to distraction…) by measuring the activity of each CL cell type during these behavioral tasks using *in vivo* calcium imaging with different cell-specific promoters to target the calcium indicator protein, GCaMP6, to the 5 different subtypes of CL cell (Zhao et al., 2011).

Next, it would be interesting to determine the effect of increasing or reducing the activity of each CL cell type during the same cognitive-related behavioral tasks using *in vivo* optogenetics. Activating each neuron at the time they are ordinarily active should evoke or enhance the behavior, while activating them at inappropriate times should disrupt the behavior. At the same time, it would be possible to determine whether such activity is necessary for each task by inhibiting the activity of these neurons: if the neuronal activity is necessary for the behavior, then inhibiting them when they are spontaneously active should disrupt the behavior.

Taken together, the results of these potential experiments should establish a causal role for each CL neuron type in various cognition-related behaviors, and they could also surmount the shortcomings of the present thesis. Developing this knowledge will be beneficial for understanding numerous brain disorders that are associated with deficits in cognitive function and abnormal CL activity, including ADHD (Dickstein et al., 2006; Castellanos et al., 2008; Wang at al., 2013), schizophrenia (Cascella et al., 2011; Cascella and Sawa, 2014), autism spectrum disorder (Wegiel, 2014), and epilepsy (Kurada et al., 2019). It is vital to completely comprehend the CL before we can properly treat such disorders.

6. MAIN FINDINGS AND CONCLUSIONS

The present Doctoral Thesis is focused on assessing the participation of the claustral neurons during different stages of the conditioning of eyelid responses —namely, *before*, *during*, and *after* learning the selected task. To accomplish this, electrophysiological recordings (extracellular single-cell and local field potentials) of CL neurons' activity have been attained from behaving rabbits. In addition, we used selective genetic and molecular tools for synaptic silencing of the CL before and after rabbits achieved the learning. In summary, the main conclusions of these experiments are the following:

6.1. Ex. 1 – Claustrum cells are involved in the acquisition of the eyeblink conditioning

- Electrophysiological, anatomical, and histological studies ensure that only CL neurons' activity has been recorded throughout these experiments.
- CL basal firing rate is quite low in resting animals, and also in response to non-significant stimuli.
- CL neurons' activity seems to be related to certain attentional, cognitive tasks since their basal firing rate increases during eyeblink conditioning, and some claustral cells respond to the paired CS/US, especially during the acquisition phase of the learning.
- CL cells activated after the paired CS/US (type A) are likely to be projecting neurons that target cortex interneurons. Their activity is related to the cognitive aspect of the acquisition —rather than the motor performance of eyelid CRs— since there is no relationship between their firing activity and the CRs development or magnitude.
- Type B neurons (which respond with inhibition to the paired CS/US) are interneurons according to their spike duration and firing pattern, and may be responsible for the silent period following the synaptic activation of the CL.

6.2. Ex. 2 – Local Field Potential oscillatory patterns are correlated in delta and low gamma bands in CL and mPFC, but not in MC, during eyeblink conditioning

- The LFP oscillatory patterns at CL-mPFC network nodes are correlated and show an amplitude-amplitude coupling between delta and low gamma frequency bands during PHASES I and III, but not during PHASE II. Instead, during the acquisition phase (PHASE II), CL neurons may inhibit prefrontal interneurons that generate those low gamma oscillations.

- MC LFPs follow a different pattern: spectral power values are increased for low frequencies (delta and theta) during the conditioning, but low gamma values remain practically unchanged.

6.3. Ex. 3 - Partial inhibition of claustrum output delays the acquisition of the conditioned responses (CRs)

- CL activity is not essential (as it is cerebellum activity) for developing conditioned eyeblink responses, although its partial inhibition generates a substantial delay in the acquisition of this learning task.
- The activity of CL cells is unlikely to be related to the retrieval of the CRs, because inhibiting their synapses after acquisition does not affect the learned eyeblinks. Furthermore, claustral neurons cease their activity once acquisition is achieved (even continuing the training), thus their activity might be involved in the association of the CS and US.

7. REFERENCES

Aiba A, Kano M, Chen C, Stanton ME, Fox GD, Herrup K, Zwingman TA, Tonegawa S. 1994. Deficient cerebellar long-term depression and impaired motor learning in mGluR1 mutant mice. Cell. 79(2):377-88.

Aksenova TI, Chibirova OK, Dryga OA, Tetko IV, Benabid AL, Villa AEP. 2003. An unsupervised automatic method for sorting neuronal spike waveforms in awake and freely moving animals. Methods 30:178–187

Alexander GE, Crutcher MD, DeLong MR. 1991. Basal ganglia-thalamocortical circuits: parallel substrates for motor, oculomotor, "prefrontal" and "limbic" functions. In Progress in brain research. (Vol. 85, pp. 119-146). Elsevier.

Alloway KD, Smith JB, Beauchemin KJ, Olson ML. 2009. Bilateral projections from rat MI whisker cortex to the neostriatum, thalamus, and claustrum: forebrain circuits for modulating whisking behavior. Journal of Comparative Neurology. 515(5):548-564.

Ammann C, Márquez-Ruiz J, Gómez-Climent MÁ, Delgado-García JM, Gruart A. 2016. The motor cortex is involved in the generation of classically conditioned eyelid responses in behaving rabbits. J Neurosci. 36:6988–7001.

Amaral DG, Cowan WM. 1980. Subcortical afferents to the hippocampal formation in the monkey. Journal of Comparative Neurology. 189(4):573-591.

Amaral DG, Insausti R. 1992. Retrograde transport of D-[3 H]-aspartate injected into the monkey amygdaloid complex. Experimental brain research. 88(2):375-388.

Andersen DL. 1968. Some striatal connections to the claustrum. Experimental neurology. 20(2):261-7.

Aou S, Woody CD, Birt D. 1992. Changes in the activity of units of the cat motor cortex with rapid conditioning and extinction of a compound eyeblink movement. J Neurosci. 12:549–559.

Arikuni T, Kubota K. 1985. Claustral and amygdaloid afferents to the head of the caudate nucleus in macaque monkeys. Neuroscience research. 2(4):239-254.

Atkinson RC, Shiffrin RM. 1968. Human memory: A proposed system and its control processes. Psychology of learning and motivation. 2(4):89-195.

Atlan G, Terem A, Peretz-Rivlin N, Groysman M, Citri A. 2017. Mapping synaptic cortico-claustral connectivity in the mouse. J Comp Neurol. 525:1381–1402.

Atlan G, Terem A, Peretz-Rivlin N, Sehrawat K, Gonzales BJ, Pozner G, Tasaka GI, Goll Y, Refaeli R, Zviran O, Lim BK, Groysman M, Goshen I, Mizrahi A, Nelken I, Citri A. 2018. The claustrum supports resilience to distraction. Curr Biol. 28:2752–2762.

Baddeley AD, Hitch G. 1974. Working memory. In *Psychology of learning and motivation* (Vol. 8, pp. 47-89). Academic press.

Bahro M, Molchan SE, Sunderland T, Herscovitch P, Schreurs BG. 1999. The effects of scopolamine on changes in regional cerebral blood flow during classical conditioning of the human eyeblink response. Neuropsychobiology. 39(4):187-95.

Barthó P, Hirase H, Monconduit L, Zugaro M, Harris KD, Buzsáki G. 2004. Characterization of neocortical principal cells and interneurons by network interactions and extracellular features. J Neurophysiol. 92:600–608.

Bartos M, Vida I, Jonas P. 2007. Synaptic mechanisms of synchronized gamma oscillations in inhibitory interneuron networks. Nat Rev Neuroscience. 8(1):45–56.

Bayat A, Joshi S, Jahan S, Connell P, Tsuchiya K, Chau D, Syed T, Forcelli P, Koubeissi MZ. 2018. A pilot study of the role of the claustrum in attention and seizures in rats. Epilepsy Research, 140:97-104.

Berger TW, Rinaldi PC, Weisz DJ, Thompson RF. 1983. Single-unit analysis of different hippocampal cell types during classical conditioning of rabbit nictitating membrane response. J Neurophysiol. 50:1197-219.

Bermudez-Rattoni F, Introini-Collison IB, McGaugh JL. 1991. Reversible inactivation of the insular cortex by tetrodotoxin produces retrograde and anterograde amnesia for inhibitory avoidance and spatial learning. Proc Natl Acad Sci USA. 88:5379-5382.

Bernstein HG, Ortmann A, Dobrowolny H, Steiner J, Brisch R, Gos T, Bogerts B. 2016. Bilaterally reduced claustral volumes in schizophrenia and major depressive disorder: a morphometric postmortem study. European archives of psychiatry and clinical neuroscience, 266(1):25-33.

Birt D, Aou S, Woody CD. 2003. Intracellularly recorded responses of neurons of the motor cortex of awake cats to presentations of Pavlovian conditioned and unconditioned stimuli. Brain research. 969(1-2):205-16.

Black AH, Prokasy WF. 1972. Classical Conditioning II: Current Theory and Research. New York: Appleton-Century. pp. 64–99.

Blázquez PM, Fujii N, Kojima J, Graybiel AM. 2002. A network representation of response probability in the striatum. Neuron. 33:973–982.

Bickel S, Parvizi J. 2019. Electrical stimulation of the human claustrum. Epilepsy & Behavior, 97:296-303.

Binks D, Watson C, Puelles L. 2019. A re-evaluation of the anatomy of the claustrum in rodents and primates—analyzing the effect of pallial expansion. Front Neuroanat. 13:34.

Boele HJ, Koekkoek SK, De Zeeuw CI. 2010. Cerebellar and extracerebellar involvement in mouse eyeblink conditioning: the ACDC model. Frontiers in cellular neuroscience. 4; 3:19.

Bokil H, Andrews P, Kulkarni JE, Mehta S, Mitra PP. 2010. Chronux: a platform for analyzing neural signals. J Neurosci Methods. 192:146–151.

Braak H, Braak, E. 1982. Neuronal types in the claustrum of man. Anatomy and embryology, 163(4):447-460.

Bruguier H, Suarez R, Manger P, Hoerder-Suabedissen A, Shelton AM, Oliver DK, Packer AM, Ferran JL, García-Moreno F, Puelles L, Molnár Z. 2020. In search of common developmental and evolutionary origin of the claustrum and subplate. Journal of Comparative Neurology.

Buchanan SL, Powell DA. 1982. Cingulate cortex: its role in Pavlovian conditioning. Journal of comparative and physiological psychology, 96(5), p.755-774.

Buchanan SL, Powell DA, Buggy J. 1984. 3H-2-deoxyglucose uptake after electrical stimulation of cardioactive sites in anterior medial cortex in rabbits. Brain research bulletin, 13(3):371-382.

Burke CJ, Tobler PN, Baddeley M, Schultz W. 2010. Neural mechanisms of observational learning. Proc Natl Acad Sci 107: 14431 –14436.

Bush G, Luu P, Posner MI 2000. Cognitive and emotional influences in anterior cingulate cortex. Trends Cogn. Sci. 4, 215–222.

Buzsáki G, Kandel A. 1998. Somadendritic back propagation of action potentials in cortical pyramidal cells of the awake rat. J Neurophysiol. 79:1587–1591.

Campolattaro MM, Halverson HE, Freeman JH. 2007. Medial auditory thalamic stimulation as a conditioned stimulus for eyeblink conditioning in rats. Learning & memory. 14(3):152-9.

Cardin JA, Carlén M, Meletis K, Knoblich U, Zhang F, Deisseroth K, Tsai LH, Moore CI. 2009. Driving fast-spiking cells induces gamma rhythm and controls sensory responses. Nature. 459(7247):663-7.

Carlier P, Jamon M. 2006. Observational learning in C57BL/6j mice. Behav Brain Res 174: 125–131.

Carman JB, Cowan WM, Powell TP. 1964. The cortical projection upon the claustrum. J Neurol Neurosurg Psychiat. 27: 46–51.

Caro-Martín CR, Delgado-García JM, Gruart A, Sánchez-Campusano R. 2018. Spike Sorting based on shape, phase and distribution features, and K-TOPS clustering with validity an error indices. Scientific Reports. 8:17796.

Caro-Martín CR, Leal-Campanario R, Sánchez-Campusano R, Delgado-García JM, Gruart A. 2015. A variable oscillator underlies the measurement of time intervals in the rostral medial prefrontal cortex during classical eyeblink conditioning in rabbits. J Neurosci. 35:14809–14821.

Carretero-Guillén A, Pacheco-Calderón R, Delgado-García JM, Gruart A. 2015. Involvement of hippocampal inputs and intrinsic circuit in the acquisition of context and cues during classical conditioning in behaving rabbits. Cerebral Cortex. 1;25(5):1278-89.

Castellanos FX, Margulies DS, Kelly C, Uddin LQ, Ghaffari M, Kirsch A, Shaw D, Shehzad Z, Di Martino A, Biswal B, Sonuga-Barke EJX, Rotrosen J, Adler LA, Milham MP. 2008. Cingulate-precuneus interactions: a new locus of dysfunction in adult attention-deficit/hyperactivity disorder. Biol Psychiat. 63:332–337.

Cascella NG, Gerner GJ, Fieldstone SC, Sawa A, Schretlen DJ. 2011. The insula-claustrum region and delusions in schizophrenia. Schizophr Res.;133(1-3):77-81.

Cascella NG, Sawa A. 2014. The claustrum in schizophrenia. In *The Claustrum* (Smythies et al. 2014, eds):237–243, Academic Press

Cebolla AM, Cheron G. 2019. Understanding neural oscillations in the human brain: from movement to consciousness and vice versa. Front Psychol. 10:1930.

Chachich ME, Powell DA. 2004. The role of claustrum in Pavlovian heart-rate conditioning in the rabbit (Oryctolagus cuniculus): anatomical, electrophysiological, and lesion studies. Behav Neurosci. 118:514–525.

Chapman PF, Steinmetz JE, Sears LL, Thompson RF. 1990. Effects of lidocaine injection in the interpositus nucleus and red nucleus on conditioned behavioral and neuronal responses. Brain research. 537(1-2):149-56.

Chen L, Bao S, Lockard JM, Kim JK, Thompson RF. 1996. Impaired classical eyeblink conditioning in cerebellar-lesioned and Purkinje cell degeneration (pcd) mutant mice. Journal of Neuroscience. 16(8):2829-38.

Chen Z, Cui L, Li M, Jiang L, Deng W, Ma X, Wang Q, Huang C, Wang Y, Collier DA, Gong Q, Li T. 2012. Voxel based morphometric and diffusion tensor imaging analysis

in male bipolar patients with first-episode mania. Prog Neuropsychopharmacol Biol Psychiatry 36:231–238

Cheron G, Dan B, Márquez-Ruiz J. 2013. Translational approach to behavioral learning: lessons from cerebellar plasticity. Neural plasticity.

Chia Z, Silberberg G, Augustine GJ. 2017. Functional properties, topological organization and sexual dimorphism of claustrum neurons projecting to anterior cingulate cortex. Claustrum. 2:1.

Chia Z, Augustine GJ, Silberberg G. 2020. Synaptic connectivity between the cortex and claustrum is organized into functional modules. Curr Biol. (Accepted)

Christian KM, Thompson RF. 2003. Neural substrates of eyeblink conditioning: acquisition and retention. Learn Mem. 10:427–455.

Christian KM, Thompson RF. 2005. Long-term storage of an associative memory trace in the cerebellum. Behav Neurosci 119(2): 526-537.

Citri A, Barretta S. 2016. Claustral delusions. Claustrum. 1:1, 31426.

Clark GA, McCormick DA, Lavond DG, Thompson RF. 1984. Effects of lesions of cerebellar nuclei on conditioned behavioral and hippocampal neuronal responses. Brain Res. 291:125-136.

Cohen DH, Randall DC, 1984. Classical conditioning of cardiovascular responses. Annual Review of Physiology, 46(1):187-197.

Colechio EM, Alloway KD. 2009. Differential topography of the bilateral cortical projections to the whisker and forepaw regions in rat motor cortex. Brain Structure and Function, 213(4-5):423-439.

Constantinidis C, Goldman-Rakic PS. 2002. Correlated discharges among putative pyramidal neurons and interneurons in the primate prefrontal cortex. J Neurophysiol. 88:3487–3497.

Crick FC. 1994. The astonishing hypothesis. New York (NY): Charles Scribner's Sons.

Crick FC, Koch C. 2005. What is the function of the claustrum? Philos Trans R Soc Lond B Biol Sci. 360:1271-1279.

Csicsvari J, Hirase H, Czurkó A, Mamiya A, and Buzsáki G. 1999. Oscillatory coupling of hippocampal pyramidal cells and interneurons in the behaving rat. J Neurosci. 19:274–287.

Damasio AR. 1994. Descartes' Error. Emotion, Reason and the Human Brain. New York (Grosset/Putnam).

Davis WB. 2008. The claustrum in autism and typically developing male children: a quantitative MRI study.

Delgado-García JM, Evinger C, Escudero M, Baker R. 1990. Behavior of Accessory Abducens and Abducens Motoneurons During Eye Retraction and Rotation in the Alert Cat**.** J Neurophysiol. 64:413-422.ç

Delgado-García JM, Gruart A. 2002. The role of interpositus nucleus in eyelid conditioned responses. The Cerebellum. 1(4):289-308.

Delgado-García JM, Gruart A. 2005. Firing activities of identified posterior interpositus nucleus neurons during associative learning in behaving cats. Brain research reviews. 49(2):367-76.

Deligkaris K, Bullmann T, Frey U. 2016. Extracellularly recorded somatic and neuritic signal shapes and classification algorithms for high-density microelectrode array electrophysiology. Front Neurosci. 10:421. doi: 10.3389/fnins.2016.00421

Dickstein SG, Bannon K, Castellanos FX, Milham MP. 2006. The neural correlates of attention deficit hyperactivity disorder: an ALE meta-analysis. J Child Psychol Psychiatry. 47:1051–1062.

Dogbevia GK, Roβmanith M, Sprengel R, Hasan MT. 2016. Flexible, AAV-equipped genetic modules for inducible control of gene expression in mammalian brain. Mol Ther Nucleic Acids. 5:e309.

Dogbevia GK, Marticorena-Alvarez R, Bausen M, Sprengel R, Hasan MT. 2015. Inducible and combinatorial gene manipulation in mouse brain. Front Cell Neurosci. 9:142.

Donoghue JP, Parham C. 1983. Afferent connections of the lateral agranular field of the rat motor cortex. Journal of Comparative Neurology. 217(4):390-404.

Doyon J, Benali H. 2005. Reorganization and plasticity in the adult brain during learning of motor skills. Current opinion in neurobiology, 15(2):161-167.

Druga R., 1966. The claustrum of the cat (Felis domestica). *Folia morphologica*, *14*(1), p.7.

Druga R., 1968. Cortico-claustral connections. II. Connections from the parietal, temporal and occipital cortex to the claustrum. *Folia morphologica*, *16*(2), p.142.

Druga R. 1982. Claustro-neocortical connections in the cat and rat demonstrated by HRP tracing technique. J Hirnforsch. 23:191-202.

Druga R., 2014. The structure and connections of the claustrum. In *The claustrum* (pp. 29-84). Academic Press.

Druga R, Chen S, Bentivoglio M. 1993. Parvalbumin and calbindin in the rat claustrum: an immunocytochemical study combined with retrograde tracing from frontoparietal cortex. Journal of chemical neuroanatomy, 6(6):399-406.

Druga R, Rokyta R, Benes V. 1990. Claustro-neocortical projections in the rhesus monkey (projections to area 6). J Hirnforsch. 31:487-94.

Du M, Liu J, Chen Z, Huang X, Li J, Kuang W, Yang Y, Zhang W, Zhou D, Bi F, Kendrick KM, Gong Q. 2014. Brain grey matter volume alterations in late-life depression. J Psychiatry Neurosci 39:130275. doi: 10.1503/jpn.130275.

Duffau H, Mandonnet E, Gatignol P, Capelle L. 2007. Functional compensation of the claustrum: lessons from low-grade glioma surgery. J Neurooncol. 81:327–329.

Edelstein LR, Denaro FJ. 2004. The claustrum: a historical review of its anatomy, physiology, cytochemistry and functional significance. Cell Mol Biol. 50(6):675-702.

Ettlinger G, Wilson WA. 1990. Cross-modal performance: behavioral processes, phylogenetic considerations and neural mechanisms. Behav. Brain Res. 40, 169–192. doi: 10.1016/0166-4328(90)90075-P

Evarts EV, Fromm C, Kroller J, Jennings VA. 1983. Motor cortex control of finely graded forces. Journal of Neurophysiology, 49(5):1199-1215.

Fallon JH, Moore RY. 1978. Catecholamine innervation of the basal forebrain IV. Topography of the dopamine projection to the basal forebrain and neostriatum. Journal of Comparative Neurology. 180(3):545-79.

Fernández-Lamo I, Delgado-García JM, Gruart A. 2018. When and where learning is taking place: multisynaptic changes in strength during different behaviors related to the acquisition of an operant conditioning task by behaving rats. Cereb Cortex. 28: 1011-1023.

Fernández-Lamo I, Sánchez-Campusano R, Gruart A, Delgado-García JM. 2016. Functional states of rat cortical circuits during the unpredictable availability of a reward-related cue. Sci Rep. 6:37650.

Fernández-Miranda JC, Rhoton AL, Kakizawa Y, Choi C, Álvarez-Linera J. 2008. The claustrum and its projection system in the human brain: a microsurgical and tractographic anatomical study. Journal of neurosurgery, 108(4):764-774.

Fodoulian L, Gschwend O, Huber C, Mutel S, Salazar R, Leone R, Renfer JR, Ekundayo K, Rodriguez I, Carleton A. 2020. The claustrum-medial prefrontal cortex network controls attentional set-shifting. bioRxiv.

Freeman Jr JH, Gabriel M. 1999. Changes of cingulothalamic topographic excitation patterns and avoidance response incubation over time following initial discriminative conditioning in rabbits. Neurobiology of learning and memory. 72(3):259-72.

Fuster JM. 1997. The Prefrontal Cortex: anatomy, physiology, and neuropsychology of the frontal lobe. 3ed Edition Lippincott-William and Wilkins Eds, Philadelphia, U.S.A. 1–315

Gabriel M, Vogt BA, Kubota Y, Poremba A, Kang E. 1991. Training-stage related neuronal plasticity in limbic thalamus and cingulate cortex during learning: a possible key to mnemonic retrieval. Behavioural brain research. 46(2):175-85.

Galarreta M, Hestrin S. 2001. Spike transmission and synchrony detection in networks of GABAergic interneurons. Science. 292:2295–2299.

Gaston KE, 1978. Brain mechanisms of conditioned taste aversion learning: A review of the literature. Physiological Psychology. 6(3):340-353.

Gattass R, Soares JG, Desimone R, Ungerleider LG. 2014. Connectional subdivision of the claustrum: two visuotopic subdivisions in the macaque. Frontiers in systems neuroscience. 8, p. 63.

Gerwig M, Kolb FP, Timmann D. 2007. The involvement of the human cerebellum in eyeblink conditioning. The Cerebellum. 6(1):38.

Gibbs CM, Prescott LB, Powell DA. 1992. A comparison of multiple-unit activity in the medial prefrontal and agranular insular cortices during Pavlovian heart-rate conditioning in rabbits. Exp Brain Res. 89:599–610.

Girgis M, Shih-Chang W. 1981. A new stereotaxic atlas of the rabbit brain. St. Louis, (MO): Warren H. Green, Inc.

Gloor C, Luft AR, Hosp JA. 2015. Biphasic plasticity of dendritic fields in layer V motor neurons in response to motor learning. Neurobiology of learning and memory, 125:189-194.

Goll Y, Atlan G, Citri A. 2015. Attention: the claustrum. Trends Neurosci. 38:486-495.

Gormezano I, Kehoe EJ, Marshall BS. 1983. Twenty years of classical conditioning research with the rabbit. Prog Psychobiol Physiol Psychol 10: 197-275.

Gormezano I, Schneiderman N, Deaux E, Fuentes I. 1962. Nictitating membrane: classical conditioning and extinction in the albino rabbit. Science. 138(3536):33-34.

Graf M, Augustine G. 2019. Inhibitory microcircuit function in the claustrum. Society for Neuroscience. Abstract 289.07.

Graf M, Nair A, Wong KL, Tang Y, Augustine GJ. 2020. Identification of mouse claustral neuron types based on their intrinsic electrical properties. Eneuro 7(4).

Grant DA, Adams JK. 1944. 'Alpha'conditioning in the eyelid. Journal of Experimental Psychology. 34(2):136.

Green JT, Arenos JD. 2007. Hippocampal and cerebellar single-unit activity during delay and trace eyeblink conditioning in the rat. Neurobiology of learning and memory. 87(2):269-84.

Gruart A, Blázquez P, Delgado-García JM. 1995. Kinematics of spontaneous, reflex, and conditioned eyelid movements in the alert cat. J Neurophysiol. 74:226–248.

Gruart A, Delgado-García JM. 1994. Discharge of identified deep cerebellar nuclei neurons related to eye blinks in the alert cat. Neuroscience. 61(3):665-81.

Gruart A, Guillazo-Blanch G, Fernández-Mas R, Jiménez-Díaz L, Delgado-García JM. 2000b. Cerebellar posterior interpositus nucleus as an enhancer of classically conditioned eyelid responses in alert cats. Journal of Neurophysiology. 1;84(5):2680-90.

Gruart A, Muñoz MD, Delgado-García JM. 2006. Involvement of the CA3-CA1 synapse in the acquisition of associative learning in behaving mice. J Neurosci. 26:1077-1087.

Gruart A, Schreurs BG, del Toro ED, Delgado-García JM. 2000a. Kinetic and frequency-domain properties of reflex and conditioned eyelid responses in the rabbit. J Neurophysiol. 83:836–852.

Haley DA, Thompson RF, Madden IV J. 1988. Pharmacological analysis of the magnocellular red nucleus during classical conditioning of the rabbit nictitating membrane response. Brain research. 454(1-2):131-9.

Halverson HE, Lee I, Freeman JH. 2010. Associative plasticity in the medial auditory thalamus and cerebellar interpositus nucleus during eyeblink conditioning. Journal of Neuroscience. 30(26):8787-96.

Hasan MT, Hernández-González S, Dogbevia G, Treviño M, Bertocchi I, Gruart A, Delgado-García JM. 2013. Role of motor cortex NMDA receptors in learning-dependent synaptic plasticity of behaving mice. Nat Commun. 4:2258.

Hattori S, Yoon T, Disterhoft JF, Weiss C. 2014. Functional reorganization of a prefrontal cortical network mediating consolidation of trace eyeblink conditioning. J Neurosci. 34:1432–1445.

Hayashi-Takagi A, Yagishita S, Nakamura M, Shirai F, Wu YI, Loshbaugh AL, Kuhlman B, Hahn KM, Kasai H. 2015. Labelling and optical erasure of synaptic memory traces in the motor cortex. Nature, 525(7569):333-338.

Heilbronner SR, Hayden BY. 2016. Dorsal anterior cingulate cortex: a bottom-up view. Annu. Rev. Neurosci. 8, 149–170.

Heiney SA, Wohl MP, Chettih SN, Ruffolo LI, Medina JF. 2014. Cerebellar-dependent expression of motor learning during eyeblink conditioning in head-fixed mice. Journal of Neuroscience. 34(45):14845-53.

Hikosaka O, Nakamura K, Sakai K, Nakahara H. 2002. Central mechanisms of motor skill learning. Current opinion in neurobiology, 12(2):217-222.

Houk JC, Buckingham JT, Barto AG. 1996. Models of the cerebellum and motor learning. Behavioral and brain sciences, 19(3):368-383.

Ishii K, Tsuji H, Tamaoka A. 2011. Mumps virus encephalitis with symmetric claustrum lesions. American Journal of Neuroradiology, 32(7): E139-E139.

Jackson J, Karnani MM, Zemelman BV, Burdakov D, Lee AK. 2018. Inhibitory control of prefrontal cortex by the claustrum. Neuron. 99:1029–1039.

Jankowski MM, Islam MN, O'Mara SM. 2017. Dynamics of spontaneous local field potentials in the anterior claustrum of freely moving rats. Brain Res. 1677:101–117.

Jankowski MM, O'Mara SM. 2015. Dynamics of place, boundary and object encoding in rat anterior claustrum. Frontiers in Behavioral Neuroscience, 9, p.250.

Jiménez-Castellanos Jr J, Reinoso-Suárez F. 1985. Topographical organization of the afferent connections of the principal ventromedial thalamic nucleus in the cat. Journal of Comparative Neurology. 236(3):297-314.

Jurado-Parras MT, Gruart A, Delgado-García JM. 2012. Observational learning in mice can be prevented by medial prefrontal cortex stimulation and enhanced by nucleus accumbens stimulation. Learning & memory.19(3):99-106.

Jurado-Parras MT, Sánchez-Campusano R, Castellanos NP, del-Pozo F, Gruart A, Delgado-García JM. 2013. Differential contribution of hippocampal circuits to appetitive and consummatory behaviors during operant conditioning of behaving mice. J Neurosci. 33:2293–2304.

Kalashnikova NS. 1972. The role of the claustrum in conditioned reflex activity. Zhurnal vysshei nervnoi deiatelnosti imeni IP Pavlova. 22(1):76-81.

Kandel ER, Schwartz JH, Jessell TM eds. 2000. Principles of neural science (Vol. 4, pp. 1227-1246). New York: McGraw-Hill.

Kapp BS, Frysinger RC, Gallagher M, Haselton JR. 1979. Amygdala central nucleus lesions: effect on heart-rate conditioning in the rabbit. Physiology & behavior, 23(6):1109-1117.

Kim J, Matney CJ, Roth RH, Brown SP. 2016. Synaptic organization of the neuronal circuits of the claustrum. J Neurosci 36:773-784.

Kim JJ, Clark RE, Thompson RF. 1995. Hippocampectomy impairs the memory of recently, but not remotely, acquired trace eyeblink conditioned responses. Behavioral neuroscience. 109(2):195.

Koekkoek SK, Den Ouden WL, Perry G, Highstein SM, De Zeeuw CI. 2002. Monitoring kinetic and frequency-domain properties of eyelid responses in mice with magnetic distance measurement technique. Journal of neurophysiology. 88(4):2124-33.

Kolb B, Whishaw IQ. 1999. Fundamentals of Human Neurophychology. New York: Freeman WH.

Kowiański P, Dziewiątkowski J, Kowiańska J, Moryś J. 1999. Comparative anatomy of the claustrum in selected species: A morphometric analysis. Brain Behav Evol. 53:44-54.

Kowiański P, Moryś J, Dziewiatkowski J, Karwacki Z, Wisniewski HM. 2000. The combined retrograde transport and unbiased stereological study of the claustrocortical connections in the rabbit. Ann Anat. 182:111-122.

Kowiański P, Moryś J, Karwacki Z, Dziewiątkowski J, Narkiewicz O. 1998. The cortico-related zones of the rabbit claustrum—study of the claustrocortical connections based on the retrograde axonal transport of fluorescent tracers. Brain Res. 784:1-2.

Kronforst-Collins MA, Disterhoft JF. 1998. Lesions of the caudal area of rabbit medial prefrontal cortex impair trace eyeblink conditioning. Neurobiology of learning and memory. 69(2):147-62.

Krupa DJ, Thompson JK, Thompson RF. 1993. Localization of a memory trace in the mammalian brain. Science. 260:989–991.

Kurada L, Bayat A, Joshi S, Koubeissi MZ. 2019. The claustrum in relation to seizures and electrical stimulation. Front Neuroanat. 13:8.

Landau E. 1919. The comparative anatomy of the nucleus amygdalae, the claustrum and the insular cortex. Journal of Anatomy, 53(Pt 4), p.351.

Lattal KM, Lattal KA. 2012. Facets of Pavlovian and operant extinction. Behavioural processes, 90(1), 1-8.

Leal-Campanario R, Delgado-García JM, Gruart A. 2006. Microstimulation of the somatosensory cortex can substitute for vibrissa stimulation during Pavlovian conditioning. Proceedings of the National Academy of Sciences. 27;103(26):10052-7.

Leal-Campanario R, Delgado-García JM, Gruart A. 2013. The rostral medial prefrontal cortex regulates the expression of conditioned eyelid responses in behaving rabbits. J Neurosci. 33:4378-4386.

Leal-Campanario R, Fairén A, Delgado-García JM, Gruart A. 2007. Electrical stimulation of the rostral medial prefrontal cortex in rabbits inhibits the expression of conditioned eyelid responses but not their acquisition. Proc Natl Acad Sci USA. 104:11459–11464.

LeVay S. 1986. Synaptic organization of claustral and geniculate afferents to the visual cortex of the cat. Journal of Neuroscience, 6(12):3564-3575.

LeVay S, Sherk H. 1981. The visual claustrum of the cat. I. Structure and connections. Journal of Neuroscience. 1(9):956-980.

Lipski J. 1981. Antidromic activation of neurones as an analytic tool in the study of the central nervous system. J Neurosci Methods. 4:1–32.

Liu J, Wu R, Johnson B, Vu J, Bass C, Li JX. 2019. The claustrum-prefrontal cortex pathway regulates impulsive-like behavior. Journal of Neuroscience, 39(50):10071-10080.

Logue AW. 1979. Taste aversion and the generality of the laws of learning. Psychological Bulletin, 86(2), p.276.

Luppi PH, Billwiller F, Fort P. 2017. Selective activation of a few limbic structures during paradoxical (REM) sleep by the claustrum and the supramammillary nucleus: evidence and function. Current Opinion in Neurobiology, 44:59-64.

McCormick DA, Connors BW, Lighthall JW, Prince DA. 1985. Comparative electrophysiology of pyramidal and sparsely spiny stellate neurons of the neocortex. Journal of neurophysiology. 54(4):782-806.

Majak K, Kowiánski P, Morýs J, Spodnik J, Karwacki Z, Wisniewski HM. 2000. The limbic zone of the rabbit and rat claustrum: a study of the claustrocingulate connections based on the retrograde axonal transport of fluorescent tracers. Anat Embryol (Berl). 201:15–25.

Marchi G, Bentivoglio M, Minciacchi D, Molinari M. 1983. Claustrocortical projections studied in the cat by means of multiple retrograde fluorescent tracing. J Comp Neurol. 215:121-134.

Maren, S., 2001. Neurobiology of Pavlovian fear conditioning. Annual review of neuroscience, 24(1):897-931.

Márquez-Ruiz J, Ammann C, Leal-Campanario R, Ruffini G, Gruart A, Delgado-García JM. 2016. Synthetic tactile perception induced by transcranial alternating-current stimulation can substitute for natural sensory stimulus in behaving rabbits. Scientific reports. 6(1):1-2.

Márquez-Ruiz J, Leal-Campanario R, Sánchez-Campusano R, Molaee-Ardekani B, Wendling F, Miranda PC, Ruffini G, Gruart A, Delgado-García JM. 2012. Transcranial direct-current stimulation modulates synaptic mechanisms involved in associative learning in behaving rabbits. Proceedings of the National Academy of Sciences. 109(17):6710-5.

Marriott BA, Do AD, Zahacy R, Jackson J. 2020. Topographic gradients define the projection patterns of the claustrum core and shell in mice. Journal of Comparative Neurology.

Masimore B, Kakalios J, Redish AD. 2004. Measuring fundamental frequencies in local field potentials. J Neurosci Methods. 138:97–105.

Mathur BN, Caprioli RM, Deutch AY. 2009. Proteomic analysis illuminates a novel structural definition of the claustrum and insula. Cereb. Cortex. 19, 2372–2379.

Mathur BN. 2014. The claustrum in review. Front Syst Neurosci. 8:48.

Mechling AE, Hübner NS, Lee HL, Hennig J, von Elverfeldt D, Harsan LA. 2014. Fine-grained mapping of mouse brain functional connectivity with resting-state fMRI. Neuroimage, 96, 203–215.

Medina JF, Nores WL, Mauk MD. 2002. Inhibition of climbing fibres is a signal for the extinction of conditioned eyelid responses. Nature. 416(6878):330-333.

Medford N, Critchley HD. 2010. Conjoint activity of anterior insular and anterior cingulate cortex: awareness and response. Brain Struct. Funct. 214, 535–549.

Meletti S, Slonkova J, Mareckova I, Monti G, Specchio N, Hon P, Giovannini G, Marcian V, Chiari A, Krupa P, Pietrafusa N. 2015. Claustrum damage and refractory status epilepticus following febrile illness. Neurology. 85(14):1224-1232.

Menon V, Uddin LQ. 2010. Saliency, switching, attention and control: a network model of insula function. Brain Struct. Funct. 214, 655–667.

Milardi D, Bramanti P, Milazzo C, Finocchio G, Arrigo A, Santoro G, Trimarchi F, Quartarone A, Anastasi G, Gaeta M. 2013. Cortical and subcortical connections of the human claustrum revealed in vivo by constrained spherical deconvolution tractography. Cerebral Cortex. 25(2):406-14.

Minciacchi D, Molinari M, Bentivoglio M, Macchi G. 1985. The organization of the ipsi- and contralateral claustrocortical system in rat with notes on the bilateral claustrocortical projections in cat. Neuroscience. 16:557–576.

Mitra PP, Bokil H. 2008. Observed Brain Dynamics. New York (NY): Oxford University Press.

Miyashita E, Keller A, Asanuma H. 1994. Input-output organization of the rat vibrissal motor cortex. Experimental brain research. 99(2):223-32.

Mohapel P, Hannesson DK, Armitage LL, Gillespie GW, Corcoran ME. 2000. Claustral lesions delay amygdaloid kindling in the rat. Epilepsia, 41(9):1095-1101.

Morcuende S, Delgado-Garcıa JM, Ugolini G. 2002. Neuronal premotor networks involved in eyelid responses: retrograde transneuronal tracing with rabies virus from the orbicularis oculi muscle in the rat. Journal of Neuroscience. 22(20):8808-18.

Morys J, Bobinski M, Wegiel J, Wisniewski HM, Narkiewicz O. 1996. Alzheimer's disease severely affects areas of the claustrum connected with the entorhinal cortex. Journal of Brain Research, 37(2):173-180.

Múnera A, Gruart A, Muñoz MD, Fernández-Mas R, Delgado-García JM. 2001. Hippocampal pyramidal cell activity encodes conditioned stimulus predictive value during classical conditioning in alert cats. J Neurophysiol, 86:2571–2582.

Naqvi NH, Rudrauf D, Damasio H, Bechara A. 2007. Damage to the insula disrupts addiction to cigarette smoking. Science, 315(5811):531-534.

Narikiyo K, Mizuguchi R, Ajima A, Shiozaki M, Hamanaka H, Johansen JP, Mori K, Yoshihara Y. 2020. The claustrum coordinates cortical slow-wave activity. Nature Neuroscience:1-13.

Nicholson DA, Freeman Jr JH. 2002. Neuronal correlates of conditioned inhibition of the eyeblink response in the anterior interpositus nucleus. Behavioral neuroscience. 116(1):22.

Norimoto H, Fenk LA, Li HH, Tosches MA, Gallego-Flores T, Hain D, Reiter S, Kobayashi R, Macias A, Arends A, Klinkmann M. 2020. A claustrum in reptiles and its role in slow-wave sleep. Nature, 578(7795):413-418.

Norman RJ, Villablanca JR, Brown KA, Schwafel JA, Buchwald JS. 1974. Classical eyeblink conditioning in the bilaterally hemispherectomized cat. Experimental Neurology. 44(3):363-80.

Olson CR, Graybiel AM. 1980. Sensory maps in the claustrum of the cat. Nature, 288:479–481.

Oswald BB, Knuckley B, Mahan K, Sanders C, Powell DA. 2009. Prefrontal control of trace eyeblink conditioning in rabbits (Oryctolagus cuniculus) II: effects of type of unconditioned stimulus (airpuff vs. periorbital shock) and unconditioned stimulus intensity. Physiol Behav. 96:67-72.

Oswald BB, Maddox SA, Powell DA. 2008. Prefrontal control of trace eyeblink conditioning in rabbits: role in retrieval of the CR? Behavioral neuroscience, 122(4), p.841.

Pacheco-Calderón R, Carretero-Guillén A, Delgado-García JM, Gruart A. 2012. Red nucleus neurons actively contribute to the acquisition of classically conditioned eyelid responses in rabbits. Journal of Neuroscience. 32(35):12129-43.

Pagani M, Bifone A, Gozzi A. 2016. Structural covariance networks in the mouse brain. Neuroimage 129, 55–63.

Patru CM, Reser D. 2015. A new perspective on delusional states: Evidence for claustrum involvement. Frontiers in Psychiatry, 6, p.158.

Pavlov I. 1927. Conditioned reflexes: An investigation of the physiological activity of the cerebral cortex. Oxford University Press, London.

Penhune VB, Steele CJ. 2012. Parallel contributions of cerebellar, striatal and M1 mechanisms to motor sequence learning. Behavioural brain research, 226(2):579-591.

Powell DA. 1999. A behavioral stages model of classical (Pavlovian) conditioning: Application to cognitive aging. Neuroscience & Biobehavioral Reviews. 23(6):797-816.

Powell DA, Churchwell J, Burriss L. 2005. Medial prefrontal lesions and Pavlovian eyeblink and heart-rate conditioning: effects of partial reinforcement on delay and trace conditioning in rabbits (Oryctolagus cuniculus). Behav Neurosci. 119:180–189.

Powell DA, Buchanan SL, Gibbs CM. 1991. Role of the prefrontal—thalamic axis in classical conditioning. Progress in brain research. 85:433-66.

Powell DA, Skaggs H, Churchwell J, McLaughlin J. 2001. Posttraining lesions of the medial prefrontal cortex impair performance of Pavlovian eyeblink conditioning but

have no effect on concomitant heart-rate changes in rabbits (Oryctolagus cuniculus). Behavioral neuroscience, 115(5), p.1029.

Preston AR, Knuttinen MG, Christoff K, Glover GH, Gabrieli JD, Disterhoft JF. 2000. The neural basis of classical eyeblink conditioning: An event-related fMRI study. In Soc. Neurosci. Abstr (Vol. 26, p. 709).

Puelles L. 2014. Development and evolution of the claustrum. In Smythies JR, Edelstein LR, Ramachandran VS, editors. *The claustrum: structural, functional, and clinical neuroscience.* San Diego: Academic Press. pp 119–176.

Puelles L, Ayad A, Alonso A, Sandoval JE, Martínez-de-la-Torre M, Medina L, Ferran JL. 2016. Selective early expression of the orphan nuclear receptor Nr4a2 identifies the claustrum homolog in the avian mesopallium: Impact on sauropsidian/mammalian pallium comparisons. Journal of Comparative Neurology, 524(3):665-703.

Rahman FE, Baizer JS. 2007. Neurochemically defined cell types in the claustrum of the cat. Brain research, 1159:94-111.

Real MÁ, Dávila JC, Guirado S. 2006. Immunohistochemical localization of the vesicular glutamate transporter VGLUT2 in the developing and adult mouse claustrum. Journal of chemical neuroanatomy, 31(3):169-177.

Reep RL, Corwin JV, Hashimoto A, Watson RT. 1987. Efferent connections of the rostral portion of medial agranular cortex in rats. Brain research bulletin. 19(2):203-21.

Remedios R, Logothetis NK, Kayser C. 2009. An auditory region in the primate insular cortex responding preferentially to vocal communication sounds. J Neurosci. 29:1034–1045.

Remedios R, Logothetis NK, Kayser C. 2010. Unimodal responses prevail within the multisensory claustrum. J Neurosci. 30:12902–12907.

Remedios R, Logothetis NK, Kayser C. 2014. A role of the claustrum in auditory scene analysis by reflecting sensory change. Front Syst Neurosci. 8:44.

Renouard L, Billwiller F, Ogawa K, Clément O, Camargo N, Abdelkarim M, Gay N, Scoté-Blachon C, Touré R, Libourel PA, Ravassard P. 2015. The supramammillary nucleus and the claustrum activate the cortex during REM sleep. Science advances, 1(3), p.e1400177.

Rescorla RA, Wagner AR. 1972. A theory of Pavlovian conditioning: Variations in the effectiveness of reinforcement and nonreinforcement. In Black AH, Prokasy WF (eds.) Classical Conditioning II: Current Theory and Research. New York: Appleton-Century. pp. 64–99.

Rescorla RA. 1988. Behavioral studies of Pavlovian conditioning. Annu Rev Neurosci. 11:329–352.

Reser DH, Richardson KE, Montibeller MO, Zhao S, Chan JM, Soares JG, Chaplin TA, Gattass R, Rosa MG. 2014. Claustrum projections to prefrontal cortex in the capuchin monkey (Cebus apella). Frontiers in systems neuroscience. 8, p.123.

Reus-García MM, Sánchez-Campusano R, Ledderose J, Dogbevia GK, Treviño M, Hasan MT, Gruart A, Delgado-García JM. 2021. The claustrum is involved in cognitive processes related to the classical conditioning of eyelid responses in behaving rabbits. Cerebral Cortex. 31(1):281-300.

Riche D, Lanoir J. 1978. Some claustro-cortical connections in the cat and baboon as studied by retrograde horseradish persocidase transport. Journal of Comparative Neurology. 177(3):435-444.

Rieke F, Warland D, de Ruyter van Steveninck R, Bialek W. 1997. Spikes: exploring the neural code. Cambridge (MA): MIT Press.

Sakamoto T, Endo S. 2010. Amygdala, deep cerebellar nuclei and red nucleus contribute to delay eyeblink conditioning in C57BL/6 mice. European Journal of Neuroscience. 32(9):1537-51.

Sánchez-Campusano R, Gruart A, Delgado-García JM. 2007. The cerebellar interpositus nucleus and the dynamic control of learned motor responses. J Neurosci. 27:6620–6632.

Schacter DL. 1987. Implicit memory: History and current status. Journal of experimental psychology: learning, memory, and cognition. 13(3):501.

Schacter DL, Wagner AD. 2013. Learning and Memory. *Principles of Neural Science*. Ed. Kandel J, Schwartz T, Jessell S, Siegelbaum A, Hudspeth. McGraw-Hill. (5th Ed.) 1441-1461.

Schade Powers A, Coburn-Litvak P, Evinger C. 2010. Conditioned eyelid movement is not a blink. J Neurophysiol. 103:641-647.

Schmajuk NA, Christiansen BA. 1990. Eyeblink conditioning in rats. Physiology & behavior. 48(5):755-8.

Sears LL, Logue SF, Steinmetz JE. 1996. Involvement of the ventrolateral thalamic nucleus in rabbit classical eyeblink conditioning. Behavioural brain research. 74(1-2):105-17.

Seeley WW, Menon V, Schatzberg AF, Keller J, Glover GH, Kenna H, Reiss AL, Greicius MD. 2007. Dissociable intrinsic connectivity networks for salience processing and executive control. J. Neurosci. 27, 2349–2356.

Shapleske J, Rossell SL, Chitnis XA, Suckling J, Simmons A, Bullmore ET, Woodruff PW, David AS. 2002. A computational morphometric MRI study of schizophrenia: effects of hallucinations. Cereb. Cortex 12 (12), 1331–1341

Shenhav A, Botvinick MM, Cohen JD. 2013. The expected value of control: an integrative theory of anterior cingulate cortex function. Neuron 79, 217–240.

Sherk H, LeVay S. 1981. Visual claustrum: topography and receptive field properties in the cat. Science. 212:87–89.

Shibuya H, Yamamoto T. 1998. Electrophysiological and morphological features of rat claustral neurons: an intracellular staining study. Neuroscience 85:1037-1049.

Siegel JJ, Mauk MD. 2013. Persistent activity in prefrontal cortex during trace eyelid conditioning: dissociating responses that reflect cerebellar output from those that do not. J Neurosci. 33:15272–15284.

Simon B, Knuckley B, Churchwell J, Powell DA. 2005. Post-training lesions of the medial prefrontal cortex interfere with subsequent performance of trace eyeblink conditioning. Journal of Neuroscience. 25(46):10740-6.

Sloniewski P, Usunoff KG, Pilgrim CH. 1986. Retrograde transport of fluorescent tracers reveals extensive ipsi-and contralateral claustrocortical connections in the rat. Journal of Comparative Neurology. 246(4):467-77.

Smith JB, Alloway KD. 2010. Functional specificity of claustrum connections in the rat: Interhemispheric communication between specific parts of motor cortex. J Neurosci. 30:16832–16844.

Smith JB, Alloway KD, Hof PR, Orman R, Reser DH, Watakabe A, Watson GD. 2018. The relationship between the claustrum and endopiriform nucleus: A perspective towards consensus on cross-species homology. Journal of Comparative Neurology. 527(2):476-99.

Smith JB, Radhakrishnan H, Alloway KD. 2012. Rat claustrum coordinates but does not integrate somatosensory and motor cortical information. Journal of Neuroscience. 32(25):8583-8588.

Smith JB, Watson GDR, Liang Z, Liu Y, Zhang N, Alloway KD. 2019. A role for the claustrum in salience processing? Front Neuroanat. 13:64.

Smythies J, Edelstein L, Ramachandran V. 2012. The Functional Anatomy of the Claustrum: The Net That Binds.

Smythies J, Edelstein L, Ramachandran V. 2014. Hypotheses relating to the function of the claustrum. Front Integr Neurosci 6:53

Sohal VS, Zhang F, Yizhar O, Deisseroth K. 2009. Parvalbumin neurons and gamma rhythms enhance cortical circuit performance. Nature. 459(7247):698-702.

Solomon PR, Vander Schaaf ER, Thompson RF, Weisz DJ. 1986. Hippocampus and trace conditioning of the rabbit's classically conditioned nictitating membrane response. Behavioral neuroscience. 100(5):729.

Spector I, Hassmannova J, Albe-Fessard D. 1974. Sensory properties of single neurons of cat's claustrum. Brain Res. 66:39–65.

Sperner J, Sander B, Lau S, Krude H, Scheffner D. 1996. Severe transitory encephalopathy with reversible lesions of the claustrum. Pediatric radiology. 26(11):769-71.

Squire LR. 1987. Memory and brain. Oxford University Press.

Sridharan D, Levitin DJ, Menon V. 2008. A critical role for the right fronto-insular cortex in switching between central-executive and default mode networks. Proc. Natl. Acad. Sci. USA 105, 12569–12574.

Stanton ME, Freeman JH, Skelton RW. 1992. Eyeblink conditioning in the developing rat. Behavioral neuroscience. 106(4):657.

Steriade M, Apostol V, Oakson G. 1971. Control of unitary activities in cerebellothalamic pathway during wakefulness and synchronized sleep. J Neurophysiol. 34:389–413.

Sweeney ST, Broadie K, Keane J, Niemann H, O'Kane CJ. 1995. Targeted expression of tetanus toxin light chain in Drosophila specifically eliminates synaptic transmission and causes behavioral defects. Neuron. 14:341-351.

Takehara-Nishiuchi K, Kawahara S, Kirino Y. 2005. NMDA receptor-dependent processes in the medial prefrontal cortex are important for acquisition and the early stage of consolidation during trace, but not delay eyeblink conditioning. Learn Mem. 12:606-614.

Ten Brinke MM, Heiney SA, Wang X, Proietti-Onori M, Boele HJ, Bakermans J, Medina JF, Gao Z, De Zeeuw CI. 2017. Dynamic modulation of activity in cerebellar nuclei neurons during pavlovian eyeblink conditioning in mice. eLife. 6:e28132.

Terem A, Gonzales BJ, Peretz-Rivlin N, Ashwal-Fluss R, Bleistein N, Reus-Garcia MM, Mukherjee D, Groysman M, Citri A. 2020. Claustral neurons projecting to frontal

cortex mediate contextual association of reward. Current Biology. 30(18): pp.3522-3532.

Thompson RF. 1988. The neural basis of basic associative learning of discrete behavioural responses. Trends in neurosciences. 11(4):152-5.

Thompson RF. 2005. In search of memory traces. Annu Rev Psychol. 56:1–23.

Thompson RF, Steinmetz JE. 2009. The role of the cerebellum in classical conditioning of discrete behavioral responses. Neuroscience. 162(3):732-55.

Torgerson CM, Irimia A, Goh SY, Van Horn JD. 2015. The DTI connectivity of the human claustrum. Hum Brain Mapp. 36:827-838.

Torgerson CM, Van Horn JD. 2014. A case study in connectomics: the history, mapping, and connectivity of the claustrum. Front. Neuroinform. 8, 83.

Trigo JA, Gruart A, Delgado-García JM. 1999. Discharge profiles of abducens, accessory abducens, and orbicularis oculi motoneurons during reflex and conditioned blinks in alert cats. J Neurophysiol 81(4): 1666-1684.

Tulving E. 1985. How many memory systems are there? American psychologist. 40(4):385.

Ungerleider LG, Desimone R, Galkin TW, Mishkin M. 1984. Subcortical projections of area MT in the macaque. Journal of Comparative Neurology. 223(3):368-386.

Venneri A, Shanks M. 2014. The claustrum and Alzheimer's disease. In *The Claustrum* (pp. 263-275). Academic Press.

Viskontas IV, Ekstrom AD, Wilson CL, Fried I. 2007. Characterizing interneuron and pyramidal cells in the human medial temporal lobe in vivo using extracellular recordings. Hippocampus. 17:49–57.

Wada JA, Tsuchimochi H. 1997. Role of the claustrum in convulsive evolution of visual afferent and partial nonconvulsive seizure in primates. Epilepsia, 38(8):897-906.

Wang Q, Ng L, Harris JA, Feng D, Li Y, Royall JJ, Oh SW, Bernard A, Sunkin SM, Koch C, Zeng H. 2017. Organization of the connections between claustrum and cortex in the mouse. Journal of Comparative Neurology. 525(6):1317-1346.

Wang X, Jiao Y, Tang T, Wang H, Lu Z. 2013. Altered regional homogeneity patterns in adults with attention-deficit hyperactivity disorder. European journal of radiology, 82(9):1552-1557.

Wang Y, Xie P, Gong H, Zhou Z, Kuang X, Wang Y, Li AA, Li Y, Liu L, Veldman MB, Daigle TL. 2019. Complete single neuron reconstruction reveals morphological

diversity in molecularly defined claustral and cortical neuron types. BioRxiv, p.675280.

Ward RL, Flores LC, Disterhoft JF. 2012. Infragranular barrel cortex activity is enhanced with learning. Journal of neurophysiology. 108(5):1278-87.

Watson JB, Rayner R. 1920. Conditioned emotional reactions. J. Exp. Psychol. 3:1–14.

Wegiel, J. 2014. Delayed development of the claustrum in autism. In *The Claustrum* (Smythies JR et al., eds): 225–235, Academic Press.

Wegiel J, Flory M, Kuchna I, Nowicki K, Ma SY, Imaki H, Wegiel J, Cohen IL, London E, Brown WT, Wisniewski T. 2014b. Brain-region–specific alterations of the trajectories of neuronal volume growth throughout the lifespan in autism. Acta neuropathologica communications, 2(1), p.28.

Wegiel J, Moryś J, Kowiański P, Ma SY, Kuchna I, Nowicki K, Imaki H, Wegiel J, Flory M, Brown WT, Wisniewski T. 2014a. Delayed development of the claustrum in autism. In The claustrum (pp. 225-235). Academic Press.

Weible AP, McEchron MD, Disterhoft JF. 2000. Cortical involvement in acquisition and extinction of trace eyeblink conditioning. Behavioral neuroscience. 114(6):1058.

Weible AP, Weiss C, Disterhoft JF. 2003. Activity profiles of single neurons in caudal anterior cingulate cortex during trace eyeblink conditioning in the rabbit. J Neurophysiol. 90:599–612.

Weiss C, Disterhoft JF. 1996. Eyeblink conditioning, motor control, and the analysis of limbic-cerebellar interactions. Behavioral and Brain Sciences. 19(3):479-81.

Weiss C, Knuttinen MG, Power JM, Patel RI, O'Connor MS, Disterhoft JF. 1999. Trace eyeblink conditioning in the freely moving rat: optimizing the conditioning parameters. Behavioral neuroscience, 113(5), p.1100.

Welsh JP, Harvey JA. 1991. Pavlovian conditioning in the rabbit during inactivation of the interpositus nucleus. J Physiol (Lond). 444:459–480.

Welzl, H, D'Adamo, P, Lipp, HP. 2001. Conditioned taste aversion as a learning and memory paradigm. Behavioural brain research, 125(1-2):205-213.

White MG, Cody PA, Bubser M, Wang HD, Deutch AY, Mathur BN. 2017. Cortical hierarchy governs rat claustrocortical circuit organization. J Comp Neurol. 525:1347–1362.

White MG, Mathur BN. 2018. Frontal cortical control of posterior sensory and association cortices through the claustrum. Brain Struct. Funct. 223, 2999–3006.

White MG, Panicker M, Mu C, Carter AM, Roberts BM, Dharmasri PA, Mathur BN. 2018. Anterior cingulate cortex input to the claustrum is required for top-down action control. Cell Reports. 22:84–95.

Witter MP, Room P, Groenewegen HJ, Lohman AH. 1988. Reciprocal connections of the insular and piriform claustrum with limbic cortex: an anatomical study in the cat. Neuroscience. 24(2):519-39.

Woody CD, Vassilevsky NN, Engel J. 1970. Conditioned eye blink: unit activity at coronal-precruciate cortex of the cat. J Neurophysiol 33(6): 851-864.

Woody CD, Yarowsky PJ. 1972. Conditioned eye blink using electrical stimulation of coronal-precruciate cortex as conditional stimulus. J Neurophysiol 35(2): 242-252.

Woody CD, Yarowsky PJ, Owens J, Black-Cleworth P, Crow T. 1974. Effect of lesions of cortical motor areas on acquisition of conditioned eye blink in the cat. J Neurophysiol 37(3): 385-394.

Zhang S, Xu M, Chang WC, Ma C, Do JPH, Jeong D, Lei T, Fan JL, Dan Y. 2016. Organization of long-range inputs and outputs of frontal cortex for top-down control. Nature Neuroscience, 19(12), p.1733.

Zhang S, Xu M, Kamigaki T, Do JP, Chang WC, Jenvay S, Miyamichi K, Luo L, Dan Y. 2014. Long-range and local circuits for top-down modulation of visual cortex processing. Science 345(6197):660-665.

Zhang X, Hannesson DK, Saucier DM, Wallace AE, Howland J, Corcoran ME. 2001. Susceptibility to kindling and neuronal connections of the anterior claustrum. J. Neurosci. 21, 3674–3687.

Zhao Y, Araki S, Wu J, Teramoto T, Chang YF, Nakano M, Abdelfattah AS, Fujiwara M, Ishihara T, Nagai T, Campbell R. 2011. An expanded palette of genetically encoded Ca^{2+} indicators. Science. 333(6051):1888–91.

Zingg B, Dong HW, Tao HW, Zhang LI. 2018. Input–output organization of the mouse claustrum. Journal of Comparative Neurology. 526(15):2428-43.

Zingg B, Hintiryan H, Gou L, Song MY, Bay M, Bienkowski MS, Foster NN, Yamashita S, Bowman I, Toga AW, Dong HW. 2014. Neural networks of the mouse neocortex. Cell 156, 1096–1111.

Zola-Morgan S, Squire LR. 1993. Neuroanatomy of memory. Annual review of neuroscience. 16(1):547-63

.

8. ANNEXES

8.1. The claustrum is involved in cognitive processes related to the classical conditioning of eyelid responses in behaving rabbits.

Cerebral Cortex, 2020;00: 1–20

doi: 10.1093/cercor/bhaa225
Original Article

ORIGINAL ARTICLE

The Claustrum is Involved in Cognitive Processes Related to the Classical Conditioning of Eyelid Responses in Behaving Rabbits

M. Mar Reus-García[1], Raudel Sánchez-Campusano[1], Julia Ledderose[2,3], Godwin K. Dogbevia[3,4], Mario Treviño[3,5], Mazahir T. Hasan[3,6,7], Agnès Gruart[1] and José M. Delgado-García[1]

[1]Division of Neurosciences, Pablo de Olavide University, Seville 4103, Spain, [2]Institute of Biochemistry, Charité—Universitätsmedizin Berlin, Berlin 10117, Germany, [3]Max Planck Institute for Medical Research, Heidelberg 69120, Germany, [4]Division of Cardiac Surgery, University of Ottawa Heart Institute, Ottawa K1Y 4W7, Canada, [5]Laboratorio de Plasticidad Cortical y Aprendizaje Perceptual, Instituto de Neurociencias, Universidad de Guadalajara, Guadalajara 44130, México, [6]Laboratory of Memory Circuits, Achucarro Basque Center for Neuroscience, Leioa 48940, Spain and [7]Ikerbasque–Basque Foundation for Science, Bilbao 48013, Spain

Address correspondence to José M. Delgado-García, Division of Neurosciences, Pablo de Olavide University, Seville 41013, Spain. Email: jmdelgar@upo.es.

Abstract

It is assumed that the claustrum (CL) is involved in sensorimotor integration and cognitive processes. We recorded the firing activity of identified CL neurons during classical eyeblink conditioning in rabbits, using a delay paradigm in which a tone was presented as conditioned stimulus (CS), followed by a corneal air puff as unconditioned stimulus (US). Neurons were identified by their activation from motor (MC), cingulate (CC), and medial prefrontal (mPFC) cortices. CL neurons were rarely activated by single stimuli of any modality. In contrast, their firing was significantly modulated during the first sessions of paired CS/US presentations, but not in well-trained animals. Neuron firing rates did not correlate with the kinematics of conditioned responses (CRs). CL local field potentials (LFPs) changed their spectral power across learning and presented well-differentiated CL–mPFC/CL–MC network dynamics, as shown by crossfrequency spectral measurements. CL electrical stimulation did not evoke eyelid responses, even in trained animals. Silencing of synaptic transmission of CL neurons by the vINSIST method delayed the acquisition of CRs but did not affect their presentation rate. The CL plays an important role in the acquisition of associative learning, mostly in relation to the novelty of CS/US association, but not in the expression of CRs.

Key words: claustrum, classical eyeblink conditioning, local field potentials, rabbits, unitary recording, virus-delivered inducible silencing of synaptic transmission

Introduction

Since the original proposal of the claustrum (CL) as a structure involved in the integration of many different cortical and subcortical neural centers in order to generate conscious sensations (Crick 1994), we have seen a notable increase in the number of structural and hodological studies dealing with its peculiar central place in the brain and regarding its putative integrative role in higher brain functions. So far, the CL has been related to consciousness (Crick and Koch 2005; Kurada et al. 2019), salience detection (Smythies et al. 2012; Remedios et al. 2014; Smith et al. 2019), and segregation of attention (Mathur 2014; Goll et al. 2015; Atlan et al. 2018), among others topics. Although a number of reviews have also proposed a role of the CL in the integration of sensory information, perceptual binding, and internal functional states to generate cognitive-related processes (Edelstein and Denaro 2004; Crick and Koch 2005; Mathur 2014; Goll et al. 2015; Citri and Barretta 2016; Jackson et al. 2018), few studies address the contribution of CL neurons to associative learning, which certainly requires all the higher brain functions mentioned above.

The classical conditioning of eyelid responses is a well-known experimental procedure for the study of the neural basis of associative learning in mammals (Thompson 2005). It is generally assumed that the acquisition and storage of this type of learning takes place in the cerebellum (Krupa et al. 1993; Christian and Thompson 2003; Ten Brinke et al. 2017) or, at least, the timed performance of the acquired responses (Welsh and Harvey 1991; Sánchez-Campusano et al. 2007), mainly regarding delay paradigms. However, other brain structures also seem to participate in those processes. For example, motor cortices (MC) pyramidal neurons in rabbits fire well in advance of conditioned response (CR) initiation (Aou et al. 1992; Ammann et al. 2016). Moreover, electrical stimulation of the eyelid M1 area evoked motor responses with profiles and kinematics similar to those of CRs during classical conditioning (Ammann et al. 2016).

Still other cortical structures have been implicated in non-motor, cognitive components of the acquisition, storage, and retrieval of eyelid CRs. For example, the hippocampus seems to be implicated in the acquisition of trace eyeblink conditioning paradigms, in which a silent gap separates conditioned stimulus (CS) and unconditioned stimulus (US) presentations (Berger et al. 1983; Thompson 2005). The activity of pyramidal hippocampal neurons is related to the salience of CS presentations across training and/or to the increasing CS/US associative strength (Rescorla 1988; Múnera et al. 2001), but not to the biomechanics of eyelid CRs, a coding property also ascribed to the rostral cingulate cortices (CC; Weible et al. 2003; Hattori et al. 2014). Likewise, specific areas of the medial prefrontal cotices (mPFC) have been proposed as participating in the proper determination of CS/US time intervals (Siegel and Mauk 2013; Caro-Martín et al. 2015) and in partial reinforcement (Powell et al. 2005). The mPFC also plays a permissive role in the initial release of eyelid CRs, because its electrical stimulation in behaving rabbits prevents the expression of CRs, but CR acquisition (Leal-Campanario et al. 2007, 2013).

The CL is the most interconnected region per volume in the brain (Torgerson et al. 2015). Given its dense reciprocal connections with the above-mentioned cortical structures described above, CL neurons could also play an important role in motor and/or nonmotor neural activities related to classical eyeblink conditioning. Furthermore, it has been reported that CL neurons respond to numerous sensory stimuli (Spector et al. 1974; Olson and Graybiel 1980; Sherk and LeVay 1981; Remedios et al. 2010), a crucial requirement for this kind of associative learning.

Different experimental laboratory species, ranging from humans to mice, have been used in the study of this thin and irregular structure. Rodents are commonly used despite the fact that they present small CLs, not very well-separated from cortex (Binks et al. 2019). Consequently, targeting the CL may be complicated, and single-unit recordings are difficult to attain when animals are awake. Because CL volume increases with the cerebral hemisphere volume (Kowiański et al. 1999), the CL of rabbits and guinea pigs offers interesting possibilities given its size and isolated location. Compared with that of mice, the rabbit CL is a prominent structure, seven times larger in volume than the CL of mice. Further, the rabbit CL is distinctly separated from surrounding structures (i.e., the insular cortex and the putamen) by the fibers of a well-developed external and extreme capsule (Girgis and Shih-Chang 1981; Kowiański et al. 1999). These advantages facilitate targeting the CL during the in vivo recordings performed here. In addition, although CL volume and shape vary across species, a vast connectivity with the cortex seems to be a well-conserved characteristic of the CL in monkeys (Druga et al. 1990), cats (Druga 1982), mice (Atlan et al. 2017), rats (Majak et al. 2000), and rabbits (Kowiański et al. 1997, 2000).

For all the above reason, rabbits were prepared for recording the unitary activity of CL neurons during classical eyeblink conditioning, using a delay paradigm since CL is a pallial subcortical structure (Binks et al. 2019). In fact, trace conditioning is preferentially related to cortical structures (Clark et al. 1984; Takehara-Nishiuchi et al. 2005; Gruart et al. 2006; Oswald et al. 2009).

Previous research has established that the integral of the rectified electromyographic (EMG) activity of the orbicularis oculi (O.O.) muscle can precisely determine eyelid position (Gruart et al. 1995; Schade Powers et al. 2010). Therefore, implanting a recording electrode in the O.O. muscle, we could ascertain whether animals closed the eye due to CS presentations (i.e., as a CR), or to US presentations (i.e., as a UR), and monitor the learning process (Gruart et al. 2000; Leal-Campanario et al. 2007). Recorded CL neurons were classified according to their firing profiles during paired CS/US presentations. Their firing rates were found to be related to the acquisition process but not to the changes in latency and strength presented by CRs across training. Local field potentials (LFPs) recorded in CL, MC, and mPFC changed their spectral powers across conditioning sessions for all the selected frequency bands. Significant delta–gamma comodulations were detected at CL–mPFC network nodes during certain conditioning phases. Finally, the inactivation of CL neuron synaptic connectivity affected the number but not the amplitude of CRs. In accordance, the CL seems to be directly involved in cognitive aspects of the process of acquiring eyeblink CRs, such as attention to CS salience (Múnera et al. 2001; Atlan et al. 2018), but not in their proper performance (Ammann et al. 2016).

Material and Methods

Experimental Animals

Experiments were carried out in male rabbits (New Zealand white albino) obtained from an authorized supplier (Isoquimen, Barcelona, Spain). Animals were 2.5–3-months old and weighing

2–2.4 kg on arrival at the Animal House facilities of Pablo de Olavide University (Seville, Spain). Upon their arrival, animals were housed in individual cages provided with a burrow and different environmental stimuli, where they were maintained for the whole experiment. The room was kept on a 12/12 h light/-dark cycle with constant ambient temperature (21 ± 1 °C) and humidity (55 ± 7%). Food and water were available ad libitum.

Experiments were carried out following European Union Council (2010/276:33–79/EU) guidelines and Spanish (BOE 34:11370-421, 2013) regulations for the use of laboratory animals in chronic experiments. Experiments were also approved by the local Ethics Committee of Pablo de Olavide University.

Surgery

Animals were anesthetized with an intramuscular injection of a ketamine–xylazine cocktail (Ketaminol, 50 mg/mL; Rompun, 20 mg/mL; and atropine sulfate, 0.5 mg/mL) at an initial dosage of 1.0 mL/kg. Anesthesia was maintained by intravenous perfusion (93% saline, 4% Ketaminol, and 3% Rompun) at a flow rate of 10 mL/kg/h.

A first group of animals ($n = 7$) were prepared for the chronic recording of unitary activity in the CL during classical eyeblink conditioning ($n = 5$) and pseudoconditioning ($n = 2$) (Figs 1A–D and 2–4). A window (2 × 5 mm) was drilled through the parietal bone centered overlying the right rostral CL (rostral corners from bregma: AP = 4 mm, $L = -4$ to -6 mm; caudal corners: AP = -1 mm, $L = -7.5$ to -9.5 mm; Girgis and Shih-Chang 1981). A recording chamber was built with acrylic cement around the window and a sterile pin was fixed to one anterolateral corner of the recording window for reference purposes. The dura mater was removed, and the cortical surface was protected with an inert plastic cover and sterile gauze between recording sessions. A silver electrode (1 mm in diameter) was attached with small screws to the right bone as a ground. All these animals were implanted bilaterally with stimulating electrodes in the M1 subdivision of the MC (AP = 2 mm, $L = +2$ mm and -2 mm; $D = 1.5$ mm, with respect to brain surface; Girgis and Shih-Chang 1981) corresponding to the eyelid motor area (Ammann et al. 2016). In addition, five of them were also implanted with electrodes aimed at the prelimbic area of the mPFC (AP = 11 mm, $L = +1$ mm and -1 mm; $D = 2.5$ mm; Girgis and Shih-Chang 1981), while the other two were implanted in the CC (AP = 4 and 0 mm, $L = +2$ and -2 mm; $D = 1.5$ mm)—namely, three areas related with classical eyeblink conditioning (Weible et al. 2003; Caro-Martín et al. 2015; Ammann et al. 2016) and projecting to the CL (Smith and Alloway 2010; Atlan et al. 2017; White et al. 2017; Jackson et al. 2018). Stimulating electrodes were made with 200 µm varnished silver wire (California Fine Wire Company, CA, USA) bared ≈0.5 mm at the tip. Finally, animals were implanted with bipolar hook electrodes in both O.O. muscles to record their EMG activity (Fig. 2A). These electrodes were handmade from multistranded Teflon-coated stainless-steel wire (A-M Systems) with a total external diameter of ≈0.2 mm and bared ≈0.5 mm at the tip. For head-holding fixation during unitary recordings, animals were implanted with a head-holding device, made from three bolts cemented to the skull perpendicular to the stereotaxic plane. Stimulating and recording electrodes were connected to two nine-pin sockets affixed to the holding system.

A second group of animals ($n = 4$) were prepared for the chronic recording of LFPs in CL, MC, and mPFC (Figs 5 and 6 and Supplementary Fig. 1A,B,D). For this experiment, animals were implanted bilaterally with recording tetrodes in the rostrodorsal part of the CL (AP = 1 mm, $L = +6.5$ and -6.5 mm; $D = 6.5$ mm; Girgis and Shih-Chang 1981) and with recording bipolar electrodes in the mPFC (AP = 11 mm, $L = +1$ and -1 mm; $D = 2.5$ mm; Girgis and Shih-Chang 1981) and in the MC (AP = 2 mm, $L = +2$ and -2 mm; $D = 1.5$ mm; Girgis and Shih-Chang 1981). These electrodes were handmade from two (bipolar) or four (tetrodes) threads of 50 µm, Teflon-coated tungsten wire (Advent Research Materials Ltd). Animals were also implanted bilaterally with recording EMG electrodes in both upper eyelids and with a ground wire. All wires were soldered to three nine-pin connectors. Finally, animals were implanted with a head-holding system as described above.

A third group of animals ($n = 8$) were infected with a mix of recombinant adeno-associated viruses (rAAVs) equipped with enhanced green fluorescent protein (EGFP) and doxycycline-dependent tetracycline-controlled genetic switches, which release tetanus toxin (TeTxLC) and tandem dimer Tomato (tdTOM) when activated (vINSIST method, see below and Supplementary Appendix 1) (Fig. 7). These animals received a total of three microinjections (each of 2 µL) of the viral suspension in each CL (rostral, AP = 4 mm, $L = +5$ and -5 mm; $D = 5$ mm; medial, AP = 2 mm, $L = +7$ and -7 mm; D = 5.5 mm; and caudal, AP = 0.5 mm, $L = +8$ and -8 mm; $D = 6$ mm; Girgis and Shih-Chang 1981). Injections were carried out in both CLs, since it has been described as a powerful functional compensation system (Duffau et al. 2007). A 5 µL microsyringe (Hamilton®) was used for injecting the rAAVs. These animals were also implanted bilaterally with recording EMG electrodes in both upper eyelids and with a ground wire. All wires were soldered to one nine-pin connector. Finally, animals were implanted with a head-holding system as described above.

Recording and Stimulating Procedures

The initial training of the animals was started 1 week after surgery and lasted for 5 days. We used a Perspex box designed to limit the animal's movements (Gruart et al. 2000; Leal-Campanario et al. 2007). The box was placed on the recording table. The recording room was kept softly illuminated and the recording table was surrounded by a black cloth. The first two recording sessions were aimed at adapting the animal to the recording conditions. No stimulus was presented during these two sessions.

The EMG activity of the O.O. muscle and LFPs were recorded using Grass P511 differential amplifiers with a bandwidth of 0.1 Hz to 10 kHz (Grass-Telefactor).

Unitary recordings from CL neurons were carried out with glass micropipettes filled with 2 M NaCl (3–5 MΩ of resistance) and filtered analogically in a bandwidth of 1 Hz to 10 kHz (AC/DC differential amplifier; model 3000, A-M Systems). On occasion, we used tungsten microelectrodes of 5 MΩ of resistance (A-M Systems) for unitary recordings and local microlesions. The recording area was approached with the help of stereotaxic coordinates (Girgis and Shih-Chang 1981), and antidromic or orthodromic field and unitary potentials were evoked by electrical stimulation of MC, CC, and/or mPFC. To determine whether the recorded and the activated neuron were the same, we used the collision test (i.e., the antidromic invasion of a soma is prevented if the antidromic action potential collides with a spontaneous orthodromic action potential; see Fig. 1G1, and Múnera et al. 2001; Ammann et al. 2016). At the end of each recording session,

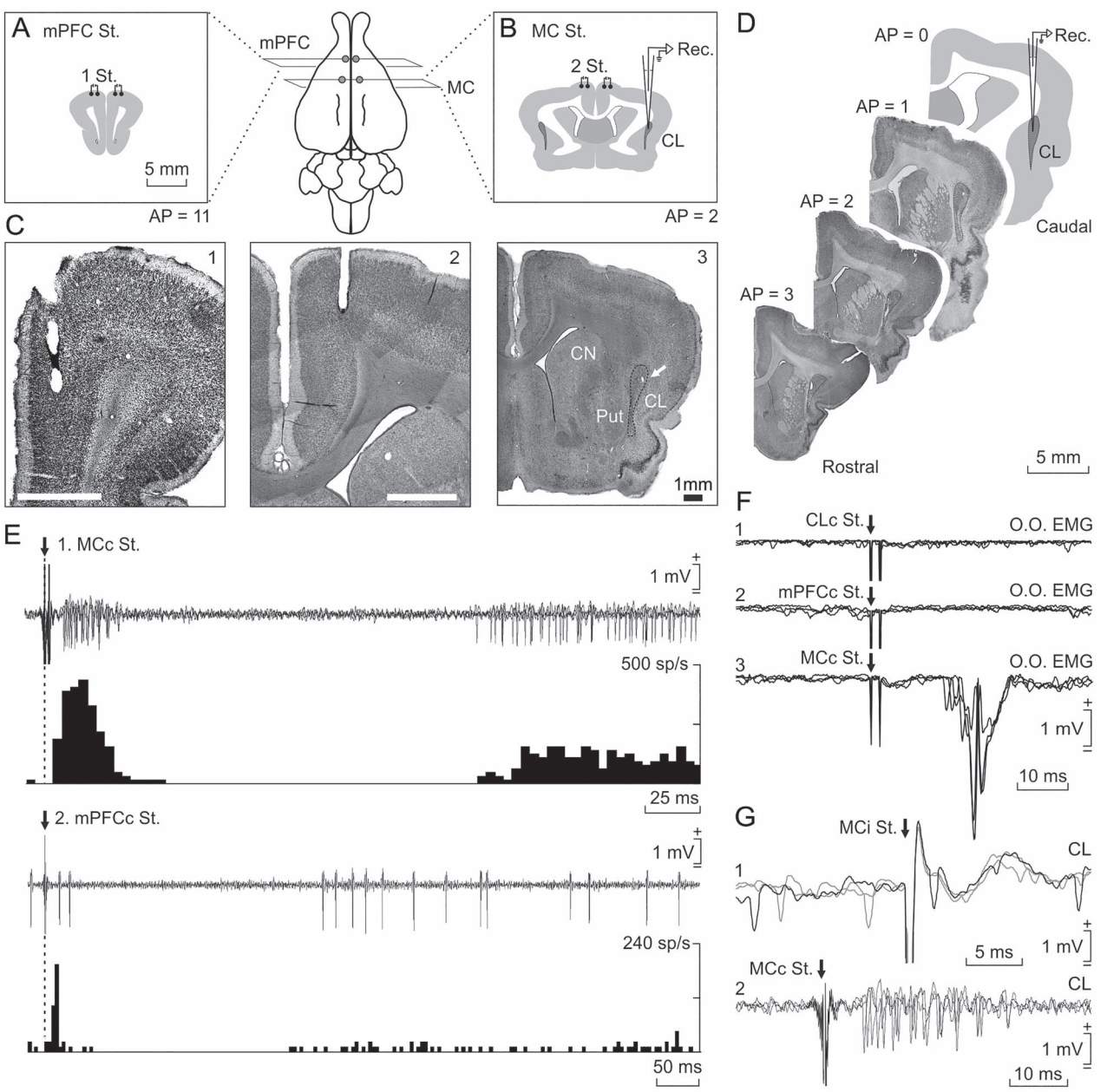

Figure 1. Location and identification of recorded neurons. Rabbits were bilaterally implanted with chronic stimulating electrodes in mPFC (*A*), M1 subdivision of MC (*B*), and CC (not illustrated). (*C*) Photomicrographs of coronal sections illustrating the location of stimulating electrodes in mPFC (1) and M1 (2). In (3), a microlesion in the dorsal CL is illustrated (arrow); it was carried out with a metal electrode implanted in a selected recording area; CN, caudate nucleus; Put, putamen. (*D*) Diagram of recording sites and images from targeted CL in four anteroposterior sections. The activity of CL neurons was recorded with glass micropipettes from rostral and central parts of the right dorsal CL (dotted line). Drawings in A, B, and D follow the atlas of Girgis and Shih-Chang (1981). (*E*) Three overlapped recordings illustrating short- and long-term synaptic activation of a CL neuron activated from the contralateral MC (1) and another one activated from the contralateral mPFC (2). Below each one is illustrated the peristimulus time histogram of 15 recordings. (*F*) From top to bottom are illustrated the EMG activity evoked in the left O.O. muscle by double pulses (2 ms interval) applied to the contralateral CL (1), mPFC (2), and MC (3). (*G*) Three overlapped recordings illustrating a CL neuron antidromically activated from the ipsilateral MC during the spike-triggered collision test (1). (2) illustrates the synaptic activation of a representative CL neuron from the contralateral MC.

the recording chamber was sterilized and closed with an inert plastic cover and sterile gauze and covered with bone wax.

Electrical stimulation of electrode-implanted sites consisted of single (square, 50 μs, 0.1–0.5 mA, positive–negative pulses with 20 μs of interval) or paired (1–2 ms of interval) pulses programmed with a CS-20 stimulator across an ISU-200-BIP isolation unit (Cibertec).

Classical Eyeblink Conditioning

Eyeblink conditioning was achieved using a delay conditioning paradigm (see Fig. 2 and Leal-Campanario et al. 2007). A 350-ms tone (600 Hz, 90 dB) was presented as CS and a 100-ms air puff (3 kg/cm^2) directed at the left cornea was used as US. The US was prepared to coterminate with the CS. The concept

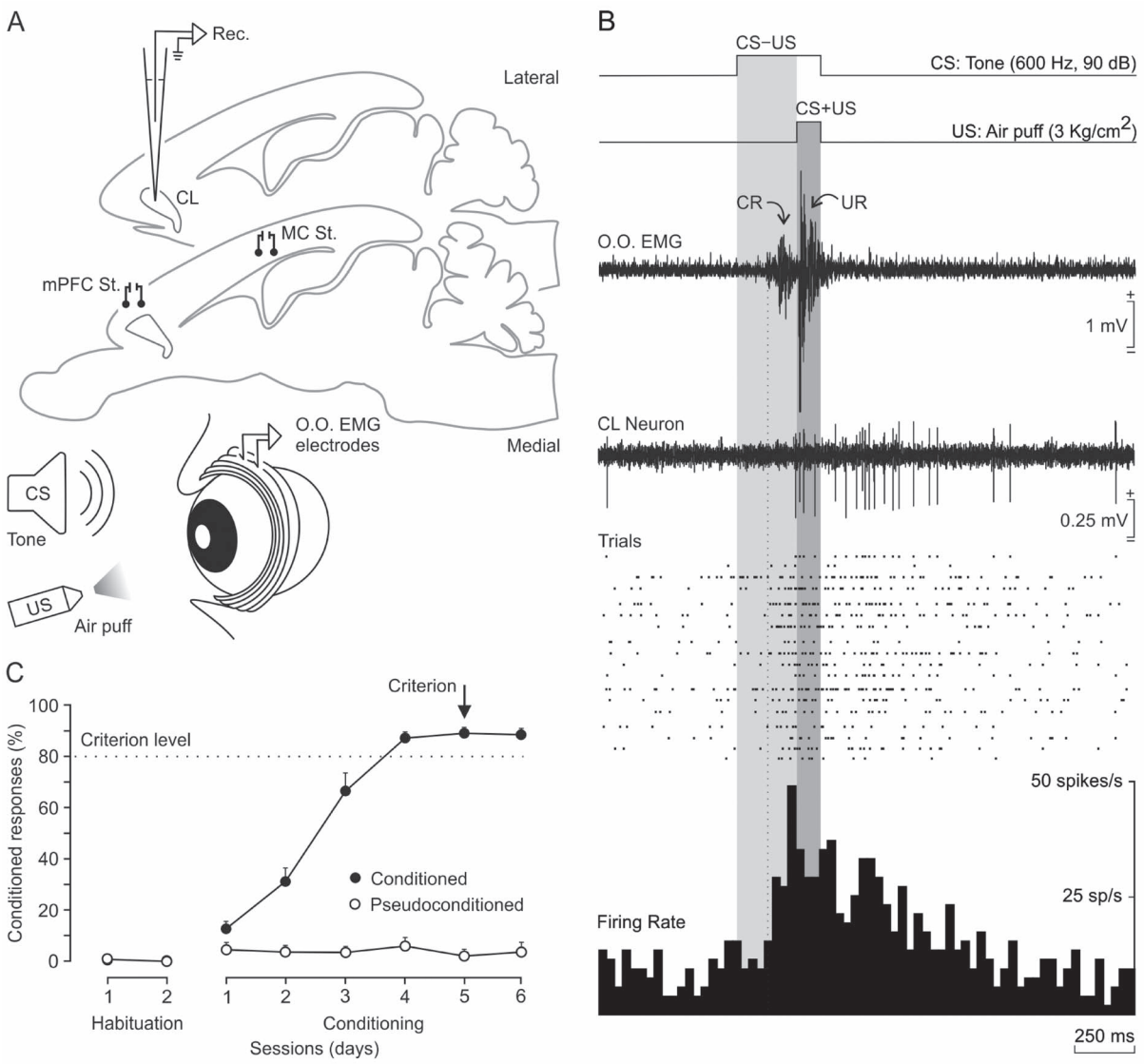

Figure 2. Classical eyeblink conditioning using a delay paradigm. (*A*) In addition to the stimulating electrodes, rabbits were implanted with EMG recording electrodes in the left O.O. muscle (O.O. EMG) aimed at recording CRs. (*B*) Representation of the delay paradigm and the firing activity of a selected CL neuron recorded during the fifth conditioning session. From top to bottom are shown: (1) the CS (a tone; 600 Hz, 90 dB, 350 ms); (2) the US (a corneal air puff; 3 kg/cm^2, 100 ms); (3) one example of the EMG activity of the O.O. muscle—note the presence of the CR in the CS–US interval as a learning-dependent response (light gray area) and the UR in the CS + US period as a reflex reaction (in dark gray area)—(4) the firing activity of a CL neuron during a CS/US presentation; (5) a raster plot of 18 successive CS/US trials; and (6) the peristimulus time histogram of all of them (in spikes/s). (*C*) Evolution of the percentage of CRs across six conditioning sessions for five conditioned and two pseudoconditioned rabbits. Note that conditioned animals reached the selected criterion (≥80% of CRs for two consecutive days) by the fifth conditioning session.

"CS/US" refers solely to the presentation of the pair of stimuli. We term "CS–US" the first 250 ms of the CS, right before the start of the US. It is during this time frame that CRs are expected to be found throughout conditioning. We considered a "CR" the presence, during the CS–US period, of the EMG activity of the left O.O. muscle lasting >10 ms and initiated >50 ms after CS onset (Gruart et al. 2000). We use "CS + US" to refer to this 100 ms coexisting period; UR will appear during this period. Recordings from the right O.O. muscle were used as a control for spontaneous and/or voluntary eyelid movements.

A function generator (AFG 3022B, Tektronix), triggered by a digital programmer (3.2-Microstim, Cibertec), was used to generate the train with tone characteristics (600 Hz, sine wave, 1 V). An amplifier (PA Amplifier FS-2035, Fonestar Systems, Madrid, Spain) converted the pulse to a tone (90 dB) via a loudspeaker located 60 cm in front of the animal. Air puffs were delivered from an air compressor (Biomedical Engineering) and applied through the opening of a plastic pipette (3 mm in diameter) attached to the animal's holding system and located 1 cm from the left cornea.

The first two sessions were aimed at adapting the animal to the experimental conditions. No stimulus was presented during these two sessions. Following them, unless otherwise indicated, animals received two habituation sessions (during which the CS was presented alone) and eight conditioning sessions (paired CS/US) ($n = 5$ rabbits). Both habituation and conditioning sessions consisted of 66 trials (6 series of 11 trials each). Successive trials were separated at random by intervals of 45–60 s

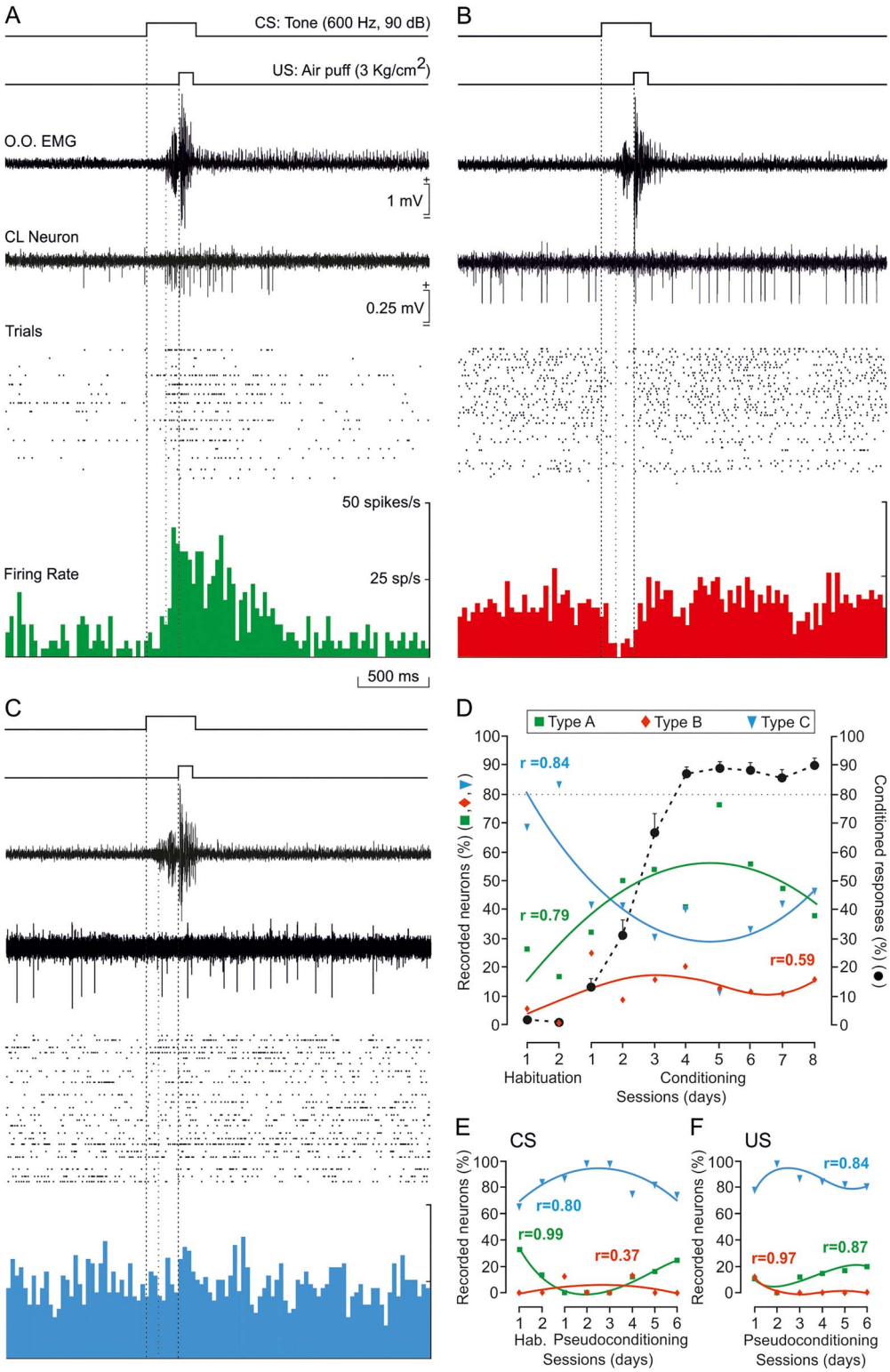

Figure 3. Types of firing rate recorded from CL neurons during classical eyeblink conditioning. (*A*) Example of a type A neuron, activated in advance of US onset, and recorded during the fifth conditioning session. (*B*) Example of a type B neuron, inhibited well in advance of the beginning of the CR, and recorded during the eighth conditioning session. (*C*) Example of a type C neuron, unrelated to the classical conditioning task, and recorded during the third conditioning session. Traces illustrated from top to bottom as in Figure 2B. Calibrations in *A* are also for *B* and *C*. (*D*) Percentages of claustral neurons ($n = 130$ from $n = 5$ rabbits) activated (green squares and lines), inhibited (red diamonds and lines), or unrelated (blue triangles and lines) to habituation and eight conditioning sessions. The black dotted line indicates the learning curve. (*E*,*F*) Percentages of CL neurons activated, inhibited, and unrelated to CS ($n = 47$ from $n = 2$ rabbits; *E*) or US ($n = 40$ from $n = 2$ rabbits; *F*) presentations during habituation and six pseudoconditioning sessions. Collected neuronal data in *D*–*F* were best represented with quadratic or higher order polynomial fits (see Supplementary Table 3). The regression coefficients (r) for the illustrated polynomial fits are indicated. The statistical performance was calculated according to the confidence interval (95%, $P < 0.05$).

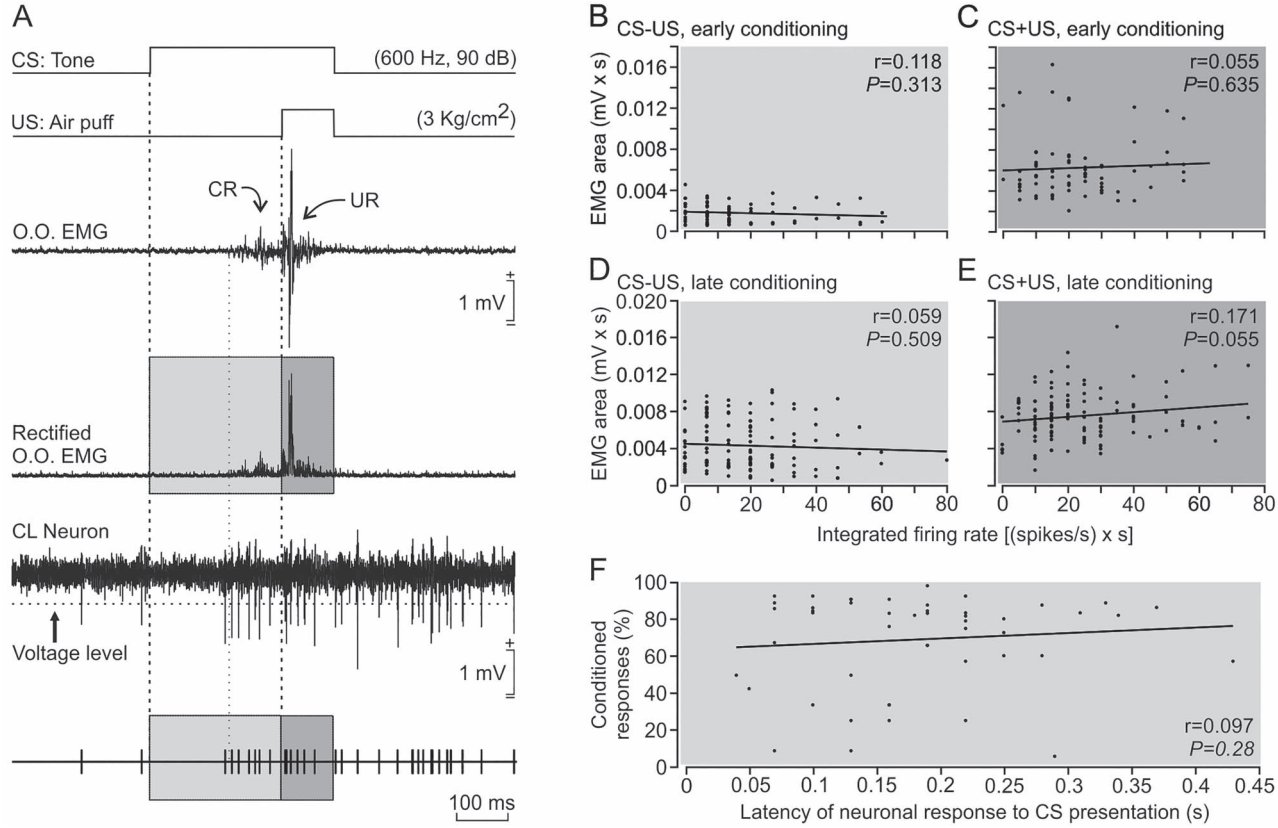

Figure 4. Relationships between changes in the firing rate of type A neurons and the EMG activity of the O.O. muscle and the percentage of CRs across conditioning. (*A*) From top to bottom are shown: a representation of the conditioning stimuli, one example of the EMG activity of the O.O. muscle with its rectified version below, the firing activity of a type A CL neuron during a CS/US presentation, and a representation of action potentials reaching the selected voltage level. For these analyses, we quantified the EMG area (mV × s) versus the integrated firing frequency [in (spikes/s) × s] during the CS–US period (light gray area) and also during CS + US interval (dark gray area)] ($n = 5$ rabbits). (*B*,*C*) Linear relationships between the EMG area and the integrated firing frequency of type A neurons for the CS–US interval (*B*) and the CS + US period (*C*) during early (first to third) conditioning sessions ($n = 75$ trials from $n = 17$ neurons). (*D*,*E*) Same relationships as in *B* and *C* but during late (fourth to eighth) conditioning sessions ($n = 127$ trials from $n = 25$ neurons). (*F*) Relationship between the activation latency of type A neurons after CS presentations and the percentage of CRs ($n = 51$ neurons). Note the low values of regression coefficients (*r*) for all the illustrated relationships (see Supplementary Table 5).

(3.2-Microstim, Cibertec). During conditioning sessions, the first trial of each one of the six series consisted of a test trial in which the CS was presented alone (a total of six test trials per session). As selected criterion for learning, the animals had to generate ≥80% of CRs in two successive conditioning sessions. Pseudoconditioned animals ($n = 2$ rabbits) received two habituation sessions as described above and six pseudoconditioning sessions (all conditioned animals learned the task and reached the criterion before the sixth conditioning session) with unpaired, randomized CS and US presentations. All sessions lasted ~80 min. Unitary and/or field recordings were carried out during all of the indicated sessions.

Histology

Once the electrophysiological experiments were finished, animals were deeply anesthetized with sodium pentobarbital (50 mg/kg, i.p.), and perfused transcardially with saline and 4% paraformaldehyde. The proper location of eyelid EMG and stimulating electrodes was checked. To facilitate the location of recording sites in the CL, a small electrolytic lesion (0.2–0–4 mA of anodic current for 30 s; CS-220 stimulator across an ISU-200-BIP isolation unit; Cibertec) was carried out during the final recording sessions and relevant coronal sections were processed for Nissl staining. Recording sites were adjusted according to the collected stereotaxic coordinates and with the location of the electrolytic marks (Fig. 1C,D and Supplementary Fig. 1D).

The vINSIST Method

We developed an advanced method for doxycycline (Dox)-controlled virus-delivered inducible silencing of synaptic transmission (vINSIST) between connected circuits. The three rAAVs contained in the injected mix were as follows: (1) rAAV–PhSYN–rtTA, (2) rAAV–Ptetbi–TeTxLC/tdTOM, and (3) rAAV–PhSYN–EGFP. We engineered the tetanus toxin light-chain coding sequence (TeTxLC) for selective cleavage of synaptobrevin-2 (Syb-2) to block synaptic transmission (Sweeney et al. 1995) into a bidirectional tetracycline promoter (P_{tet}bi) (Hasan et al. 2013; Dogbevia et al. 2015, 2016) with TeTxLC on one side and tandem dimer Tomato gene (tdTOM, expressing red fluorescent protein) on the other (rAAV–Ptetbi–TeTxLC/tdTOM). A reverse tetracycline transactivator (rtTA) and EGFP are independently expressed under the human synapsin promoter (rAAV–PhSYN–rtTA and rAAV–PhSYN–EGFP), so rtTA-infected cells will be traceable in green. With the addition of Dox, a hydrophobic

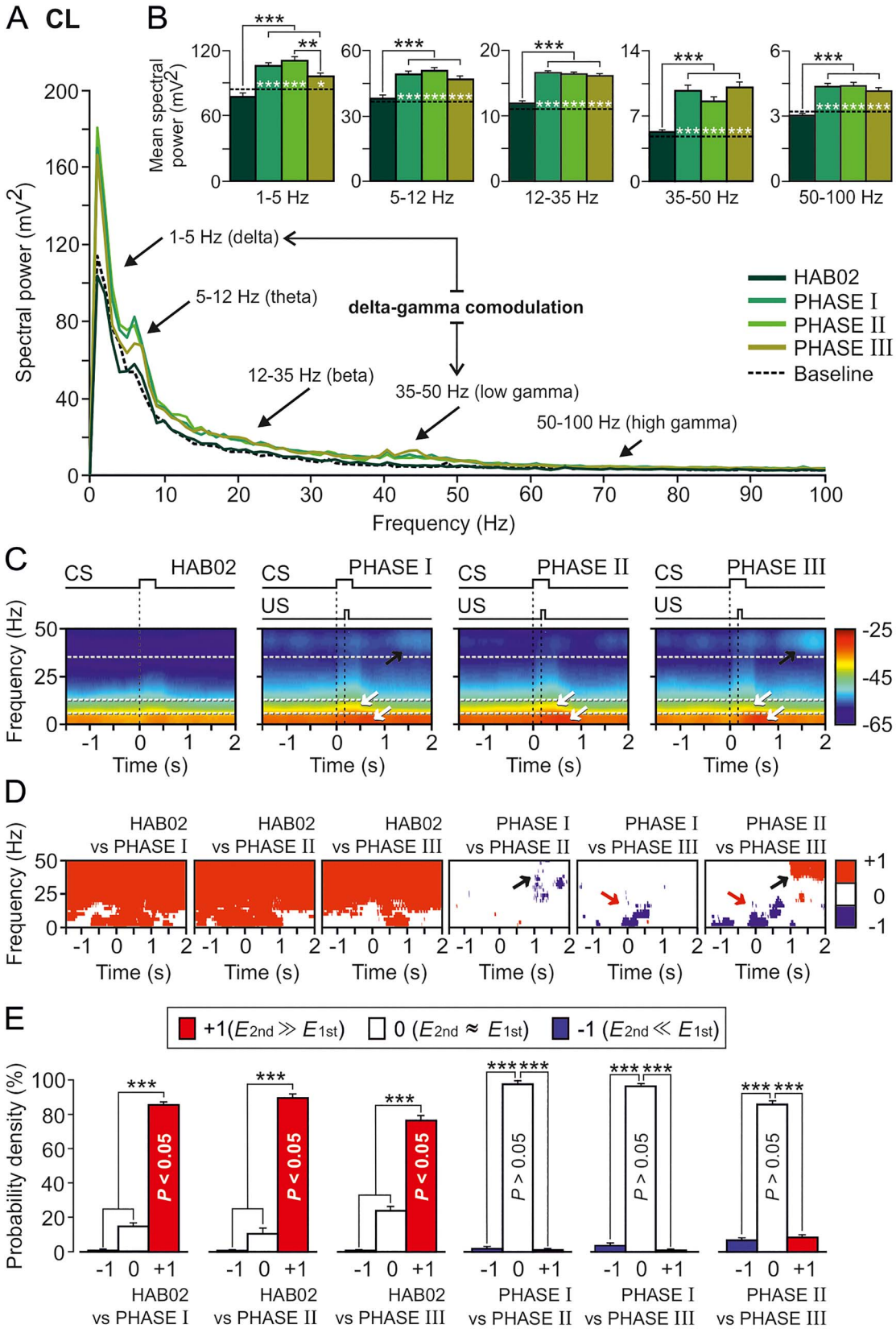

Figure 5. Spectral analyses of LFPs recorded in the CL during classical eyeblink conditioning. LFPs were recorded during habituation and conditioning phases from four rabbits. (*A*) Mean power spectra of LFPs recorded in the CL for 120 3.5 s frames (between 1.5 s before and 2 s after CS presentation) for four of the conditions (HAB02, phase I, phase II, and phase III) and for 3.5 s baseline frames (taken from HAB02 sessions but including no stimulus). The black arrows indicate the spectral ranges

derivative of tet that rapidly crosses the blood–brain–barrier, rtTA binds $\mathbf{P}_{tet}$bi and activates the expression of TeTxLC (to silence synaptic transmission) and tdTOM (thus the inhibited location will glow in red; Fig. 7 and Supplementary Fig. 2 and Supplementary Appendix 1).

Rabbit Brain Slices

Brains from the vINSIST-injected rabbits were fixed in PFA (4%) at 4 °C overnight. Brains were then cut by a vibratome (Leica VT 1000S) in sections 140 µm thick. The sections were mounted in glycerol (80% in PBS + 2.5% DAPCO). Slices were imaged on a confocal laser scanning microscope (Leica TCS SP5) using a 10× air objective and a 20× oil immersion objective and a 488 nm argon laser. Images were taken in z-stacks of 2 and 3 µm on the 10× and the 20× objectives, respectively.

Data Collection and Analysis

The unrectified EMG activity of the O.O. muscle, the unitary activity of CL neurons, LFPs recorded in the CL, and 1-volt rectangular pulses corresponding to CS and US presentations were acquired online through an 8-channel analog-to-digital converter (CED 1401-plus, CED, Cambridge, UK), and transferred to a computer for quantitative offline analysis. Data were sampled at 4 kHz for LFP recordings, 5 kHz for EMG activities, and 25 kHz for unitary recordings, with an amplitude resolution of 12 bits.

Computer programs (Spike2 and SIGAVG from CED) were used to display unrectified and rectified EMG, unitary activities, and LFPs (Figs 2–6 and Supplementary Fig. 1). As illustrated in Figures 1–4, the recorded neuron was generally easy to identify. In the case of multiple unitary recordings in which it was difficult to identify a single cell, a spike sorting (from Spike2, CED) was carried out. In all cases, an event channel was created for each identified neuron in which each event corresponded to a single spike. The representation programs enabled display of event rasters of unitary activities and the poststimulus time histograms (PSTHs). Following Rieke et al. (1997), PSTHs were converted to firing rates as a function of time (i.e., in spikes/s) for the characterization of the firing properties of the CL neurons. For the classification of the CL neurons in different groups, we used not only their firing rate profiles but also spike duration parameters (see Supplementary Fig. 3 and Supplementary Appendix 2).

Programs also enabled quantifying the activation latencies of CRs (ms) and unitary recordings (ms), the rectified EMG areas (mV × s or mV × ms), and the integrated firing rate [(spikes/s) × s] (Caro-Martín et al. 2015; Ammann et al. 2016).

Statistical analyses for unitary and EMG activities were carried out using the Sigma Plot 11.0 package (Sigma Plot) and the Statistics MATLAB Toolbox (version 9.4, R2018a; The MathWorks) for Windows, for a statistical significance level of $P < 0.05$. Mean values are followed when necessary by their standard error mean (SEM). Statistical differences of mean values were determined by analysis of variance (ANOVA). Regression analyses were carried out using ≥50 measurements collected from at least four animals.

From spectral analyses, we selected LFP epochs lasting 3.5 s (1.5 s preceding and 2 s following CS presentation). Analyses in the frequency domain were carried out in accordance with the following frequency bands: delta (1–5 Hz), theta (5–12 Hz), beta (12–35 Hz), low gamma (35–50 Hz), and high gamma (50–100 Hz). The processing of LFP recordings both in the frequency domain by means of fast Fourier transforms (FFT; Figs 5A and 6A,D,G,J) and in the time–frequency domain by means of multitaper Fourier transforms (mTFT; Figs 5C and 6C,F,I,L) were carried out using homemade programs (Jurado-Parras et al. 2013; Fernández-Lamo et al. 2016) written in the MATLAB platform (version 9.4, R2018a; The MathWorks) and customized scripts of Chronux (Mitra and Bokil 2008; Bokil et al. 2010) software (versions 2.11/R2014 and 2.12/R2018. Website: http://chronux.org/). Probability maps for the comparison of pairs of spectrograms were generated following previous descriptions by our group (Fernández-Lamo et al. 2016). In addition, to assess the putative spectral couplings between different oscillatory activities from LFP recordings, the crossfrequency correlation (Masimore et al. 2004) as a measure of comodulation and the power–power spectral ratios were calculated (see Supplementary Appendix 3).

For multivariate statistics assessments, both parametric (Fisher ANOVA *F*-tests, without or with repeated measures) and nonparametric [ANOVA tests on ranks, without repeated measures (Kruskal–Wallis ANOVA)] methods were used to assess the statistical significance of differences between groups, followed by the appropriate test (Holm–Sidak, Tukey–Kramer, or Student–Newman–Keuls tests, in this order of priority when the group sizes are equal; and the Dunn's test when the sizes are different) for all the pairwise multiple-comparison analyses (Jurado-Parras et al. 2013; Fernández-Lamo et al. 2016).

corresponding to delta (1–5 Hz), theta (5–12 Hz), beta (12–35 Hz), and low- (35–50 Hz) and high- (50–100) gamma bands. Although the fundamental contribution to CL power spectrum was determined by delta and theta frequency bands, prominent (well-differentiated) power peaks appeared in delta and low gamma bands during phases I and III. Therefore, the resulting delta–gamma comodulation is also indicated. (*B*) Histograms of mean spectral powers for all the defined frequency bands. Note that the start of conditioning phases significantly increased the spectral powers in the five frequency bands (Tukey–Kramer multiple comparison test: HAB02 and Baseline vs. phases I, II, and III; $^{***}P < 0.001$). Also note that baseline values (dotted black line) were very similar to those collected during the presentation of the unpaired CS (HAB02). (*C*) Time–frequency representations (spectrograms; $N_T \times K = 600$ tapered Fourier transforms) corresponding to data from HAB02 and conditioning phases I, II, and III illustrated in *A* and *B*. Note that maximum spectral powers (see the color calibration bar at the right) for delta and theta occurred during and shortly after CS/US presentations, in the three conditioning phases (white arrows), but maxima for low gamma appeared 1 s after the CS/US, during phases I and III (black arrows). (*D*) Multiple comparisons between the different spectrograms and their corresponding probabilistic maps according to the jackknifed variance criterion. Red (inference type +1; power in first spectrogram ≫ power in second spectrogram) and blue (inference type −1; power in first spectrogram ≪ power in second spectrogram) indicate significant statistical differences ($P < 0.05$; jackknifed estimates of the variance), and white (inference type 0; power in first spectrogram ≈ power in second spectrogram) indicates no significant differences ($P > 0.05$). Black arrows indicate that the spectral powers in the low-gamma frequency band were higher in phases I and (especially) III when comparing with phase II; that increment occurred at the end (range between 1 and 2 s after the CS/US presentation) of the analyzed epoch. Red arrows show how, in contrast, spectral powers in low frequencies were higher in phases I and (especially) II when comparing with phase III during and slightly after the CS/US presentation. (*E*) Histograms of mean probability densities. Here, it is very evident ($^{***}P < 0.001$, Tukey–Kramer test) that there are statistically significant differences ($P < 0.05$, red bars) between the habituation (HAB02) and the conditioning (I, II, and III) phases in practically the whole time–frequency range. Although they present some specific significant differences in delta, theta, and low gamma bands, the three conditioning sessions are not statistically different overall ($P > 0.05$, white bars).

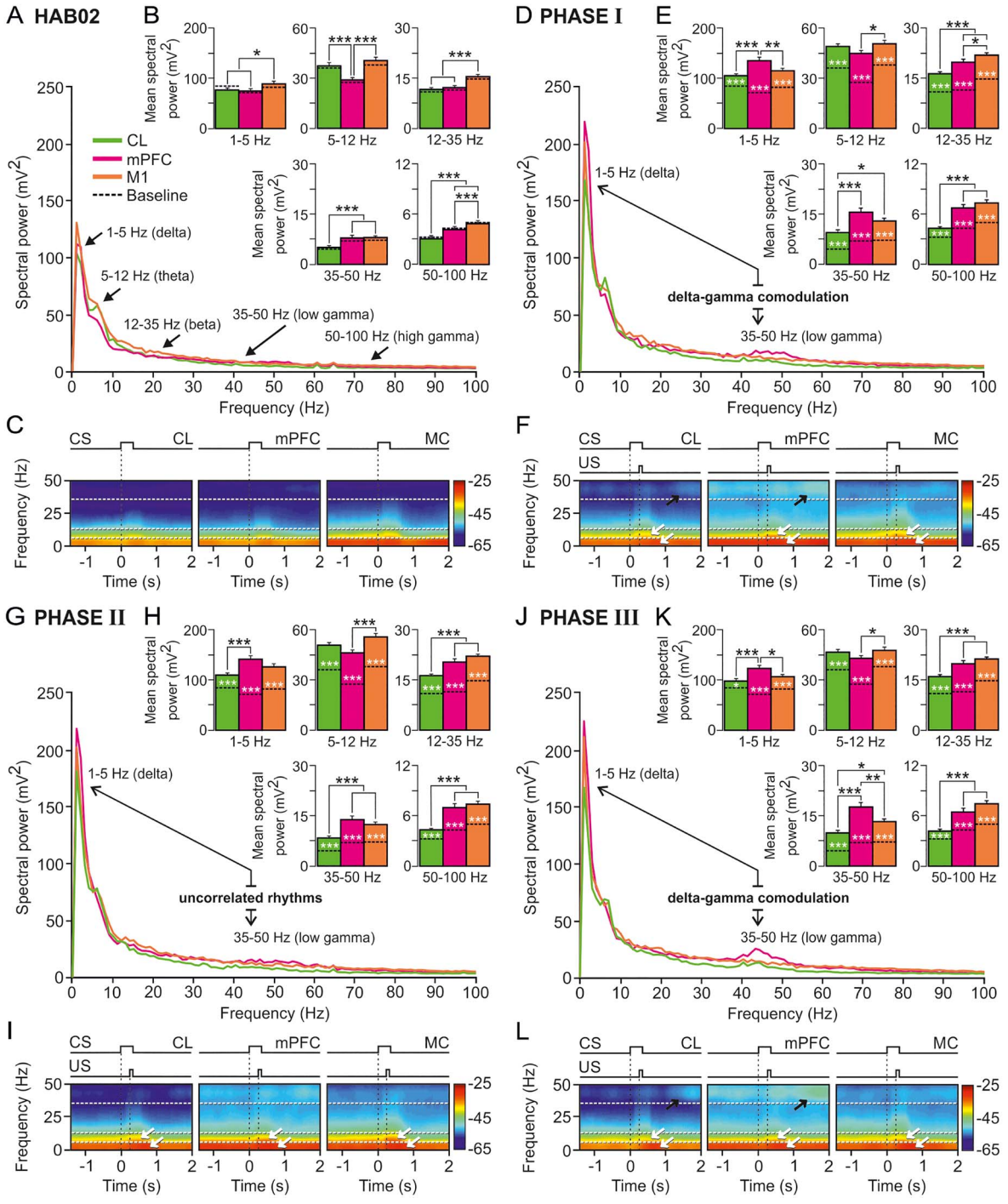

Figure 6. Spectral analyses of LFPs recorded in CL (green), mPFC (magenta), and MC (orange) during classical eyeblink conditioning. (*A*) Mean power spectra of LFPs recorded in the three recording sites between 1.5 s before and 2 s after the CS initiation during the second habituation session (HAB02). Black arrows indicate spectral ranges corresponding to delta (1–5 Hz), theta (5–12 Hz), beta (12–35 Hz), and low- (35–50 Hz) and high- (50–100) gamma bands. (*B*) Histograms of mean spectral powers for all frequency bands. Baseline values (collected from HAB02 sessions, including no stimulus) are also represented (dotted black line inside the bars); note that they are very similar to those collected during the presentation of the unpaired CS (HAB02). (*C*) Spectrograms corresponding to data illustrated in *A*, *B*. Note that the maximum values of spectral power (see the color calibration bar at the right) appeared during and after CS presentations, and the fundamental contribution to the spectral power was determined by delta and theta bands. (*D–L*) Same representations and analyses for LFPs recorded in CL, mPFC, and MC during phase I (*D–F*), phase II (*G–I*), and phase III (*J–L*). Note that the most-prominent and -differentiated power peaks appeared in delta, theta (white arrows in the spectrograms), and low gamma (black arrows in the spectrograms) bands for the mPFC and CL spectra during conditioning phases I and III (but not during phase II, just when CL neuron activation reached its maximum firing rates). This suggests the possibility of delta–gamma comodulations in *D* and *J* but uncorrelated rhythms in panel *G*. For all the multiple comparisons (Tukey–Kramer test: $^{*}P < 0.05$; $^{**}P < 0.01$; $^{***}P < 0.001$).

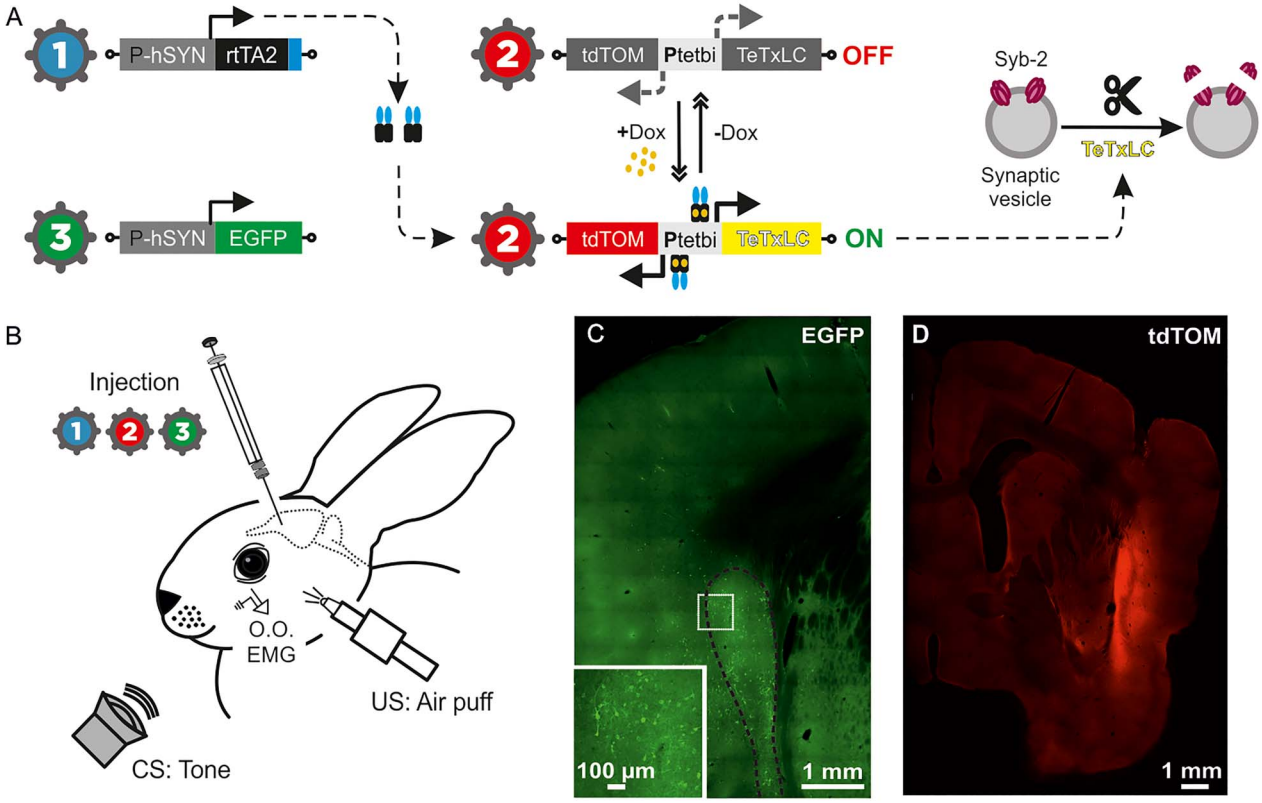

Figure 7. Animal preparation for classical eyeblink conditioning following virus-delivered inducible silencing of synaptic transmission (vINSIST) of CL neurons. (*A*) The three injected viruses were as follows: (1) rAAV–P_{hSYN}–rtTA; (2) rAAV–P_{tet}bi–TeTxLC/tdTOM; and (3) rAAV–P_{hSYN}–EGFP. With the vINSIST method, the reverse tetracycline trans activator (rtTA) is expressed under a human synapsin specific promoter (P_{hSYN}) and the tetanus toxin light chain (TeTxLC) and tdTomato (tdTOM) are under a bidirectional tet responder promoter (P_{tet}bi). Only under doxycycline (Dox) treatment, rtTA binds the P_{tet}bi to express simultaneously TeTxLC, which blocks synaptic transmission, and tdTOM, a tracer that we used to identify the inhibited zone. Virus 3 acted as a post hoc histological tracer for validating the degree of precision and the expression of rtTA. (*B*) Diagram illustrating the animal's injections with the rAAVs and its preparation for the classical conditioning of eyelid responses. (*C*) Photomicrographs from CL infected neurons glowing green due to EGFP fluorescent protein generated by the administered virus 3. The large white square is an amplification of the smaller one. (*D*) Photomicrograph from the inhibited CL glowing red due to tdTOM fluorescent protein generated by the activation of the P_{tet}bi by dox administration.

Results

Location and Identification of Claustral Neurons

Because of its substantial connectivity with the MC, the CC, and the mPFC (Kowiański et al. 1997; Majak et al. 2000; Smith and Alloway 2010; Mathur 2014; White et al. 2018; Smith et al. 2019) and its significantly larger size, the rostral and central portion of the dorsal CL was targeted for electrophysiological recordings. In accordance with Kowiański et al. 1997, that region in rabbits corresponds mainly to the somatosensory and motor protection zones, perhaps also including the auditory and PFC projections areas. The recording area was initially approached using available stereotaxic coordinates (Girgis and Shih-Chang 1981). As illustrated in Figure 1E, recorded neurons were identified by their orthodromic (i.e., synaptic) activation from the MC and the mPFC. Occasionally, they were also activated from the CC (not illustrated). In the absence of conditioning stimuli, the spontaneous activity of CL neurons recorded here ($n = 315$ from seven rabbits) presented irregular, low firing rates (5–25 spikes/s). Synaptic and/or antidromic activation was recorded when stimulating MC, mPFC, or CC in 81.90% (258/315) of the cases (Supplementary Table 1).

The electrical stimulation of either MC evoked a characteristic early (~10 ms) and late (~150 ms) activation of most (contralateral: 39.44%; ipsilateral: 66.9%) CL neurons, including a noticeable intermediate silent period (Fig. 1E1,G2). Repeated MC stimulations (at 0.1 Hz) increased the mean firing rate of CL neurons (to 50 spikes/s) for the ~300 ms following the silent period. CL neurons (15.59%) were also antidromically activated from the ipsilateral MC with the help of the collision test (Fig. 1G1, see Methods). Mean activation latencies were 3.12 ± 0.13 ms (mean ± SEM; $n = 20$; range: 2.02–4.53 ms). Additional support for the antidromic nature of spike activation was that it followed stimulation frequencies of up to 300 Hz. Finally, the electrical stimulation of either of the two implanted mPFC sites drove preferentially neurons located deeper in the CL (contralateral: 9.15%; ipsilateral: 10.06%) with a similar profile (i.e., short, late activations separated by a silent period; Fig. 1E2), but with a longer activation latency and a smaller increase in the firing rates of the activated neurons (to 25 spikes/s). With regard to the CL neurons stimulated ipsilaterally from CC, almost half of them (44%) responded to stimuli presented to the rostral CC (AP: 4 mm) and 32% to the caudal part (AP: 0 mm). They were also activated antidromically in 9.09% of the cases from the

rostral CC and in 12.5% of the cases from its caudal part, suggesting the presence of bidirectional projections between CL and CC (Chia et al. 2020).

Small electrolytic-lesion marks made with tungsten electrodes at the end of the recording sessions indicated that recorded neurons occupied a dorsal position in the rostral part of the CL (Fig. 1C,D). With the help of these electrolytic marks and collected information regarding stereotaxic coordinates, we show the location of recorded CL neurons ($n = 315$) included in this study. Figure 1D illustrates that the recorded neurons formed a cell column (AP: 0–3 mm; *L*: 5.5–6.25 mm) in between the striatum and the insular cortex. Note that in its thickest portion, the size of rabbit CL can be ~1 mm (Kowiański et al. 1999).

As previously reported (Ammann et al. 2016), the MC area that we stimulated was clearly related to eyelid movements: stimulation there (twin pulses separated by a 2 ms interval) evoked short-latency activation (16.6 ± 0.4 ms; range 15.1–18.7 ms) of the contralateral O.O. muscle (Fig. 1F3). In contrast, applying similar stimuli to the CL (Fig. 1F1), mPFC (Fig. 1F2), or CC (not illustrated) did not activate this muscle.

Firing Activity of Claustral Neurons During Classical Eyeblink Conditioning

For eyeblink conditioning, animals were presented with a tone as CS and, 250 ms later, with a 100 ms air puff aimed at the left cornea as US (Fig. 2A,B). Apart from two preliminary recording sessions to adapt the animals to the recording devices, activity of CL neurons was recorded for two habituation sessions (only CS was presented) and eight conditioning sessions (paired CS/US, $n = 5$), or six pseudoconditioning sessions (randomized CS and US, $n = 2$). Mean learning curves of conditioned and pseudoconditioned animals are illustrated in Figure 2C. Although conditioned animals reached the selected criterion by the fifth session, training was maintained up to the eighth session. The aim was to identify and record neurons both during the acquisition process and when the learning curve reached asymptotic values. Those acquisition values were similar to those collected in rabbits when using the same delay conditioning paradigm and recording characteristics (Gruart et al. 2000; Leal-Campanario et al. 2007; Caro-Martín et al. 2015; Ammann et al. 2016).

Neurons were classified in three different groups (A–C) depending on their firing activity during presentations of paired stimuli (Figs 2B, 3A–C and Supplementary Table 2). The following analysis only includes neurons recorded for ≥8 trials during conditioning ($n = 130$ neurons from $n = 5$ rabbits) or pseudoconditioning sessions ($n = 47$ neurons from $n = 2$ rabbits); otherwise, sorting them depending on their activity was very ambiguous. All the selected neurons were also activated by at least one of the stimulating electrodes (MC, mPFC, and/or CC) to ensure that the recording site was the CL.

Type A neurons recorded during conditioning sessions ($n = 59$) were characterized by a >30% increase in their firing rate during CS/US presentations and even after them (Figs 2B and 3A). In the absence of the paired stimuli, type A neurons presented an irregular, low (15–20 spikes/s) discharge rate. Type A neurons were rarely activated during single-stimulus presentations of any sensory modality. As a whole, the averaged firing rate of type A neurons increased 293.02 ± 29.56% compared with baseline values acquired immediately before CS presentations ($H = 50.900$ with one degree of freedom; $P < 0.001$; Kruskal–Wallis one-way ANOVA on ranks). The activation of these neurons took place 175.5 ± 11.5 ms ($n = 57$; range 50–430 ms) after the CS presentation—namely, well after the mean value for the beginning of CRs (156.7 ± 13.8; range 76–231 ms). The activation lasted 476.8 ± 33.5 ms, that is, very much longer than the CS + US interval. In addition, the mean peak activity of type A neurons took place slightly after the CS/US presentations (380 ± 39.5 ms after CS onset). In Figure 2B is illustrated a type A neuron recorded from a well-trained animal during the fifth conditioning session. The cell was activated after CR initiation (i.e., 164 and 129 ms after CS onset, respectively). The averaged firing rate of this neuron increased 330.43% steadily from its early activation until surpassing the end of the US by >600 ms [$F_{(1,8)} = 58.533$; $P < 0.001$; one-way ANOVA *F*-test]. Its firing rate peaked right before (229 ms after the CS) the US presentation and reached ~50 spikes/s. In contrast, the type A neuron illustrated in Figure 3A started increasing its firing rate almost at the same time as CR onset (~160 ms after the CS) but also reached its peak firing rate before the US (208 ms). Here again, the increase in firing rate (593.51% more than its baseline) surpassed the end of the US by >600 ms [$F_{(1,8)} = 80.365$; $P < 0.001$; one-way ANOVA *F*-test].

Type B neurons recorded during conditioning sessions ($n = 16$) were characterized by a ≥30% decrease in their firing rate during CS/US presentations (Fig. 3B). In the absence of paired stimuli, type B neurons presented an irregular spontaneous firing rate (20–30 spikes/s), some 133–150% higher than that presented by type A neurons. As already described for type A neurons, type B cells were rarely found during single-stimulus presentations of any sensory modality. The averaged firing rate of type B neurons decreased 59.59 ± 5.82% compared with baseline values ($H = 38.434$ with one degree of freedom; $P < 0.001$; Kruskal–Wallis one-way ANOVA on ranks). Overall, the inhibition of type B neurons took place from 60.0 ± 18.7 to 266.6 ± 25.2 ms after CS presentations (mostly during the CS–US interval); hence, their inhibition occurred before the mean value for the beginning of CRs (156.7 ± 13.8; range 76–231 ms). As an example, Figure 3B illustrates a type B neuron recorded from a well-trained animal during the eighth conditioning session. This neuron was inhibited 65 ms following CS presentation, well before CR onset (111 ms after the CS) and recovered its baseline activity (~250 ms after the CS); that is, by US presentation. This neuron presented a decrease of 79.16% of its activity during approximately 185 ms [$F_{(1,7)} = 62.395$; $P < 0.001$; one-way ANOVA *F*-test].

Type C neurons recorded during conditioning sessions ($n = 55$) presented an irregular firing rate (20–30 spikes/s) that was not modified by any stimulus present in the recording room, including the paired CS/US presentation during conditioning sessions ($H = 0.678$ with one degree of freedom; $P = 0.41$; Kruskal–Wallis one-way ANOVA on ranks). See an example in Figure 3C. This neuron did not change its firing rate in response to CS/US presentations; its baseline values—obtained 500 ms before CS onset—were very similar to those obtained 500 ms after the CS (25.74 and 26.50 spikes/s respectively) [$F_{(1,8)} = 0.127$; $P = 0.731$; one-way ANOVA *F*-test].

Remarkably, the percentage of these three types of neuron was modified across habituation and conditioning sessions but not during pseudoconditioning. As illustrated in Figure 3D, the evolution in the relative percentage of type A (green), B (red), and C (blue) neurons across training was best represented with quadratic or higher order polynomial fits (Supplementary Table 3). Thus, during the two habituation sessions, type C neurons represented 68.42% and 83.33% of recorded units, respectively, while type A neurons were only 26.32% and 16.67%, and type B less than 5%. During the first

five conditioning sessions (prelearning and learning phase, up until rabbits reached the selected criterion), these percentages changed notably for types A and C neurons. The number of type A neurons showed a growing trend, reaching its highest value around CON05 and reaching values of 76.47% of recorded units. In contrast, the number of type C neurons decreased, showing its lowest value also at CON05 (11.76%). From CON06 on (when the percentage of CRs reached asymptotic values), this trend flipped again, and by CON08 type C neurons were the most numerous cells recorded (46.15% for type C; 38.46% for type A). Type B cells presented rather low, constant values ($12.27 \pm 2.26\%$, ranging from 0 to 25% of recorded units) across sessions, and no trend was detected.

As indicated in Figure 3E,F and Supplementary Table 3, no changes in the relative percentages of types A, B, and C neurons were observed during pseudoconditioning sessions. In response to single CS presentations, the percentage of the recorded type C neurons remained at high levels, while the percentages of types A and B neurons maintained low levels across training [Fig. 3E, types A (10.64%), B (4.26%), and C (85.11%)]. Similar results were collected during single US presentations [Fig. 3F, types A (12.5%), B (2.5%), and C (85%)]. The reliability of these data is confirmed by the results obtained for the two habituation sessions when only the CS was presented (Fig. 3D,E).

Taken together, recorded CL cells did not respond to single stimuli (even when presented at high intensities), as during pseudoconditioning. Type A neurons did respond with an increase of firing activity to the same stimuli when they were presented together (paired CS/US); in this situation, their percentage increased in conjunction with the development of CRs, until animals reached the learning criterion—that is, when the acquisition phase was finished. The burst of activity presented by type A neurons followed the initiation of CRs. In contrast, type B neurons decreased their activity during the CS–US interval, but the number of recorded units remained low across sessions and no particular evolution was observed. Their inhibition preceded CR onset. Interestingly, the number of recorded neurons not related to CS and US presentations (type C) decreased during the first conditioning sessions until animals reached criterion. This suggests a recruitment of type A CL neurons, at the expense of type C cells, during CR acquisition.

Because firing rate profiles and spike durations vary between pyramidal cells and interneurons (Buzsáki and Kandel 1998; Csicsvari et al. 1999; Constantinidis and Goldman-Rakic 2002; Barthó et al. 2004; Viskontas et al. 2007), we used these two criteria to discriminate principal (projecting neurons) and nonprincipal units (putative inhibitory interneurons) from neuronal recordings. Following the analytical procedures detailed in Supplementary Table 4, Supplementary Fig. 3, and Supplementary Appendix 2, no significant differences ($P > 0.05$) were observed between the spike durations of types A and C neurons. Only the cluster of spikes from type B neurons showed shorter spike durations (0.88 ± 0.01, range 0.80–0.92 ms) than those of type A cluster (1.04 ± 0.01, range 0.94–1.09 ms). The multiple comparison demonstrated that there was a statistically significant difference ($H = 16.26$ with one degree of freedom; $P < 0.001$; Kruskal–Wallis one-way ANOVA on ranks) between the mean values of the spike duration (see Supplementary Table 4). These differences in spike duration together with their different firing patterns, suggest that type B neurons could represent a population of CL interneurons, while types A and C neurons might represent projecting neurons.

Changes in the Firing Rate of Type A Neurons in Relation to the Development of Conditioned Responses Across Conditioning

We also checked the putative relationships between the discharge rates of type A neurons during the acquisition process and EMG activity of the left O.O. muscle collected during the corresponding sessions and trials (Fig. 4). For this, we quantified the integrated firing rate [in (spikes/s) × s] of type A neurons during the CS–US (Fig. 4A,B,D) and CS + US (Fig. 4A,C,E) periods and represented it against the EMG area (in mV × s) of the rectified EMG activity of the left O.O. muscle ($n = 5$ animals; Supplementary Table 5). We determined the linear relationships between these two variables in early (from first to third) and late (from fourth to eighth) conditioning sessions during the CS–US interval (early conditioning, Fig. 4B; late conditioning, Fig. 4D), and also during the CS + US period (early conditioning, Fig. 4C; late conditioning, Fig. 4E). None of these four representations (Fig. 4B–E) indicated the presence of a linear relationship ($r \geq 0.6$).

Finally, it is well known that training reduces the latency of CRs with respect to CS presentation (see details and references in Gruart et al. 1995). If claustral neuron activity is related to the development and/or expression of CRs then type A neurons in well-trained animals should decrease their initiation latency with respect to CS onset. Accordingly, we checked whether the activation latency of type A neurons to CS presentation was inversely correlated to the percentage of CRs. As illustrated in Figure 4F, we found that there was no linear relationship between these two variables. Taken together, these results indicate that type A neurons are not related with the EMG activity of the O.O. muscle during the acquisition process.

Analysis of LFPs Recorded in CL, MC, and mPFC During the Classical Conditioning of Eyelid Responses

During the unitary recording sessions, we noticed the presence of specific changes in LFPs recorded in the CL across conditioning, particularly in the gamma band (Cebolla and Cheron 2019). In order to have consistent recordings of selected CL sites during all training sessions, we prepared four additional rabbits with chronically implanted tetrodes in the right CL (Supplementary Fig. 1D). For comparative purposes, those animals were also chronically implanted with recording bipolar electrodes in mPFC and MC (Supplementary Fig. 1D). To avoid any distortion of LFP recordings, no electrical stimulation of the implanted sites was carried out in this group of animals.

Representative LFPs collected from CL, MC, and mPFC are shown in Supplementary Figure 1A,B. Those examples exhibit 3.5 s frames (from 1.5 s before to 2 s after CS presentations) taken from the second habituation (Supplementary Fig. 1A) and the eighth conditioning sessions (Supplementary Fig. 1B). It can be seen that conditioning increases LFP amplitudes in the three recording sites and evokes the presence of a high-frequency oscillation following the paired CS/US presentation in CL and mPFC recorded traces (Supplementary Fig. 1B).

Figures 5 and 6 illustrate the spectral analysis of LFPs (in 3.5 s frames, as those shown in Supplementary Fig. 1A,B) recorded during baseline and the second habituation session, and also during three conditioning sessions that represent different learning stages (Supplementary Fig. 1C): phase I (before learning, <12% of CRs, $5.95 \pm 2.16\%$; mean ± SEM); phase II (during acquisition, ~50% of CRs, $47.45 \pm 2.93\%$); and phase III (after learning, >85% of CRs, $94.27 \pm 2.22\%$). Those phases

were selected following a previous study from our laboratory (Fernández-Lamo et al. 2018). Time frames from phases I to III included the paired CS/US presentations, while habituation sessions included only the CS, and baseline sessions did not include any stimulus.

Figure 5 shows the results for the analysis of the LFP recordings carried out in the CL. As plotted in Figure 5A,B, baseline and habituation did not show any difference in the mean spectral power of the five selected bands [delta (1–5 Hz), theta (5–12 Hz), beta (12–35 Hz), low gamma (35–50 Hz), and high gamma (50–100 Hz)], whereas during the conditioning phases it increased significantly in all the frequency bands (Tukey–Kramer multiple comparison test: HAB02 and Baseline vs. phases I, II, and III; $P < 0.001$; ***).

Following Fernández-Lamo et al. (2016), for a more-precise dynamic analysis of spectral powers computed from LFPs, we selected moving time-windows of 500 ms (shifted in 10 ms increments) and we calculated multitapered Fourier transforms. Thus, time–frequency representations were computed for the 3.5 s LFP frames recorded in the CL for habituation and phases I, II, and III (Fig. 5C). The illustrated spectrograms correspond to 600 tapered Fourier transforms, each corresponding to the average of 120 frames × 5 tapers. Collected results indicate that the maximum power values appeared during the CS + US interval and 0.75 s following it, throughout the subsequent conditioning phases. This is particularly visible in lower frequency bands (delta, theta; Fig. 5C, white arrows), but it is also present in the higher frequency bands (beta, low gamma and high gamma). Likewise, notice the increase of the spectral power in the low gamma band 1 s after the CS/US presentation shown in phases I and III spectrograms, but not in phase II (Fig. 5C, black arrows).

Figure 5D represents probabilistic maps for the multiple comparisons between pairs of spectrograms, where red (inference type +1) and blue (inference type −1) indicate significant statistical differences ($P < 0.05$; jackknifed estimates of the variance), and white (inference type 0) indicates no significant differences ($P > 0.05$). It can be seen clearly that spectral powers of LFPs recorded during conditioning sessions were higher than those recorded during habituation (red, inference type +1), mainly during and after CS/US presentations. Specific differences were observed when comparing the three selected conditioning phases: between phases I and III versus phase II, mainly in low gamma band (see the black arrows 1 s after the CS/US presentation), and between phases I and II versus phase III for low frequencies (red arrows). The probability density histograms (Fig. 5E) allowed us to verify the aforementioned results.

It is noticeable in all the representations (Fig. 5A–D) that spectral power of phase II is the highest in low frequencies before and during the CS/US presentations (in which is similar to phase I). In contrast, the peak in low gamma frequency 1 s after the CS/US present in phases I and III is missing in phase II. The increment of the low gamma spectral power during phases I and III respect to phase II in this specific temporal range (between 1 and 2 s after CS presentation) could be a CL cognitive-control inference.

Alternatively, Figure 6 illustrates a comparative spectral analysis of the LFPs recordings carried out in CL (green), mPFC (magenta), and MC (orange) simultaneously. Figure 6A–C shows mean spectra (*A*), histograms of mean spectral power (*B*), and time–frequency spectrograms (*C*) of these tree recording sites during habituation. Figure 6, *D–FG–I* and *J–L* provides the same information about conditioning phases I, II, and III respectively. In addition, in the multiple comparison histograms (Fig. 6B,E,H,K), the difference to the baseline values is shown (dotted black line). The histograms also further illustrate that the above-indicated changes in spectral power for LFPs collected in the CL when comparing habituation versus any of the conditioning phases were present in mPFC and MC as well, and they were even stronger (Tukey–Kramer multiple comparison test: HAB02 and Baseline vs. phases I, II, and III; $P < 0.001$, white asterisk).

CL results were detailly described and analyzed above, hence data from mPFC and MC LFP recordings are going to be evaluated next. The changes we observed in CL LPF spectra seem to be present and even greater in mPFC ones. Apparently, both structures follow a similar spectral pattern. The two structures increased their LFP spectral power in delta (1–5 Hz) during phases I and II (even though both increased, power values from mPFC became statistically different that those from CL, $P < 0.001$), and reduced it notably in phase III. In addition, they both raised remarkably their spectral power for low gamma band (35–50 Hz) in phases I and III (Fig. 6E,K, 35–50 Hz plots; Fig. 6F,L, see black arrows). Curiously, mPFC is the one recording site whose theta band (5–12 Hz) spectral powers grew the most compared with habituation session, but its values remained unchangeable throughout the three conditioning phases. On the other hand, LFP recordings from MC did not follow the same spectral patterns as those from CL and mPFC. Its spectral powers did increase in phases I and II specially for low frequencies (delta and theta), but in contrapositions to CL and mPFC, LFP from MC did not experience any noticeable change for the low gamma values across phases I, II, and III (*$P < 0.05$; **$P < 0.01$; ***$P < 0.001$; Tukey–Kramer test).

None of the three structures presented any remarkable change in beta (12–35 Hz) and high gamma (50–100 Hz) bands, except the general increase of spectral power in all the five bands produced presumably due to the conditioning itself.

Finally, comodulation analysis by means of the crossfrequency couplings and the computation of the power–power spectral ratios between different frequency bands indicated that the strength of these crossfrequency interactions changes dynamically and differentially, between the LFP oscillatory activities from CL, mPFC, or MC. In summary, the LFP oscillatory patterns at CL–mPFC network nodes were correlated with coordinated dynamic changes in delta and low-gamma powers. In contrast, at the CL–MC network nodes, the power dynamics in delta and gamma frequency bands were uncorrelated. In relation to the above, see further comments and detailed statistical results in Supplementary Appendix 3.

Effects of Blocking CL Output on the Acquisition Curve and on the EMG Activity of the Orbicularis Oculi Muscle During Classical Eyeblink Conditioning

In a final experimental step, we studied the putative effects of blocking CL neuron output on learning and/or performance of conditioned eyeblink responses. For this, we used a novel method for virus-delivered inducible silencing of synaptic transmission (vINSIST, see Methods, and Supplementary Fig. 2 and Supplementary Appendix 1). A homogeneous cocktail of three rAAVs was injected at three different sites (2 µL each) in the two CLs (Fig. 7). With the vINSIST method, we were able not only to silence the synaptic transmission in CL after doxycycline treatment, but also to target infected (EGFP, green) and inhibited (tdTOM, red) CL neurons (Fig. 7C).

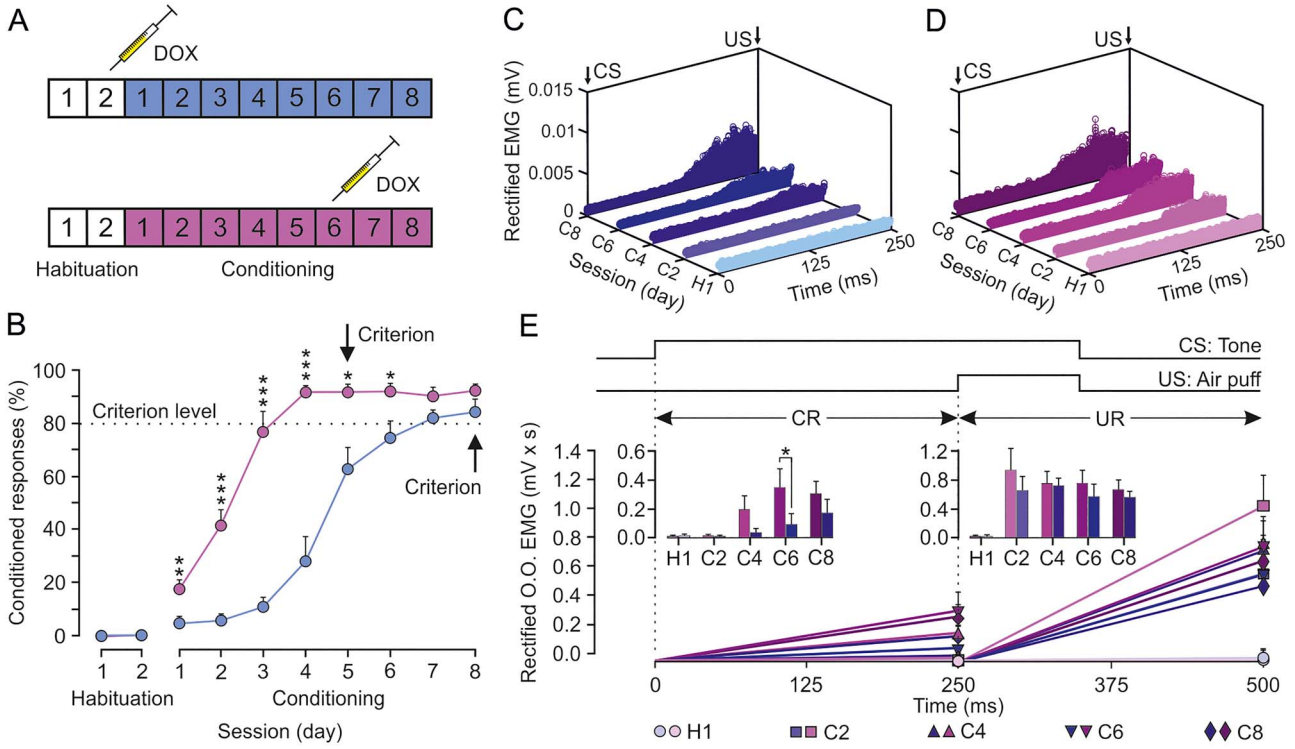

Figure 8. Classical conditioning of eyelid responses during the inhibition of both CLs. CL neurons were inhibited by the local injection of a cocktail of rAAVs equipped with doxycycline (Dox)-dependent tetracycline-controlled genetic switches, which release tetanus toxin (TeTxLC) when activated. (*A*) Animals ($n = 8$) were classically conditioned using a delay paradigm following two protocols: half of them (blue group) were injected with Dox after the second habituation session and the other half (magenta group) after the sixth conditioning session. (*B*) Learning curves corresponding to the two groups of animals. Data are presented as mean ± SEM (see the multiple comparison reports: $^{*}P < 0.05$; $^{**}P < 0.01$; $^{***}P < 0.001$; Holm–Sidak or Tukey–Kramer tests). (*C*) Rectified EMG activity of the left O.O. muscle from the blue group during the CS–US interval (CRs time gap) and collected for the indicated habituation and conditioning sessions ($n = 50$ trials per session from $n = 4$ animals). (*D*) Same representation for magenta group. Note the earlier and larger CRs attained by this group during CS–US interval. (*E*) Quantitative analysis of cumulative areas (in mV × ms) of the rectified EMG activity of the left O.O. muscle recorded during the CS–US interval (CR time gap) and during the 250 ms following it (CS + US interval plus 150 ms, UR time gap) for the five indicated sessions. The insets illustrate the differences in net EMG areas between the two groups ($^{*}P < 0.05$) during the CS–US (CRs) and the CS + US intervals (URs). No differences were found between groups for URs.

A total of eight rAAV-injected rabbits were classically conditioned using a delay paradigm; four of them were injected with doxycycline following the second habituation session (before the learning has even started; the blue group) and the other four were injected following the sixth conditioning session (after the learning has been achieved; the magenta group) (Fig. 8A). As illustrated in Figure 8B, animals included in the early inhibited CLs group (blue) presented a significantly delayed learning curve [$F_{(7,42)} = 14.179$; $P < 0.001$; two-way ANOVA *F*-test, with one factor repetition] with respect to values collected from the late-inhibited CLs group (magenta). In contrast, the activation of the injected rAAVs in the magenta group after the sixth conditioning session (i.e., once the learning criterion has been reached) produced no noticeable effects.

In regard to the EMG activity of the O.O. muscle during the CS–US interval (Fig. 8C–E), the early inactivation of both CLs in the blue group significantly decreased the mean area of the rectified EMG during the intermediate conditioning sessions, but control values were reached by the eighth conditioning session [$F_{(3,18)} = 7.287$; $P = 0.002$; two-way ANOVA *F*-test, with one factor repetition; see inset in Fig. 8E]. In contrast, there were no significant differences for the evoked URs shown during the CS + US period [$F_{(3,18)} = 3.036$; $P = 0.056$; two-way ANOVA *F*-test, with one factor repetition].

In summary, the early inactivation of both CLs delayed the acquisition of a classical conditioning task without affecting its performance, but their inactivation in well-trained animals had no effect. Therefore, we conclude that CL neurons are involved in the cognitive component of the eyeblink conditioning, rather that the motor.

Discussion

We have found that CL neurons exhibit changes in their activity during classical eyeblink conditioning in behaving rabbits. Their firing properties were related to cognitive aspects of the acquisition process rather than the kinematics of the CR. Below we discuss our findings in detail and consider the potential role of the CL in cognitive-like functions involved in associative learning.

Location and Identification of Claustral Neurons

Specific details were considered to ensure that recordings were carried out in the CL. Even though rabbit CL is far easier to access, due to its significantly larger size (compared with mouse CL), its differential and dense connectivity (anti- and ortho-dromic) with MC, mPFC, and CC (Carman et al. 1964; Crick and Koch 2005;

Mathur 2014; Chia et al. 2017; Atlan et al. 2018; White et al. 2018) and its spontaneous firing rate (Spector et al. 1974; Chachich and Powell 2004) are key to identifying the recorded zone. The electrolytic marks in the postmortem tissues confirmed that the region recorded was the CL.

CL neurons were easily activated synaptically from MC, mPFC, and CC, but their antidromic activation was much more difficult. This could be the result of their extensive branching into different cortical areas (Marchi et al. 1983; Minciacchi et al. 1985; Majak et al. 2000), which would certainly hinder the antidromic invasion of their somas (Steriade et al. 1971; Lipski 1981). As supported by the present results and in the multiunit recordings carried out in rabbit CL during Pavlovian heart rate conditioning by Chachich and Powell (2004), CL neurons presented a low, irregular spontaneous firing that was not easily modulated by the single presentation of stimuli used as CS or US. This characteristic firing helped to differentiate CL from nearby nuclei while recording. For instance, insular neurons in rabbits present inconstant, low-magnitude responses during classical conditioning (Gibbs et al. 1992). Moreover, insular neurons in monkeys seem to be involved in integrative complex processing of sounds and vocal communications (Remedios et al. 2009), while—as reported here—CL neurons are not very active when presented with single stimuli of any sensory modality. Finally, the inactivation of the insular cortex by tetrodotoxin evokes different effects to those reported here for the CL (Bermudez-Rattoni et al. 1991). On the other hand, striatal cells present a characteristic low-frequency stable tonic firing that can be modulated during classical eyeblink conditioning but with response profiles pretty different (Blázquez et al. 2002) to those reported here for types A and B neurons.

Finally, action potentials recorded in fiber tracks and long dendrites present a quite different shape than those recorded near neuron somas (Delgado-García et al. 1990; Deligkaris et al. 2016). That is why we dismiss the possibility of having been recording in the extreme or external capsule or dendrites located outside the nucleus. Thus, we are positive that the neuronal activity analyzed in this work has been recorded in the CL.

Firing Activity of Claustral Neurons During Classical Eyeblink Conditioning

Type A neurons reported here presented activation profiles similarly to those of other cortical neurons recorded in rabbits during delay eyeblink conditioning. For instance, Leal-Campanario et al. (2013) identified mPFC pyramidal neurons that presented a delayed firing with respect to CS presentation. Caro-Martín et al. 2015 ("late mPFC neurons") and Ammann et al. 2016 ("type C pyramidal MC neurons") also recorded similar cells. In addition, CL neurons recorded by Chachich and Powell (2004) presented a late and longer lasting increase in their discharge rate during paired CS/US presentations similarly to type A neurons reported here. In contrast, they did not report the presence of cells that responded with inhibition (type B neurons), probably due to their multiunit recording procedures. Even using single-unit recordings as carried out here, finding type B neurons was challenging. Inhibition was perceptible only when neurons had high baseline firing rates and the recording was held for a long time. Type C neurons did not respond to any stimuli, not even to the paired CS/US presentations. They represented more than 75% of the recorded cells during habituation and pseudoconditioning sessions (when single or unpaired stimuli were presented), but they became less frequent during the learning phase. In fact, they seemed to be replaced by type A neurons, whose number increased considerably (Fig. 3*D*–*F*). Although the spike durations of types A and C neurons were similar and they presented an inverse relation across conditioning, the fact that they presented different baseline firing rates prevent considering them as member of the same CL population.

Moreover, this work clearly shows how types A and B neurons respond to the presentations of the paired CS/US. Therefore, we believe they must play a role in this type of associative learning. Claustral type A neurons increased their activity with the association of the paired CS/US during the acquisition of the CRs. However, we reject the possibility that their function during the learning phase is related to the motor performance of the CRs, for three main reasons: (1) CRs appeared mostly before type A neurons discharged (156.7 ± 13.8 and 175.5 ± 11.5 ms after the CS, respectively), so there is no way their activation could produce or modulate the movement of the eyelid. (2) The first CRs started appearing very soon in the training and they became larger and more numerous until the learning curve reached asymptotic values (around the fifth session). If type A neurons were necessary for the proper execution of the CRs, their activation should be maintained specifically during the last conditioning sessions, when more and bigger CRs are delivered. On the contrary, these data show that after the fifth session, type A neuron number starts to decrease (Fig. 3*D*). And (3) the regression analysis dismisses any linear relationship between the discharge rates of type A neurons and the EMG activity of the O.O. muscle ($r \geq 0.6$), both for the CS–US period, where CRs are expected (Fig. 4*B*,*D*,*F*) and for the CS + US interval, when URs appeared (Fig. 4*C*,*E*). On top of that, it was usual to find CS/US trials with type A neuron firing activity and no CR, and vice versa. It can be concluded then that type A neurons are not related to the correct performance of the eyelid CRs. Alternatively, it is more plausible that their role is related to attentional, cognitive processes, since type A cell activity is mainly required during the acquisition phase: once the CRs are fully developed and the learning is achieved, no more activation in the CL is recorded. Furthermore, claustrocortical connections are expected to produce inhibition of their target cortices, especially in PFC (Jackson et al. 2018). Therefore, we hypothesize that type A cell activity will suppress cortical areas during the learning phase.

In contrast, given their firing profiles during conditioning and the short duration of their spikes, type B neurons are expected to be interneurons and not project out of the CL. They certainly did respond to the CS/US before the initiation of the CRs (60 ± 18 and 156.7 ± 13.8 ms after the CS, respectively), but it is unlikely that their inhibition is somehow involved in the CR performances. Rather, they might be part of an inhibitory inner circuitry. Anyhow, as said before, more data are needed to clarify with regard to type B neurons.

Analysis of LFPs Recorded in CL, MC, and mPFC During the Classical Conditioning of Eyelid Responses

According to data obtained from LFPs recorded in CL (Fig. 5), habituation and baseline results barely differed, and single CS presentations did not produce any change in spectral power, as has already been indicated for single-unit recordings. In contrast, the CS/US association increased the spectral power of all the frequency bands. Comparing spectral power changes (Fig. 5*C*) with single-unit activation (Fig. 3*D*) throughout phases I, II, and III, we noticed several remarkable details: (1) In the prelearning stage (phase I), there was a perceptible increase of

low-frequency (delta and theta) spectral powers, and simultaneously (during and slightly after the CS/US presentation) a few type A neurons started firing. One second after the CS, there was a slight increase of low gamma spectral power. (2) During the acquisition stage (phase II), delta and theta spectral powers were the highest simultaneously (during and slightly after the CS/US presentation) with the increased firing of type A neurons. One second after the CS, the low gamma peak had disappeared. And (3) when learning had been achieved (phase III), delta and theta presented the lowest spectral powers during and slightly after the CS/US, while type A neurons were rarely recorded. Yet, one second after the CS, the low gamma band presented its highest value, with a prominent peak.

To sum up, the spectral patterns (power–power ratios and amplitude–amplitude comodulations) suggest that the couplings in which delta–gamma comodulation appears in CL LFPs seem to depend on the learning phase. Not only are they absent during habituation sessions, but also, the strength of these crossfrequency interactions changed differentially during phases I, II, and III. Moreover, those patterns seem to be tightly related to the single-unit activities. Available information concerning LFP recordings carried out in CL of behaving rats indicates a similar modulation between two frequency bands (1–4 and 8–12 Hz) during spontaneous behaviors (Jankowski et al. 2017), although frequency bands in rats and rabbits are not equivalent.

Data collected from LFP recordings carried out in CL, mPFC, and MC are quite intriguing. Despite the fact that MC recordings seem to follow a completely different pattern, mPFC recordings also presented a distinctive increment of spectral power in low-gamma frequencies during some conditioning phases, as described above for CL recordings. Thus, LFPs recorded from CL–mPFC network nodes show an amplitude–amplitude coupling between delta and low-gamma frequency bands during phases I and III. In contrast, during the acquisition stage (phase II) the low gamma peak disappeared in CL and mPFC and delta–gamma comodulation was not found. In single-unit recording experiments, it was also during the acquisition sessions that the percentage of type A neurons was greater, reaching its highest value at the end of this stage (Fig. 3*D*). These cells fired from 175.5 ± 11.5 to 476.8 ± 33.5 ms after the CS presentations and ≈500 ms after that, the expected low-gamma peak was missing. Thus, firing activities of CL neurons could prevent the presence of low-gamma oscillations. Additionally, as Jackson et al. (2018) have reported using optogenetic activation of CL neurons, it is likely that CL type A cells target mPFC interneurons which inhibit pyramidal neurons. Those inhibited mPFC neurons could generate the low-gamma oscillations described in phases I and III (especially considering that spectral power values for low gamma were higher in mPFC than in CL). After the acquisition period (i.e., in phase III), CL neurons become silent and mPFC might again generate low gamma oscillations. This would also explain why in phase I, the low-gamma peak is small: there are already a few CL neurons firing, but not sufficient to inhibit PFC activity as they do in phase II.

In contrast, MC does increase its spectral power values for low frequencies (delta and theta) across conditioning, but not for low gamma. This fact helps to verify that this peak in the low-gamma band is specific and is not occurring all-brain-wide due to signal contamination. In accordance, it can be suggested that the power dynamics at CL nodes could be related to cognitive-like functions (CL and mPFC LFPs are correlated) rather than to the motor neural control (CL and MC LFPs are uncorrelated) during classical eyeblink conditioning (contrary to the predominant motor control role played by MC circuits for the generation of eyelid-conditioned responses (CRs) as described by Ammann et al. 2016).

Notice that for LFP experiments, we use special electrodes to avoid multiunitary recording that could affect low- and/or high-gamma amplitudes. Thus, the delta–gamma couplings in the CL–mPFC network nodes were due to genuine interactions between spectral patterns of two LFP oscillations, and not to spike contamination from the local firing of CL and/or mPFC neurons. These LFP spectral patterns should endorse the proposal of the delta-associated gamma oscillations described here as a new type of CL–mPFC coupling, directly involved in cognitive processes related to this type of associative learning. Indeed, results presented here further support evidence (White et al. 2018) of a cognitive control system, where CL is subservient to network function (mainly top–down) rather than an integrator of sensory cortical information.

CL Inactivation Delayed Learning During Classical Eyeblink Conditioning

Regarding the inhibition of CL neuron afferences, the injections of the vINSIST rAAVs were minimal and local, in order to avoid spill over adjacent structures. Hence, it is unlikely that the entire CL was reached by injected viruses. Nevertheless, the partial inactivation of both CLs evoked a noticeable delay in the acquisition of CRs, without affecting URs. This delay in CR acquisition was evident not only in a qualitative sense (there were fewer CRs in early conditioning sessions; Fig. 8*B*), but also in a quantitative one (when CRs started appearing, they were considerably smaller; Fig. 8*C–E*). In contrast, we could not find any significant difference between the URs of blue and magenta groups; thus, CL shutdown affected the cognitive component of the task, but not the motor one. Furthermore, Chachich and Powell (2004) attained similar results—a delay in the acquisition of a classical heart rate conditioning—following permanent bilateral electrolytic lesion in the CL of rabbits. These results, together with the data illustrated in Figure 4, confirmed that CL neurons are not related to the kinematics of eyelid CRs, further support our previous statement about the CL being involved in the cognitive components of this type of associative learning.

In opposition to the role in the motor aspects of conditioned eyeblinks played by the cerebellum (Welsh and Harvey 1991; Krupa et al. 1993; Christian and Thompson 2003; Sánchez-Campusano et al. 2007; Ten Brinke et al. 2017) and the MC (Aou et al. 1992; Ammann et al. 2016), we believe that CL may be part of the several brain structures implicated in the cognitive component, mainly the hippocampus (Rescorla 1988; Múnera et al. 2001), CC (Weible et al. 2003; Hattori et al. 2014), and the mPFC (Powell et al. 2005; Leal-Campanario et al. 2007; Siegel and Mauk 2013; Caro-Martín et al. 2015).

The cognitive role of CL neurons could be related to the attentional process triggered by CS/US association, as reported by Goll et al. (2015). Furthermore, this putative role of the CL in the attentional and cognitive components of classical eyeblink conditioning has also been proposed for CL in other types of learning task, as a sort of resilience to distraction (Atlan et al. 2018). As shown here, reduction in claustral activities produces a noticeable deficit in the cognitive components of classical eyeblink conditioning. It has also been reported that CL presents a heightened activity in patients with attention deficit hyperactivity disorder as compared with controls

(Dickstein et al. 2006; Castellanos et al. 2008). Therefore, it is possible that a specific activation–inhibition balance of the CL cell population is needed to cope with complex cognitive challenges that require recruiting attention.

According to the present results, CL neurons are not activated by single and/or irrelevant stimuli of any sensory modality. In fact, they are activated by paired CS/US associations until the moment when CRs reach asymptotic values in their expression levels. In conclusion, the CL seems to play an important role in the proper acquisition of classical conditioning tasks, mostly in attentional processes related to CS/US association.

Supplementary Material

Supplementary material can be found at *Cerebral Cortex* online.

Funding

Spanish Ministry of Economy and Competitiveness (BFU2017-82375-R to A.G. and J.M.D.-G.); Max Planck Society (to G.K.D., M.T., J.L., and M.T.H.); a Charité Postdoctoral Research fellowship (to J.L.); Fritz Thyssen Stiftung (to M.T.H.); NeuroCure Charite Berlin (to M.T.H.); Ikerbasque—Basque Foundation of Science (to M.T.H.), Achucarro Basque Center for Neuroscience (to M.T.H.); and the Spanish Ministry of Economy and Business under the framework of ERA-NET Neuron (to A.G. and M.T.H.).

Notes

We wish to thank Mr José A. Santos Naharro for the development of electronic equipment, Mr José M. González Martín for his help in the surgical room, and Mr Pablo Sierra Márquez and Mr Roger Churchill for revising the final version of the manuscript. Authors thank Drs Britta J. Eickholt, Matthew E. Larkum, and Rolf Sprengel for allowing us the use of their facilities. *Conflict of Interest*: None declared.

Authors' Contributions

Conception and design of the experiments: M.M.R.-G., A.G., J.M.D.-G. Performance of the experiments: M.M.R.-G., J.M.D.-G. Contribution of new analytic tools and representation programs: R.S.-C., J.L., G.K.D., M.T., M.T.H. Data analysis: M.M.R.-G., R.S.-C., J.M.D.-G. Preparation of the illustrations: M.M.R.-G., R.S.C., A.G. Drafting of the paper: M.M.R.-G., R.S.-C., A.G., J.M.D.-G. All authors revised the final version of the manuscript.

References

Ammann C, Márquez-Ruiz J, Gómez-Climent MÁ, Delgado-García JM, Gruart A. 2016. The motor cortex is involved in the generation of classically conditioned eyelid responses in behaving rabbits. *J Neurosci*. 36:6988–7001.

Aou S, Woody CD, Birt D. 1992. Changes in the activity of units of the cat motor cortex with rapid conditioning and extinction of a compound eyeblink movement. *J Neurosci*. 12:549–559.

Atlan G, Terem A, Peretz-Rivlin N, Groysman M, Citri A. 2017. Mapping synaptic cortico-claustral connectivity in the mouse. *J Comp Neurol*. 525:1381–1402.

Atlan G, Terem A, Peretz-Rivlin N, Sehrawat K, Gonzales BJ, Pozner G, Tasaka GI, Goll Y, Refaeli R, Zviran O *et al*. 2018. The claustrum supports resilience to distraction. *Curr Biol*. 28:2752–2762.

Barthó P, Hirase H, Monconduit L, Zugaro M, Harris KD, Buzsáki G. 2004. Characterization of neocortical principal cells and interneurons by network interactions and extracellular features. *J Neurophysiol*. 92:600–608.

Berger TW, Rinaldi PC, Weisz DJ, Thompson RF. 1983. Single-unit analysis of different hippocampal cell types during classical conditioning of rabbit nictitating membrane response. *J Neurophysiol*. 50:1197–1219.

Bermudez-Rattoni F, Introini-Collison IB, McGaugh JL. 1991. Reversible inactivation of the insular cortex by tetrodotoxin produces retrograde and anterograde amnesia for inhibitory avoidance and spatial learning. *Proc Natl Acad Sci USA*. 88:5379–5382.

Blázquez PM, Fujii N, Kojima J, Graybiel AM. 2002. A network representation of response probability in the striatum. *Neuron*. 33:973–982.

Binks D, Watson C, Puelles L. 2019. A re-evaluation of the anatomy of the claustrum in rodents and primates—analyzing the effect of pallial expansion. *Front Neuroanat*. 13:34.

Bokil H, Andrews P, Kulkarni JE, Mehta S, Mitra PP. 2010. Chronux: a platform for analyzing neural signals. *J Neurosci Methods*. 192:146–151.

Buzsáki G, Kandel A. 1998. Somadendritic back propagation of action potentials in cortical pyramidal cells of the awake rat. *J Neurophysiol*. 79:1587–1591.

Carman JB, Cowan WM, Powell TP. 1964. The cortical projection upon the claustrum. *J Neurol Neurosurg Psychiatry*. 27:46–51.

Caro-Martín CR, Leal-Campanario R, Sánchez-Campusano R, Delgado-García JM, Gruart A. 2015. A variable oscillator underlies the measurement of time intervals in the rostral medial prefrontal cortex during classical eyeblink conditioning in rabbits. *J Neurosci*. 35:14809–14821.

Castellanos FX, Margulies DS, Kelly C, Uddin LQ, Ghaffari M, Kirsch A, Shaw D, Shehzad Z, Di Martino A, Biswal B *et al*. 2008. Cingulate-precuneus interactions: a new locus of dysfunction in adult attention-deficit/hyperactivity disorder. *Biol Psychiatry*. 63:332–337.

Cebolla AM, Cheron G. 2019. Understanding neural oscillations in the human brain: from movement to consciousness and vice versa. *Front Psychol*. 10:1930.

Chachich ME, Powell DA. 2004. The role of claustrum in Pavlovian heart rate conditioning in the rabbit (*Oryctolagus cuniculus*): anatomical, electrophysiological, and lesion studies. *Behav Neurosci*. 118:514–525.

Chia Z, Silberberg G, Augustine GJ. 2017. Functional properties, topological organization and sexual dimorphism of claustrum neurons projecting to anterior cingulate cortex. *Claustrum*. 2:1.

Chia Z, Augustine GJ, Silberberg G. 2020. Synaptic connectivity between the cortex and claustrum is organized into functional modules. *Curr Biol*. 30:2777–2790.

Christian KM, Thompson RF. 2003. Neural substrates of eyeblink conditioning: acquisition and retention. *Learn Mem*. 10:427–455.

Citri A, Barretta S. 2016. Claustral delusions. *Claustrum*. 1(1):31426.

Clark GA, McCormick DA, Lavond DG, Thompson RF. 1984. Effects of lesions of cerebellar nuclei on conditioned behav-

ioral and hippocampal neuronal responses. *Brain Res*. 291: 125–136.
Constantinidis C, Goldman-Rakic PS. 2002. Correlated discharges among putative pyramidal neurons and interneurons in the primate prefrontal cortex. *J Neurophysiol*. 88:3487–3497.
Crick FC. 1994. *The astonishing hypothesis*. New York (NY): Charles Scribner's Sons.
Crick FC, Koch C. 2005. What is the function of the claustrum? *Philos Trans R Soc Lond B Biol Sci*. 360:1271–1279.
Csicsvari J, Hirase H, Czurkó A, Mamiya A, Buzsáki G. 1999. Oscillatory coupling of hippocampal pyramidal cells and interneurons in the behaving rat. *J Neurosci*. 19:274–287.
Delgado-García JM, Evinger C, Escudero M, Baker R. 1990. Behavior of accessory abducens and abducens motoneurons during eye retraction and rotation in the alert cat. *J Neurophysiol*. 64:413–422.
Deligkaris K, Bullmann T, Frey U. 2016. Extracellularly recorded somatic and neuritic signal shapes and classification algorithms for high-density microelectrode array electrophysiology. *Front Neurosci*. 10:421. doi: 10.3389/fnins.2016.00421.
Dickstein SG, Bannon K, Castellanos FX, Milham MP. 2006. The neural correlates of attention deficit hyperactivity disorder: an ALE meta-analysis. *J Child Psychol Psychiatry*. 47:1051–1062.
Dogbevia GK, Roβmanith M, Sprengel R, Hasan MT. 2016. Flexible, AAV-equipped genetic modules for inducible control of gene expression in mammalian brain. *Mol Ther Nucleic Acids*. 5:e309.
Dogbevia GK, Marticorena-Alvarez R, Bausen M, Sprengel R, Hasan MT. 2015. Inducible and combinatorial gene manipulation in mouse brain. *Front Cell Neurosci*. 9:142.
Druga R. 1982. Claustro-neocortical connections in the cat and rat demonstrated by HRP tracing technique. *J Hirnforsch*. 23:191–202.
Druga R, Rokyta R, Benes V. 1990. Claustro-neocortical projections in the rhesus monkey (projections to area 6). *J Hirnforsch*. 31:487–494.
Duffau H, Mandonnet E, Gatignol P, Capelle L. 2007. Functional compensation of the claustrum: lessons from low-grade glioma surgery. *J Neurooncol*. 81:327–329.
Edelstein LR, Denaro FJ. 2004. The claustrum: a historical review of its anatomy, physiology, cytochemistry and functional significance. *Cell Mol Biol*. 50(6):675–702.
Fernández-Lamo I, Delgado-García JM, Gruart A. 2018. When and where learning is taking place: multisynaptic changes in strength during different behaviors related to the acquisition of an operant conditioning task by behaving rats. *Cereb Cortex*. 28:1011–1023.
Fernández-Lamo I, Sánchez-Campusano R, Gruart A, Delgado-García JM. 2016. Functional states of rat cortical circuits during the unpredictable availability of a reward-related cue. *Sci Rep*. 6:37650.
Gibbs CM, Prescott LB, Powell DA. 1992. A comparison of multiple-unit activity in the medial prefrontal and agranular insular cortices during Pavlovian heart rate conditioning in rabbits. *Exp Brain Res*. 89:599–610.
Girgis M, Shih-Chang W. 1981. *A new stereotaxic atlas of the rabbit brain*. St. Louis (MO): Warren H. Green, Inc.
Goll Y, Atlan G, Citri A. 2015. Attention: the claustrum. *Trends Neurosci*. 38:486–495.
Gruart A, Blázquez P, Delgado-García JM. 1995. Kinematics of spontaneous, reflex, and conditioned eyelid movements in the alert cat. *J Neurophysiol*. 74:226–248.
Gruart A, Muñoz MD, Delgado-García JM. 2006. Involvement of the CA3-CA1 synapse in the acquisition of associative learning in behaving mice. *J Neurosci*. 26:1077–1087.
Gruart A, Schreurs BG, del Toro ED, Delgado-García JM. 2000. Kinetic and frequency-domain properties of reflex and conditioned eyelid responses in the rabbit. *J Neurophysiol*. 83:836–852.
Hasan MT, Hernández-González S, Dogbevia G, Treviño M, Bertocchi I, Gruart A, Delgado-García JM. 2013. Role of motor cortex NMDA receptors in learning-dependent synaptic plasticity of behaving mice. *Nat Commun*. 4:2258.
Hattori S, Yoon T, Disterhoft JF, Weiss C. 2014. Functional reorganization of a prefrontal cortical network mediating consolidation of trace eyeblink conditioning. *J Neurosci*. 34:1432–1445.
Jackson J, Karnani MM, Zemelman BV, Burdakov D, Lee AK. 2018. Inhibitory control of prefrontal cortex by the claustrum. *Neuron*. 99:1029–1039.
Jankowski MM, Islam MN, O'Mara SM. 2017. Dynamics of spontaneous local field potentials in the anterior claustrum of freely moving rats. *Brain Res*. 1677:101–117.
Jurado-Parras MT, Sánchez-Campusano R, Castellanos NP, del-Pozo F, Gruart A, Delgado-García JM. 2013. Differential contribution of hippocampal circuits to appetitive and consummatory behaviors during operant conditioning of behaving mice. *J Neurosci*. 33:2293–2304.
Kowiański P, Dziewiątkowski J, Kowiańska J, Moryś J. 1999. Comparative anatomy of the claustrum in selected species: a morphometric analysis. *Brain Behav Evol*. 53:44–54.
Kowiański P, Moryś J, Dziewiatkowski J, Karwacki Z, Wisniewski HM. 2000. The combined retrograde transport and unbiased stereological study of the claustrocortical connections in the rabbit. *Ann Anat*. 182:111–122.
Kowiański P, Moryś J, Karwacki Z, Dziewiątkowski J, Narkiewicz O. 1997. The cortico-related zones of the rabbit claustrum—study of the claustrocortical connections based on the retrograde axonal transport of fluorescent tracers. *Brain Res*. 784:1–2.
Krupa DJ, Thompson JK, Thompson RF. 1993. Localization of a memory trace in the mammalian brain. *Science*. 260:989–991.
Kurada L, Bayat A, Joshi S, Koubeissi MZ. 2019. The claustrum in relation to seizures and electrical stimulation. *Front Neuroanat*. 13:8.
Leal-Campanario R, Delgado-García JM, Gruart A. 2013. The rostral medial prefrontal cortex regulates the expression of conditioned eyelid responses in behaving rabbits. *J Neurosci*. 33:4378–4386.
Leal-Campanario R, Fairén A, Delgado-García JM, Gruart A. 2007. Electrical stimulation of the rostral medial prefrontal cortex in rabbits inhibits the expression of conditioned eyelid responses but not their acquisition. *Proc Natl Acad Sci USA*. 104:11459–11464.
Lipski J. 1981. Antidromic activation of neurones as an analytic tool in the study of the central nervous system. *J Neurosci Methods*. 4:1–32.
Majak K, Kowiánski P, Morýs J, Spodnik J, Karwacki Z, Wisniewski HM. 2000. The limbic zone of the rabbit and rat claustrum: a study of the claustrocingulate connections based on the retrograde axonal transport of fluorescent tracers. *Anat Embryol*. 201:15–25.
Marchi G, Bentivoglio M, Minciacchi D, Molinari M. 1983. Claustrocortical projections studied in the cat by means of multiple retrograde fluorescent tracing. *J Comp Neurol*. 215:121–134.

Masimore B, Kakalios J, Redish AD. 2004. Measuring fundamental frequencies in local field potentials. *J Neurosci Methods*. 138:97–105.

Mathur BN. 2014. The claustrum in review. *Front Syst Neurosci*. 8:48.

Minciacchi D, Molinari M, Bentivoglio M, Macchi G. 1985. The organization of the ipsi- and contralateral claustrocortical system in rat with notes on the bilateral claustrocortical projections in cat. *Neuroscience*. 16:557–576.

Mitra PP, Bokil H. 2008. *Observed brain dynamics*. New York (NY): Oxford University Press.

Múnera A, Gruart A, Muñoz MD, Fernández-Mas R, Delgado-García JM. 2001. Hippocampal pyramidal cell activity encodes conditioned stimulus predictive value during classical conditioning in alert cats. *J Neurophysiol*. 86:2571–2582.

Olson CR, Graybiel AM. 1980. Sensory maps in the claustrum of the cat. *Nature*. 288:479–481.

Oswald BB, Knuckley B, Mahan K, Sanders C, Powell DA. 2009. Prefrontal control of trace eyeblink conditioning in rabbits (Oryctolagus cuniculus) II: effects of type of unconditioned stimulus (airpuff vs. periorbital shock) and unconditioned stimulus intensity. *Physiol Behav*. 96:67–72.

Powell DA, Churchwell J, Burriss L. 2005. Medial prefrontal lesions and Pavlovian eyeblink and heart rate conditioning: effects of partial reinforcement on delay and trace conditioning in rabbits (*Oryctolagus cuniculus*). *Behav Neurosci*. 119:180–189.

Remedios R, Logothetis NK, Kayser C. 2009. An auditory region in the primate insular cortex responding preferentially to vocal communication sounds. *J Neurosci*. 29:1034–1045.

Remedios R, Logothetis NK, Kayser C. 2010. Unimodal responses prevail within the multisensory claustrum. *J Neurosci*. 30:12902–12907.

Remedios R, Logothetis NK, Kayser C. 2014. A role of the claustrum in auditory scene analysis by reflecting sensory change. *Front Syst Neurosci*. 8:44.

Rescorla RA. 1988. Behavioral studies of Pavlovian conditioning. *Annu Rev Neurosci*. 11:329–352.

Rieke F, Warland D, de Ruyter van Steveninck R, Bialek W. 1997. *Spikes: exploring the neural code*. Cambridge (MA): MIT Press.

Sánchez-Campusano R, Gruart A, Delgado-García JM. 2007. The cerebellar interpositus nucleus and the dynamic control of learned motor responses. *J Neurosci*. 27:6620–6632.

Schade Powers A, Coburn-Litvak P, Evinger C. 2010. Conditioned eyelid movement is not a blink. *J Neurophysiol*. 103:641–647.

Sherk H, LeVay S. 1981. Visual claustrum: topography and receptive field properties in the cat. *Science*. 212:87–89.

Siegel JJ, Mauk MD. 2013. Persistent activity in prefrontal cortex during trace eyelid conditioning: dissociating responses that reflect cerebellar output from those that do not. *J Neurosci*. 33:15272–15284.

Smith JB, Alloway KD. 2010. Functional specificity of claustrum connections in the rat: interhemispheric communication between specific parts of motor cortex. *J Neurosci*. 30:16832–16844.

Smith JB, Watson GDR, Liang Z, Liu Y, Zhang N, Alloway KD. 2019. A role for the claustrum in salience processing? *Front Neuroanat*. 13:64.

Smythies J, Edelstein L, Ramachandran V. 2012. Hypotheses relating to the function of the claustrum. *Front Integr Neurosci*. 6:53.

Spector I, Hassmannova J, Albe-Fessard D. 1974. Sensory properties of single neurons of cat's claustrum. *Brain Res*. 66:39–65.

Steriade M, Apostol V, Oakson G. 1971. Control of unitary activities in cerebellothalamic pathway during wakefulness and synchronized sleep. *J Neurophysiol*. 34:389–413.

Sweeney ST, Broadie K, Keane J, Niemann H, O'Kane CJ. 1995. Targeted expression of tetanus toxin light chain in Drosophila specifically eliminates synaptic transmission and causes behavioral defects. *Neuron*. 14:341–351.

Takehara-Nishiuchi K, Kawahara S, Kirino Y. 2005. NMDA receptor-dependent processes in the medial prefrontal cortex are important for acquisition and the early stage of consolidation during trace, but not delay eyeblink conditioning. *Learn Mem*. 12:606–614.

Ten Brinke MM, Heiney SA, Wang X, Proietti-Onori M, Boele HJ, Bakermans J, Medina JF, Gao Z, De Zeeuw CI. 2017. Dynamic modulation of activity in cerebellar nuclei neurons during pavlovian eyeblink conditioning in mice. *Elife*. 6:e28132.

Thompson RF. 2005. In search of memory traces. *Annu Rev Psychol*. 56:1–23.

Torgerson CM, Irimia A, Goh SY, Van Horn JD. 2015. The DTI connectivity of the human claustrum. *Hum Brain Mapp*. 36:827–838.

Viskontas IV, Ekstrom AD, Wilson CL, Fried I. 2007. Characterizing interneuron and pyramidal cells in the human medial temporal lobe in vivo using extracellular recordings. *Hippocampus*. 17:49–57.

Weible AP, Weiss C, Disterhoft JF. 2003. Activity profiles of single neurons in caudal anterior cingulate cortex during trace eyeblink conditioning in the rabbit. *J Neurophysiol*. 90:599–612.

Welsh JP, Harvey JA. 1991. Pavlovian conditioning in the rabbit during inactivation of the interpositus nucleus. *J Physiol (Lond)*. 444:459–480.

White MG, Cody PA, Bubser M, Wang HD, Deutch AY, Mathur BN. 2017. Cortical hierarchy governs rat claustrocortical circuit organization. *J Comp Neurol*. 525:1347–1362.

White MG, Panicker M, Mu C, Carter AM, Roberts BM, Dharmasri PA, Mathur BN. 2018. Anterior cingulate cortex input to the claustrum is required for top-down action control. *Cell Rep*. 22:84–95.